OPTIMIZATION OF HYBRID RENEWABLE ENERGY SOURCES USING METAHEURISTIC ALGORITHMS

A THESIS

Submitted in the fulfilment of the requirement for the award of the degree of

DOCTOR OF PHILOSOPHY

By

JYOTI GUPTA

(Registration Number: 901904003)

Under the Supervision of

Dr. Parag Nijhawan
Associate Professor, EIED

Dr. Souvik Ganguli
Assistant Professor, EIED

THAPAR INSTITUTE
OF ENGINEERING & TECHNOLOGY
(Deemed to be University)

Electrical and Instrumentation Engineering Department

Thapar Institute of Engineering & Technology, Patiala -147004

PUNJAB (INDIA)

September -2022

CERTIFICATE

I hereby certify that the work which is being presented in the thesis entitled, ***"OPTIMIZATION OF HYBRID RENEWABLE ENERGY SOURCES USING METAHEURISTIC ALGORITHMS"*** in the partial fulfilment of the requirement for the award of the Degree of ***Doctor of Philosophy***, submitted to ***Electrical & Instrumentation Engineering Department*** of **Thapar Institute of Engineering & Technology, Patiala**, is an authentic record of my own work carried under the supervision of **Dr. Parag Nijhawan and Dr. Souvik Ganguli**. It refers other researcher's work which is duly listed in the reference section. The matter contained in this thesis has not been submitted, neither in part nor in full to any other university except as reported in the text and references.

Place: Patiala
Date: 29th Sept 2022

Jyoti Gupta.
Jyoti Gupta
(Registration No. 901904003)

This is to certify that the above statement made by the candidate is correct and true to best of our knowledge.

Parag.
Dr. Parag Nijhawan
(Associate Professor)

Ganguli
Dr. Souvik Ganguli
(Assistant Professor)

ABSTRACT

The need for power is rising on a daily basis all across the world. Due to the finite supply of fossil fuels, it is critical to develop innovative non-renewable energy systems that can reduce reliance on conventional energy sources. Solar photovoltaic (PV) is most common alternative renewable energy source due to availability in abundance. Recently, Proton Exchange Membrane Fuel Cells (PEMFCs) is also gaining popularity as the feasible method for sustainable power generation to meet the ever-increasing electricity demand with no greenhouse gases emission. The optimal operation of PV and PEMFC needs to be ensured to exploit its advantages to the maximum limit. In this direction, there is an extensive need for parameter extraction of PV and PEMFC. Many researchers have applied evolutionary optimization approaches are used to estimate the PV and PEMFCs parameters as the precise modeling of these cells still to deliver good model.

In all engineering areas, optimization is a frequent mathematical issue. Finding the finest possible/desirable option is what it actually implies. Optimization issues are so diverse and numerous, strategies for tackling them should be an emerging research area. The nature of optimization methods can be stochastic. As computationally efficient alternatives to deterministic approaches, bio-inspired stochastic optimization algorithms have been developed. Meta-heuristics are based on the iterative improvement of a population of solutions (as in Evolutionary algorithms and Swarm based algorithms) or a single solution and often use randomization and local search to solve an optimization issue.

In this thesis, the work objective is to enhance the optimization algorithm to overcome the process's variety and premature convergence. This can be possible by modification meta-heuristic algorithm by using chaos theory or hybridization of algorithm. In a nonlinear system, chaos is a deterministic and random process that refers to initial conditions. The behaviour of the nonlinear system will dramatically change if there are small changes in the initial values. Besides, a chaotic system has complex characteristics such as certainty, randomness, and sensitivity initial conditions, and even a good internal structure. Based on these features, the diversity of the population should be retained and therefore prevent entering into an optimum local search and improve the probability of reaching a global optimum. This feature of chaos theory is explored on different optimization algorithm to increase the accuracy of parameter extraction of PV and PEMFC.

A hybrid off-grid renewable energy system is needed to reduce reliance on traditional energy supplies, and to enhance the reliability of the renewable energy system. The process of selecting the appropriate combinations of components and their costs in order to produce an affordable, dependable and effective alternative energy supply is known as hybrid system optimization. Hybrid energy technology can meet the energy needs of community very effectively. The goal of improving hybrid energy system control, size, and component selection is to offer society with a cost-effective electric power solution. One of the objective of this thesis aims to use the proposed hybrid chaotic algorithm for optimal sizing of hybrid renewable energy system. The solar/fuel cell/biomass hybrid renewable energy system is considered for the continuation of supply. The outcome of the proposed algorithm and parent algorithm is compared with Hybrid Optimization of Multiple Energy Resources (HOMER) software.

Keywords: Renewable Energy, Solar Photovoltaic, Proton Exchange Membrane Fuel Cells, Optimization, Bio Inspired Algorithms, Chaos Theory, Hybrid Optimization of Multiple Energy Resources.

ACKNOWLEDGMENT

- At the outset, I would like to acknowledge my sincere gratitude and appreciation of my supervisors Dr. Parag Nijhawan, Associate Professor, and Dr. Souvik Ganguli, Assistant Professor, Electrical and Instrumentation Engineering Department, Thapar Institute of Engineering and Technology, Patiala, for their invaluable guidance and time throughout my research work. They were always available and eager to help and advice, whether my problem be professional or personal. Their cooperation, support, and motivation are the primary reason for my completion of this dissertation. This research would not have been possible without their inspiration.
- I would like to take this opportunity to express my sincere gratitude to all faculty members of the Electrical and Instrumentation Engineering Department (EIED), especially advisory committee members, namely Dr. R.S. Kaler (Professor & Head, EIED), Dr. Amit Dhir (Associate Professor, School of Energy and Environment), Dr. Surya Prakash (Associate Professor, EIED) and Dr. Suman Bhullar (Assistant Professor, EIED) for their valuable suggestions and feedbacks. The inputs provided by them and their critical appraisal during each stages of this research were invaluable.
- I would express my dearest gratitude to my fellow research scholars, some of whom I have come to share a special bond throughout my thesis. Manish Kumar Singla is the one who helped me a lot, and the times we spent and the memories we shared will always be etched in my memory. He was always there as a friend whenever I needed him. Thank you for your unending support.
- No words of mine can be sufficient to express my thanks and respect to my Parents. They have been a constant and untiring source of support and motivation to me all through this time. I am also grateful to my husband who were always there for me through this journey.

In the end, I thank the Almighty for giving me his blessing throughout my research work and providing me strength enough to accomplish this research work.

Jyoti Gupta

TABLE OF CONTENT

LIST OF FIGURES

LIST OF TABLE

LIST OF ABBREVIATIONS

ABC	Artificial Bee Colony
AC	Alternating Current
AD	Anaerobic Digestion
AE	Absolute Error
ALO	Ant Lion Optimizer
AO	Aquila Optimizer
ASC	Annualized System Cost
ASO	Atom Search Optimization
BPP	Biogas Power Plant
BWO	Black Widow Optimization
CBSSO	Chaotic Binary Shark Smell Optimization
CCSO	Chaotic Chicken Swarm Optimization
ChOA	Chimp Optimization Algorithm
CMA	Chaotic Mayfly Algorithm
COA	Coyote Optimization Algorithm
COE	Cost of Energy
CSO	Chicken Swarm Optimization
CTSA	Chaotic Tunicate Swarm Algorithm
CUF	Capacity Utilization Factory
CPU	Central Processing Unit
CRF	Capital Recovery Factor

DA	Dragonfly Algorithm
DC	Direct Current
DDM	Double Diode Model
DE	Differential Evolution
DF	Degree of Freedom
ESS	Energy Storage System
FA	Firefly Algorithm
FC	Fuel Cell
FC-EPSO	Fractional Chaotic Ensemble Particle Swarm Optimizer
FPA	Flower Pollination Algorithm
GOA	Grasshopper Optimization Algorithm
GWOCSA	Grey Wolf Optimization Cuckoo Search Algorithm
HGWO	Hybrid Grey Wolf Optimizer
HHO	Harris Hawks Optimizer
HCPSOSMA	Hybrid Chaotic Particle Swarm Optimization Slime Mould Algorithm
HISA	Hybrid Interior Search Algorithm
HOMER	Hybrid Optimization of Multiple Energy Resources
HPS	Hybrid Power System
HRES	Hybrid Renewable Energy System
HS	Harmony Search
IAE	Individual Absolute Error
IEC	International Electro-technical Commission

ISA	Interior Search Algorithm
LCOE	Levelised Cost of Energy
LPSP	Loss of Power Supply Probability
MA	Mayflies Algorithm
MAE	Maximal Absolute Error
MATLAB	Matrix Laboratory
MBE	Mean Bias Error
MFO	Month-Flame Optimizer
MILP	Mixed Integer Linear Programming
MOPSO	Multi-objective Particle Swarm Optimization
MS	Mean Square
MSA	Moth Search Algorithm
MVO	Multi Verse Optimizer
NASA	National Aeronautics and Space Administration
NPC	Net Present Cost
O&M	Operational and Maintenance Cost
OSCs	Organic Solar Cells
PEMFC	Proton Exchange Membrane Fuel Cell
PSO	Particle Swarm Optimization
PV	Photovoltaic
RMSE	Root Mean Square Error
SCA	Sine Cosine Algorithm

SD	Standard Deviation
SDM	Single diode Model
SFO	Sunflower Optimization
SMA	Slime Mould Algorithm
SS	Sum of Squares
SSE	Sum of Square Error
SSO	Salp Swarm Optimizer
STC	Standard Temperature Condition
sTLBO	Sanitised Teacher Learning Based Optimization
TDM	Triple Diode Model
TNPC	Total Net Present Cost
TSA	Tunicate Swarm Algorithm
TSD	Total Square Deviation
VSA	Vortex Search Algorithm
WOA	Whale Optimization Algorithm

LIST OF SYMBOLS

A	Surface Area
$\overrightarrow{A_b}$ and $\overrightarrow{A_c}$	Variable Parameter
Ae	Area of the Solar Photovoltaic Generator
$\vec{B}$	New Search Agent Locations
b	Parametric Variable
C_f	Best Solution Found by All Iterations
CN	Number of Chicks
C_{O2}	Cathode Side Concentration of the Oxygen
D	Individual Dimension
d_1, d_2, d_3	Random Variable Number
DW_{bg}	Calorific Value of Biomass Gasifier
$\vec{E}$	SM location
$\overrightarrow{E_A(l)}$ and $\overrightarrow{E_B(l)}$	Individuals Selected from the Swarm Randomly
$\overrightarrow{E_b}$	Peak Odour Concentration
E_{Nernst}	Open Circuit Voltage
f	Fitness of Individual Chicken
F_{bg}	Biomass Gasifier's Yearly Output Electricity
f_{cp}	Energy Conditioning Efficiency
FL	Parameter that Implies the Chick Would Follow their Mother for Foraging of Food

f_r	Module Efficiency
$\vec{H}$	Force of Gravity
$H(j)$	$\vec{E}$ Fitness
HN	Number of Hens
I	Output Current
I_{fc}	Current Generated by the Cell
I_o, I_{o1}, I_{o2}	Saturation Current
I_{ph}	Photovoltaic Current
$\vec{J}$	Water Flow Advection in Deep Ocean
J_{bio}	Cost of Biomass Gasifier
$J_{converter}$	Cost of Converter
J_e	Cost of Electrolyzer
J_{fc}	Cost of Fuel Cell
J_{ht}	Cost of Hydrogen Tank
J_{IHRES}	Sum of Cost Integrated Hybrid Renewable Energy System
J_{max}	Maximum Current Density
J_{spv}	Cost of the Solar PV Panel
$\overrightarrow{JT}$	Position of Food Source
J_a^t	Current Position of Mayflies
K	Boltzmann's Constant
k	Index of the Rooster

l	Membrane Thickness
l	Current Iteration
lb	Lower Bound
M	Specific Range of Random Value
m	Mother Hen
M_E	Electrical Efficiency
M_{FC}	Overall Efficiency of Fuel Cell
MN	Number of Mother Hens
M_R	Efficiency of Fuel Cell
M_T	Thermal Efficiency
N	Population Size
$\vec{N}$	Social Forces Between the Search Agents
N_{cells}	Number of Cells Connected in Series
$N(0,\sigma^2)$	Gaussian Distribution
N_{oct}	Nominal Operating Temperature
N_q	Solar Radiation
P_a	Pressure at the Anode
P_c	Pressure at the Cathode
PH_a	Anode Relative Vapour Humidity
P_{H2}	Partial Pressure of Hydrogen
P_{H2O}	Water Saturation Pressure
P_{O2}	Partial Pressure of Oxygen

q	Electron Charge
Q_a	Ambient Temperature
Q_{bg}	Biomass Gasifier System Rating
Q_c	Cell Temperature
q_{min}	Initial Speed
q_{max}	Subordinate Speed
Q_{ref}	Reference Cell Temperature
R_C	Contact of the Resistance
RH_C	Cathode Relative Vapour Humidity
R_M	Membrane Surface Resistance
RN	Number of Roosters
R_S	Series Resistance
R_{Sh}	Shunt Resistance
T	PV Cell Temperature
T_{fc}	Operating Cell Temperature
ub	Upper Bound
V	Voltage of PV Cell
$V_{activation}$	Activation Voltage Drop
V_{cell}	Voltage of Each Cell
$V_{concentration}$	Concentration Voltage Drop
V_{ohmic}	Ohmic Voltage Drop
V_{stack}	Stack Output Voltage

V_{ab}^{t+1}	Velocity of Female Mayflies
$\overrightarrow{W}$	SM Weights
w_f	Worst Solution
$\overrightarrow{XE}$	Distance Between the Food Source And Search Agent
$\overrightarrow{X_X}$	Tunicate Position
z	Current Iteration
$\alpha, \alpha_1, \alpha_2$	Diode Ideality Factor
σ^2	Variance
ε	Smallest Constant to Avoid Zero Division Error
$\xi_1, \xi_2, \xi_3, \xi_4;$	Semi-Empirical Coefficients
$x_i^j(t)(i \in [1, \cdots, N])$	Individual Position
ρM	Membrane Material of Specific Resistance
λ	Adjustable Empirical Variable
$\Omega_1 M^{-\alpha R_l^2}$ and $\Omega_2 M^{-\alpha R_l^2}$	Constants
H	Efficiency of Solar Photovoltaic
β	Temperature Coefficient
η_{bg}	Overall Efficiency of the Biomass Gasifier

LIST OF PUBLICATIONS

SCI/SCIE

1. Gupta, J., Nijhawan, P., & Ganguli, S. (2021). Parameter extraction of solar PV cell models using novel metaheuristic chaotic tunicate swarm algorithm. *International Transactions on Electrical Energy Systems*, *31*(12), e13244. (Impact Factor: 2.860) (SCIE).
2. Gupta, J., Nijhawan, P., & Ganguli, S. (2021). Parameter estimation of different solar cells using a novel swarm intelligence technique. *Soft Computing*, 1-31. (Impact Factor: 3.646) (SCIE).
3. Gupta, J., Nijhawan, P., & Ganguli, S. (2021). Optimal parameter estimation of PEM fuel cell using slime mould algorithm. *International Journal of Energy Research*, *45*(10), 14732-14744. (Impact Factor: 5.164) (SCIE).
4. Gupta, J., Nijhawan, P., & Ganguli, S. (2021). Parameter estimation of fuel cell using chaotic Mayflies optimization algorithm. *Advanced Theory and Simulations*, *4*(12), 2100183. (Impact Factor: 4.004) (SCIE).
5. Gupta, J., Nijhawan, P., & Ganguli, S. (2021). Optimal sizing of different configuration of photovoltaic, fuel cell, and biomass-based hybrid energy system. *Environmental Science and Pollution Research*, 1-16. (Impact Factor: 4.223) (SCI).

PATENT

1. Nijhawan, P., Gupta, J., & Ganguli, S. (2021). HYBRID ENERGY GENERATION SYSTEM. *Australian Government Innovation Patent,* Patent Number AU2021101651A4.

CHAPTER 1 INTRODUCTION

1.1 Overview

Energy has increasingly been acknowledged as human societies guiding power and has been applied to human value and impact in human evolution. For this cause, energy supply is one of the most critical aspects in the present era that has a significant effect on foreign affairs and the growth of countries. Over the past decades and centuries, as well as in the newly developed world, the global pattern in energy consumption has centered on the extensive usage of fossil fuels to maintain that these sources of energy supply approximately 90% of the planet's energy demands [1-2]. The unsuitable use of fossil fuels has resulted in environmental problems that hinder people's well-being and health, so it is expected that it will eventually suffer irreparable harm [3]. The most difficult aspect of using fossil fuels is the long term regeneration of oil and emission of carbon from the world's energy and energy cycle over millions of years. This direct oil emissions, along with the greenhouse gases it produces, increases global temperatures and triggers abnormal environmental changes including polar ice melting and increasing groundwater levels, storms, flooding, droughts, and famines, pest outbreaks, rats, and infectious diseases [4-5]. On the other hand, environmental issues and emissions have been compounded by unintended and reckless usage of these energy sources [6-7]. Their deteriorating condition is another problem associated with fossil fuel use. As a result, in contrast to the above, the development of clean energies and green energy sources is inexhaustible, has no issues competing with fossil fuel sources, and, most notably, is accessible in certain parts of the country. The designing of most efficient system is big issue for researchers.

Many academics researched computational paradigms that replicated intelligent bio-inspired processes in the form of computer algorithms, inspired by various characteristics found in biological systems [8-9]. They aimed to replicate the inherent benefits of such biological systems in order to solve complicated modeling, simulation, and optimization challenges. In this context, significant emphasis has been dedicated to optimization problems, whose complexity has unlocked a rich substratum from which numerous bio-inspired population-based heuristic techniques have grown each balancing computing efficiency and optimality of solutions in their own unique way. While the early contributions in this field were generally based on observation and replication of Darwinian evolutionary processes, the number of bio-inspired solutions in the literature has exploded in recent years, with a wide range of inspiring rationales [10]. When focusing on other elements of optimization, such as multi-objective criteria, developing

(dynamic) optimization problems, or networked computing techniques, to name a few, this observed blossoming of fresh bio-inspiration optimization approaches becomes even more intense [11]. Recently new theory is introduced which approaches that use chaotic variables instead of random variables are referred to as chaotic optimization algorithms in random-based optimization algorithms. Because of the non-repetition and ergodicity of chaos, metaheuristic algorithms can perform overall searches at faster speeds than stochastic searches based on probabilities [12-13].

The most effective and feasible alternative among numerous existing sources of renewable energy is solar photovoltaic cell based energy sources [14-15]. The advancement of PV technologies has attracted significant attention in the evaluation, control and maximum power point tracking of PV systems for the reliable modeling and parameter estimation that can closely reflect the I-V nonlinear characteristics of the solar cells [16-17]. Although mathematical models have been proposed to explain the nonlinear behaviour of PV structures, two parameter circuit equivalent models are typically used in operation, such as single diode and double diode model [18]. The performance of these models is calculated largely by the parameters of their models, but these parameters are frequently inaccessible and differ in terms of defects, ageing and changing operating conditions [19]. As a result, correct understanding of these criteria is critical for PV system's performance assessment, maximum power point tracking, and quality control. However, single and double diode model tacit transcendental equations hinder specific elementary functions [20]. In order to evaluate these model parameters on the basis of the calculated I-V data of the PV cell and module, it is therefore, expected and essential to design appropriate and reliable techniques.

The issue of extracting the parameters of the PV cells and module models can be turned into an optimization problem, and an objective function ought to be specified. A certain amount of distortion in the outcomes of the calculated I-V data in the quest space is nonlinear and multimodal, comprising several local optimal values, which causes difficulties in constructing the process of estimating one parameter [21-22]. In general, while estimating the parameters of PV models, there are two classes of methods: deterministic method and heuristic method. A variety of model constraints, such as convexity and differentiability, are needed when using deterministic techniques. Furthermore, its initial approach greatly affects the efficiency of the deterministic technology [23]. As a consequence, the conclusions obtained via deterministic methods are unsatisfactory and unpredictable. Heuristic algorithms, on the other hand have certain apparent

benefits, such as enforcing no constraints on problem structure, flexibility in logical and computational terms, and being exemplary for multimodal issues [24-25]. Therefore, in the past few years, several heuristic approaches have been used and developed to determine the parameters of PV models [26-28]. While these heuristic methods have provided quite stable and reliable results relative to deterministic methods, it is still challenging to find the global optimum for most heuristic algorithms. The main reason for this is that calculating PV model parameters is a multimodal problem with many local architecture and optimization problems. Furthermore, many heuristic methods have their own algorithm specific control parameters, and their performance is heavily influenced by the choices of algorithm specific control parameters, in addition to two normal parameters, namely population size and generation number. An incorrect tuning also raises the computational stress, but also succeeds in early termination. Therefore, it is still a challenge to build a successful heuristic algorithm for evaluating the most optimized parameters for PV models. The literature review reveals that primarily researchers take the fundamental model of the solar PV cell into account, i.e. single diode model (SDM) and double diode model (DDM) for calculation of the electric parameter. There is relatively limited research on triple diode model (TDM) owing to the higher degree of difficulty and the rise in the number of unknown parameters [29]. These models, however, justified their accuracy and performance in multi-crystalline solar cells rather than the basic one. In literature, the conventional optimization algorithm was proposed with TDM which really consumes more time in computation. These sophisticated models can be recommended from parameter extraction for a more effective algorithm with more precision and less execution time.

Fuel cells are a part of power generation systems that are becoming increasingly common around the world because they are safe, quiet, and cost-effective. Numerous cells are integrated into the fuel cell system through their lateral systems. A fuel cell transforms chemical energy directly into electrical energy [30]. A fuel cell's energy storage function is not like that of a battery; a fuel cell transfers energy from one state to the other without consuming the materials in the batteries. Provided its high reactivity, availability, and environmental emissions, hydrogen gas is used as an ideal fuel in fuel cells. The problem of green energy is a complex and up-to-date controversy and will overtake fossil fuels soon. Fuel cell devices are increasing and being commercialized rapidly [31-32]. A fuel cell comprised of an anode, cathode, and electrolyte may be recognized as the smallest operational system of the fuel cell. This conversion is simple and yields a high profit [33-

34]. The PEMFC seems to be the most common type of fuel cell. The high-performance PEMFC power generation is having a reliability of about 40 to 50 per cent for various power scales [36-37].

Despite developments in PEM fuel cell modeling, the PEM fuel cell system is a complicated nonlinear, multivariable system that is difficult to describe using traditional techniques [38]. It is vital to identify the parameters of the models using optimization techniques in order to increase the accuracy of the models and make the basic model better represent the PEM fuel cell performance [39]. All optimization approaches used in the literature aim to reduce the relative error between experimental and calculated data by a substantial amount. The traditional approaches for modeling and parameter estimation of PEMFC often fail to yield a good PEMFC model. The underlying meta-heuristic, on the other hand, is frequently caught in the local minimum. As a result, the primary goal is to develop a novel meta-heuristic technique for the PEMFC stack model's optimal parameter collection [40]. The objective is to enhance the optimization algorithm to overcome the process's variety and premature convergence.

Renewable-based hybrid energy systems have gained popularity in recent years as a result of environmental concerns, non-availability of a single source 24 hours a day, continually rising energy demand and fuel prices, and fossil fuel depletion. Solar based generation technologies, in particular, have emerged as viable and ecologically being solutions for supplying power in remote or off-grid places. Due to the unpredictable nature of solar resources, the most significant disadvantage of a standalone solar based energy system is its need on power backup [41]. Fortunately, because to ongoing technological advancements, alternative renewable energy sources such as biomass, biogas, and fuel cells have been incorporated alongside solar power. Biomass appears to be a more realistic alternative among the renewable energy options discussed above, particularly in the case of agriculture-rich countries. Biomass may be used to produce a variety of products, including heat, power, and biofuels [42]. Electricity generated by biomass gasifier’s is becoming more popular, especially in rural regions, thanks to developments in biomass gasification technology. Plants that generate electricity from biomass have a high load factor and are cost-effective. PV, wind, and other renewable energy sources had been linked with biomass power generation. PV-biomass with or without storage, both stand-alone and grid-connected, is viewed as a feasible and cost-effective solution for energy production, particularly in poor nations [43].

Another key goal is to evaluate energy generating technology in conjunction with monetary evaluation to get the best size of the hybrid power system (HPS) including solar, fuel cell, biomass to ensure constant power output while spending the least amount of money. To efficiently and economically utilize sustainable resources, the proper size of source components is critical. Optimal sizing approaches can help to ensure a low initial cost while still getting the most out of HPS components. Optimal sizing of sources is a strategy for specifying the size of an HPS by decreasing system components while maintaining the system's dependability [44]. Over sizing the HPS equipment will increase the system's cost, while under sizing would result in power failure. As a result, enough care should be given to planning a consistent power system at the lowest possible cost. Many academics presented their findings on size strategies used to construct the best HPS setup. Technical and economic goals are the most important factors to consider while developing an HPS.

1.2 Literature Survey

1.2.1 Literature Review on Bio-inspired Algorithms

Mirjalali [45] developed the Ant Lion Optimizer (ALO), a revolutionary nature-inspired algorithm. The ALO algorithm is based on the natural hunting mechanism of ant lions. The random movement of ants, constructing traps, trapping of ants in traps, collecting preys, and re-building traps are the five key processes of hunting prey. In three stages, the proposed methodology is evaluated and the outcome of these stages suggests excellence of proposed algorithm.

Mirjalali [46] introduced the Sine Cosine Approach (SCA), a revolutionary population-based optimization algorithm for tackling optimization issues. Using a mathematical model based on sine and cosine functions, the SCA generates numerous initial random candidate solutions and needs them to fluctuate outwards or towards the ideal answer. The suggested technique is able to successfully explore multiple areas of a search space, avoid local optima, converge towards the global optimum, and utilize potential parts of a search space during optimization, as evidenced by test functions and performance metrics.

Mirjalali [47] presented the Dragonfly Algorithm (DA), a revolutionary swarm intelligence optimization. The DA algorithm takes its inspiration from the static and dynamic swarming behaviours of dragonflies in nature. Modelling the social interaction of dragonflies in navigating, seeking for meals, and avoiding opponents whether swarming dynamically or statistically is used to design two crucial phases of optimization: exploration and exploitation. Several mathematical

test functions and one real-world case study serve as qualitative and quantitative benchmarks for the proposed algorithm.

Mirjalali [48] introduced the Multi-Verse Optimizer (MVO), a revolutionary nature-inspired algorithm. This algorithm's major inspirations are three cosmological concepts: white hole, black hole, and worm hole. Exploration, exploitation, and local search are all performed using mathematical models of these three notions. The proposed algorithm is first used to solve nineteen benchmarked functions. It is then used to resolve complex engineering problems to prove its effectiveness. The proposed algorithm is then compared to four well-known algorithms in order to validate the results. The findings show that the suggested algorithm outperforms the top algorithms in the literature on the majority of test beds.

Wang [49] devised a new type of metaheuristic algorithm named the Moth Search Algorithm (MSA), which is inspired by the photo tax is and Lévy flights of moths. The MSA technique is compared to five other metaheuristic optimization algorithms in a series of experiments on fourteen fundamental benchmarks in order to demonstrate its better performance. The results show that MSA outperforms five other approaches on the majority of test functions and engineering scenarios.

Mirjalali *et al.* [50] developed the Whale Optimization Algorithm (WOA) is a revolutionary nature-inspired meta-heuristic optimization algorithm that replicates the social behaviour of humpback whales. The bubble-net hunting approach inspired the algorithm. Twenty-nine mathematical optimization tasks and six structural design challenges are used to test WOA. The WOA algorithm outperforms both state-of-the-art meta-heuristic algorithms and traditional approaches in terms of optimization outcomes.

Saremi *et al.* [51] devised the Grasshopper Optimization Algorithm (GOA), nature-inspired meta-heuristic optimization algorithm. For tackling optimization issues, the suggested approach mathematically models and simulates the behaviour of grasshopper swarms in nature. To evaluate and validate the GOA algorithm performance subjectively and quantitatively, it is benchmarked on a set of test issues. The findings reveal that the suggested method outperforms other well-known and recently published algorithms in the literature.

Zhao *et al.* [52] introduced a new form of meta-heuristic optimization approach based on atom dynamics i.e. Atom Search Optimization (ASO). It is a population-based iterative heuristic optimization technique that may be used to solve a wide range of optimization issues. ASO

mathematically describes and mimics nature's atomic motion model, in which atoms move with one another via interaction forces. The experimental findings show that ASO can beat other well-known metaheuristic algorithms.

Pierezan *et al.* [53] proposed the Coyote Optimization Algorithm (COA), a population-based metaheuristic for optimization inspired by the canis latrans species. It makes a contribution by developing a novel algorithmic framework and procedures for balancing exploration and exploitation. The COA's performance is investigated using a set of boundary restricted real parameter optimization benchmarks and a comparison with other nature-inspired meta-heuristics. The COA is capable of identifying promising solutions, according to numerical data and non-parametric statistical significance tests, and it beats other meta-heuristics on most functions studied.

Heidari *et al.* [54] devised the Harris Hawks Optimizer (HHO), a revolutionary nature-inspired optimization methodology. The cooperative behaviour and pursuit manner of Harris' hawks in nature, known as surprise pounce, is the fundamental inspiration for HHO. To design an optimization method, this work mathematically duplicates such dynamic patterns and behaviours. On 29 benchmark problems and numerous real-world engineering challenges, the effectiveness of the proposed HHO optimizer is tested by comparing it to other nature-inspired approaches. When compared to well-established metaheuristic approaches, the statistical findings and comparisons reveal that the HHO algorithm delivers highly promising and occasionally competitive outcomes.

Kishke *et al.* [55] introduced the Chimp Optimization Algorithm (ChOA), a unique metaheuristic algorithm inspired by chimps' individual intellect and sexual drive in collective hunting, which differs from that of other social predators. The suggested ChOA algorithm is put to the test in three stages. In terms of convergence speed, the risk of becoming trapped in local minimums, and exploration and exploitation, the findings are compared to many newly suggested meta-heuristic algorithms. Statistical tests were also used to determine the significance of the findings. The ChOA outperforms the other benchmark optimization methods, according to the results.

Abualigah *et al.* [56] proposed the Aquila Optimizer (AO), a unique population-based optimization approach, which is inspired by the Aquila's natural behaviours when collecting prey. As a result, the proposed AO algorithm's optimization procedures are divided into four categories: selecting the search space with a high soar and vertical stoop, exploring within a diverge search space with a contour flight and short glide attack, exploiting within a converge search space with a low flight

and slow descent attack, and swooping with a walk and grab prey. A set of experimental series is done to validate the new optimizer's capacity to discover the best solution for various optimization issues. The superiority of the created AO algorithm is justified in the AO results.

Gandomi *et al*. [13] The Firefly Algorithm (FA), a recently created metaheuristic optimization algorithm, simulates the social behaviour of fireflies by mimicking its flashing and attraction qualities. Authors incorporate chaos into FA in this work in order to boost its global search mobility for robust global optimization. On benchmark issues with various chaotic maps, in-depth analyses are conducted. To modify the enticing movement of the firefly in the algorithm, 12 distinct chaotic maps are used. The results reveal that some chaotic FAs outperform the regular FA significantly.

1.2.2 Literature Review on Parameter Estimation of PV Models

Allam *et al.* [57] proposed the Moth-Flame Optimizer (MFO) as an appropriate optimization algorithm for a three-diode model of multi-crystalline silicon solar cells. The outcomes of the proposed technique were compared to Hybrid Evolutionary and Flower Pollination Algorithms in order to verify its effectiveness. The MFO method has the lowest Mean Bias Error (MBE), Root Mean Square Error (RMSE), Absolute Error (AE), and greatest coefficient of determination, according to the results.

Jaldi *et al.* [58] developed a new parameter estimation strategy based on a combination of various methods like analytical method, evolutionary computation method, and derived approach. To demonstrate the usefulness of the suggested method, several performance indices were estimated for various solar PV panels using proposed and existing methodologies.

Ouada *et al.* [59] described a new way to developing a comprehensive MATLAB/Simulink simulator for solar generators that is based on a three-diode equivalent circuit and takes into account seven parameters while just requiring the characteristics listed on the manufacturer's data sheet. The simulator supports a vast array combination with excellent accuracy for characterizing any solar generator. The simulator's results are validated to those of a recently reported simulator as well as experimental data.

Chenche *et al.* [60] for a single diode model, authors examine four techniques for estimating the physical parameters of photovoltaic devices. To compare the applicability of each approach, two of the most efficient photovoltaic technologies, mono and multi-junction devices, are employed under various temperature and solar radiation conditions. Three of the four parameter estimation

approaches are analytic, while the fourth, the generalized reduced gradient, is based on an algorithm for non-linear problem optimization. The various approaches are summarized, and a comparison study utilizing experimental data from the literature is undertaken, showing the benefits and drawbacks of each method.

Qais *et al.* [61] extracted nine unknown parameters of the three-diode photovoltaic (PV) model using a novel application of the Coyote Optimization Algorithm (COA). The COA-PV model is validated by numerical results obtained under various environmental variables such as temperature and irradiation change.

Wei *et al.* [62] presented a Particle Swarm Optimization (PSO) based parameter extraction technique for a three-diode lumped parameter model of organic solar cells (OSCs). PSO with a parameter extraction technique like this can be a useful tool for extracting the appropriate parameters of an OSC's lumped parameter model.

Qais *et al.* [63] proposed a Sunflower Optimization Algorithm (SFO) which is an accurate and simple approach for modeling PV modules. Two parameters (parallel resistance and photo-generated current) were determined analytically from the nine parameters of a three-diode model, and the remaining parameters were optimized using the described algorithm. The efficiency of the proposed method, as well as its I-V and P-V properties, were verified using data collected at various environmental variations. The margin of error for these results is less than 0.5 percent.

Yousari *et al.* [64] presented a new optimization algorithm called Fractional Chaotic Ensemble Particle Swarm Optimizer (FC-EPSO) for precisely modeling solar PV modules. A new method to meta-heuristic algorithms is provided in FC-EPSO, in which fractional chaos maps are included into the algorithm to improve accuracy and reliability. Several statistical studies and comparisons are carried out for validation reasons using the most recent state-of-the-art algorithms. The proposed algorithm's correctness and consistency are demonstrated by statistical metrics and comparative investigations. The new technique can simulate experimental datasets with less variation, a faster convergence rate, and a shorter execution time.

Chenouard *et al.* [65] proposed an internal branch and bound algorithm for parameter extraction of different types of PV models. The minimization of the Maximal Absolute Error (MAE) is evaluated and compared to the Root Mean Square Error (RMSE). On all three models, the proposed optimization algorithm's performance is studied and tested. It features good convergence and statistical analysis under a variety of operating situations and for a variety of models. The

calculated current-voltage (I-V) and power-voltage (P-V) performance characteristics of the tested cells are quite close to the experimental data and compete with previous efforts in the literature.

Elazab *et al.* [66] presented a new algorithm of the Grasshopper Optimization Algorithm (GOA) for parameter estimation of three diode model. By comparing the proposed PV model's results to the experimental results of these commercial PV modules, the suggested PV model is evaluated. The GOA-based PV model's efficiency is assessed by comparing its numerical findings to those of other optimization method-based PV models.

Qais *et al.* [67] proposed a new method for extracting parameters from the three-diode model that combines computation with the Harris Hawk Optimization (HHO) algorithm. Instead of intensive PV modeling studies, this objective function was displayed based on datasheet values. The proposed method's absolute current inaccuracy was compared to that of existing approaches.

Bisht *et al.* [68] devised a novel technique based on sanitized teaching learning-based optimization (s-TLBO) for the parameters estimation. The suggested technique is used to evaluate PV attributes and relative error for various solar panels, and the results are compared to recent algorithms. The suggested algorithm, it was found, delivers PV characteristics that are quite near to actual features.

Singla *et al.* [69] proposed hybrid technique based on the Grey Wolf Optimizer Cuckoo Search Algorithm (GWOCSA) to extract the parameters of various PV cell models. GWOCSA is used to produce parameter optimization results, which are then compared to those achieved using five different techniques. The superiority of proposed algorithm is established using ranking test, statistical error analysis, and sensitivity temperature variation.

1.2.3 Literature Review on Parameter Estimation of Proton Exchange Membrane fuel cell (PEMFC)

Ali *et al.* [70] explored a novel use of the Grey Wolf Optimizer (GWO), a nature-inspired metaheuristic optimization technique, to estimate PEMFC model parameters. Five commercial PEMFCs were used to test the suggested GWO-based technique. It was also evaluated against other algorithms for additional validation, and very comparable results were found.

Fergany [71] presented the Grasshopper Optimization Algorithm (GOA) for extraction of proton exchange membrane fuel cells unknown parameters. The goal was to minimize the objection function defined as sum of square errors (SSE) between the experimental data and the estimated results. The obtained results highlighted the survivability and effectiveness of the GOA-based procedure in steady-state and dynamic simulations.

Fergany [72] introduced an innovative application of a recently developed heuristic-based technique, the Salp Swarm Optimizer (SSO), to determine the optimal values for unknown PEMFC model parameters. The objective function was represented by the total square deviations (TSD) between both the actual and calculated results. The results showed that the proposed SSO-based strategy was successful in accurately describing the PEMFC model.

Fathy *et al.* [73] described the multi-verse optimizer (MVO), a recently developed optimization tool, is used to determine the best parameters of a proton exchange membrane fuel cell (PEMFC) under specific operating conditions. In the presence of two types of parameter restrictions, four sets of experimental voltage stack are considered; two of them are used for the optimization process, while the other two are used for model validation. The results show that MVO is the best option among the others since it has a lower fitness function and a shorter convergence time.

Gong *et al.* [74] proposed a decomposition method for PEMFC modeling, in which the unknown parameters were split into two categories: nonlinear and linear. The optimization approaches were only used to optimize the nonlinear unknown parameters, which were then used to find the linear parameters. Our approach dramatically lowered computational resources while producing high-quality solutions, according to the results.

Fathy *et al.* [75] provides a novel hybrid optimization approach for predicting the optimal undetermined parameters of the proton exchange membrane fuel cell that combines the vortex search algorithm (VSA) with differential evolution (DE). VSA and DE hybridization is recommended to improve VSA's performance and prevent it from falling into local optima; DE is utilized as a local search strategy to promote VSA's exploitation process. The study is carried out on a variety of PEMFCs modules, and the results are compared to those obtained using other methods. The collected findings validated the proposed method's superiority and dependability.

Priya *et al.* [76] proposed the Flower Pollination Algorithm (FPA), which was used to extract unknown model parameters for fuel cells with various attributes and ratings. To demonstrate convergence speed, computational efficiency, level of complexity, reliance on the initial solution, and ability to locate the global optimum, comprehensive comparisons were made in terms of model parameter values, sum of squared error, individual absolute error, and relative error values.

Duan *et al.* [77] presented a Satin Bowerbird Algorithm (SBA), a new optimizer, which was implemented for the assessment of the PEMFC performance standards. Among the other well-known techniques, the sum of squared error and standard deviation calculated for the specified

optimizer were among the lowest. Furthermore, the provided method was validated using experimental data, which revealed that the experimental and modeling data were in good agreement.

Han *et al.* [78] proposed a novel optimization approach called Chaotic Binary Shark Smell Optimization (CBSSO), to estimate undetermined parameters of the PEMFC model. The CBSSO is a recently presented Meta-Heuristic algorithm that has demonstrated acceptable ability in parameter identification and optimization scenarios. Furthermore, the suggested method's findings are compared to those of alternative methods. Based on the acquired results, this proposed method outperforms other well-known methods in terms of convergence and accuracy.

Xu *et al.* [79] provided a robust two-level eagle strategy based on the JAYA and Nelder-Mead simplex algorithms. The JAYA algorithm was used for coarse global exploration in the proposed strategy, and the Neldere-Mead simplex search algorithm was used for intensive local search. The proposed strategy proved to be a promising approach for estimating PEMFC parameters.

Kler *et al.* [80] introduced the Hybrid Interior Search Algorithm (HISA), which was created utilizing evolutionary mutation and crossover operators to improve the Interior Search Algorithm (ISA) modeling capacity. Based on the results of the extensive simulations given, it was determined that HISA outperforms the basic ISA in terms of fitter solutions, resilience, and convergence rate, and so represents a feasible optimization strategy for fuel cell parameter extraction.

Fergany *et al.* [81] presented a new usage of the Whale Optimization Approach (WOA) to retrieve unidentified PEMFC model parameters. WOA is used directly to minimize the objective function given a set of constraints. The findings based on WOA were compared to other outcomes based on competing optimization approaches.

Miao *et al.* [82] proposed the Hybrid Grey Wolf Optimizer (HGWO), a novel metaheuristic method. The basic Grey Wolf Optimizer was hybridized by incorporating crossover and mutation operators into the optimization process to improve efficiency in evaluating the major parameters of PEMFC. During the search, the adopted operators boost the search potential capability while also avoiding entrapment in the local optima. The suggested Hybrid Grey Wolf Optimizer was utilized to estimate the model of PEMFC, and the results reveal a good efficiency of the proposed Hybrid Grey Wolf Optimizer.

Fathy *et al.* [83] proposed the LSHADE-EpSin optimization algorithm to tackle the PEMFC parameter extraction problem using a unique solution methodology based on employing an ensemble sinusoidal parameter adaption coupled with L-SHADE. The suggested methodology is tested on four commercial PEMFCs, and the results are compared to those achieved using other recently developed optimization algorithms. The results reveal that the technique provided employing the LSHADE-Ep Sin algorithm is effective in calculating the best PEMFC parameters under various operating situations.

Singla *et al.* [84] proposed a novel approach called black widow optimization (BWO) is proposed for evaluating PEMFC undetermined parameters. BWO optimization results are then compared to those achieved using five other algorithms. To prove BWO's superiority, the two data sheets of the PEMFCs are subjected to a comprehensive error analysis. When compared to the results achieved with the rest of the algorithms, the generated recommended algorithm produces better outcomes. After computing the error, a non-parametric test is run, indicating that the BWO is superior to the other algorithms under consideration.

1.2.4 Literature Review on Optimal Sizing of Biomass-Based Systems

Heydari *et al.* [85] suggested a hybrid system in which PV system area and the size of the biomass system's engine–generator was optimized using the Harmony Search (HS) algorithm to reduce the system's total net present cost (TNPC) during its lifespan. The loss of power supply probability (LPSP) concept was used to ensure the intended system's dependability. The collected findings show that a PV/biomass generating system is more promising than a single PV or biomass system in the analyzed location.

Singh *et al.* [86] provided an optimum sizing technique for a PV-biomass hybrid energy system that is both freestanding and grid-connected. The ideal hybrid system design with the lowest levelised cost of energy while lowering the yearly cost of the system was discovered using a recently developed Artificial Bee Colony (ABC) algorithm. The findings of the ABC method and the Hybrid Optimization of Multiple Energy Resources (HOMER) were compared briefly.

Lai *et al.* [87] proposed a deterministic strategy for sizing a solar photovoltaic (PV) and energy storage system (ESS) with anaerobic digestion (AD), biogas power plant (BPP) in Kenya, Africa, to satisfy a proportionate scaled-down demand of the national load. For solar panel size, Particle Swarm Optimization using Interior Point Method was adopted. The goal was to make the system's Levelised Cost of Energy (LCOE) as low as possible.

Singh *et al.* [88] describes a hybrid PV-wind generation system with biomass and storage to meet a small area's electrical load needs. A recently proposed swarm-based artificial bee colony (ABC) technique is used for optimum component sizing. The findings are compared to those produced using software tool (HOMER), and the particle swarm optimization (PSO) method, to demonstrate the strength of the suggested technique. The findings show that the ABC algorithm has an excellent convergence characteristic and the potential to provide high-quality output.

Sawle *et al.* [89] developed an optimum planning strategy for PV, wind, and biomass hybrid energy systems with backup power sources such as a battery bank and a diesel engine. Using GA and PSO, the cost of energy (COE) was reduced as an objective function. To show the hybrid system's techno-economic feasibility, the reliability was calculated using the loss of power supply probability (LPSP).

Sawle *et al.* [90] proposed the optimum hybrid power system. Using GA, PSO, BFPSO, and TLBO optimization approaches, a new multi-objective function with six independent objectives of the hybrid renewable system was proposed to determine the optimal configuration of parameters. TLBO's performance was determined to be superior to those of others.

Eteiba *et al.* [91] proposed a techno-economic assessment of an off-grid PV/Biomass hybrid system. The goal was to use the Harmony Search (HS) algorithm, the Flower Pollination Algorithm (FPA), the Firefly Algorithm (FA), and the Artificial Bee Colony Algorithm (ABC) to find the best solution for the sizing problem. Among the other algorithms, the FA had the shortest execution time and the best performance.

Heng *et al.* [92] employed deterministic constrained optimization and stochastic optimization methodologies to analyze uncertainties in the biomass-integrated micro-grid, which supplied both electricity and heat. Monte Carlo simulation was used to examine uncertainty in weather and economic assumptions, resulting in a probability density function for energy costs.

Gonzalez *et al.* [93] described a multi-objective optimization based on the usage of the genetic algorithm to optimize a grid-connected PV-wind-biomass HRES technique based on economic and environmental factors. The data are presented in a Pareto front, which is a useful tool for decision-makers since it illustrates the trade-off between opposing criteria.

Zheng *et al.* [94] suggested a load shifting algorithm to reduce the operational costs of a biomass combined heat and power based micro-grid system which is based on economic linear

programming with model predictive control. In Davis, California, a case study for a notional utility grid-connected micro-grid application was investigated.

Samy *et al.* [95] proposed a multi-objective particle swarm optimization (MOPSO) approach to address the sizing problem for the proposed biomass and fuel cell micro-grid from an economical point of view, namely the cost of energy (COE). The MOPSO method seeks to minimize the loss of power supply probability (LPSP) to a minimum in order to reduce the COE to lower levels. Statistical analysis has also been completed to investigate the correctness of the introduced technique's results.

Kumar *et al.* [96] presented a mixed integer linear programming (MILP)-based optimization to determine the optimal size of solar, biomass and battery based hybrid renewable energy system. The economic feasibility of various micro-grids has been shown. The optimization model is tested using six distinct real-world case studies from India. The techno-economic analysis was given for each case study's scenario and compared to the existing solution.

1.3 Research Gaps

Based on in-depth literature, identified research gaps are:

1. Metaheuristic algorithms has been deeply study and explored by various researchers. Common variants like binary, chaotic and hybrid of the bio-inspired algorithm can be developed and can be justified of different applications.
2. After intense literature survey it is concluded that very little research is available on three diode modeling of solar PV cells. Researchers mainly focus on single diode and double diode modeling.
3. Different types of hybrid system are presented by researchers. Optimal sizing of hybrid renewable system is also explored. Still, hybrid system which includes fuel cell and biomass had not been reported in the literature.

1.4 Objectives of Research Work

Based on the reviewed literature and identified research gap, the proposed research work caters to address the following objectives:

5.1 Parameter estimation of multi-diode photovoltaic models using metaheuristic algorithms.

5.2 Electrical parameter estimation of proton exchange membrane fuel cells.

5.3 Optimal sizing of different configurations of photovoltaic, fuel cell and biomass based hybrid energy systems.

1.5 Thesis Contribution

The main contributions of the thesis are as follows:

New metaheuristic algorithms are being developed: Chaotic and hybrid topologies are being developed on different metaheuristic algorithms. Novel PSO and SMA based chaotic hybrid optimization algorithm is designed.

Parameter estimation of solar as well as fuel cell: The developed algorithms are used to extract unknown parameters of solar as well as fuel cell. The outcome errors are justified using non parametric test.

Designing of new hybrid energy system: New photovoltaic, fuel cell and biomass based renewable energy system is designed. The proposed design is also patented.

Optimal sizing of new hybrid renewable energy system: Novel PSO and SMA based chaotic hybrid optimization algorithm is implemented on proposed hybrid renewable energy system.

1.6 Thesis Organization

This thesis comprises of further five chapters as follows:

CHAPTER 1 presents the comprehensive overview of renewable energy mostly fuel cell, solar and biomass. The introduction about metaheuristic algorithm along with chaos theory is discussed. This chapter mainly emphases on the review of various problems as well as approaches for parameter estimation of solar energy as well as fuel cell. Along with this, a brief discussion about the biomass based hybrid energy system is also presented. After this research gap along with objectives are also mentioned at end. In next chapter, the parameter extraction of solar PV cell is explored with the meta-heuristic algorithms.

CHAPTER 2 comprises of brief introduction to the solar PV cell, in addition to which this section offers a detailed description of the mathematical modeling of the solar cell. The proposed algorithms, such as the chaotic tunicate algorithm and chaotic chicken swarm algorithm, are presented in depth, as well as the findings. For a better understanding, a summary of the results is offered at the conclusion. In next chapter, the parameter extraction of fuel cell is explored with the meta-heuristic algorithms.

CHAPTER 3 includes the detail explanation about the mathematical modeling of fuel cell in continuation to brief introduction of fuel cell. Proposed algorithms i.e. slime mould algorithm and chaotic mayfly algorithm is explained along with the detail discussion of the results. At the end overview of results are presented for better understanding. In next chapter, the optimal sizing of

the proposed hybrid system is carried out and results are compared between Homer and proposed algorithm.

CHAPTER 4 presents the comprehensive overview about Optimal sizing of different configurations of photovoltaic, fuel cell and biomass based hybrid energy systems. The proposed hybrid energy system is evaluated using homer as proposed hybrid algorithms. The outcome is compared with each other. After detail research on the meta-heuristic algorithms detail conclusion and future scope is also presented.

CHAPTER 5 includes conclusions of the research along with future work is also present

CHAPTER 2 PARAMETER ESTIMATION OF SOLAR PV CELL

2.1 Introduction

Through previous years, renewable energy is regarded as a very efficient alternative to fossil fuel to meet the rising energy demand. Solar energy is the primary energy source among various renewable energy resources due to its sufficient availably across the world [97-98]. Photovoltaic has attained immense attention nowadays [99]. Precise modeling and detailed knowledge are thus required for photovoltaic systems. The output power of the PV system is highly nonlinear i.e., it produces varying power with the change in voltage and current with respect to environment condition [100]. Therefore, the PV system should be operated at MPP for maximum efficiency [101]. PV standard values like open-circuit voltage (V_{open}), short circuit current (I_{short}), saturation current (I_d), photocurrent (I_{pv}), diode ideality factor (n), series resistance (R_{se}), and shunt resistance (R_p) needed to obtain the appropriate parameter values. But sometime PV module manufacture does not provide some vital information such as saturation current (I_d), photocurrent (I_{pv}), diode ideality factor (n), series resistance (R_{se}), and shunt resistance (R_p) [102].

The parameter estimation of renewable energy is referred to as the optimization problem. Various approaches like analytical method, metaheuristic methods, and combination of meta-heuristics and analytical methods are addressed by different researchers to extract the unknown electrical parameter of the PV model [103]. The manufacturer data of the PV module provides the value of the basic components of the equation at standard conditions and operating conditions. In the analytical method, unknown parameters of the PV model are extracted utilizing the I-V curve data and data sheets information [104]. These methods suffer problems in extracting the value of parameters of complex models like three diodes and sometimes even consider the initial values or ignore the resistive effect which results in inaccurate parameters [105]. Due to these various drawbacks, the metaheuristic method was introduced [106]. In the combination of metaheuristic and analytical methods, parameter estimation of the solar cells is carried out, where one or two parameters are extracted using the analytical approach, and the rest are extracted using a metaheuristic approach.

Thus, it is observed from the literature, that researchers mainly considered the basic model of PV i.e. single diode model (SDM) and double diode model (DDM) for electrical parameter estimation. Very little research is being performed on the three diode models (TDM) due to a higher degree of complexity with the increase in the number of unknown parameters [63]. However, these models justified their efficiency and accuracy in multi-crystalline solar cells more than the basic

model. A more efficient algorithm with more accuracy should be proposed from parameter extraction to these advanced models. The metaheuristic optimization technique operates with the principle of optimizing the random particles in the defined space to obtain the fitness function through a repetitive process [107].

2.2 Mathematical Modeling of PV Cells

(a) Single Diode Model (SDM)

Different diode models have been used to explore the characteristics of PV. Most common and popular in the literature is the single-diode model, abbreviated as SDM, and is represented with the help of Fig. 2.1.

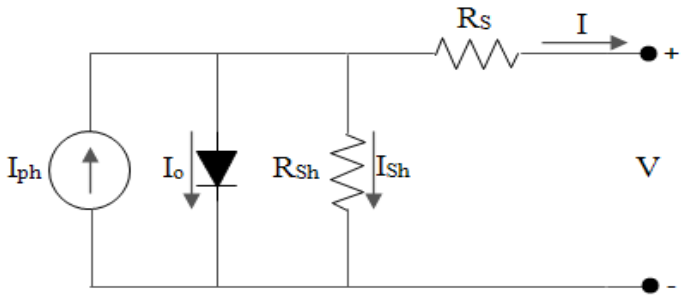

Fig. 2.1 Single-Diode Model of a PV Cell

Mathematically, the load current can be represented in equation 2.1 as

$$I = I_{ph} - I_o\left[exp\left(\frac{q(V+IR_S)}{\alpha KT}\right) - 1\right] - \frac{V+IR_S}{R_{Sh}} \tag{2.1}$$

where

$I_{ph}, I_o, q, k, T, V$and I are photovoltaic current, saturation current, electron charge, Boltzmann's constant, PV cell temperature, output voltage, and output current respectively.

To obtain the five unknown parameters ($I_{ph}, I_o, \alpha, R_S, R_{Sh}$), the open circuit, short circuit, and maximum power point equations are used as given below.

At open circuit $I = 0$ and $V = V_{OC}$; then equation 2.1 becomes;

$$0 = I_{ph} - I_o\left[exp\left(\frac{qV_{OC}}{\alpha KT}\right) - 1\right] - \frac{V_{OC}}{R_{Sh}} \tag{2.2}$$

Therefore;

$$I_{ph} = I_o\left[exp\left(\frac{qV_{OC}}{\alpha KT}\right) - 1\right] + \frac{V_{OC}}{R_{Sh}} \tag{2.3}$$

At the instant of a short circuit $V = 0$ and $I = I_{SC}$; then equation 2.1 becomes;

$$I_{SC} = I_{ph} - I_o \left[exp\left(\frac{qI_{SC}R_S}{\alpha KT}\right) - 1 \right] - \frac{I_{SC}R_S}{R_{Sh}} \tag{2.4}$$

Therefore;

$$I_{ph} = I_{SC} + I_o \left[exp\left(\frac{qI_{SC}R_S}{\alpha KT}\right) - 1 \right] + \frac{I_{SC}R_S}{R_{Sh}} \tag{2.5}$$

(b) Double Diode Model (DDM)

The refined version of SDM is Double Diode Model. In DDM, an additional diode is incorporated in parallel with the basic SDM which represents the space charge recombination. The circuit of DDM is thus shown in Fig. 2.2.

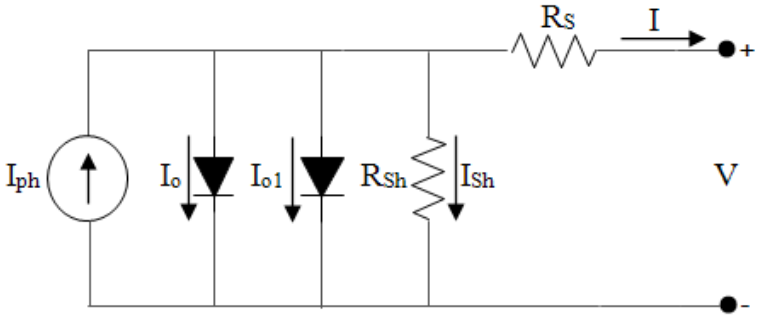

Fig. 2.2 Double-Diode Model of a PV Cell

From Fig. 2.2, the load current equation of DDM is thus given by

$$I = I_{ph} - I_o \left[exp\left(\frac{q(V+IR_S)}{\alpha KT}\right) - 1 \right] - I_{o1} \left[exp\left(\frac{q(V+IR_S)}{\alpha_1 KT}\right) - 1 \right] - \frac{V+IR_S}{R_{sh}} \tag{2.7}$$

where I_{o1}, α_1 is the saturation current and ideality factor for the new diode.

Seven undefined DDM parameters need to be extracted that are $I_{ph}, I_o, \alpha, R_S, R_{Sh}, I_{o1}, \alpha_1$. Thus, we find two extra parameters as compared with SDM. The other equations like a short circuit, open circuit, and maximum power point can be modified accordingly and described below.

During open circuit $I = 0$ and $V = V_{OC}$; then equation 2.7 becomes;

$$0 = I_{ph} - I_o \left[exp\left(\frac{qV_{OC}}{\alpha KT}\right) - 1 \right] - I_{o1} \left[exp\left(\frac{qV_{OC}}{\alpha_1 KT}\right) - 1 \right] - \frac{V_{OC}}{R_{Sh}} \tag{2.8}$$

Therefore;

$$I_{ph} = I_o\left[exp\left(\frac{qV_{OC}}{\alpha KT}\right) - 1\right] + I_{o1}\left[exp\left(\frac{qV_{OC}}{\alpha_1 KT}\right) - 1\right] + \frac{V_{OC}}{R_{Sh}} \quad (2.9)$$

When there is a short circuit $V = 0$ and $I = I_{SC}$; then equation 2.7 becomes;

$$I_{SC} = I_{ph} - I_o\left[exp\left(\frac{qI_{SC}R_S}{\alpha KT}\right) - 1\right] - I_{o1}\left[exp\left(\frac{qI_{SC}R_S}{\alpha_1 KT}\right) - 1\right] - \frac{I_{SC}R_S}{R_{Sh}} \quad (2.10)$$

Therefore;

$$I_{ph} = I_{SC} + I_o\left[exp\left(\frac{qI_{SC}R_S}{\alpha KT}\right) - 1\right] + I_{o1}\left[exp\left(\frac{qI_{SC}R_S}{\alpha_1 KT}\right) - 1\right] + \frac{I_{SC}R_S}{R_{Sh}} \quad (2.11)$$

(c) Three Diode Model (TDM)

In the TDM, three diodes are connected in parallel in the PV cell model as represented in Fig.2.3. The third diode denotes the effect of leakage current and grain boundaries.

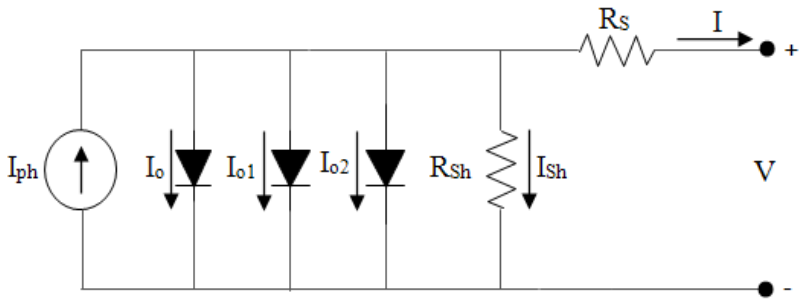

Fig. 2.3 Three-Diode Model of a PV Cell

The current equation of the TDM is thus formulated as

$$I = I_{ph} - I_o\left[exp\left(\frac{q(V+IR_S)}{\alpha KT}\right) - 1\right] - I_{o1}\left[exp\left(\frac{q(V+IR_S)}{\alpha_1 KT}\right) - 1\right] - I_{o2}\left[exp\left(\frac{q(V+IR_S)}{\alpha_2 KT}\right) - 1\right] - \frac{V+IR_S}{R_{sh}} \quad (2.13)$$

The nine unidentified parameters of TDM to be extracted are $I_{ph}, I_o, \alpha, I_{o1}, \alpha_1, I_{o2}, \alpha_2, R_S, R_{Sh}$. Once again, there are two extra parameters as compared to DDM. The open circuit, short circuit and the maximum power conditions are given below.

At open circuit $I = 0$ and $V = V_{OC}$; then equation 2.13 becomes;

$$0 = I_{ph} - I_o\left[exp\left(\frac{qV_{OC}}{\alpha KT}\right) - 1\right] - I_{o1}\left[exp\left(\frac{qV_{OC}}{\alpha_1 KT}\right) - 1\right] - I_{o2}\left[exp\left(\frac{qV_{OC}}{\alpha_2 KT}\right) - 1\right] - \frac{V_{OC}}{R_{Sh}} \quad (2.14)$$

Therefore;

$$I_{ph} = I_o\left[exp\left(\frac{qV_{OC}}{\alpha KT}\right) - 1\right] + I_{o1}\left[exp\left(\frac{qV_{OC}}{\alpha_1 KT}\right) - 1\right] + I_{o2}\left[exp\left(\frac{qV_{OC}}{\alpha_2 KT}\right) - 1\right] + \frac{V_{OC}}{R_{Sh}} \quad (2.15)$$

At the time of a short circuit $V = 0$ and $I = I_{SC}$; then equation 2.13 becomes;

$$I_{SC} = I_{ph} - I_o\left[exp\left(\frac{qI_{SC}R_S}{\alpha KT}\right) - 1\right] - I_{o1}\left[exp\left(\frac{qI_{SC}R_S}{\alpha_1 KT}\right) - 1\right] - I_{o2}\left[exp\left(\frac{qI_{SC}R_S}{\alpha_2 KT}\right) - 1\right] - \frac{I_{SC}R_S}{R_{Sh}} \quad (2.16)$$

Therefore;

$$I_{ph} = I_{SC} + I_o\left[exp\left(\frac{qI_{SC}R_S}{\alpha KT}\right) - 1\right] + I_{o1}\left[exp\left(\frac{qI_{SC}R_S}{\alpha_1 KT}\right) - 1\right] + I_{o2}\left[exp\left(\frac{qI_{SC}R_S}{\alpha_2 KT}\right) - 1\right] + \frac{I_{SC}R_S}{R_{Sh}} \quad (2.17)$$

2.3 Proposed Algorithms and Outcomes

2.3.1 Tunicate Swarm Algorithm (TSA)

Tunicate has the potential to locate a food supply in the sea. However, in the provided search space, there is no information about the food source. In this article, to find the best food supply the tunicate behaviours are used. Swarm intelligence and jet propulsion are the two forms of behaviours [108-109]. A tunicate must fulfill three requirements in order to mathematically model jet propulsion behaviour i.e., to prevent disputes between search agents, step towards the best search agent's location, and stay close to the best search agent. On the other hand, the behaviour of swarm is it will keep other search agents up to date on the best optimal solution. The foregoing paragraphs cover the statistical modeling of these actions.

- **Mathematical Modeling**

(a) To Prevent Disputes Between Search Agents

Vector $\vec{B}$ is used to calculate new search agent locations as shown in equation (2.18-2.20) to prevent collisions with other search agents (i.e., other tunicates).

$$\vec{B} = \frac{\vec{H}}{\vec{N}} \quad (2.18)$$

$$\vec{H} = d_2 + d_3 - \vec{J} \quad (2.19)$$

$$\vec{J} = 2.d_1 \tag{2.20}$$

Where, the force of gravity is represented by $\vec{H}$, the water flow advection in deep ocean is represented by $\vec{J}$, the random variable number which lies between the range of [0, 1] are represented by d_1, d_2, d_3. The social forces between the search agents is represented by $\vec{N}$. The vector $\vec{N}$ is calculated as shown in equation 2.21[108-109].

$$\vec{N} = [q_{min} + (d_1.q_{max} - q_{min})] \tag{2.21}$$

Where, the initial speed is represented by q_{min}, and subordinate speed is represented by q_{max}, to make the social interaction. The value of initial speed is 1 and subordinate speed is 4 is considered.

(b) Step Towards the Best Search Agent's Location

Since preventing neighbour confrontation, the search agents continue in the path of the better neighbour as shown in equation 2.22.

$$\overrightarrow{XE} = \left[\overrightarrow{JT} - rand.\overrightarrow{X_X}(z)\right] \tag{2.22}$$

Where, the distance between the food source and search agent is represented as $\overrightarrow{XE}$, the value as random number lies between the range of [0, 1], the position of food source is represented as $\overrightarrow{JT}$, the tunicate position is represented as $\overrightarrow{X_X}$, and the current iteration is represented by z.

(c) Stay Close to The Best Search Agent

It is possible for the search agent to retain its position as the best search agent (i.e., food source) as shown in equation 2.23.

$$\overrightarrow{X_X(z)} = \begin{cases} \overrightarrow{JT} + \vec{B}.\overrightarrow{XE}, & if\ rand\ \geq 0.5 \\ \overrightarrow{JT} - \vec{B}.\overrightarrow{XE}, & if\ rand\ < 0.5 \end{cases} \tag{2.23}$$

(d) Behaviour of Swarm

To mathematically replicate tunicate's swarm behaviour, the first two optimal solutions are saved, and other search agents' positions are modified based on the best search agents' positions. To describe tunicate swarm behaviour, the following formula has been formulated as shown in equation 2.24.

$$\overrightarrow{X_X(z+1)} = \frac{\overrightarrow{X_X(z)} + \overrightarrow{X_X(z+1)}}{Z + d_1} \tag{2.24}$$

The stopping criteria defines that if obtained optimal value for a particular iteration is better than the previous stored optimal value than the obtained value will be consider the best value. The pseudo code of TSA is represented in Fig. 2.4. The flowchart of TSA is represented in Fig. 2.5.

Input: Tunicate population $\overrightarrow{Xx}$
Output: Optimal fitness value $\overrightarrow{JT}$
procedure TSA
Initialize the parameters $\vec{B}$, $\vec{H}$, $\vec{J}$, $\vec{N}$ and $\text{Max}_{\text{iteraticons}}$
Define q_{min} parameters
Define q_{max} parameters
Define *Swarm* parameters
while ($z < \text{Max}_{\text{iteraticons}}$) **do**
for i ←1 to 2 **do**
$\overrightarrow{JT}$ ←**ComputeFitness** ($\vec{P}p$)
$d_1, d_2, d_3, r_{and} \leftarrow Rand()$
$\vec{N} \leftarrow [\, q_{min} + (d_1 * q_{max} - q_{min})]$
$\vec{J} \leftarrow 2 * d_1$
$\vec{H} \leftarrow d_2 + d_3 - \vec{J}$
$\vec{B} \leftarrow \vec{H} / \vec{N}$
$\overrightarrow{XY} \leftarrow \text{abs}(\overrightarrow{JT} - r_{and} * \overrightarrow{Xx}(z))$
if($r_{and} \leq 0.5$) **then**
$Swarm \leftarrow Swarm + \overrightarrow{JT} + \vec{B} * \overrightarrow{XE}$
else
$Swarm \leftarrow Swarm + \overrightarrow{JT} - \vec{B} * \overrightarrow{XE}$
end if
end for
$\overrightarrow{Xx}(z) \leftarrow Swarm/(2+d_1)$
$Swarm \leftarrow 0$
Update the parameters $\vec{B}$, $\vec{H}$, $\vec{J}$and $\vec{N}$
$z \leftarrow z+1$
end while
return $\overrightarrow{JT}$
end procedure
procedure COMPUTEFITNESS ($\overrightarrow{Xx}$)
for i ←1 to n **do**
$\mathbf{FIT}_P$ [i] ← FitnessFunction ($\overrightarrow{Xx}(\vec{i},:)$)
end for
$\mathbf{FIT}_{Pbest}$ ← **BEST**(FIT_P [i])
return $\mathbf{FIT}_{Pbest}$
end procedure
procedure BEST(FIT_P)
Best ← FIT_P[0]
for i ←1 to n **do**
if (FIT_P [i]<*Best*) **then**
Best ← FIT_P[i]
end if
end for
return *Best*
end procedure

Fig. 2.4 Pseudo code of TSA

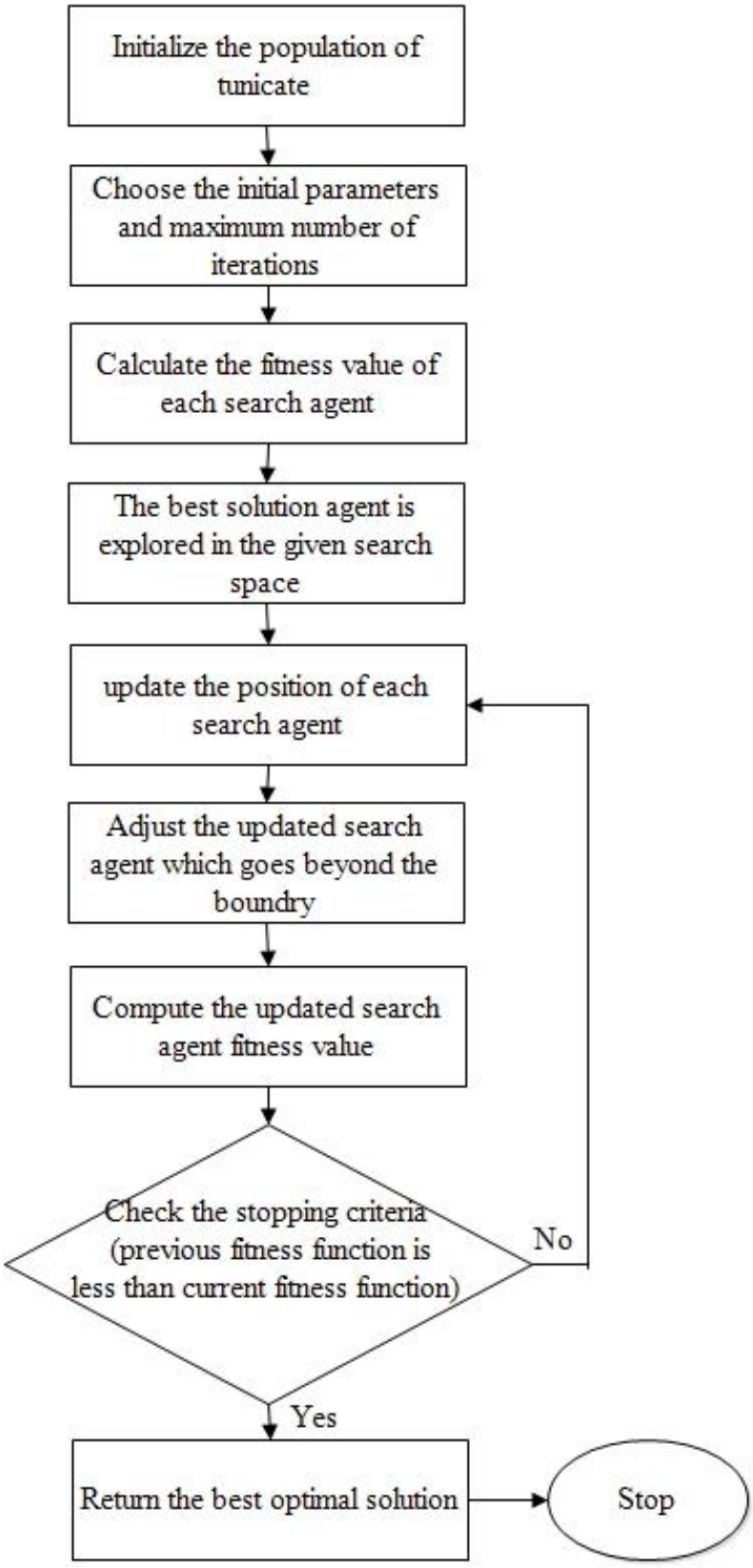

Fig. 2.5 Flow Chart of TSA

- **New Chaotic Tunicate Swarm Algorithm (CTSA) Technique**

Chaotic maps have numerous remunerations in metaheuristic algorithm and it can be observed from previous work [110]. The benefits of chaotic maps are explored in our proposed (TSA) algorithm. The problem of the TSA to get stuck in the local minimum which can be eliminated with the help chaotic maps to assist the TSA algorithm to explore the search space in a better way. The parameter 'z' (current iteration) is used in equation 2.24 of the classical TSA method, is varied chaotically using the five maps to yield better results as compared to the original approach. Pseudo code of CTSA is represented in Fig. 2.6. The flowchart of chaotic tunicate swarm algorithm is represented in Fig. 2.7

Input: Tunicate population $\overrightarrow{Xx}$
Output: Optimal fitness value $\overrightarrow{JT}$
procedure TSA
Initialize the parameters $\vec{B}$, $\vec{H}$, $\vec{J}$, $\vec{N}$ and $\text{Max}_{\text{iterations}}$
Define q_{min} parameters
Define q_{max} parameters using chaotic maps
Define *Swarm* parameters
while (z< $\text{Max}_{\text{iterations}}$) **do**
for i ←1 to 2 **do**
$\overrightarrow{JT}$ ←**ComputeFitness** ($\vec{P}p$)
d_1, d_2, d_3, r_{and} ← *Rand()*
$\vec{N}$ ← [q_{min} + (d_1 * q_{max} - q_{min})]
$\vec{J}$ ←2* d_1
$\vec{H}$ ← d_2+d_3- $\vec{J}$
$\vec{B}$ ← $\vec{H}$ /$\vec{N}$
$\overrightarrow{XY}$ ←abs($\overrightarrow{JT}$ - r_{and} *$\overrightarrow{Xx}$(z))
if($r_{and} \leq 0.5$) **then**
Swarm ← *Swarm* +$\overrightarrow{JT}$ +$\vec{B}$ *$\overrightarrow{XE}$
else
Swarm ← *Swarm* +$\overrightarrow{JT}$-$\vec{B}$ *$\overrightarrow{XE}$
end if
end for
$\overrightarrow{Xx}$ (z)← *Swarm*/(2+d_1)
Swarm ← 0
Update the parameters $\vec{B}$, $\vec{H}$, $\vec{J}$and $\vec{N}$
z ← z+1
end while
return $\overrightarrow{JT}$
end procedure
procedure COMPUTEFITNESS ($\overrightarrow{Xx}$)
for i ←1 to n **do**
FIT$_P$ [i] ← FitnessFunction ($\overrightarrow{Xx}(\vec{i},:)$)
end for
FIT$_{Pbest}$ ← **BEST**(*FIT*$_P$ [i])
return **FIT**$_{Pbest}$
end procedure
procedure BEST(*FIT*$_P$)
Best ← *FIT*$_P$[0]
for i ←1 to n **do**
if (FIT$_P$ [i]<*Best*) **then**
Best ← *FIT*$_P$[i]
end if
end for
return *Best*
end procedure

Fig. 2.6 Pseudo code of CTSA

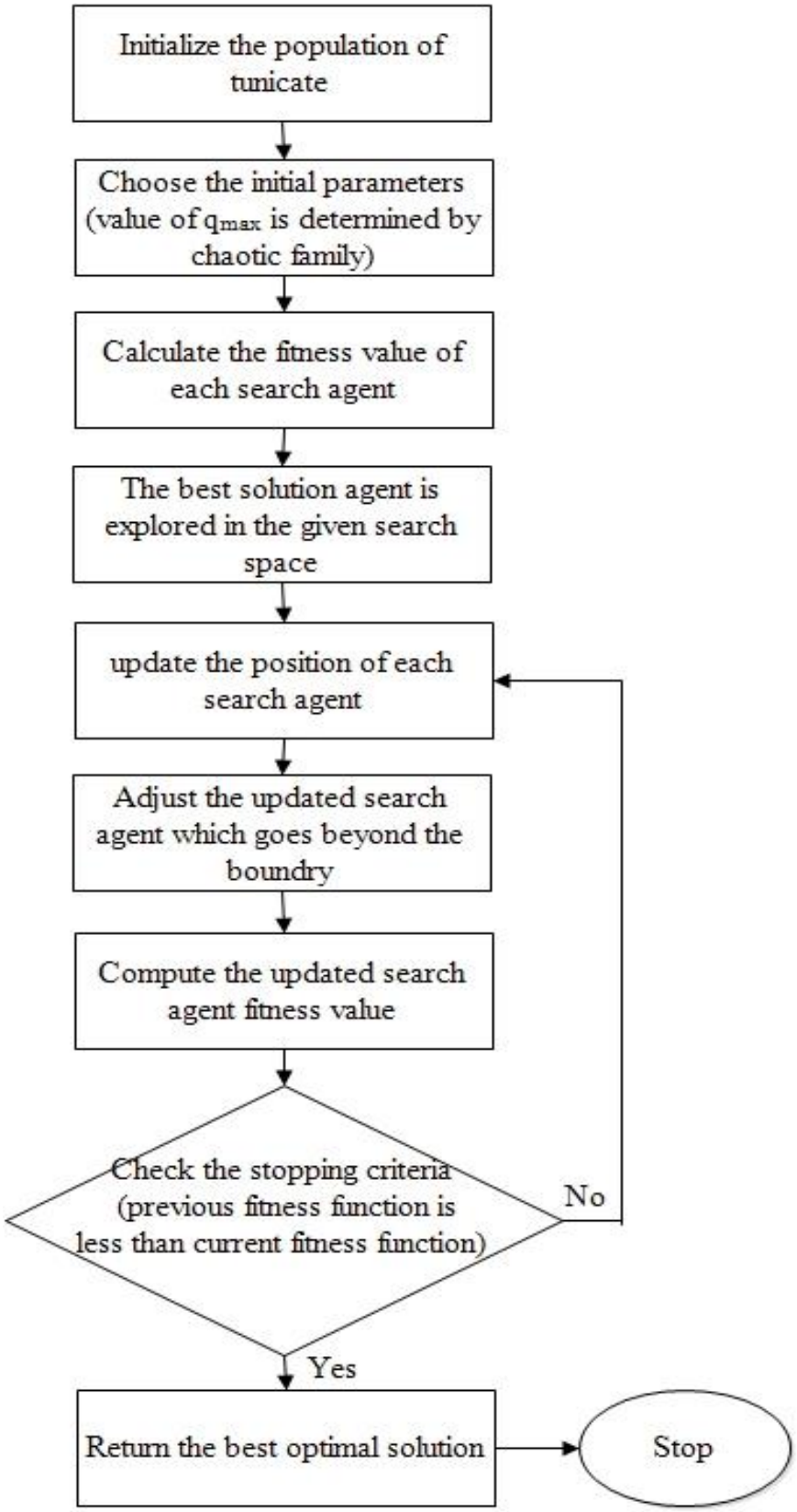

Fig. 2.7 Flow Chart of CTSA

2.3.1.1 Outcomes of TSA

The 57 mm diameter commercial silicon R.T.C France solar cell under 1000w/m^2 at 33^{o}C [111] is derived from the I-V data of the double diode model and triple diode model is used for the solar PV parameter extraction. Solar PV model parameter extraction issues are solved by CTSA in this section to further analyze the performance of CTSA. The referred algorithms of each chaotic map and their detailed equation of each chaotic map is described in Table 2.1. The search range of the parameter for the double PV models is represented in Table 2.2. From the Table 2.2, I_{pv} is the photovoltaic current, $\alpha_1, \alpha_2, \alpha_3$ is the output current, the series and shunt resistance is denoted as R_S and R_{Sh}, and diode saturation current is denoted as I_{o1}, I_{o2}, I_{o3}. The data sheet of the double diode model and triple diode solar PV model for the parameter estimation is represented in Table 2.3. Some well-known meta-heuristics algorithms are compared, in order to check the CTSA performance. All the algorithms are iterated for the 1000 iterations along with the 50 search agents. Two cases of PV cell model are discussed below.

Table 2.1 List of Chaotic Maps

Map Name	Function	Range	Referred Algorithm
Chebyshev map	$x_{k+1} = \cos(k \cos^{-1}(x_k))$	(-1,1)	CTSA1
Circle map	$x_{k+1} = x_k + \mathrm{b} - (\mathrm{a} - 2\pi) \sin(2\pi x_k) mod(1)$	(0,1)	CTSA2
Mouse map	$x_{k+1} = \begin{cases} 0 & x_k = 0 \\ 1/x_k mod(1) & otherwise \end{cases}$	(0,1)	CTSA3
Iterative map	$x_{k+1} = \sin(a\pi/x_k)$	(-1,1)	CTSA4
Logistic map	$x_{k+1} = a x_k (1 - x_k)$	(0,1)	CTSA5

Table 2.2 Parameter Search Range for the PV Models

Parameter	R.T.C. France	
	Lower bound	Upper bound
I_{pv} (A)	0	1
I_{o1}, I_{o2}, I_{o3} (uA)	0	1
R_S (ohm)	0	0.5
R_{Sh} (ohm)	0	100
$\alpha_1, \alpha_2, \alpha_3$	1	2

Table 2.3 Data Sheet for the Parameter Estimation

Company	R.T.C France
Model	-
Vm [V]	0.4507
Im [A]	0.6894
Voc [V]	0.5728
Isc [A]	0.7603
Ns [Cells]	1
T [oC]	33

Case 1: Double Diode Model

Table 2.4 represents the best extracted parameters and the corresponding RMSE values which are calculated at standard temperature condition (STC) for the double diode model. Table 2.4 shows the seven unknown parameters as well as the root mean square error and computation time per second. From the computation time it is clear that the variants of the chaotic family are better than the rest of the compared algorithms. The best RMSE of the chaotic maps of CTSA then the rest of the compared algorithms is concluded in Table 2.5. From above all the results, it is concluded that the variants of chaotic family have better accuracy and performance than the rest of the algorithms compared.

Table 2.4 Parameter Estimation of Double Diode Model at STC

Parameters → / **Algorithms ↓**	$\mathbf{I_{pv}}$	$\boldsymbol{\alpha_1}$	$\boldsymbol{\alpha_2}$	$\mathbf{R_S}$	$\mathbf{R_{Sh}}$	$\mathbf{I_{o1}}$	$\mathbf{I_{o2}}$	**Computation time/second**
CTSA1	0.7797	1.2471	1.2339	0.0499	11.248	0.4	0.6395	1.1885
CTSA2	0.6979	1.0703	1.6214	0.1926	10.379	0.3261	0.4748	1.2502
CTSA3	0.6172	1.4635	1.5856	0.1774	43.7972	0.3114	0.1321	1.2962
CTSA4	0.7532	1.3616	1.3867	0.1287	12.2601	0.3651	0.2651	1.1204
CTSA5	0.7813	1.4324	1.4801	0.0236	41.4550	0.3539	0.5	1.2214
PSO	0.7713	1.2699	1.5824	0.2593	31.1945	0.4607	0.4288	17.4532
TSA	0.7633	1.0361	1.4404	0.1880	56.1147	0.4903	0.1277	2.5278
HHO	0.7772	1.3443	1.4246	0.0205	14.7727	0.7541	0.3207	10.8942
ALO	0.7503	1.3017	1.2450	0.4034	72.3518	0.1403	0.1233	15.0214
ASO	0.7328	1.3387	1.3247	0.3662	1.2242	0.2216	0.2045	9.5214

Table 2.5 Statistical Results of RMSE for Double Diode Model at STC

Statistical Results → Algorithms ↓	Minimum	Average	Maximum	S.D
CTSA1	1.2156E-08	3.3564E-08	9.4505E-08	3.4771E-08
CTSA2	2.3175E-07	4.0794E-07	8.4942E-07	2.6065E-07
CTSA3	1.6768E-07	4.9110E-07	8.9923E-07	3.5296E-07
CTSA4	1.0239E-08	2.1185E-08	9.6017E-08	3.9865E-08
CTSA5	1.7232E-07	3.1145E-07	9.7127E-07	3.5340E-07
PSO	0.1181	0.3120	0.1998	0.3849
TSA	1.1145E-04	2.3866E-06	8.6502E-04	3.3593E-04
HHO	0.0017	0.0030	0.0075	0.0025
ALO	0.0120	0.0289	0.0873	0.0321
ASO	0.0011	0.0026	0.0098	0.0038

Fig. 2.8 shows the best convergence curve of R.T.C. France model attained by PSO, HHO, TSA, ALO, ASO, CTSA1, CTSA2, CTSA3, CTSA4, and CTSA5. The efficiency of CTSA is obtained from the convergence graph. It also shows that variant of chaotic family has a higher pace of convergence than the rest of the other compared algorithms. After extraction of the solar PV model parameters, the power and output current corresponding to the measured voltage can be conveniently estimated. For the further demonstration of CTSA's accuracy, Table 2.6, Table 2.7, Table 2.8 and Table 2.9 showed the measured output, current and individual absolute error (IAE) values.

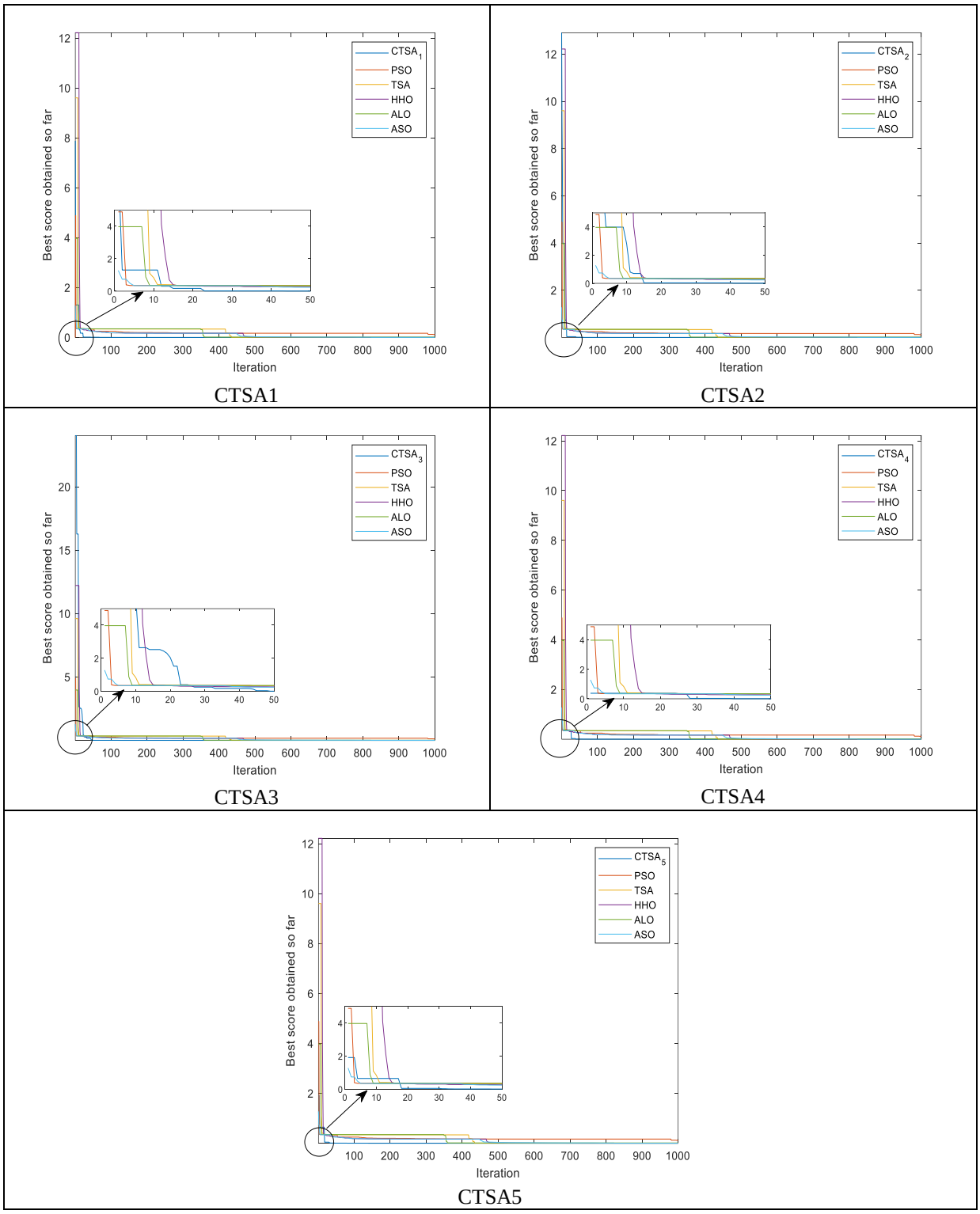

Fig. 2.8 Best Convergences Curve of Double Diode Model at STC for Each Variant of CTSA with Other Compared Algorithm

Table 2.6 Calculated Current for Double Diode Model for Each Variant of CTSA

V_L Measured Voltage (V)	I_L Measured Current (A)	CTSA1		CTSA2		CTSA3		CTSA4		CTSA5	
		I_L Calculated Current (A)	IAE	I_L Calculated Current (A)	IAE	I_L Calculated Current (A)	IAE	I_L Calculated Current (A)	IAE	I_L Calculated Current (A)	IAE
-0.2057	**0.7640**	0.7663	0.0030	0.7651	0.0014	0.7610	0.0039	0.7626	0.0018	0.7631	0.0012
-0.1291	**0.7620**	0.7638	0.0024	0.7637	0.0022	0.7696	0.0098	0.7623	0.0004	0.7620	0.0000
-0.0588	**0.7605**	0.7625	0.0026	0.7625	0.0026	0.7682	0.0101	0.7610	0.0007	0.7610	0.0006
0.0057	**0.7605**	0.7622	0.0022	0.7614	0.0011	0.7670	0.0085	0.7604	0.0001	0.7601	0.0006
0.0646	**0.7600**	0.7611	0.0014	0.7603	0.0004	0.7659	0.0077	0.7611	0.0014	0.7592	0.0010
0.1185	**0.7590**	0.7600	0.0013	0.7594	0.0005	0.7549	0.0054	0.7589	0.0001	0.7584	0.0007
0.1678	**0.7570**	0.7585	0.0020	0.7585	0.0019	0.7539	0.0041	0.757	0.0000	0.7577	0.0009
0.2132	**0.7570**	0.7580	0.0013	0.7576	0.0008	0.7530	0.0054	0.7565	0.0007	0.7569	0.0001
0.2545	**0.7555**	0.7568	0.0017	0.7566	0.0015	0.7519	0.0048	0.7579	0.0032	0.7560	0.0007
0.2924	**0.7540**	0.7551	0.0015	0.7554	0.0019	0.7523	0.0022	0.7541	0.0001	0.7546	0.0008
0.3269	**0.7505**	0.7524	0.0025	0.7535	0.0040	0.7509	0.0005	0.7515	0.0013	0.7523	0.0024
0.3585	**0.7465**	0.7476	0.0015	0.7401	0.0086	0.7436	0.0039	0.7475	0.0013	0.7481	0.0021
0.3873	**0.7385**	0.7393	0.0011	0.7342	0.0059	0.7358	0.0037	0.7402	0.0023	0.7405	0.0027
0.4137	**0.7280**	0.7251	0.0040	0.7237	0.0060	0.7222	0.0080	0.7275	0.0007	0.7273	0.0009
04373	**0.7065**	0.7028	0.0052	0.7066	0.0002	0.7006	0.0084	0.7072	0.0010	0.7006	0.0085
0.4590	**0.6755**	0.6691	0.0095	0.6797	0.0061	0.6673	0.0123	0.6757	0.0003	0.6589	0.0251
0.4784	**0.6320**	0.6328	0.0012	0.6309	0.0018	0.6311	0.0015	0.6314	0.0010	0.6315	0.0008
0.4960	**0.5730**	0.5727	0.0005	0.5777	0.0081	0.5730	0.0000	0.5730	0.0000	0.5627	0.0184
0.5119	**0.4990**	0.4970	0.0040	0.4993	0.0006	0.4954	0.0074	0.4993	0.0006	0.4949	0.0083
0.5365	**0.4130**	0.4186	0.133	0.4132	0.0005	0.4166	0.0087	0.4160	0.0072	0.4107	0.0057

0.5398	**0.3165**	0.3106	0.0191	0.3123	0.0135	0.3141	0.0076	0.3205	0.0125	0.3128	0.0119
0.5521	**0.2120**	0.2108	0.0056	0.2139	0.0088	0.2104	0.0075	0.2161	0.0190	0.2197	0.0352
0.5633	**0.1035**	0.1024	0.0104	0.1020	0.0150	0.1044	0.0089	0.1037	0.0019	0.1017	0.0177
0.5736	**-0.0100**	-0.0135	0.2618	-0.0106	0.0525	-0.0114	0.1253	-0.0124	0.1935	-0.0132	0.2403
0.5833	**-0.1230**	-0.1219	0.0093	-0.1232	0.0016	-0.1213	0.0138	-0.1243	0.0105	-0.1218	0.0100
0.5900	**-0.2100**	-0.2085	0.0071	-0.2103	0.0014	-0.2101	0.0005	-0.2099	0.0005	-0.2098	0.0011
Sum of IAE			**0.3756**		**0.1490**		**0.2801**		**0.2621**		**0.3977**

Table 2.7 Calculated Current of Double Diode Model for Compared Algorithms

V_L Measured Voltage (V)	**I_L Measured Current (A)**	**TSA**		**ASO**		**HHO**		**ALO**		**PSO**	
		I_L Calculated Current (A)	**IAE**	**I_L Calculated Current (A)**	**IAE**	**I_L Calculated Current (A)**	**IAE**	**I_L Calculated Current (A)**	**IAE**	**I_L Calculated Current (A)**	**IAE**
-0.2057	**0.7640**	0.7525	0.0152	0.7610	0.0039	0.7793	0.0197	0.7663	0.0030	0.7550	0.0118
-0.1291	**0.7620**	0.7499	0.0160	0.7595	0.0032	0.7776	0.0201	0.7648	0.0036	0.7537	0.0109
-0.0588	**0.7605**	0.7475	0.0173	0.7582	0.0029	0.7761	0.0201	0.7634	0.0038	0.7524	0.0106
0.0057	**0.7605**	0.7453	0.0203	0.7570	0.0045	0.7746	0.0182	0.7622	0.0022	0.7513	0.0121
0.0646	**0.7600**	0.7433	0.0224	0.7559	0.0054	0.7733	0.0172	0.7610	0.0013	0.7503	0.0129
0.1185	**0.7590**	0.7415	0.0235	0.7548	0.0054	0.7421	0.0227	0.7600	0.0013	0.7493	0.0128
0.1678	**0.7570**	0.7397	0.0232	0.7539	0.0040	0.7710	0.0181	0.7589	0.0026	0.7484	0.0113
0.2132	**0.7570**	0.7381	0.0255	0.7529	0.0053	0.7698	0.0167	0.7579	0.0012	0.7475	0.0125
0.2545	**0.7555**	0.7364	0.0258	0.7518	0.0048	0.7686	0.0170	0.7567	0.0016	0.7466	0.0118
0.2924	**0.7540**	0.7344	0.0265	0.7503	0.0048	0.7269	0.0372	0.7551	0.0014	0.7454	0.0115
0.3269	**0.7505**	0.7317	0.0256	0.7479	0.0034	0.7643	0.0180	0.7524	0.0025	0.7434	0.0094
0.3585	**0.7465**	0.7274	0.0262	0.7435	0.0039	0.7598	0.0175	0.7476	0.0015	0.7401	0.0085

0.3873	**0.7385**	0.7201	0.0254	0.7358	0.0036	0.7120	0.0371	0.7393	0.0011	0.7341	0.0058
0.4137	**0.7280**	0.7078	0.0284	0.7222	0.0079	0.7388	0.0146	0.7250	0.0040	0.7236	0.0059
04373	**0.7065**	0.6885	0.0260	0.7006	0.0084	0.7181	0.0162	0.7028	0.0052	0.7066	0.0001
0.4590	**0.6755**	0.6589	0.0251	0.6672	0.0123	0.6466	0.0446	0.6691	0.0095	0.6796	0.0061
0.4784	**0.6320**	0.6175	0.0234	0.6207	0.0180	0.6528	0.0319	0.6227	0.0148	0.6408	0.0138
0.4960	**0.5730**	0.5626	0.0183	0.5597	0.0236	0.5854	0.0212	0.5627	0.0182	0.5876	0.0250
0.5119	**0.4990**	0.4948	0.0082	0.4853	0.0281	0.5149	0.0308	0.4900	0.0183	0.5193	0.0390
0.5365	**0.4130**	0.3229	0.2787	0.2966	0.3923	0.3381	0.2214	0.3085	0.3384	0.3432	0.2033
0.5398	**0.3165**	0.3217	0.0164	0.3001	0.0559	0.3357	0.0572	0.3105	0.0191	0.3322	0.0474
0.5521	**0.2120**	0.2197	0.0352	0.1941	0.0919	0.2303	0.0798	0.2082	0.0178	0.2138	0.0088
0.5633	**0.1035**	0.1117	0.0734	0.0844	0.2258	0.1088	0.0493	0.1024	0.0103	0.0819	0.2626
0.5736	**-0.0100**	-0.0063	0.5832	-0.0254	0.6068	-0.0103	0.0313	-0.0037	1.6634	-0.0021	0.6392
0.5833	**-0.1230**	-0.1178	0.0437	-0.1403	0.1234	-0.1881	0.3463	-0.1148	0.0708	-0.2215	0.4448
0.5900	**-0.2100**	-0.2037	0.0358	-0.2212	0.0509	-0.1077	0.9495	-0.1935	0.0852	-0.3444	0.3903
Sum of IAE			**1.4846**		**1.7002**		**2.1748**		**2.3032**		**5.2296**

Table 2.8 Calculated Power of Double Diode Model for Each Variant of CTSA

P_L Measured Power (W)	**CTSA1**		**CTSA2**		**CTSA3**		**CTSA4**		**CTSA5**	
	P_L Calculated Power (W)	**IAE**	**P_L Calculated Power (W)**	**IAE**	**P_L Calculated Power (W)**	**IAE**	**P_L Calculated Power (W)**	**IAE**	**P_L Calculated Power (W)**	**IAE**
-0.1572	-0.1576	0.0030	-0.1574	0.0014	-0.1565	0.0039	-0.1569	0.0018	-0.1570	0.0012
-0.0984	-0.0986	0.0024	-0.0986	0.0022	-0.0994	0.0098	-0.0984	0.0004	-0.0984	0.0000
-0.0447	-0.0448	0.0026	-0.0448	0.0026	0.0452	0.0101	-0.0447	0.0007	-0.0447	0.0006
0.0043	0.0043	0.0022	0.0043	0.0011	0.0044	0.0085	0.0043	0.0001	0.0043	0.0006

0.0491	0.0492	0.0014	0.0491	0.0004	0.0495	0.0077	0.0492	0.0014	0.0490	0.0010
0.0899	0.0901	0.0013	0.0900	0.0005	0.0895	0.0054	0.0899	0.0001	0.0899	0.0007
0.1270	0.1273	0.0020	0.1273	0.0019	0.1265	0.0041	0.1270	0.0000	0.1271	0.0009
0.1614	0.1616	0.0013	0.1615	0.0008	0.1605	0.0054	0.1613	0.0007	0.1614	0.0001
0.1923	0.1926	0.0017	0.1926	0.0015	0.1913	0.0048	0.1929	0.0032	0.1924	0.0007
0.2205	0.2208	0.0015	0.2209	0.0019	0.2200	0.0022	0.2205	0.0001	0.2207	0.0008
0.2453	0.2460	0.0025	0.2463	0.0040	0.2455	0.0005	0.2457	0.0013	0.2459	0.0024
0.2676	0.2680	0.0015	0.2653	0.0086	0.2666	0.0039	0.2680	0.0013	0.2682	0.0021
0.2860	0.2863	0.0011	0.2843	0.0059	0.2850	0.0037	0.2867	0.0023	0.2868	0.0027
0.3012	0.3000	0.0040	0.2994	0.0060	0.2988	0.0080	0.3101	0.0007	0.3009	0.0009
0.3090	0.3073	0.0052	0.3090	0.0002	0.3064	0.0084	0.3093	0.0010	0.3064	0.0085
0.3101	0.3071	0.0095	0.3120	0.0061	0.3063	0.0123	0.3101	0.0003	0.3025	0.0251
0.3023	0.3027	0.0012	0.3018	0.0018	0.3019	0.0015	0.3021	0.0010	0.3021	0.0008
0.2842	0.2841	0.0005	0.2865	0.0081	0.2842	0.0000	0.2842	0.0000	0.2791	0.0184
0.2554	0.2544	0.0040	0.2556	0.0006	0.2536	0.0074	0.2556	0.0006	0.2533	0.0083
0.2174	0.2246	0.133	0.2217	0.0005	0.2235	0.0087	0.2232	0.0072	0.2203	0.0057
0.1708	0.1676	0.0191	0.1686	0.0135	0.1696	0.0076	0.1730	0.0125	0.1688	0.0119
0.1170	0.1164	0.0056	0.1181	0.0088	0.1162	0.0075	0.1193	0.0190	0.1213	0.0352
0.0583	0.0577	0.0104	0.0574	0.0150	0.0588	0.0089	0.0584	0.0019	0.0573	0.0177
-0.0057	-0.0078	0.2618	-0.0061	0.0525	-0.0066	0.1253	-0.0071	0.1935	-0.0075	0.2403
-0.0717	-0.0711	0.0093	-0.0719	0.0016	-0.0708	0.0138	-0.0725	0.0105	-0.0710	0.0100
-0.1239	-0.1230	0.0071	-0.1240	0.0014	-0.1240	0.0005	-0.1238	0.0005	-0.1238	0.0011
Sum of IAE		**0.3756**		**0.1490**		**0.2801**		**0.2621**		**0.3977**

Table 2.9 Calculated Power of Double Diode Model for Compared Algorithms

P_L Measured Power (W)	TSA		ASO		HHO		ALO		PSO	
	P_L Calculated Power (W)	IAE	P_L Calculated Power (W)	IAE	P_L Calculated Power (W)	IAE	P_L Calculated Power (W)	IAE	P_L Calculated Power (W)	IAE
-0.1572	-0.1548	0.0152	-0.1565	0.0039	-0.1603	0.0197	-0.1576	0.0030	-0.1553	0.0118
-0.0984	-0.0968	0.0160	-0.0980	0.0032	-0.1004	0.0201	-0.0987	0.0036	-0.0973	0.0109
-0.0447	-0.0439	0.0173	-0.0445	0.0029	-0.0456	0.0201	-0.0448	0.0038	-0.0442	0.0106
0.0043	0.0042	0.0203	0.0043	0.0045	0.0044	0.0182	0.0043	0.0022	0.0042	0.0121
0.0491	0.0480	0.0224	0.0488	0.0054	0.0499	0.0172	0.0491	0.0013	0.0484	0.0129
0.0899	0.0878	0.0235	0.0894	0.0054	0.0879	0.0227	0.0900	0.0013	0.0888	0.0128
0.1270	0.1241	0.0232	0.1265	0.0040	0.1293	0.0181	0.1273	0.0026	0.1255	0.0113
0.1614	0.1273	0.0255	0.1605	0.0053	0.1641	0.0167	0.1616	0.0012	0.1593	0.0125
0.1923	0.1874	0.0258	0.1913	0.0048	0.1956	0.0170	0.1926	0.0016	0.1900	0.0118
0.2205	0.2147	0.0265	0.2194	0.0048	0.2125	0.0372	0.2207	0.0014	0.2179	0.0115
0.2453	0.2392	0.0256	0.2444	0.0034	0.2498	0.0180	0.2459	0.0025	0.2430	0.0094
0.2676	0.2607	0.0262	0.2665	0.0039	0.2724	0.0175	0.2680	0.0015	0.2653	0.0085
0.2860	0.2789	0.0254	0.2849	0.0036	0.2757	0.0371	0.2863	0.0011	0.2843	0.0058
0.3012	0.2928	0.0284	0.2987	0.0079	0.3056	0.0146	0.2999	0.0040	0.2993	0.0059
0.3090	0.3011	0.0260	0.3063	0.0084	0.3140	0.0162	0.3073	0.0052	0.3090	0.0001
0.3101	0.3024	0.0251	0.3062	0.0123	0.2967	0.0446	0.3071	0.0095	0.3119	0.0061
0.3023	0.2954	0.0234	0.2969	0.0180	0.3123	0.0319	0.2979	0.0148	0.3065	0.0138
0.2842	0.2790	0.0183	0.2776	0.0236	0.2903	0.0212	0.2791	0.0182	0.2915	0.0250
0.2554	0.2533	0.0082	0.2484	0.0281	0.2635	0.0308	0.2508	0.0183	0.2658	0.0390
0.2174	0.1732	0.2787	0.1591	0.3923	0.1814	0.2214	0.1655	0.3384	0.1841	0.2033

0.1708	0.1737	0.0164	0.1620	0.0559	0.1812	0.0572	0.1676	0.0191	0.1793	0.0474
0.1170	0.1213	0.0352	0.1071	0.0919	0.1272	0.0798	0.1149	0.0178	0.1180	0.0088
0.0583	0.0629	0.0734	0.0475	0.2258	0.0613	0.0493	0.0577	0.0103	0.0461	0.2626
-0.0057	-0.0036	0.5832	-0.0145	0.6068	-0.0059	0.0313	-0.0021	1.6634	-0.0012	0.6392
-0.0717	-0.0687	0.0437	-0.0818	0.1234	-0.1097	0.3463	-0.0670	0.0708	-0.1292	0.4448
-0.1239	-0.1202	0.0358	-0.1305	0.0509	-0.0635	0.9495	-0.1141	0.0852	-0.2032	0.3903
Sum of IAE		**1.4846**		**1.7002**		**2.1748**		**2.3032**		**5.2296**

Furthermore, Fig. 2.9, Fig. 2.10, Fig. 2.11 and Fig. 2.12 show the I-V and P-V curves of the R.T.C France model. From Fig. 2.9 and Fig. 2.11 it is clear that the measured value and calculated values is almost same and the error of the proposed algorithm is less. From Fig. 2.10 and Fig. 2.12 it is clear that the measured value and calculated values is varying with each other. In the Fig. 2.9, Fig. 2.10, Fig. 2.11 and Fig. 2.12 the blue line represents the measured values and red line indicated the calculated values. It can be concluded that the all the chaotic variants of the proposed algorithm have better accuracy than the compared algorithms.

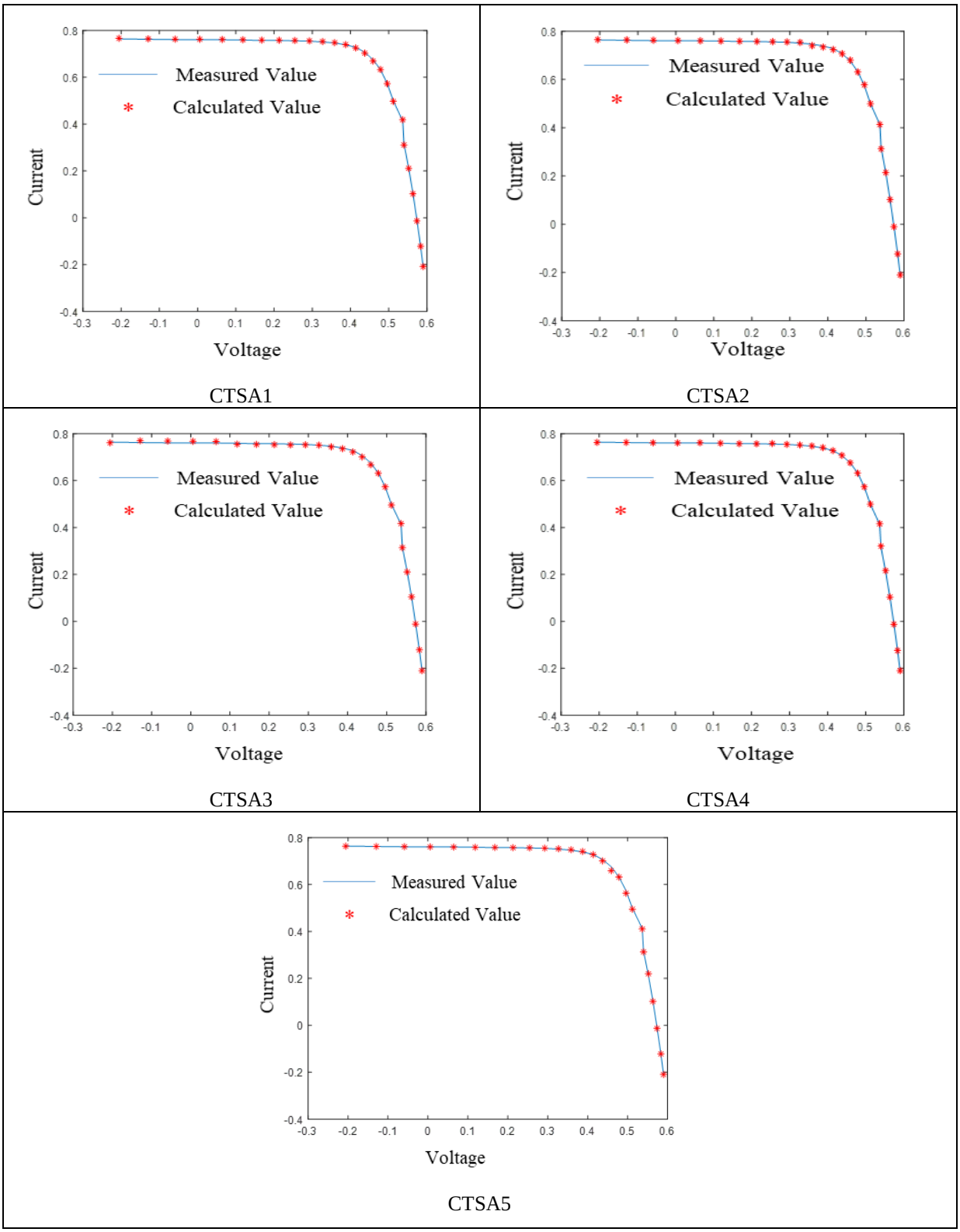

Fig. 2.9 I-V Characteristics Curve Obtained of Double Diode Model by Variant of Chaotic Family

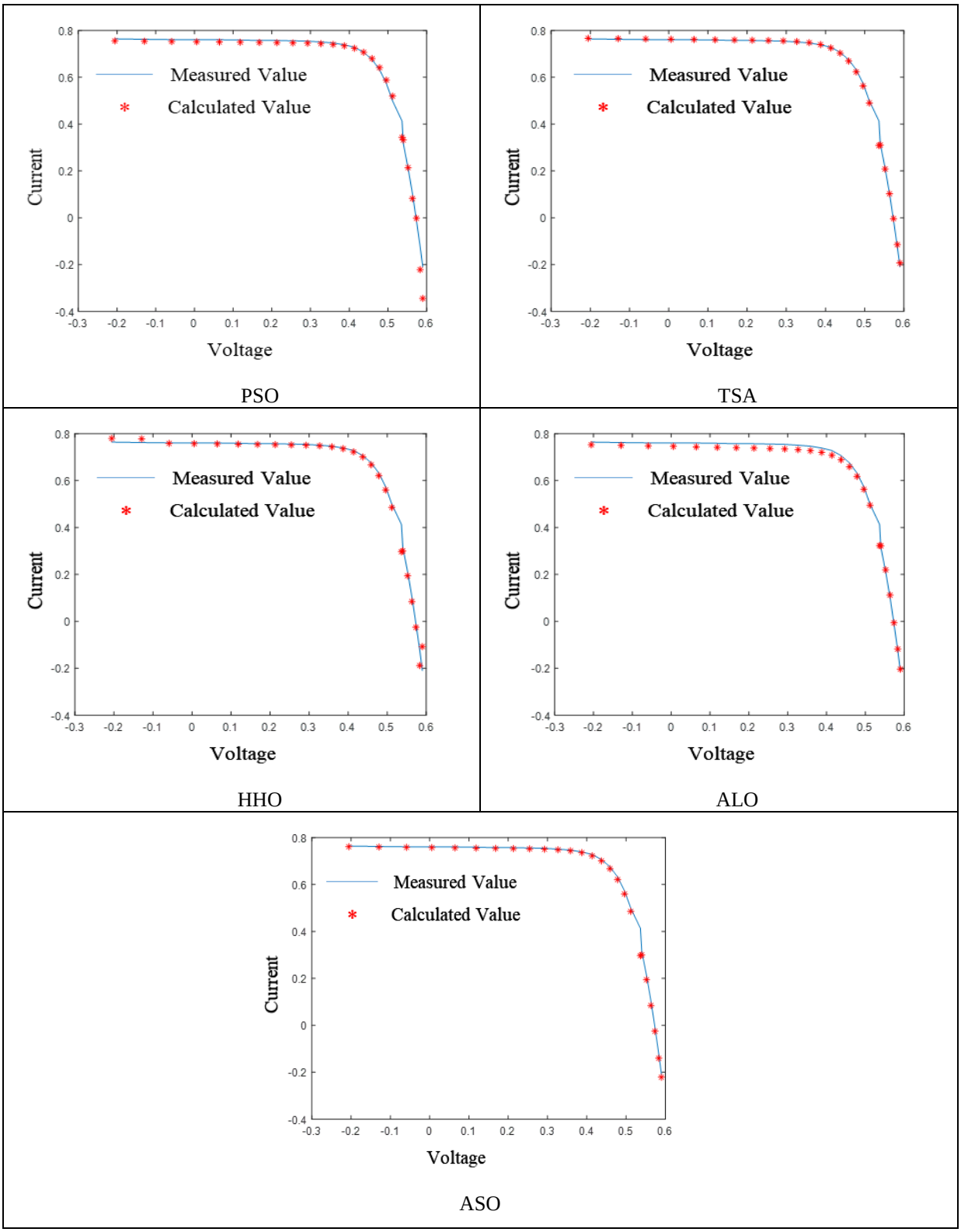

Fig. 2.10 I-V Characteristics Curve Obtained of Double Diode Model by Compared Algorithms

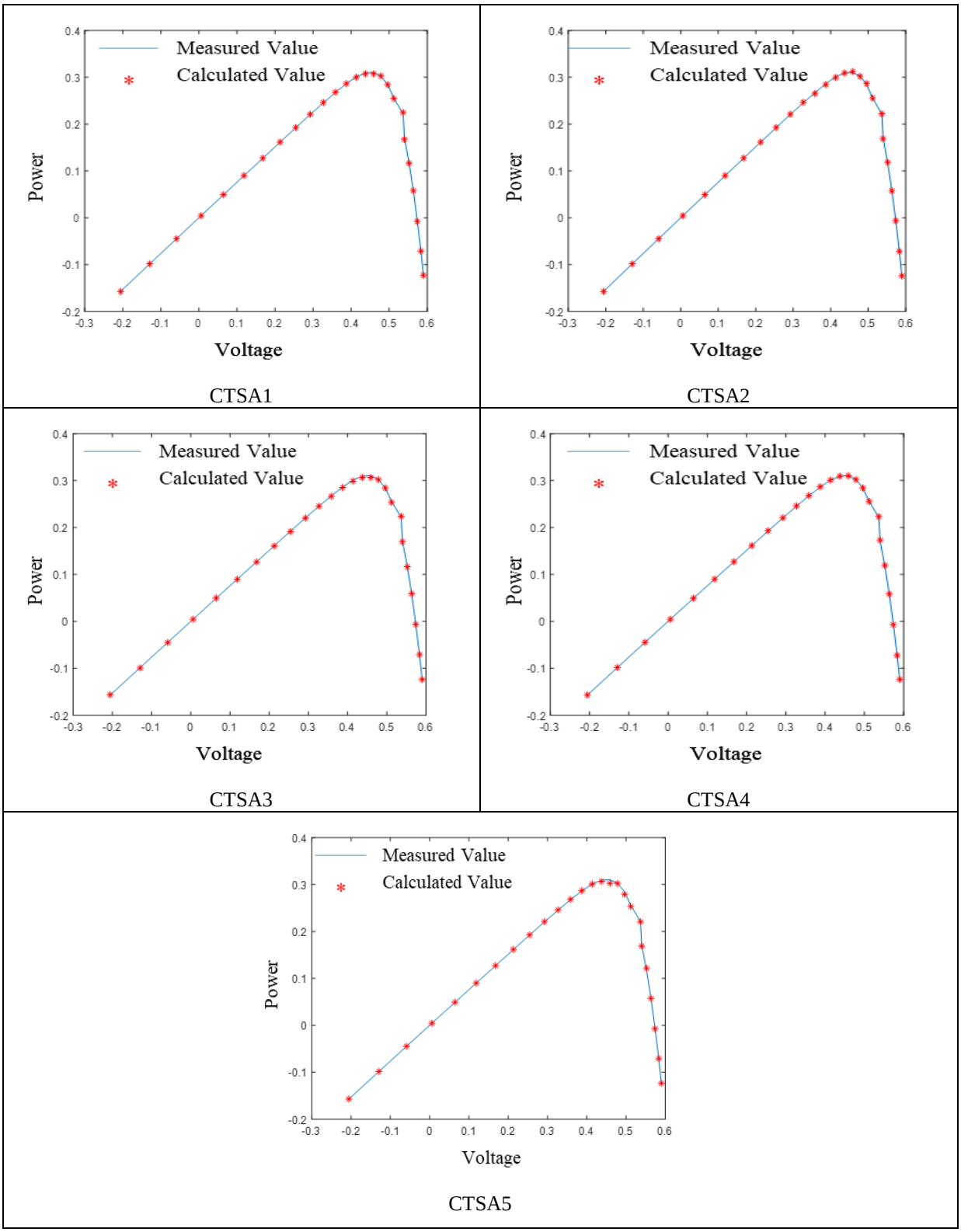

Fig. 2.11 P-V Characteristics Curve Obtained of Double Diode Model by Variant of Chaotic Family

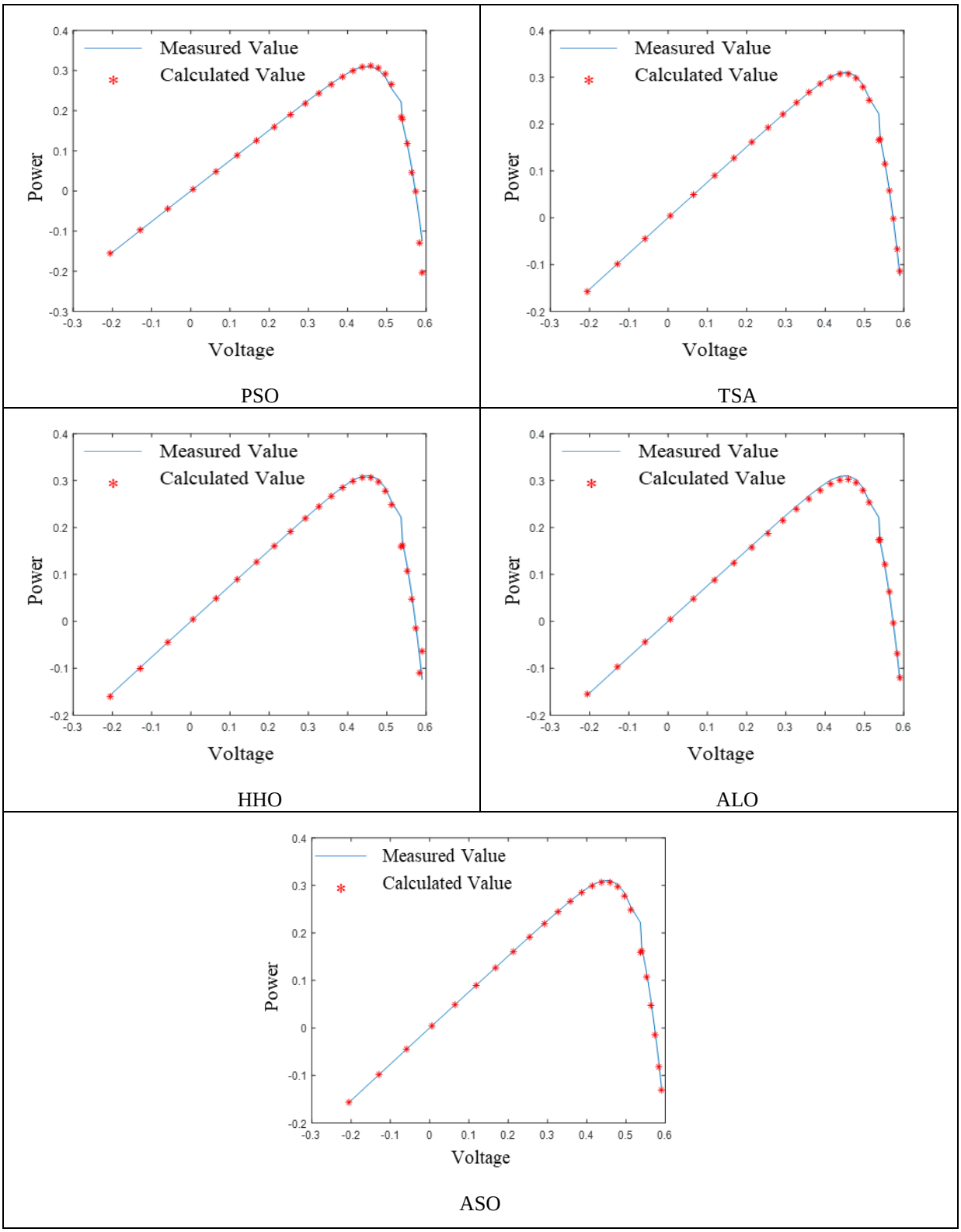

Fig. 2.12 P-V Characteristics Curve Obtained of Double Diode Model by Compared Algorithms

Table 2.10 represents the parameter estimation of double diode for solar PV cell at different temperature with RMSE. Variation of the RMSE depicts the output pattern of the PV cells.

Table 2.10 Temperature Analysis of Double Diode Model Solar PV Cell

Temperature →	**-5ºC**	**0 ºC**	**5 ºC**	**10 ºC**	**15 ºC**	**20 ºC**	**25 ºC**	**30 ºC**	**Algorithms ↓**
	268.15 K	**273.15 K**	**278.15 K**	**283.15 K**	**288.15 K**	**293.15 K**	**298.15 K**	**303.15 K**	
Parameters ↓									
$\mathbf{I_{pv}}$	0.7675	0.8047	0.7543	0.7630	0.8370	0.7853	0.7898	0.7587	
$\boldsymbol{\alpha_1}$	1.0101	1.1123	1.9905	1.0928	1.7042	1.3820	1.5417	1.8403	
$\boldsymbol{\alpha_2}$	1.0099	1.1650	1.8194	1.9789	1.1852	1.4317	1.5214	1.4894	
$\mathbf{R_S}$	0.0704	0.05059	0.1567	0.0021	0.0374	0.0384	0.0142	0.1873	**CTSA1**
$\mathbf{R_{Sh}}$	12.0658	10.3568	11.3963	30.6614	48.1534	22.5267	41.5102	11.0241	
$\mathbf{I_{o1}}$	0.1411	0.7697	0.1822	0.6760	0.1352	0.7054	0.9114	0.5872	
$\mathbf{I_{o2}}$	0.2814	0.1348	0.8320	0.6514	0.2578	0.7512	0.6254	0.2714	
RMSE Error	3.6690 E-08	4.1085 E-08	4.9105 E-08	3.0414 E-08	4.1324 E-08	4.3373 E-08	3.3764 E-08	3.6448 E-08	
$\mathbf{I_{pv}}$	0.7317	0.7686	0.7347	0.8571	0.7383	0.7372	0.7421	0.7472	
$\boldsymbol{\alpha_1}$	1.0008	1.8304	1.1674	1.0856	1.1698	1.2508	1.3611	1.0117	
$\boldsymbol{\alpha_2}$	1.0001	1.0559	1.7719	1.0659	1.1660	1.2119	1.0274	1.7885	**CTSA2**
$\mathbf{R_S}$	0.1441	0.0326	0.0324	0.1356	0.0212	0.0403	0.1605	0.1428	
$\mathbf{R_{Sh}}$	12.1130	41.2300	21.7746	51.9282	81.9642	41.8020	31.5023	48.3257	
$\mathbf{I_{o1}}$	0.1506	0.3703	0.1042	0.7624	0.2541	0.9526	0.2548	0.6529	
$\mathbf{I_{o2}}$	0.6847	0.1761	0.1721	0.2929	0.1689	0.0924	0.6050	0.2309	
RMSE Error	4.6960 E-07	3.8332 E-07	4.9534 E-07	3.6283 E-07	2.3580 E-07	3.9943 E-07	3.3219 E-07	3.5252 E-07	
$\mathbf{I_{pv}}$	0.8512	0.8342	0.7709	0.8196	0.8075	0.8167	0.7902	0.7744	
$\boldsymbol{\alpha_1}$	1.3632	1.0211	1.8181	1.4810	1.0142	1.3395	1.8797	1.7733	
$\boldsymbol{\alpha_2}$	1.1206	1.7368	1.1879	1.7567	1.0371	1.3678	1.8905	1.7585	
$\mathbf{R_S}$	0.0391	0.1827	0.1250	0.0359	0.0217	0.0752	0.0593	0.1258	**CTSA3**
$\mathbf{R_{Sh}}$	97.8181	59.8008	65.8152	10.4458	10.2990	18.8358	51.2288	11.0551	
$\mathbf{I_{o1}}$	0.1468	0.1109	0.5155	0.2408	0.1206	0.1736	0.1879	0.7567	
$\mathbf{I_{o2}}$	0.1832	0.1766	0.7192	0.1371	0.0367	0.0895	0.0755	0.0841	
RMSE Error	3.6700 E-07	3.8948 E-07	4.6116 E-07	4.3050 E-07	4.2534 E-07	3.3067 E-07	3.9419 E-07	4.3845 E-07	
$\mathbf{I_{pv}}$	0.8281	0.8414	0.7742	0.8017	0.8199	0.7882	0.7992	0.7809	
$\boldsymbol{\alpha_1}$	1.9538	1.0062	1.7459	1.6718	1.0649	1.0005	1.8171	1.8171	
$\boldsymbol{\alpha_2}$	1.2326	1.0223	1.0178	1.2391	1.9466	1.0086	1.1225	1.8705	

R_S	0.1880	0.1695	0.1620	0.0203	0.0411	0.1824	0.1270	0.1508	**CTSA4**
R_{Sh}	20.2867	96.4613	10.7139	37.9492	10.7062	71.0011	48.1244	11.2954	
I_{o1}	0.4821	0.2559	0.6354	0.1000	0.2700	0.5089	0.1989	0.1031	
I_{o2}	0.9347	0.1766	0.7192	0.5693	0.3947	0.2484	0.1008	0.1548	
RMSE Error	4.2742 E-08	3.6645 E-08	3.9748 E-08	3.1683 E-08	3.8151 E-08	4.1780 E-08	4.3598 E-08	3.9575 E-08	
I_{pv}	0.7971	0.7905	0.8448	0.8133	0.8085	0.7996	0.7709	0.8196	**CTSA5**
α_1	1.0126	1.0803	1.1151	1.3338	1.4159	1.1915	1.8779	1.8181	
α_2	1.6987	1.2679	1.4780	18532	1.6619	1.5919	1.6035	1.0037	
R_S	0.0403	0.0238	0.1131	0.535	0.0285	0.0055	0.1250	0.0359	
R_{Sh}	11.0370	41.6191	81.2212	10.0088	15.8122	31.9396	19.4468	50.4458	
I_{o1}	0.2433	0.5384	0.1563	0.1468	0.2408	0.2775	0.1109	0.2031	
I_{o2}	0.7283	0.5503	0.1104	0.2778	0.3387	0.1766	0.1030	0.5693	
RMSE Error	4.8091 E-07	4.2748 E-07	3.3269 E-07	4.1639 E-07	3.9605 E-07	4.7627 E-07	3.0127 E-07	4.5060 E-07	

- **Non-Parametric Test**

The three non-parametric tests are performed. First the statistical result of Friedman ranking test [112] as shown in Table 2.11. From this test, it is clear that the first rank is secured by CTSA4, second rank is secured by CTSA1, and third rank is secured CTSA5 with CTSA2, CTSA3, TSA, ASO, HHO, ALO and PSO to follow.

Table 2.11 Friedman Ranking Test of Double Diode Model for Solar PV Cell at STC

Algorithms	Friedman Ranking
CTSA1	2
CTSA2	4
CTSA3	5
CTSA4	1
CTSA5	3
PSO	10
TSA	6
HHO	8
ALO	9
ASO	7

Second non-parametric test done is Wilcoxon's rank sum test [113]. Wilcoxon's rank sum test is applied in comparison of all variants of chaotic family with all rest of the compared algorithms as shown in Table 2.12 for the solar PV model

Table 2.12 Wilcoxon's Rank Sum Test p Values of Double Diode Model

Algorithms	PSO	TSA	HHO	ALO	ASO
CTSA1	1.5214E-11	1.5012E-11	1.5716E-11	1.5901E-11	1.5614E-11
CTSA2	1.5301E-11	1.5846E-11	1.5037E-11	1.5278E-11	1.5147E-11
CTSA3	1.5368E-11	1.5104E-11	1.5697E-11	1.5421E-11	1.5370E-11
CTSA4	1.5601E-11	1.5871E-11	1.5661E-11	1.5304E-11	1.5201E-11
CTSA5	1.5812E-11	1.5634E-11	1.5083E-11	1.5941E-11	1.5889E-11

Last non-parametric test performed is Kruskal-Wallis test [114]. The list of graphs obtained from the research, as well as the CTSA mean and median rank is seen in Fig. 2.13 and Fig. 2.14, showing that CTSA results are substantially different from those of other groups. The findings of the Anova Kruskal-Wallis test are shown in Table 2.13. The probability chi square value is calculated using this test. With a significance level of 95 percent, this test proves that all variants of CTSA outperform the other compared algorithms. From the Table 2.13, the significance of the degree of freedom (DF) refers to the maximum number of logically independent values, which are values that have the freedom to vary, in the data sample. Similarly, the significance of sum of squares (SS) express the total variation that can be attributed to various factors. The significance of the mean squares (MS) used to determine whether factors are significant or not. This non-parametric test explicitly shows that a recently developed chaotic family variant is much more reliable and precise than the other algorithms.

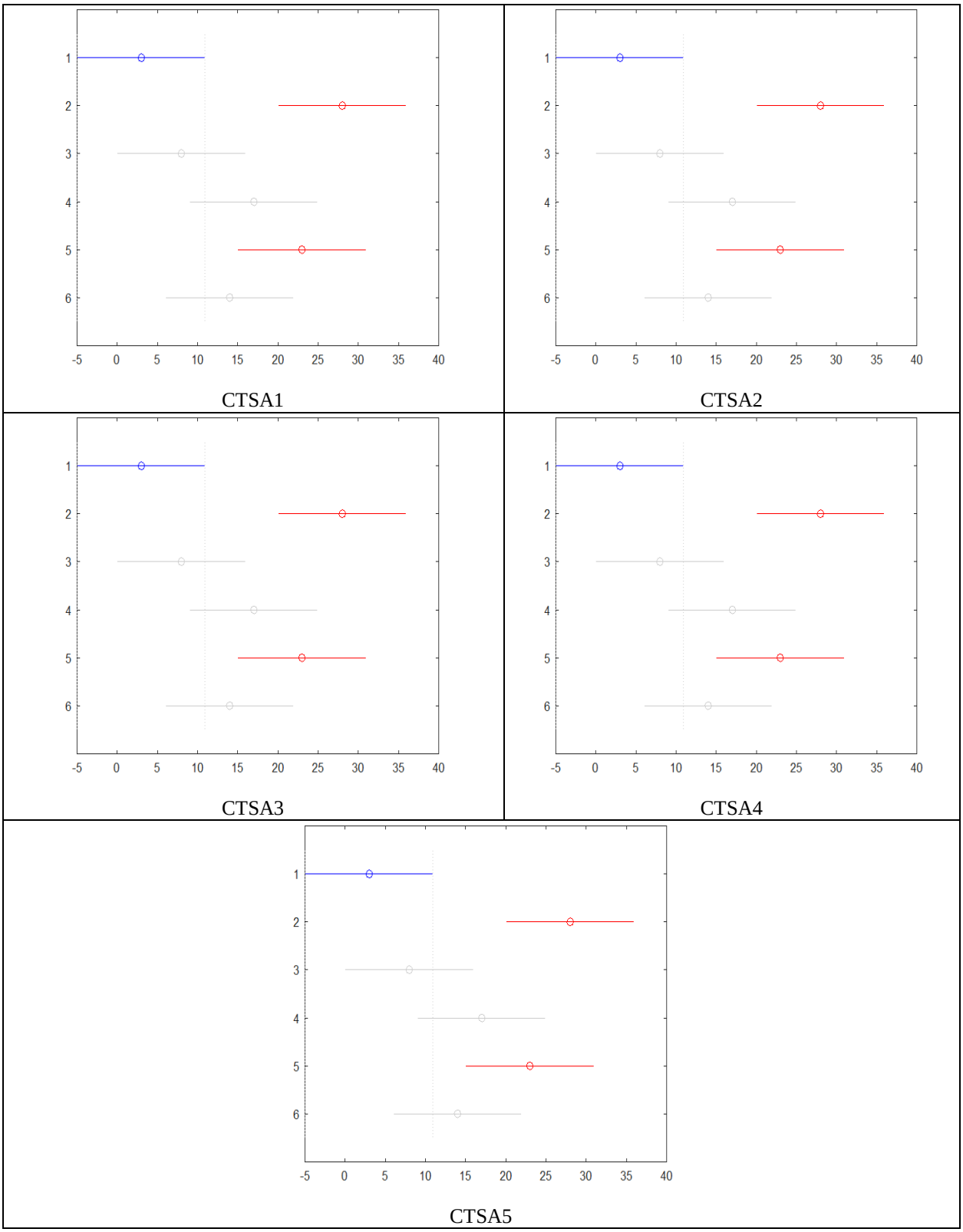

Fig. 2.13 Multiple Comparisons of Mean Rank using Kruskal-Wallis Test of Double Diode Model

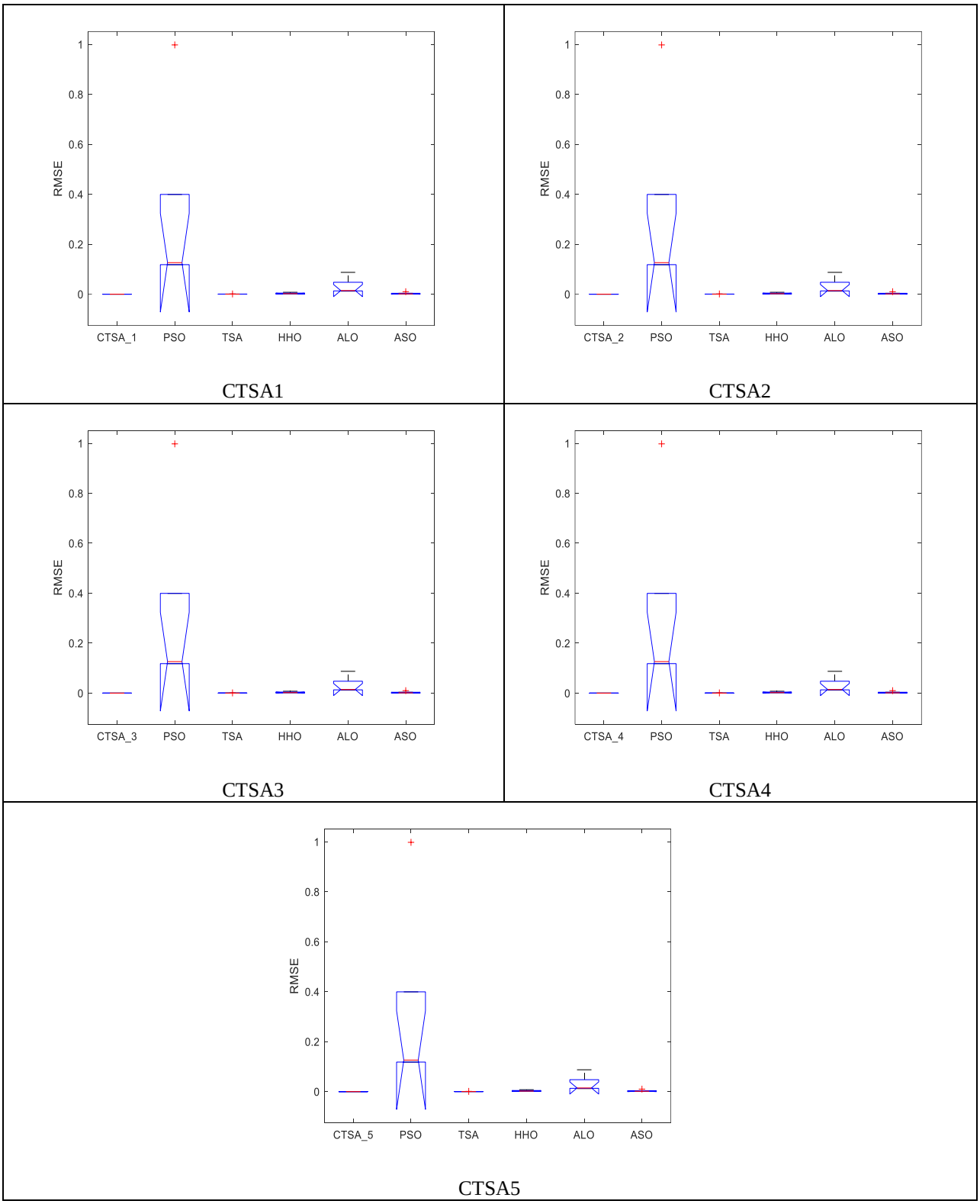

Fig. 2.14 Multiple Comparisons of Median Rank using Kruskal-Wallis Test of Double Diode Model

Table 2.13 Anova Kruskal-Wallis Test for Double Diode Model

SOURCE	SS (Sum of Squares)	DF (degree of Freedom)	MS (Mean Squares)	Chi-sq	Prob>Chi-sq	Algorithms
Columns	507199.5	5	101439.9	175	6.25672E-36	**CTSA1**
Error	28994	180	161	-	-	
Total	536193.5	185	-	-	-	
Columns	507199.5	5	101439.9	175	6.23994E-36	**CTSA2**
Error	28963	180	161	-	-	
Total	536162.5	185	-	-	-	
Columns	507199.5	5	101439.9	175	6.25197E-36	**CTSA3**
Error	28984	180	161	-	-	
Total	536184.5	185	-	-	-	
Columns	507199.5	5	101439.9	175	6.24889E-36	**CTSA4**
Error	28978	180	161	-	-	
Total	536177.5	185	-	-	-	
Columns	507199.5	5	101439.9	175	6.25563E-36	**CTSA5**
Error	28992.5	180	161	-	-	
Total	536193	185	-	-	-	

Case 2: Triple Diode Model

Table 2.14 represents the best extracted parameters and the corresponding RMSE values which are calculated at standard temperature condition (STC) for the triple diode model. Table 2.14 shows the nine unknown parameters as well as the root mean square error and computation time per second. From the computation time it is clear that the variants of the chaotic family are better than the rest of the compared algorithms. The best RMSE of the chaotic maps of CTSA then the rest of the compared algorithms is concluded in Table 2.14. At STC the statistical results of the solar PV model are represented in Table 2.15. From above all the results, it is concluded that the variants of chaotic family have better accuracy and performance than the rest of the algorithms compared.

Table 2.14 Parameter Estimation of Triple Diode Model at STC

Parameter → / **Algorithms ↓**	**I_{pv}**	**α_1**	**α_2**	**α_3**	**R_S**	**R_{Sh}**	**I_{o1}**	**I_{o2}**	**I_{o3}**	**Computation time/second**
CTSA1	0.8771	1.4924	1.4497	1.1667	0.0833	29.3941	0.5	0.7560	0.6640	1.2658
CTSA2	0.8507	1.5304	1.2387	1.3956	0.1247	12.2957	0.5416	0.4247	0.2770	1.3520
CTSA3	0.8152	1.0395	1.0765	1.5923	0.1852	28.0305	0.2422	0.7512	0.4675	1.3056
CTSA4	0.9436	1.5129	1.3969	1.4247	0.1247	38.5420	0.6626	0.7359	0.6650	1.2290
CTSA5	0.7301	1.0110	1.1108	1.2420	0.0286	34.8557	0.4772	0.4877	0.4083	1.3859
PSO	0.8369	1.4054	1.5270	1.4874	0.0926	56.1121	0.4973	0.3217	0.3059	18.5421
TSA	0.9207	1.6969	1.5145	1.3308	0.1471	23.9128	0.4651	0.3969	0.4731	3.2568
HHO	0.8413	1.1388	1.1480	1.1487	0.1463	59.0120	0.2736	0.2932	0.1424	9.8754
ALO	0.8408	1.1241	1.1453	1.0573	0.1247	55.0993	0.2535	0.3014	0.1772	13.5841
ASO	0.8354	1.5351	1.3343	1.5872	0.1933	54.0631	0.3637	0.3996	0.3704	11.8412

Table 2.15 Statistical Results of Triple Diode Model at STC

Statistical Results → / **Algorithms ↓**	**Minimum**	**Average**	**Maximum**	**S.D**	**Error**
CTSA1	1.2142E-07	3.9642E-07	9.6688E-07	2.2859E-07	**RMSE**
CTSA2	1.0036E-06	3.4906E-06	9.4766E-06	2.7057E-06	
CTSA3	1.0487E-07	5.3721E-07	9.6712E-07	2.9049E-07	
CTSA4	1.3161E-07	2.7393E-07	2.6865E-07	1.3109E-07	
CTSA5	1.1557E-06	3.2032E-06	8.9966E-06	2.2296E-06-	
PSO	0.1480	0.2584	0.4940	0.0865	
TSA	1.2038E-04	3.8211E-04	9.2882E-04	2.7281E-04	
HHO	0.0012	0.0044	0.0095	0.0023	
ALO	0.0112	0.0413	0.0952	0.0269	
ASO	0.0010	0.0055	0.0096	0.0029	

Fig. 2.15 shows the best convergence curve of R.T.C. France model attained by PSO, HHO, TSA, ALO, ASO, CTSA1, CTSA2, CTSA3, CTSA4, and CTSA5. The efficiency of CTSA is obtained from the convergence graph. It also shows that variant of chaotic family has a higher pace of convergence than the rest of the other compared algorithms. After extraction of the solar PV model parameters, the power and output current corresponding to the measured voltage can be conveniently estimated. For the further demonstration of CTSA's accuracy, Table 2.16, Table 2.17, Table 2.18 and Table 2.19 showed the measured output, current and individual absolute error (IAE) values.

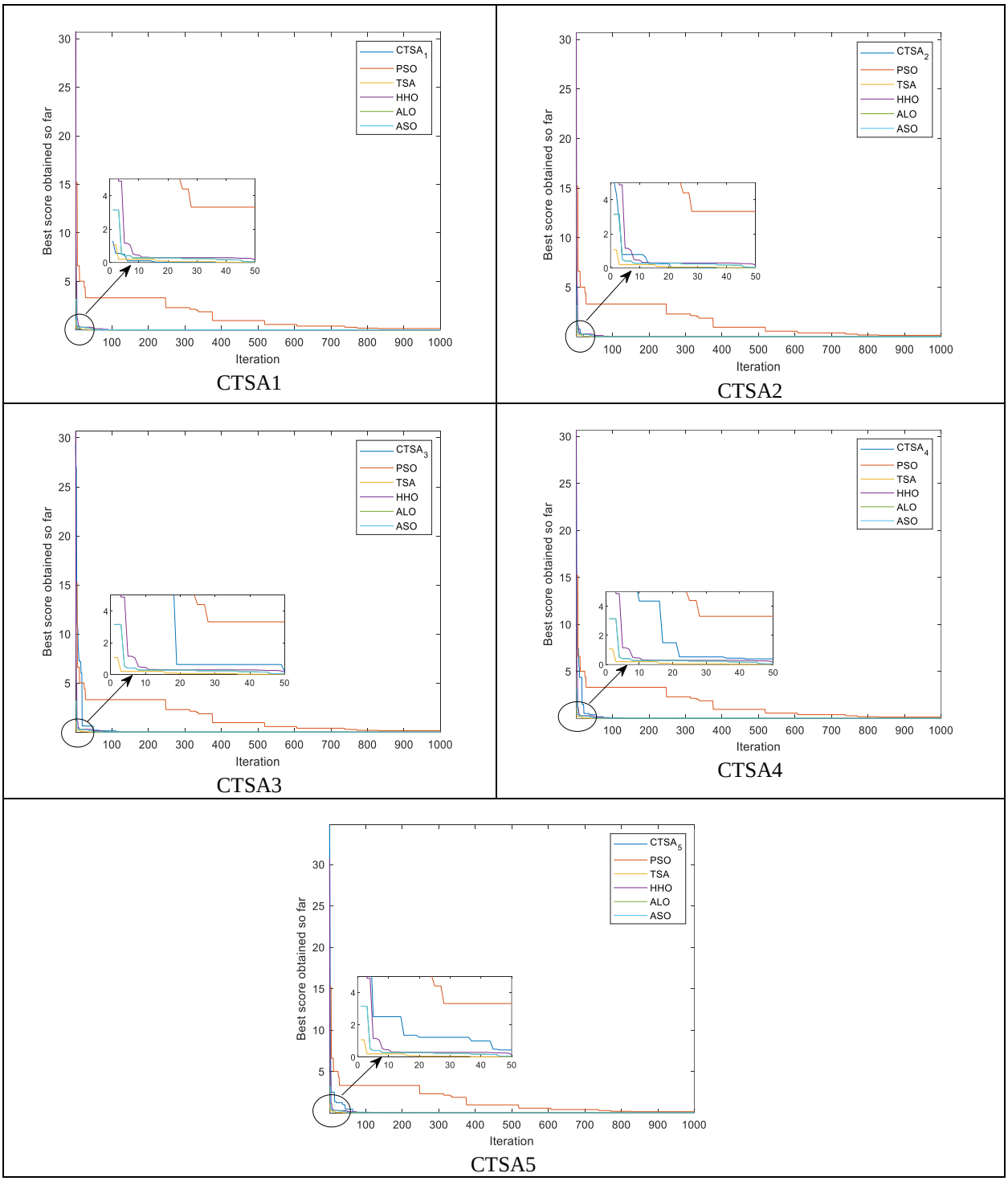

Fig. 2.15 Best Convergences Curve of Triple Diode Model at STC for Each Variant of CTSA with Other Compared Algorithm

Table 2.16 Calculated Current of Triple Diode Model for Each Variant of CTSA

V_L Measured Voltage (V)	I_L Measured Current (A)	CTSA1		CTSA2		CTSA3		CTSA4		CTSA5	
		I_L Calculated Current (A)	IAE	I_L Calculated Current (A)	IAE	I_L Calculated Current (A)	IAE	I_L Calculated Current (A)	IAE	I_L Calculated Current (A)	IAE
-0.2057	**0.7640**	0.7631	0.0009	0.7636	0.0004	0.7640	0.0000	0.7638	0.0002	0.7639	0.0001
-0.1291	**0.7620**	0.7620	0.0000	0.7623	0.0003	0.7626	0.0006	0.7625	0.0005	0.7625	0.0005
-0.0588	**0.7605**	0.7610	0.0005	0.7605	0.0000	0.7613	0.0008	0.7613	0.0008	0.7612	0.0007
0.0057	**0.7605**	0.7601	0.0004	0.7604	0.0001	0.7601	0.0004	0.7602	0.0003	0.7601	0.0004
0.0646	**0.7600**	0.7592	0.0008	0.7611	0.0011	0.7591	0.0009	0.7591	0.0009	0.7590	0.0010
0.1185	**0.7590**	0.7584	0.0006	0.7592	0.0002	0.7581	0.0009	0.7582	0.0008	0.7580	0.0010
0.1678	**0.7570**	0.7577	0.0007	0.7574	0.0004	0.7572	0.0002	0.7573	0.0003	0.7571	0.0001
0.2132	**0.7570**	0.7569	0.0001	0.7565	0.0005	0.7562	0.0008	0.7564	0.0006	0.7572	0.0002
0.2545	**0.7555**	0.7560	0.0005	0.7555	0.0000	0.7552	0.0003	0.7554	0.0001	0.7552	0.0003
0.2924	**0.7540**	0.7546	0.0006	0.7541	0.0001	0.7538	0.0002	0.7540	0.0000	0.7538	0.0002
0.3269	**0.7505**	0.7523	0.0018	0.7501	0.0004	0.7515	0.0010	0.7517	0.0012	0.7515	0.0010
0.3585	**0.7465**	0.7481	0.0016	0.7464	0.0001	0.7475	0.0010	0.7476	0.0011	0.7475	0.0010
0.3873	**0.7385**	0.7405	0.0020	0.7384	0.0001	0.7392	0.0007	0.7403	0.0018	0.7402	0.0017
0.4137	**0.7280**	0.7273	0.0007	0.7284	0.0004	0.7275	0.0005	0.7274	0.0006	0.7275	0.0005
04373	**0.7065**	0.7065	0.0000	0.7065	0.0000	0.7071	0.0006	0.7069	0.0004	0.7072	0.0007
0.4590	**0.6755**	0.6746	0.0009	0.6755	0.0000	0.6756	0.0001	0.6752	0.0003	0.6757	0.0002
0.4784	**0.6320**	0.6303	0.0017	0.6329	0.0009	0.6314	0.0006	0.6320	0.0000	0.6314	0.0006
0.4960	**0.5730**	0.5722	0.0008	0.5725	0.0005	0.5730	0.0000	0.5727	0.0003	0.5730	0.0000
0.5119	**0.4990**	0.5009	0.0019	0.4989	0.0001	0.5013	0.0023	0.5001	0.0011	0.4993	0.0003
0.5365	**0.4130**	0.4163	0.0033	0.4128	0.0002	0.4150	0.0020	0.4160	0.0030	0.4160	0.0030

0.5398	**0.3165**	0.3114	0.0051	0.3163	0.0002	0.3172	0.0007	0.3188	0.0023	0.3205	0.0040
0.5521	**0.2120**	0.2127	0.0007	0.2111	0.0009	0.2139	0.0019	0.2161	0.0041	0.2143	0.0023
0.5633	**0.1035**	0.1037	0.0002	0.1034	0.0001	0.1036	0.0001	0.1037	0.0002	0.1036	0.0001
0.5736	**-0.0100**	-0.0100	0.0000	-0.0098	0.0002	-0.0099	0.0001	-0.0100	0.0000	-0.0098	0.0002
0.5833	**-0.1230**	-0.1236	0.0006	-0.1232	0.0002	-0.1231	0.0001	-0.1243	0.0013	-0.1229	0.0001
0.5900	**-0.2100**	-0.2109	0.0009	-0.2101	0.0001	-0.2114	0.0014	-0.2099	0.0001	-0.2077	0.0023
Sum of IAE			**0.0273**		**0.0075**		**0.0180**		**0.0223**		**0.0224**

Table 2.17 Calculated Current of Triple Diode Model for Compared Algorithms

V_L Measured Voltage (V)	**I_L Measured Current (A)**	**TSA**		**ASO**		**HHO**		**ALO**		**PSO**	
		I_L Calculated Current (A)	**IAE**	**I_L Calculated Current (A)**	**IAE**	**I_L Calculated Current (A)**	**IAE**	**I_L Calculated Current (A)**	**IAE**	**I_L Calculated Current (A)**	**IAE**
-0.2057	**0.7640**	0.7714	0.0097	0.7659	0.0025	0.7526	0.0150	0.7711	0.0092	0.7577	0.0082
-0.1291	**0.7620**	0.7705	0.0111	0.7624	0.0006	0.7519	0.0134	0.7683	0.0083	0.7561	0.0076
-0.0588	**0.7605**	0.7697	0.0119	0.7592	0.0016	0.7512	0.0123	0.7658	0.0070	0.7547	0.0076
0.0057	**0.7605**	0.7689	0.0109	0.7562	0.0055	0.7505	0.0132	0.7635	0.0040	0.7534	0.0094
0.0646	**0.7600**	0.7682	0.0107	0.7536	0.0084	0.7499	0.0133	0.7614	0.0019	0.7521	0.0103
0.1185	**0.7590**	0.7675	0.0111	0.7511	0.0104	0.7494	0.0127	0.7595	0.0006	0.7510	0.0105
0.1678	**0.7570**	0.7669	0.0129	0.7488	0.0109	0.7489	0.0108	0.7576	0.0009	0.7499	0.0093
0.2132	**0.7570**	0.7663	0.0121	0.7466	0.0138	0.7483	0.0115	0.7559	0.0014	0.7488	0.0109
0.2545	**0.7555**	0.7655	0.0131	0.7445	0.0147	0.7475	0.0105	0.7541	0.0018	0.7474	0.0107
0.2924	**0.7540**	0.7645	0.0137	0.7421	0.0159	0.7464	0.0101	0.7519	0.0027	0.7454	0.0114
0.3269	**0.7505**	0.7626	0.0159	0.7392	0.0152	0.7443	0.0082	0.7489	0.0020	0.7421	0.0112
0.3585	**0.7465**	0.7591	0.0166	0.7348	0.0158	0.7404	0.0081	0.7442	0.0029	0.7362	0.0138

0.3873	**0.7385**	0.7524	0.0185	0.7279	0.0144	0.7333	0.0069	0.7365	0.0026	0.7260	0.0171
0.4137	**0.7280**	0.7401	0.0164	0.7167	0.0157	0.7210	0.0096	0.7236	0.0060	0.7085	0.0273
04373	**0.7065**	0.7200	0.0188	0.6991	0.0104	0.7015	0.0070	0.7034	0.0042	0.6818	0.0361
0.4590	**0.6755**	0.6881	0.0183	0.6721	0.0049	0.6716	0.0057	0.6727	0.0040	0.6420	0.0520
0.4784	**0.6320**	0.6427	0.0167	0.6338	0.0029	0.6299	0.0031	0.6296	0.0036	0.5887	0.0733
0.4960	**0.5730**	0.5824	0.0162	0.5818	0.0151	0.5752	0.0038	0.5720	0.0016	0.5220	0.0977
0.5119	**0.4990**	0.5085	0.0188	0.5152	0.0314	0.5078	0.0175	0.4994	0.0009	0.4444	0.1227
0.5365	**0.4130**	0.3168	0.3035	0.3457	0.1944	0.3388	0.2189	0.3169	0.3031	0.2526	0.6345
0.5398	**0.3165**	0.3251	0.0265	0.3330	0.0498	0.3370	0.0608	0.3061	0.0338	0.3165	0.0002
0.5521	**0.2120**	0.2213	0.0424	0.2173	0.0245	0.2367	0.1045	0.1863	0.1374	0.1732	0.2233
0.5633	**0.1035**	0.1153	0.1029	0.0877	0.1797	0.1307	0.2085	0.0546	0.8928	0.0825	0.2538
0.5736	**-0.0100**	-0.0111	0.1046	-0.0542	0.8155	-0.0218	0.5432	-0.0869	0.8849	-0.0304	0.6720
0.5833	**-0.1230**	-0.0964	0.2757	-0.2132	0.4231	-0.0941	0.3069	-0.2431	0.4942	-0.0758	0.6208
0.5900	**-0.2100**	-0.1702	0.2331	-0.3363	0.3756	-0.178	0.1776	-0.3621	0.4201	-0.1403	0.4964
Sum of IAE			**1.3633**		**2.2739**		**1.8146**		**3.2329**		**3.4495**

Table 2.18 Calculated Power of Triple Diode Model for Each Variant of CTSA

P_L Measured Power (W)	**CTSA1**		**CTSA2**		**CTSA3**		**CTSA4**		**CTSA5**	
	P_L Calculated Power (W)	**IAE**	**P_L Calculated Power (W)**	**IAE**	**P_L Calculated Power (W)**		**P_L Calculated Power (W)**	**IAE**	**P_L Calculated Power (W)**	**IAE**
-0.1572	-0.1570	0.0002	-0.1571	0.0001	-0.1571	0.0000	-0.1571	0.000	-0.1571	0.0000
-0.0984	-0.0984	0.0000	-0.0984	0.0000	-0.0984	0.0001	-0.0984	0.00001	-0.0984	0.0001
-0.0447	-0.0447	0.0000	-0.0447	0.0000	-0.0448	0.0000	-0.0448	0.0000	-0.0448	0.0000
0.0043	0.0043	0.0000	0.0043	0.0000	0.0043	0.0000	0.0043	0.0000	0.0043	0.0000

0.0491	0.0490	0.0001	0.0492	0.0001	0.0490	0.0001	0.0490	0.0001	0.0490	0.0001
0.0899	0.0899	0.0001	0.0900	0.0000	0.0898	0.0001	0.0898	0.0001	0.0898	0.0001
0.1270	0.1271	0.0001	0.1271	0.0001	0.1271	0.0000	0.1271	0.0001	0.1270	0.0000
0.1614	0.1614	0.0000	0.1613	0.0001	0.1612	0.0002	0.1613	0.0001	0.1641	0.0000
0.1923	0.1924	0.0001	0.1923	0.0000	0.1922	0.0001	0.1923	0.0000	0.1922	0.0001
0.2205	0.2207	0.0002	0.2205	0.0000	0.2204	0.0001	0.2205	0.0000	0.2204	0.0001
0.2453	0.2459	0.0006	0.2452	0.0001	0.2457	0.0003	0.2457	0.0004	0.2457	0.0003
0.2676	0.2682	0.0006	0.2676	0.0000	0.2680	0.0003	0.2680	0.0004	0.2680	0.0003
0.2860	0.2868	0.0008	0.2860	0.0000	0.2863	0.0003	0.2867	0.0007	0.2867	0.0007
0.3012	0.3009	0.0003	0.3013	0.0002	0.3010	0.0002	0.3009	0.0003	0.3010	0.0002
0.3090	0.3090	0.0000	0.3089	0.0000	0.3092	0.0003	0.3091	0.0002	0.3092	0.0003
0.3101	0.3097	0.0004	0.3100	0.0000	0.3101	0.0000	0.3099	0.0001	0.3101	0.0001
0.3023	0.3015	0.0008	0.3028	0.0004	0.3020	0.0003	0.3023	0.0000	0.3021	0.0003
0.2842	0.2838	0.0004	0.2840	0.0002	0.2842	0.0000	0.2840	0.0002	0.2842	0.0000
0.2554	0.2564	0.0010	0.2554	0.0000	0.2566	0.0012	0.2560	0.0006	0.2556	0.0001
0.2174	0.2192	0.0017	0.2174	0.0001	0.2185	0.0010	0.2190	0.0016	0.2190	0.0016
0.1708	0.1681	0.0028	0.1708	0.0001	0.1712	0.0004	0.1721	0.0012	0.1730	0.0022
0.1170	0.1174	0.0004	0.1165	0.0005	0.1181	0.0010	0.1193	0.0023	0.1183	0.0013
0.0583	0.0584	0.0001	0.0582	0.0001	0.0583	0.0000	0.0584	0.0001	0.0584	0.0001
-0.0057	0.0057	0.0000	-0.0056	0.0001	-0.0057	0.0000	-0.0057	0.0000	-0.0056	0.0001
-0.0717	-0.0721	0.0004	-0.0718	0.0001	-0.0718	0.0000	-0.0725	0.0008	-0.0717	0.0000
-0.1239	-0.1244	0.0005	-0.1239	0.0000	-0.1247	0.0008	-0.1238	0.0001	-0.1225	0.0014
Sum of IAE		**0.0115**		**0.0026**		**0.0069**		**0.0093**		**0.0094**

Table 2.19 Calculated Power of Triple Diode Model for Compared Algorithms

P_L Measured Power (W)	TSA		ASO		HHO		ALO		PSO	
	P_L Calculated Power (W)	IAE	P_L Calculated Power (W)	IAE	P_L Calculated Power (W)	IAE	P_L Calculated Power (W)	IAE	P_L Calculated Power (W)	IAE
-0.1572	-0.1587	0.0097	-0.1576	0.0025	-0.1548	0.0150	-0.1586	0.0092	-0.1558	0.0082
-0.0984	-0.0995	0.0111	-0.0984	0.0006	-0.0970	0.0134	-0.0992	0.0083	-0.0976	0.0076
-0.0447	-0.0452	0.0119	-0.0446	0.0016	-0.0441	0.0123	-0.0450	0.0070	-0.0443	0.0076
0.0043	0.0043	0.0109	0.0043	0.0055	0.0042	0.0132	0.0043	0.0040	0.0042	0.0094
0.0491	0.0496	0.0107	0.0486	0.0084	0.0484	0.0133	0.0491	0.0019	0.0485	0.0103
0.0899	0.0909	0.0111	0.0890	0.0104	0.0888	0.0127	0.0900	0.0006	0.0889	0.0105
0.1270	0.1286	0.0129	0.1256	0.0109	0.1256	0.0108	0.1271	0.0009	0.1258	0.0093
0.1614	0.1633	0.0121	0.1591	0.0138	0.1595	0.0115	0.1611	0.0014	0.1596	0.0109
0.1923	0.1948	0.0131	0.1894	0.0147	0.1902	0.0105	0.1919	0.0018	0.1902	0.0107
0.2205	0.2235	0.0137	0.2170	0.0159	0.2182	0.0101	0.2190	0.0027	0.2179	0.0114
0.2453	0.493	0.0159	0.2416	0.0152	0.2433	0.0082	0. 2448	0.0020	0.2426	0.0112
0.2676	0.2721	0.0166	0.2635	0.0158	0.2654	0.0081	0.2668	0.0029	0.2639	0.0138
0.2860	0.2914	0.0185	0.2819	0.0144	0.2840	0.0069	0.252	0.0026	0.2811	0.0171
0.3012	0.3062	0.0164	0.265	0.0157	0.2983	0.0096	0.2993	0.0060	0.2931	0.0273
0.3090	0.3148	0.0188	0.3057	0.0104	0.3067	0.0070	0.3076	0.0042	0.2981	0.0361
0.3101	0.3158	0.0183	0.3085	0.0049	0.3082	0.0057	0.3087	0.0040	0.2947	0.0520
0.3023	0.3074	0.0167	0.3032	0.0029	0.3013	0.0031	0.3012	0.0036	0.2816	0.0733
0.2842	0.2889	0.0162	0.2885	0.0151	0.2853	0.0038	0.2837	0.0016	0.2589	0.0977
0.2554	0.2603	0.0188	0.2637	0.0314	0.2599	0.0175	0.2556	0.0009	0.2275	0.1227
0.2174	0.1699	0.3035	0.1855	0.1944	0.1817	0.2189	0.1700	0.3031	0.1355	0.6345

0.1708	0.1755	0.0265	0.1798	0.0498	0.1819	0.0608	0.1652	0.0338	0.1708	0.0002
0.1170	0.1222	0.0424	0.1199	0.0245	0.1307	0.1045	0.0102	0.1374	0.0956	0.2233
0.0583	0.0649	0.1029	0.0494	0.1797	0.0736	0.2085	0.0308	0.8928	0.0464	0.2538
-0.0057	-0.0064	0.1046	-0.0311	0.8155	-0.0125	0.5432	-0.0498	0.8849	-0.0174	0.6720
-0.0717	-0.0562	0.2757	-0.1243	0.4231	-0.0548	0.3069	-0.1418	0.4942	-0.0442	0.6208
-0.1239	-0.1005	0.2331	-0.1985	0.3756	-0.1052	0.1776	-0.2136	0.4201	-0.0828	0.4964
Sum of IAE		**1.3633**		**2.2739**		**1.8146**		**3.2329**		**3.4495**

Furthermore, Fig. 2.16, Fig. 2.17, Fig. 2.18 and Fig. 2.19 shows the I-V and P-V curves of the R.T.C France model. From Fig. 2.16 and Fig. 2.18, it is clear that the measured value and calculated values is almost same and the error of the proposed algorithm is less. In the Fig. 2.16, Fig. 2.17, Fig. 2.18 and Fig. 2.19 the red line represents the measured values and blue line indicated the calculated values. From the Fig. 2.16 and Fig. 2.17 the x-axis represents the voltage and y-axis represents the current, similarly for Fig. 2.18 and Fig. 2.19 the x-axis represents the voltage and y-axis represents the power. Even the sensitivity of the atmospheric temperature was measured under the specific operating environment condition after measuring the error.

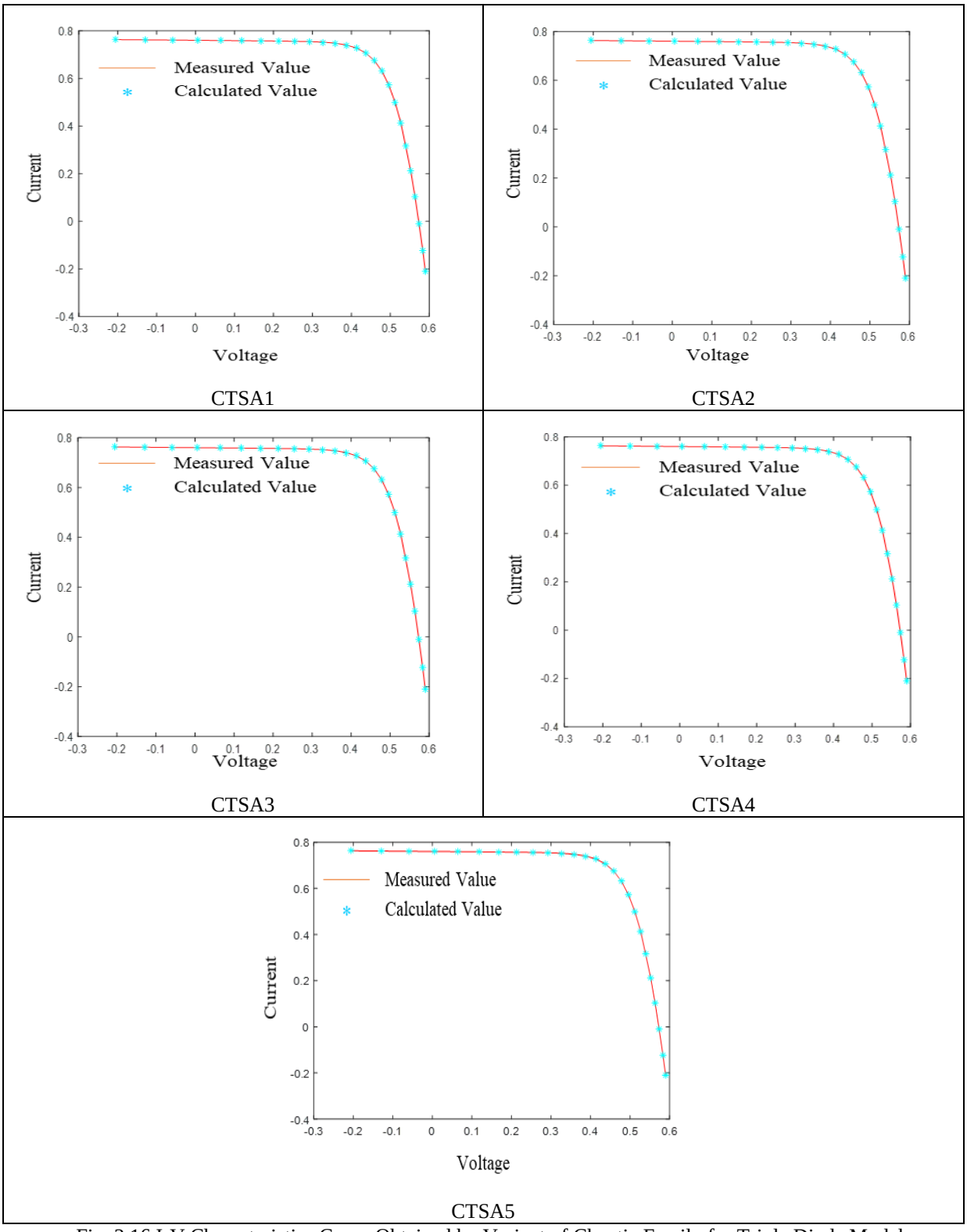

Fig. 2.16 I-V Characteristics Curve Obtained by Variant of Chaotic Family for Triple Diode Model

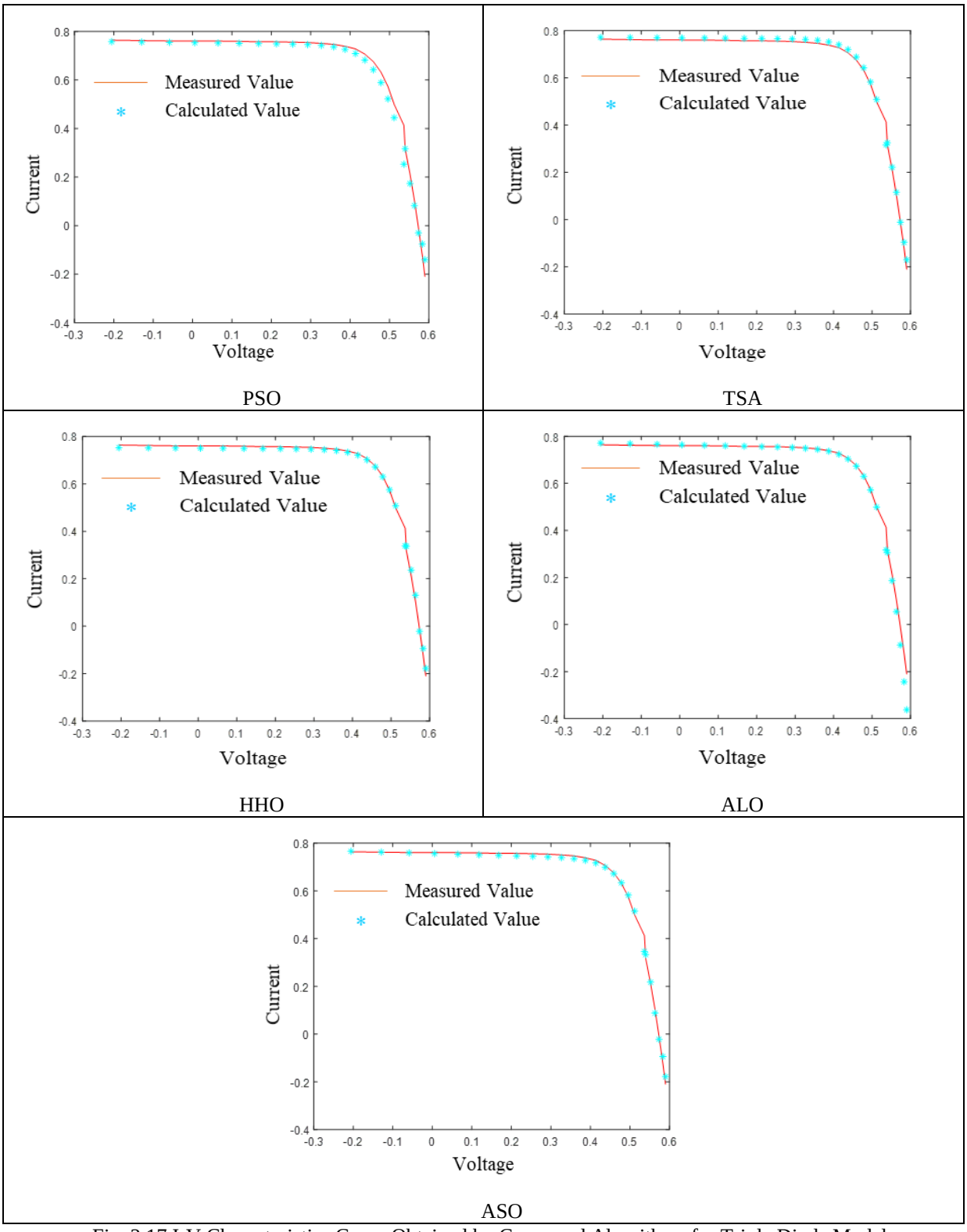

Fig. 2.17 I-V Characteristics Curve Obtained by Compared Algorithms for Triple Diode Model

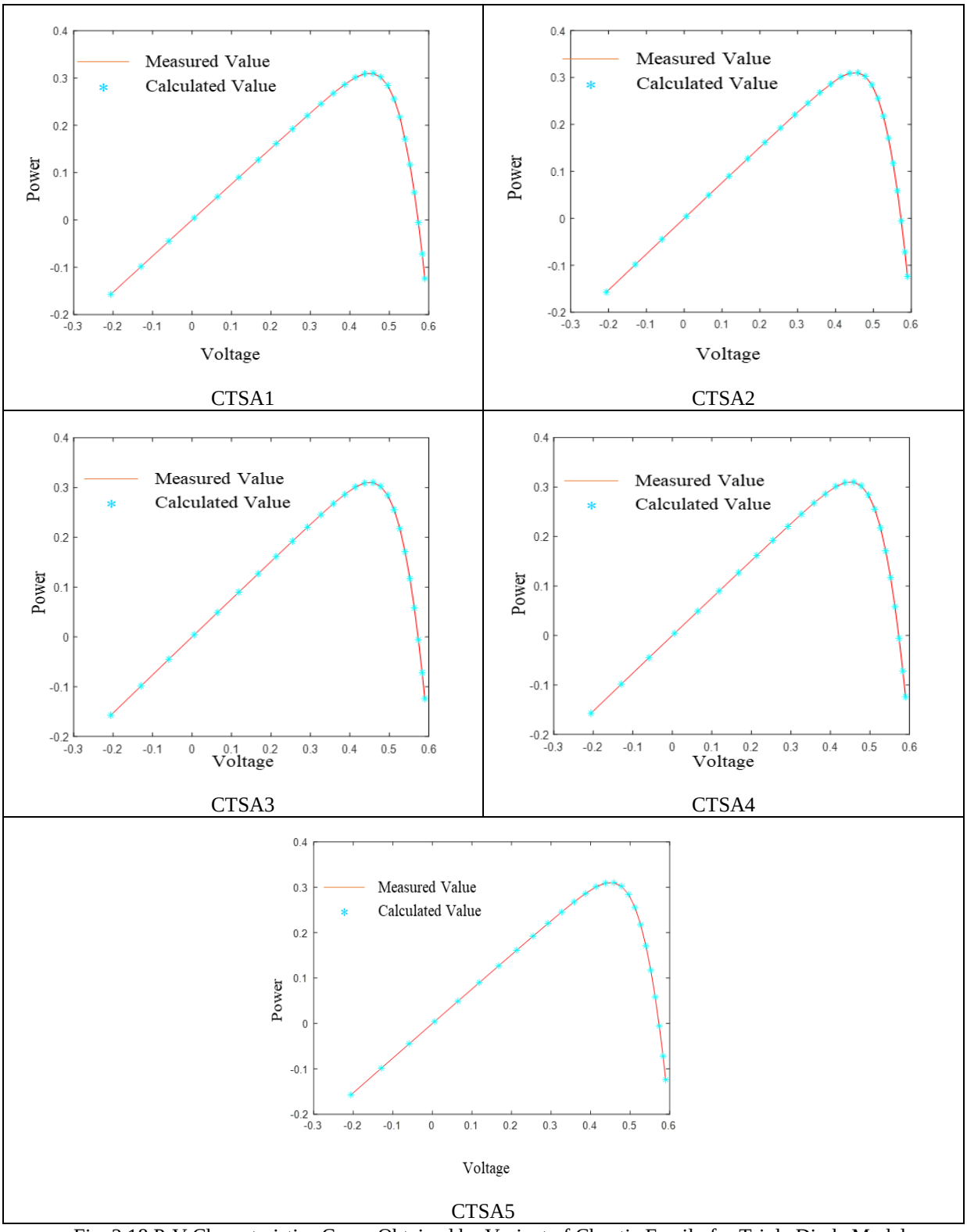

Fig. 2.18 P-V Characteristics Curve Obtained by Variant of Chaotic Family for Triple Diode Model

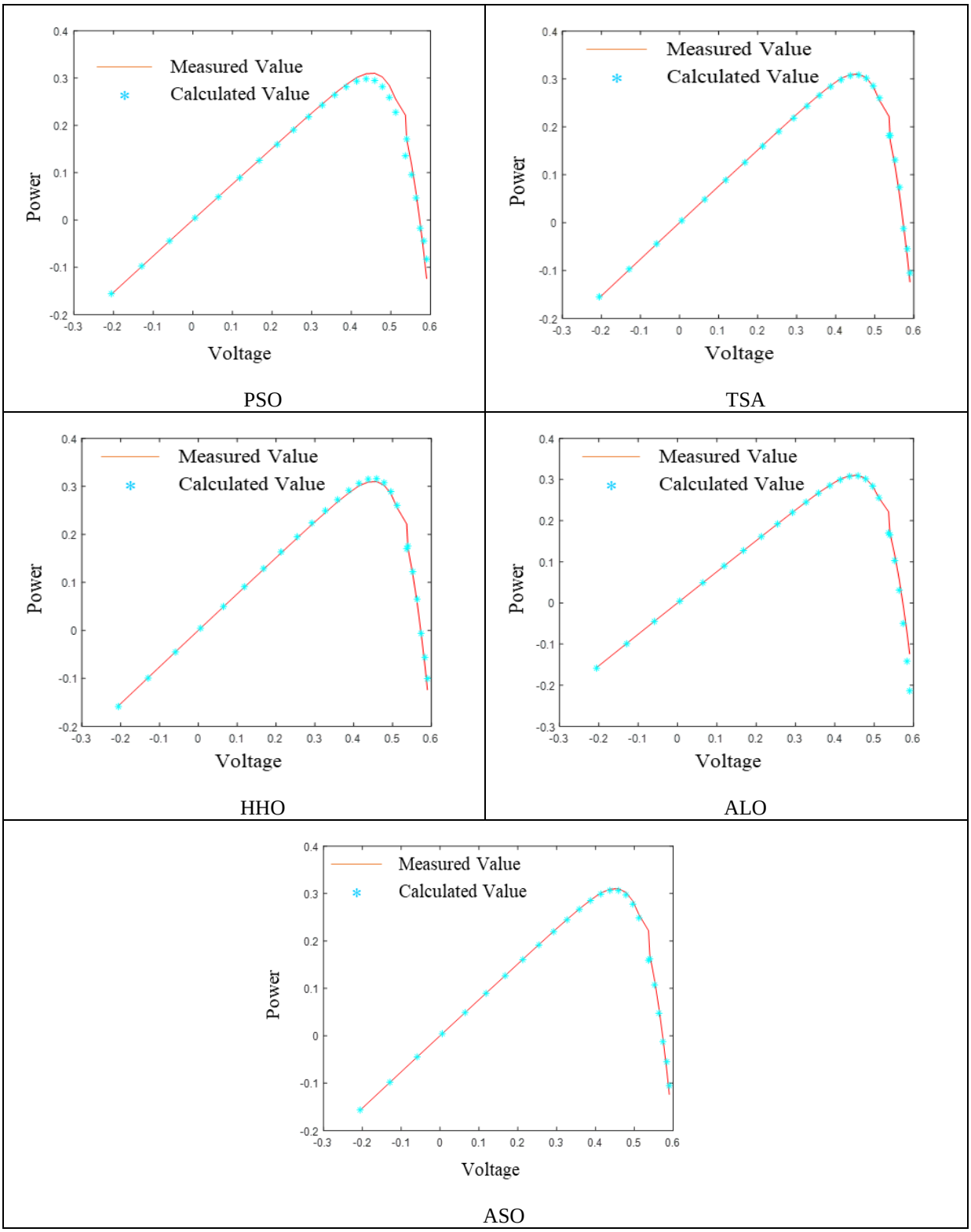

Fig. 2.19 P-V Characteristics Curve Obtained by Compared Algorithms for Triple Diode Model

Table 2.20 represents the parameter estimation of triple diode for solar PV cell at different temperature with RMSE. Variation of the RMSE depicts the output pattern of the PV cells.

Table 2.20 Temperature Analysis of Triple Diode Solar PV cell

Temperature→	**-5 ºC**	**0 ºC**	**5 ºC**	**10 ºC**	**15 ºC**	**20 ºC**	**25 ºC**	**30 ºC**	**Algorithm↓**
	268.15 K	**273.15K**	**278.15 K**	**283.15 K**	**288.15 K**	**293.15 K**	**298.15 K**	**303.15 K**	
Parameters↓									
$\mathbf{I_{pv}}$	0.9616	0.8948	0.9522	0.7695	0.8644	0.9616	0.8948	0.9522	
$\boldsymbol{\alpha_1}$	1.5634	1.4970	1.7744	1.4846	1.4530	1.3791	1.4579	1.7025	
$\boldsymbol{\alpha_2}$	1.2714	1.3783	1.3138	1.9969	1.5974	1.4043	1.1250	1.5969	
$\boldsymbol{\alpha_3}$	1.5684	1.5122	1.5389	1.4531	1.4916	1.3308	1.7969	1.2469	
$\mathbf{R_S}$	0.1508	0.1431	0.1512	0.1325	0.1265	0.1643	0.1247	0.1643	
$\mathbf{R_{Sh}}$	21.5369	28.5254	30.3881	34.4369	31.5616	19.9254	24.1553	31.5281	**CTSA1**
$\mathbf{I_{o1}}$	0.9127	0.4248	0.5298	0.7789	0.7120	0.7127	0.7197	0.4723	
$\mathbf{I_{o2}}$	0.3578	0.2643	0.9788	0.6514	0.4473	0.8000	0.5968	0.7513	
$\mathbf{I_{o3}}$	0.7172	0.7783	0.5491	0.7975	0.2017	0.3172	0.2912	0.4427	
RMSE Error	2.8034 E-07	2.8772E -07	4.5039 E-07	5.0714 E-07	5.1378 E-07	5.9011 E-07	6.7633 E-07	9.6688 E-07	
$\mathbf{I_{pv}}$	0.9320	0.8042	0.7898	0.7045	0.8588	0.8261	0.7431	0.6944	
$\boldsymbol{\alpha_1}$	1.0410	1.3305	1.2029	1.1975	1.3698	1.5140	1.3685	1.0300	
$\boldsymbol{\alpha_2}$	1.4369	1.1590	1.1124	1.3460	1.0881	1.1397	1.1081	1.0368	
$\boldsymbol{\alpha_3}$	1.3333	1.0431	1.2477	1.1370	1.3969	1.3157	1.3070	1.0048	
$\mathbf{R_S}$	0.1039	0.0113	0.1463	0.0180	0.1463	0.0048	0.0410	0.0132	
$\mathbf{R_{Sh}}$	13.9521	38.9387	24.4191	26.9191	19.5972	25.3826	42.0647	25.4627	**CTSA2**
$\mathbf{I_{o1}}$	0.7925	0.6427	0.4932	0.3072	0.5490	0.4755	0.4751	0.4218	
$\mathbf{I_{o2}}$	0.7772	0.4472	0.7164	0.4148	0.5478	0.5931	0.4479	0.1825	
$\mathbf{I_{o3}}$	0.5431	0.2764	0.4970	0.3844	0.8648	0.7827	0.4224	0.4037	
RMSE Error	1.6742 E-06	1.78245 E-06	2.9497 E-06	3.3387 E-06	4.9807 E-06	6.1978 E-06	6.7258 E-06	9.4766 E-06	
$\mathbf{I_{pv}}$	0.9154	0.9209	0.8451	0.8948	0.8915	0.9181	0.9661	0.8966	
$\boldsymbol{\alpha_1}$	1.3659	1.1972	1.3333	1.4912	1.7969	1.7793	1.4282	1.3579	
$\boldsymbol{\alpha_2}$	1.3125	1.5968	1.706	1.3991	1.2912	1.5702	1.3180	1.5969	
$\boldsymbol{\alpha_3}$	1.4058	1.4015	1.1667	1.3969	1.6247	1.6073	1.4974	1.2043	
$\mathbf{R_S}$	0.1251	0.1291	0.0833	0.1247	0.1271	0.1305	0.1039	0.2463	
$\mathbf{R_{Sh}}$	21.4179	8.5989	20.4951	20.6995	21.6605	13.0941	22.9049	32.6445	**CTSA3**
$\mathbf{I_{o1}}$	0.5544	0.0620	0.5939	0.4291	0.5631	0.7891	0.7835	0.7625	
$\mathbf{I_{o2}}$	0.5778	0.4512	0.2560	0.7343	0.5969	0.4205	0.6641	0.5512	

$\mathbf{I_{o3}}$	0.4404	0.6309	0.5977	0.5130	0.4979	0.4962	0.8333	0.9691	
RMSE Error	4.0548 E-07	4.4421E -07	5.6346 E-07	7.7504 E-07	8.8875 E-07	8.9438 E-07	8.9758 E-07	9.6712 E-07	
$\mathbf{I_{pv}}$	0.7780	0.8647	0.6964	0.8068	0.6821	0.8180	0.7676	0.7894	**CTSA4**
$\boldsymbol{\alpha_1}$	1.1191	1.4175	1.1440	1.2000	1.0303	1.2176	1.1530	1.3063	
$\boldsymbol{\alpha_2}$	1.3140	1.4047	1.1975	1.1795	1.0606	1.3794	1.3103	1.4853	
$\boldsymbol{\alpha_3}$	1.0779	1.1305	1.0904	1.3820	1.2657	1.1461	1.1588	1.0351	
$\mathbf{R_S}$	0.1051	0.1274	0.156	0.1297	0.1427	0.1118	0.1091	0.0079	
$\mathbf{R_{Sh}}$	35.635 2	16.4722	55.367 9	41.830 5	25.308 3	53.458 4	48.206 6	42.506 9	
$\mathbf{I_{o1}}$	0.6680	0.3190	0.3711	0.0763	0.4692	0.6594	0.7437	0.7272	
$\mathbf{I_{o2}}$	0.3272	0.6000	0.4800	0.4816	02868	0.7504	0.4831	0.4899	
$\mathbf{I_{o3}}$	0.4355	0.7534	0.3060	0.7222	0.4650	0.7220	0.3853	0.6522	
RMSE Error	1.8898 E-06	2.7301E -07	2.7415 E-07	3.0647 E-07	3.5486 E-07	3.8439 E-07	4.3983 E-07	5.9893 E-07	
$\mathbf{I_{pv}}$	0.8546	0.8407	0.8476	0.6529	0.6369	0.6863	0.5908	0.7992	**CTSA5**
$\boldsymbol{\alpha_1}$	1.1795	1.3593	1.1969	1.3232	1.0227	1.1969	1.1579	1.3753	
$\boldsymbol{\alpha_2}$	1.2979	1.0029	1.4530	1.1140	1.0205	1.2179	1.2343	1.5530	
$\boldsymbol{\alpha_3}$	1.0049	1.5789	1.2349	1.3006	1.5395	1.2527	1.0577	1.3698	
$\mathbf{R_S}$	0.1463	0.0440	0.1473	0.0537	0.1046	0.1473	0.1046	0.0251	
$\mathbf{R_{Sh}}$	34.893 0	30.2536	29.026 7	32.351 5	21.472 4	43.525 6	23.625 5	37.812 4	
$\mathbf{I_{o1}}$	0.6007	0.6960	0.5841	0.3104	0.4474	0.5344	0.3094	0.7640	
$\mathbf{I_{o2}}$	0.3231	0.6001	0.5017	0.3777	0.4246	0.4015	0.2244	0.6938	
$\mathbf{I_{o3}}$	0.5194	0.3276	0.6315	0.1308	0.2994	0.3940	0.3117	0.5020	
RMSE Error	2.2786 E-06	2.7451E -06	2.9074 E-06	3.0582 E-06	3.3923 E-06	5.4392 E-06	6.9317 E-04	8.9966 E-06	

- **Non-Parametric Tests**

The three non-parametric tests are performed. First the statistical result of Friedman ranking test as shown in Table 2.21 [112]. From this test, it is clear that the first rank is secured by CTSA4, second rank is secured by CTSA1, and third rank is secured CTSA3 with CTSA2, CTSA5, TSA, HHO, ASO, ALO and PSO to follow.

Table 2.21 Friedman Ranking Test for Triple Diode Solar PV Cell at STC

Algorithms	Friedman Ranking
CTSA1	2
CTSA2	4
CTSA3	3
CTSA4	1
CTSA5	5
PSO	10
TSA	6
HHO	7
ALO	9
ASO	8

Second non-parametric test done is Wilcoxon's rank sum test [113]. Wilcoxon's rank sum test is applied in comparison of all variants of chaotic family with all rest of the compared algorithms as shown in Table 2.22 for the solar PV model.

Table 2.22 Wilcoxon's Rank Sum Test p Values of Triple Diode Model

Algorithms	PSO	TSA	HHO	ALO	ASO
CTSA1	1.3871E-11	1.3628E-11	1.3806E-11	1.3822E-11	1.3847E-11
CTSA2	1.3961E-11	1.3717E-11	1.3896E-11	1.3912E-11	1.3936E-11
CTSA3	1.3896E-11	1.3653E-11	1.3830E-11	1.3847E-11	1.3871E-11
CTSA4	1.3953E-11	1.3709E-11	1.3887E-11	1.3904E-11	1.3928E-11
CTSA5	1.3896E-11	1.3653E-11	1.3830E-11	1.3847E-11	1.3871E-11

Last non-parametric test performed is Kruskal-Wallis test [114]. The list of graphs obtained from the research, as well as the CTSA mean and median rank is seen in Fig. 2.20 and Fig. 2.21, showing that CTSA results are substantially different from those of other groups. The findings of the Anova Kruskal-Wallis test are shown in Table 2.23. The probability chi square value is calculated using this test which is 175. With a significance level of 95 percent, this test proves that all variants of CTSA outperform the other compared algorithms. From the Table 2.23, the significance of the degree of freedom (DF) refers to the maximum number of logically independent values, which are values that have the freedom to vary, in the data sample. Similarly, the significance of sum of squares (SS) express the total variation that can be attributed to various factors. The significance of the mean squares (MS) used to determine whether factors are significant or not. This non-parametric test explicitly shows that a recently developed chaotic family variant is much more reliable and precise than the other algorithms.

Outcome of all the non-parametric test justifies the higher accuracy and reliability of the proposed algorithm as compared to other algorithms.

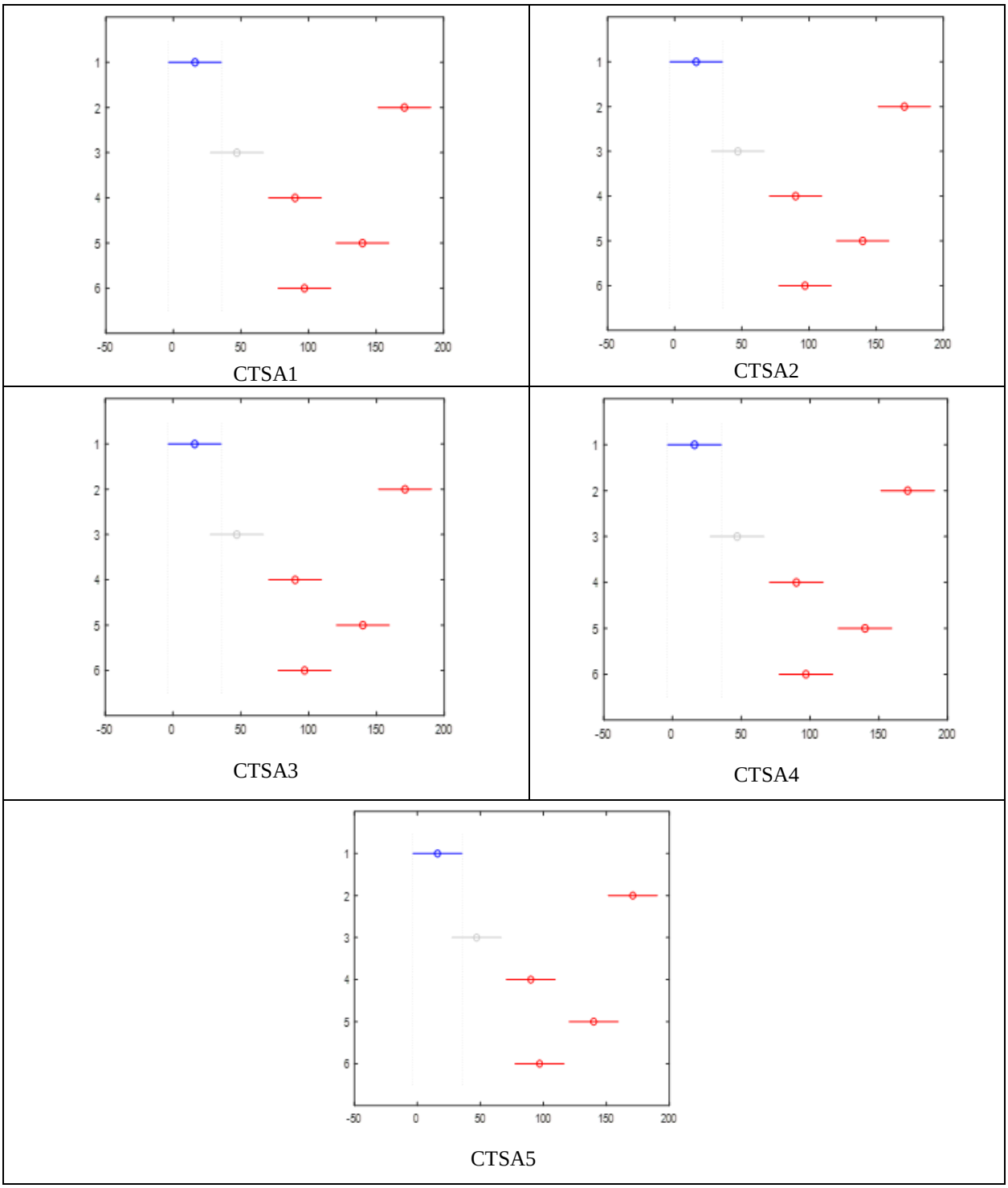

Fig. 2.20 Multiple Comparisons of Mean Ranks using Kruskal-Wallis Test for Triple Diode Model

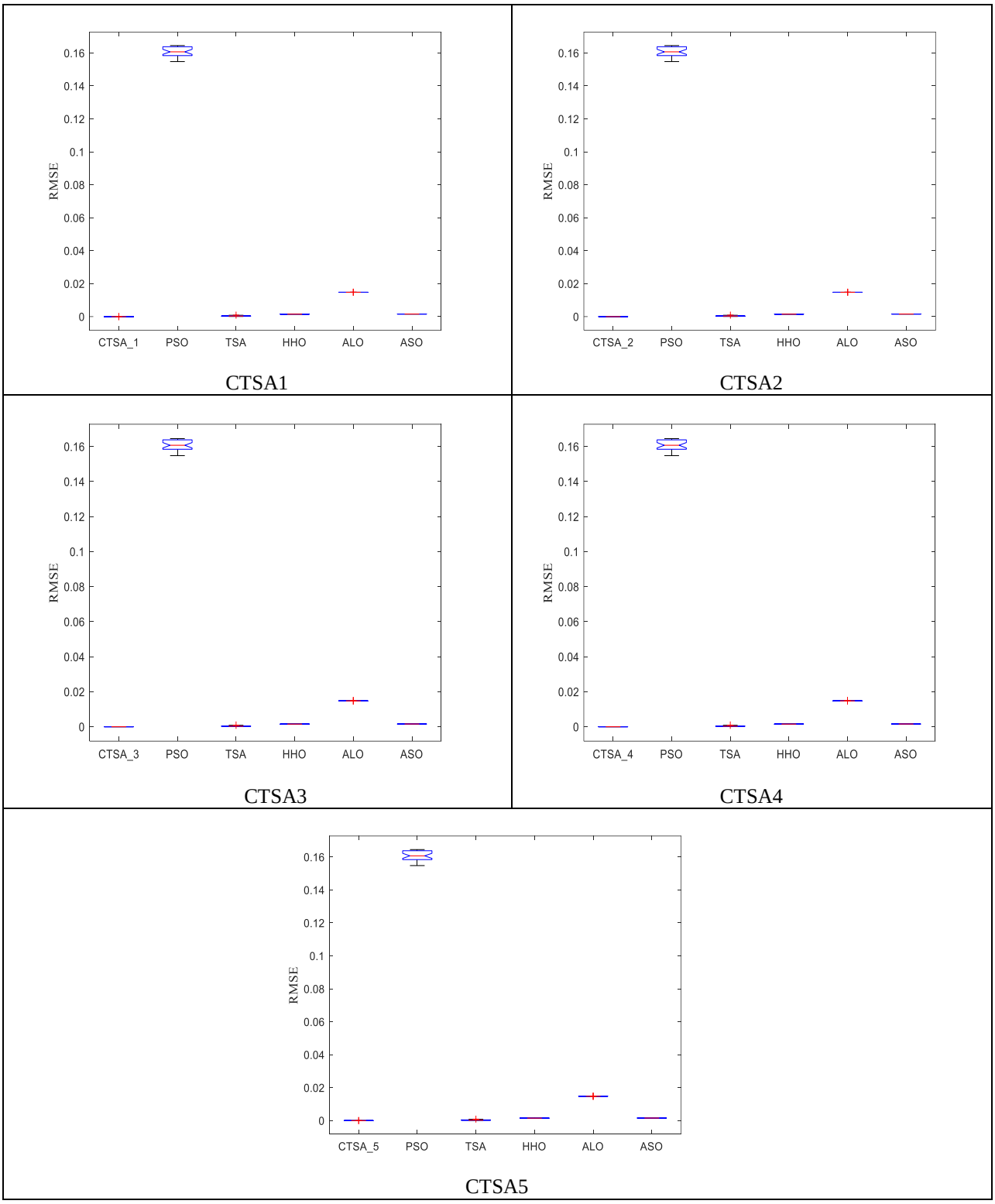

Fig. 2.21 Multiple Comparisons of Median Rank using Kruskal-Wallis Test for Triple Diode Model

Table 2.23 Annova Kruskal-Wallis Test for Triple Diode Model

SOURCE	SS	DF	MS	Chi-sq	Prob>Chi-sq	Algorithms
Columns	507199.5	5	101439.9	175	6.24887E-36	**CTSA1**
Error	28979.5	180	161	-	-	
Total	536179	185	-	-	-	
Columns	507199.5	5	101439.9	175	6.25435E-36	**CTSA2**
Error	28985	180	161	-	-	
Total	536184.5	185	-	-	-	
Columns	507199.5	5	101439.9	175	6.25034E-36	**CTSA3**
Error	28981	180	161	-	-	
Total	536180.5	185	-	-	-	
Columns	507199.5	5	101439.9	175	6.25385E-36	**CTSA4**
Error	28984.5	180	161	-	-	
Total	536184	185	-	-	-	
Columns	507199.5	5	101439.9	175	6.25034E-36	**CTSA5**
Error	28981	180	161	-	-	
Total	536180.5	185	-	-	-	

2.3.2 Chicken Swarm Optimization

Chicken swarm optimization (CSO) is a newly developed metaheuristic bio-inspired algorithm [115]. CSO is inspired by the behaviours and the hierarchical structure of swarm of chicken during the food search, where individual chicken denotes a possible solution to an optimization problem. For simplicity, to idealize the behaviour of chickens the mentioned algorithm assumes the following four rules, which are described below.

(a) Swam of chicken is mainly comprised of several groups. Each group comprises a dominant rooster and a couple of hens and chicks.

(b) Fitness values of the chicken swam lead to the formation of groups and their identification as rooster, hen, and chicks. The rooster is the group head so the chicken with the fittest value is declared as the group head or rooster of a particular group. The chickens with the poorest fittest value would be declared as chicks and the rest chicken is declared as hens. Further, the number of chicks should be less than the number of hens.

(c) Rooster and hen relationships are established randomly so the hen could choose any group randomly to stay within. Similarly, the mother hens and child chick relationship is also established abruptly. The hierarchal order, dominance relationship, and mother-child relationship in each group will remain touched within G iterations. Every update in their statues

takes place after several time iterations to uphold the population diversity and to reduce any chance of local convergence.

(d) Hens follow their dominant rooster and chick follow their mother hen for the search of food, though they may preclude the ones from eating their food. It is assumed that the dominant rooster of each group would arbitrarily rob the good food that is already found by another rooster.

Further, *RN*, *HN*, *CN*, and *MN* represent the number of roosters, the hens, the chicks, and the mother hens, respectively. This has the fittest value among chicken, so it is presumed to be the head of the rooster of the group, where the *CN* is the worst ones so it would be referred to as chicks. The left ones are assumed as hens. N is the population size, D is the individual dimension and the individual position can be represented by $x_i^j(t)(i \in [1,\cdots,N],\ j \in [1,\cdots,D]$ in the t[th] iteration. The position update of the rooster could be described in equation 2.25-2.26 as follows:

$$x_i^j(t+1) = x_i^j(t) * [1 + N(0,\sigma^2)] \tag{2.25}$$

$$\sigma^2 = \begin{Bmatrix} 1 & f_i \le f_k \\ exp\left[\frac{(f_k - f_i)}{|f_i + \varepsilon|}\right] & otherwise \end{Bmatrix} \tag{2.26}$$

$$k \in [1, RN]\ , k \neq i$$

Where $N(0,\sigma^2)$ the Gaussian distribution and 0 is is the mean and σ^2 is the variance, ε denotes the smallest constant to avoid zero division error, 'k' denotes the index of the rooster from other groups, 'f' symbolizes the fitness of individual chicken correspondingly.

The position update of the hen could be described in equation 2.27-2.29 as follows:

$$x_i^j(t+1) = x_i^j(t) + S_1 * rand * \left[x_{r1}^j(t) - x_i^j(t)\right] + S_2 * rand * \left[x_{r2}^j(t) - x_i^j(t)\right] \tag{2.27}$$

$$S_1 = exp\left\{\frac{(f_i - f_{r1})}{[abs(f_i) + \varepsilon]}\right\} \tag{2.28}$$

$$S_2 = \exp(f_{r2} - f_i) \tag{2.29}$$

Where $rand$ denotes the uniformly distributed random number within [0,1], $r1 \in [1,\cdots,N]$is an index of the rooster which is the group-mate of the hen ith, $r2 \in [1,\cdots,N]$is an index of the chicken (rooster or hen) which is randomly selected from the swarm and $r_1 \neq r_2$.

The position update of the chicks could be described in equation 2.30

$$x_i^j(t+1) = x_i^j(t) + FL \times \left[x_m^j(t) - x_i^j(t)\right] \tag{2.30}$$

Where m indicates the mother hen of the i^{th} chick and *FL* is a parameter that implies the chick would follow their mother for foraging of food. Considering the individual differences, the value

of *FL* for each chick is made to vary between 0 and 2. Pseudo code of CSO is described in Fig. 2.22. Flow chart of CSO is presented in Fig. 2.23.

A population of 'N' chickens is initialized and the related parameters are defined;

Obtain the fitness values of 'N' chickens, *t=0;*

While (t < Max_Iterations)

If (t % G = = 0)

Rank the fitness values of the chickens and establish the hierarchal order in the swarm;

Divide the swarm into different groups, and obtain the relationship between the chicks and mother hens in a group;

End if

For *i = 1 : N*

If *i* = = rooster (Update its position);

End if

If *i* = = hen (Update its position);

End if

If *i* = = chick (Update its position);

End if

Evaluate the new solution;

If the new solution is better than the previous, update the solution;

End for

End while

Fig. 2.22 Pseudo code of CSO

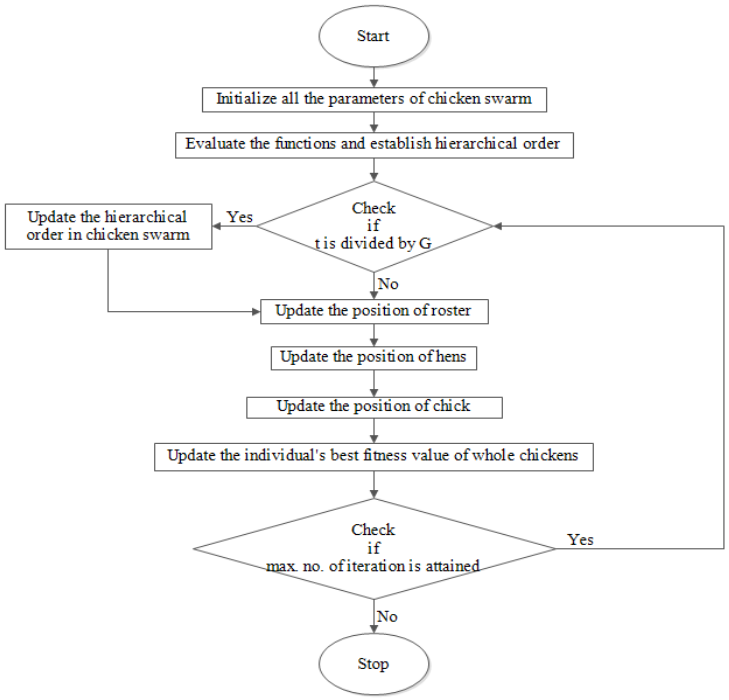

Fig.2.23 Flow Chart of CSO

- **New Chaotic Chicken Swarm Optimization (CCSO) Technique**

The benefit of the chaotic maps in metaheuristic algorithms is well explored in the literature [111]. The problem of the CSO to get stuck in the local minimum is eliminated with the help of chaotic maps to assist the CSO algorithm to explore the search space in a better way. In this algorithm, the parameter *FL* is used in equation (2.30) of the classical CSO method, is varied chaotically using the ten maps to yield better results as compared to the original approach. The pseudo-code of the proposed technique is shown in Fig. 2.24 for a better understanding of the readers along with this flow chart of CCSO is also presented in Fig. 2.25. Ten chaotic maps as well as referred algorithms are explained in Table 2.24.

A population of 'N' chickens is initialized and the related parameters are defined;

Obtain the fitness values of 'N' chickens, *t=0;*

While (t < Max_Iterations)

If (t % G = = 0)

Rank the fitness values of the chickens and establish the hierarchal order in the swarm;

Divide the swarm into different groups, and obtain the relationship between the chicks and mother hens in a group;

End if

For *i = 1 : N*

If *i* = = rooster (Update its position);

End if

If *i* = = hen (Update its position);

End if

If *i* = = chick (Update its position);

[FL parameter in chick position is chaotically varied instead of conventional CSO]

End if

Evaluate the new solution;

If the new solution is better than the previous, update the solution;

End for

End while

Fig. 2.24 Pseudo code of CCSO

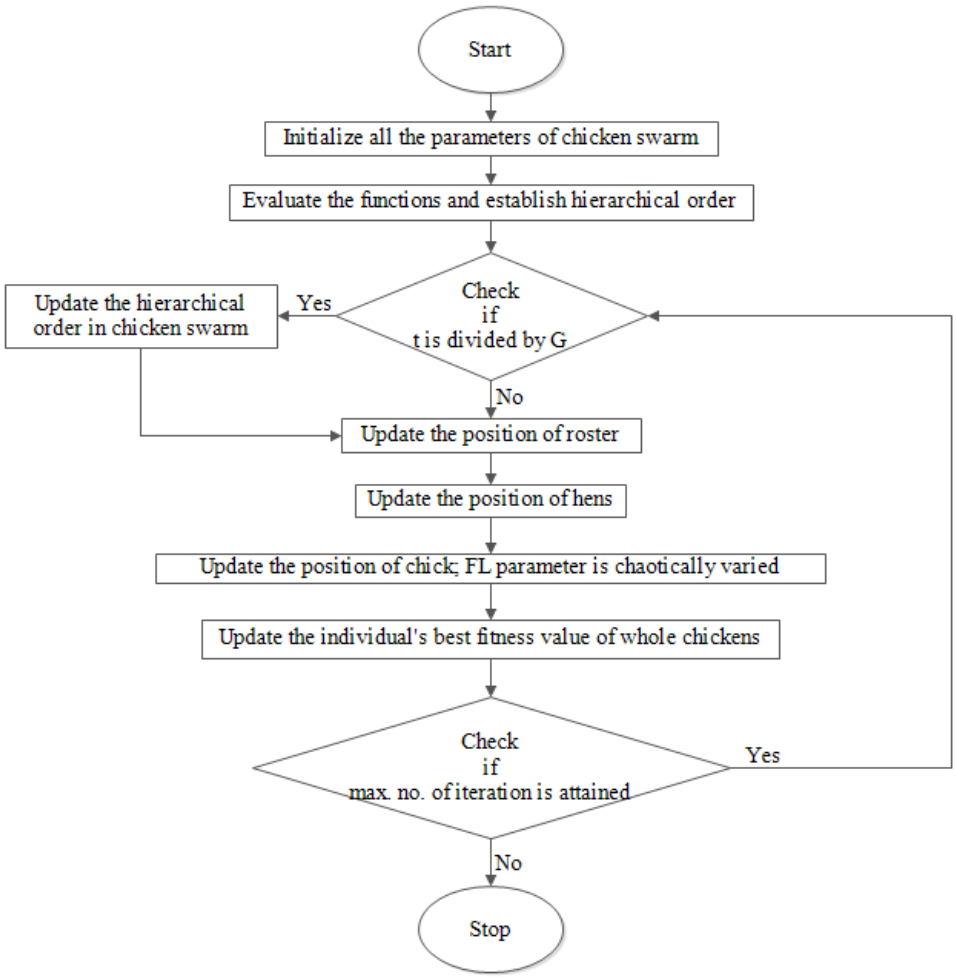

Fig. 2.25 Flow Chart of CCSO

Table 2.24 List of Chaotic Maps

Map Name	Definition	Referred Algorithm
Chebyshev map	$x_{k+1} = \cos(k \cos^{-1}(x_k))$	**CCSO1**
Circle map	$x_{k+1} = x_k + \mathrm{b} - (\mathrm{a} - 2\pi)\sin(2\pi x_k) mod(1)$	**CCSO2**
Gauss map	$x_{k+1} = \begin{cases} 0 & x_k = 0 \\ 1/x_k mod(1) & otherwise \end{cases}$	**CCSO3**
Iterative map	$x_{k+1} = \sin(a\pi/x_k)$	**CCSO4**
Logistic map	$x_{k+1} = a x_k(1 - x_k)$	**CCSO5**
Piecewise map	$x_{k+1} = \begin{cases} \frac{x_k}{P} & 0 \le x_k < P \\ \frac{x_k - P}{0.5 - P} & P \le x_k < 0.5 \\ \frac{1 - P - x_k}{0.5 - P} & 0.5 \le x_k < 1 - P \\ \frac{1 - x_k}{P} & 1 - P \le x_k < 1 \end{cases}$	**CCSO6**
Sine map	$x_{k+1} = \frac{a}{4}\sin(\pi x_k)$	**CCSO7**

Singer map	$x_{k+1} = \mu(7.86x_k - 23.31x_k^2 + 28.75x_k^3 - 13.3028.75x_k^4$	**CCSO8**
Sinusoidal map	$x_{k+1} = ax_k^2 \sin(\pi\, x_k)$	**CCSO9**
Tent map	$x_{k+1} = \begin{cases} \frac{x_k}{0.7} x_k < 0.7 \\ \frac{10}{3}(1 - x_k) \quad x_k \geq 0.7 \end{cases}$	**CCSO10**

2.3.2.1 Outcomes of CCSO

In this section, three famous commercial modules are utilized for the estimation of the parameters of the TDM model. In this regard, the practical PV modules are CS6K 280M [107], KC200GT [66], and MSX-60 [66], which are fabricated by Canadian, Kyocera, and Solarex, respectively. Table 2.25 illustrates the values of the electrical performance of the mentioned commercial PV modules under the STC condition.

Table 2.25 Datasheet Values of PV Modules at STC Conditions

Company	**Canadian solar**	**Kyocera**	**Solarex**
Model	**CS6K-280M**	**KC200GT**	**MSX-60**
Cell type	**Mono-crystalline**	**Multicrystal**	**Poly-crystalline**
Pm [W]	280	200	60
Vm [V]	31.5	26.3	17.1
Im [A]	8.89	7.61	3.5
Vo [V]	38.5	32.9	21.1
Isc [A]	9.43	8.21	3.8
Ns[cells]	60	54	36
Ki	0.053%/°C	0.00318A/°C	0.065%/°C
Kv	−0.31%/°C	−0.123V/°C	−0.08V/°C

The number of search agents considered for the experiments is 50 and the maximum iteration is taken as 1000 for all the algorithms. The results of the proposed heuristic algorithm are compared with the other algorithms namely (CSO, DA, ALO, MVO, WOA, GOA, SCA, SSA, HHO, and ASO). The electrical parameters of the TDM are evaluated with the proposed method as well as the algorithms meant for comparison. The metaheuristic approaches used to obtain the parameters are stochastic i.e. their outcomes change on every test run. Hence, there is the requirement of finding some popular statistical measures of the error function for a set of independent test runs. Thus, 30 test runs are carried out to get meaningful statistical measures. The minimum and the maximum value as the average and the standard deviation of the error functions are thus recorded. Besides, non-parametric tests (Wilcoxon's rank-sum test, Kruskal-Wallis test, Wilcoxon's rank

test with Holm-Bonferroni correction) are also performed to certify the significances of the obtained results. The results of the test models considered in this work are thus discussed below.

Case 1: In this case Canadian solar (CS6K 280M mono-crystalline) commercial module is examined. All the earlier mention algorithms are executed to extract all the nine parameters of the TDM. Table 2.26 describes the extracted parameters of the Triple Diode Model.

Table 2.26 Parameter Estimation of Triple Diode Model for Canadian Solar Model

Parameters → **Algorithms ↓**	**I_{pv}**	**α_1**	**α_2**	**α_3**	**R_S**	**R_{Sh}**	**I_{o1}**	**I_{o2}**	**I_{o3}**
CCSO1	9.4302	1.7057	1.7495	1.7537	0.0059	411.3706	2.2168E-07	3.9402E-07	5.0675E-07
CCSO2	9.4302	1.6884	1.7412	1.8431	0.0081	456.1701	3.3946E-07	4.3468E-07	3.1319E-07
CCSO3	9.4302	1.5593	1.8777	1.7947	0.0095	446.3377	3.6246E-07	2.4166E-07	3.5841E-07
CCSO4	9.4302	1.6470	1.6948	1.8248	0.0099	446.8661	2.8017E-07	3.2204E-07	3.6688E-07
CCSO5	9.4302	1.7011	1.7236	1.7694	0.0066	432.5930	3.2903E-07	3.9987E-07	3.3506E-07
CCSO6	9.4302	1.6996	1.6713	1.8001	0.0081	417.9113	2.8271E-07	3.7024E-07	4.5862E-07
CCSO7	9.4302	1.8023	1.7156	1.7307	0.0072	415.1717	4.5389E-07	3.9385E-07	4.7702E-07
CCSO8	9.4303	1.7093	1.6845	1.7447	0.0123	421.0451	3.9214E-07	3.4401E-07	3.5347E-07
CCSO9	9.4302	1.7406	1.6909	1.7957	0.0117	441.2769	2.8295E-07	3.7913E-07	4.6381E-07
CCSO10	9.4303	1.7344	1.6349	1.8037	0.0165	387.3281	2.4279E-07	3.3020E-07	3.0763E-07
CSO	9.4376	1.6469	1.8064	1.6449	0.0139	432.4226	3.9518E-07	5.9630E-07	3.3322E-07
DA	9.6699	1.6259	1.6190	1.6970	0.1113	307.1956	3.5008E-07	4.6534E-07	4.8815E-07
ALO	9.4656	1.7093	1.6624	1.7716	0.0128	330.8411	6.1475E-07	6.1565E-07	5.1381E-07
MVO	9.5086	1.5588	1.5704	1.4607	0.0012	236.3761	3.8308E-07	2.8418E-07	3.2500E-07
WOA	9.5761	1.7507	1.5937	1.5514	0.0925	304.4203	5.4441E-07	4.5941E-07	5.0330E-07
GOA	9.6851	1.7206	1.6887	1.7157	0.2185	489.0740	3.8567E-07	3.6657E-07	4.5994E-07
HHO	9.7083	1.6468	1.7031	1.6678	0.2661	315.3751	5.5896E-07	5.6685E-07	5.4425E-07
SCA	9.4827	1.2621	1.2784	1.1406	0.0184	318.5973	1.5203E-07	2.1090E-07	1.6321E-07

SSA	9.5144	1.5928	1.6413	1.6907	0.0678	299.7689	4.3274E-07	4.6313E-07	4.7420E-07
ASO	9.4309	1.6649	1.6284	1.6768	0.0161	318.0123	3.4217E-07	4.4015E-07	3.4157E-07

Table 2.27 shows the statistical results of parameters (minimum, maximum, mean, and standard deviation) of SSE. The outcome of results the least SSE error is obtained by chaotic variants of proposed CSO algorithm in comparison to all compared algorithms. Hence proving the accuracy of proposed algorithm.

Table 2.27 Statistical Results of the SSE for Triple Diode Model for Canadian Solar Model

Statistical Results→ Algorithms↓	**Minimum**	**Average**	**Maximum**	**Standard Deviation**
CCSO1	1.4023E-10	9.5216E-10	5.7216E-10	2.8057E-10
CCSO2	1.0560E-10	8.7443E-10	3.9869E-10	2.4290E-10
CCSO3	1.1183E-10	8.3524E-10	4.7752E-10	2.6303E-10
CCSO4	1.0264E-10	9.5535E-10	3.6780E-10	1.7832E-10
CCSO5	1.4738E-10	9.4900E-10	4.1216E-10	2.4793E-10
CCSO6	1.0088E-10	9.1990E-10	4.3307E-10	2.0608E-10
CCSO7	1.0984E-10	9.2319E-10	4.0673E-10	2.5310E-10
CCSO8	1.0835E-10	9.9470E-10	3.9582E-10	2.6872E-10
CCSO9	1.2123E-10	8.8779E-10	4.2975E-10	2.5122E-10
CCSO10	1.0242E-10	8.2570E-10	3.0926E-10	2.2288E-10
CSO	1.2038E-04	9.2882E-04	3.8389E-04	2.7729E-04
DA	0.1040	0.4080	0.2531	0.0890
ALO	0.0012	0.0095	0.0045	0.0023
MVO	0.0010	0.0096	0.0040	0.0026
WOA	0.0112	0.0952	0.0397	0.0258
GOA	0.0231	0.0935	0.0501	0.0199
SCA	0.0102	0.0861	0.0307	0.0171
SSA	0.0107	0.0804	0.0321	0.0209
HHO	0.1002	0.6044	0.2637	0.1696
ASO	0.0010	0.0096	0.0056	0.0028

Moreover, the convergences curve of the TDM is plotted to prove the significance of the extracted error value. Fig. 2.26 shows the list of convergences curve of each variant of CCSO with other compared algorithms (CSO, DA, ALO, MVO, WOA, GOA, SCA, SSA, HHO, ASO). Similarly, the plot in Fig. 2.26 clearly shows that the proposed methods supersede the algorithms used for comparison. Fig. 2.27 shows the I-V curves of all variants of CCSO. The resultant curves resemble the standard I-V curve of the solar model proving the accuracy of the proposed technique. On a similar note, Fig. 2.28 shows the P-V curves of all variants of CCSO. The curves look very much

similar to the standard P-V curve of the solar model proving the accuracy of the proposed approach.

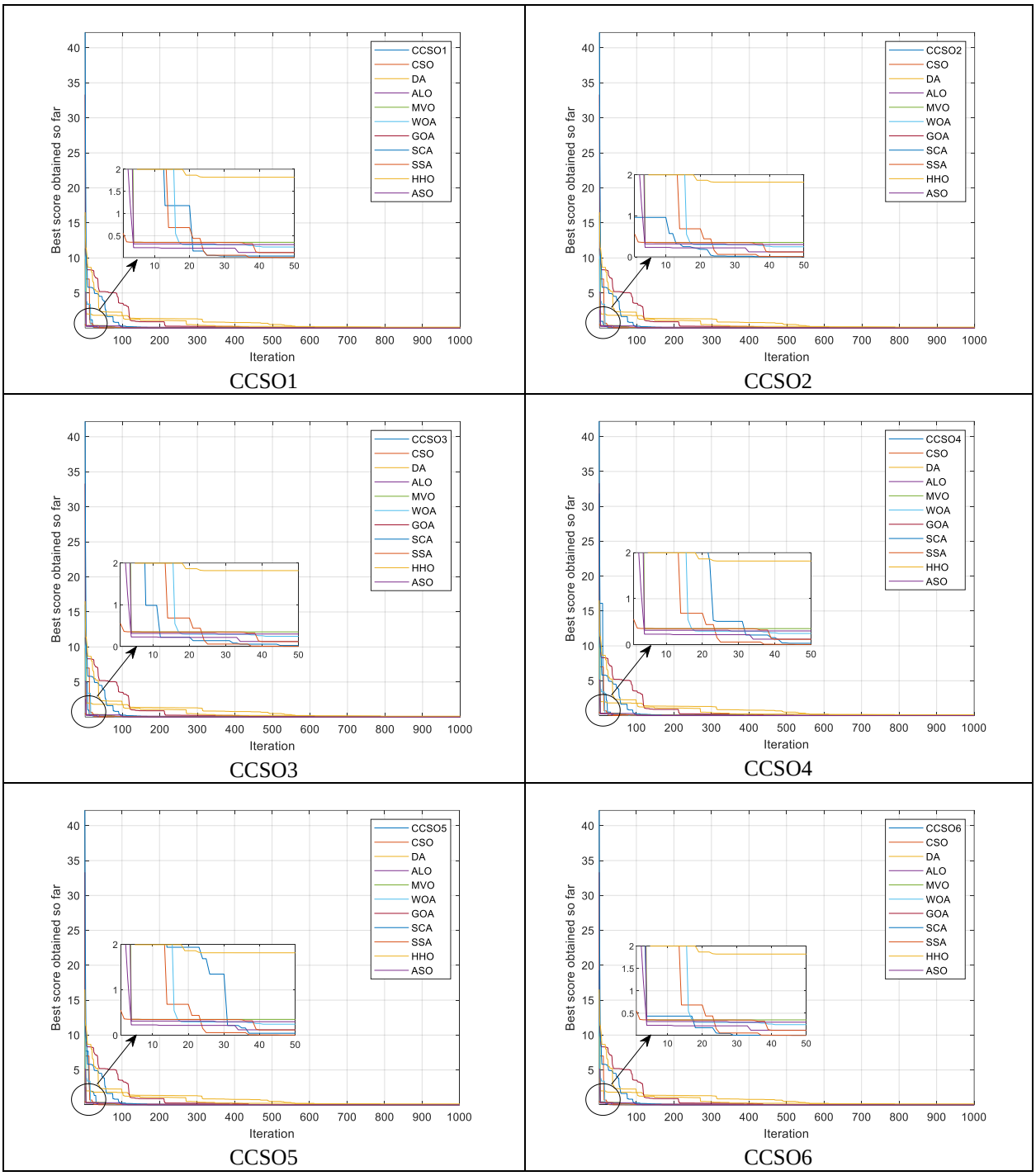

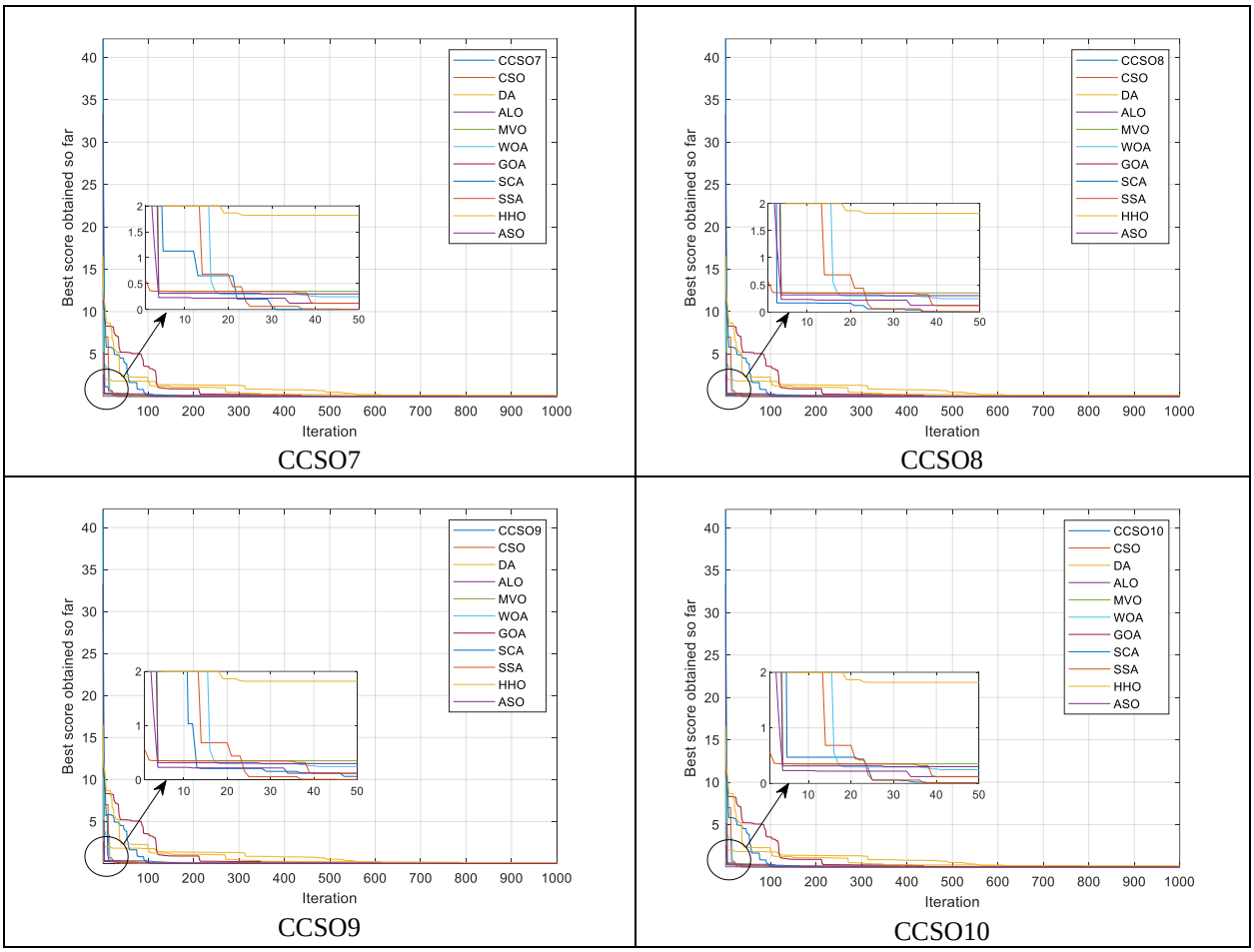

Fig. 2.26 Convergences Curves of the Each Variant of CCSO with Other Compared Algorithm for Canadian Solar Model

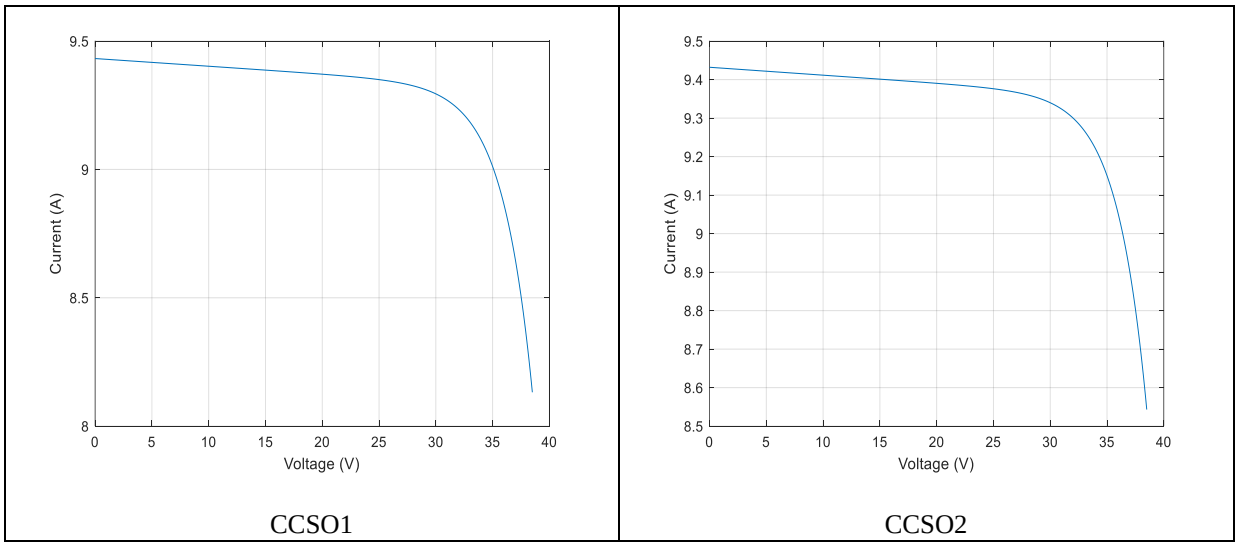

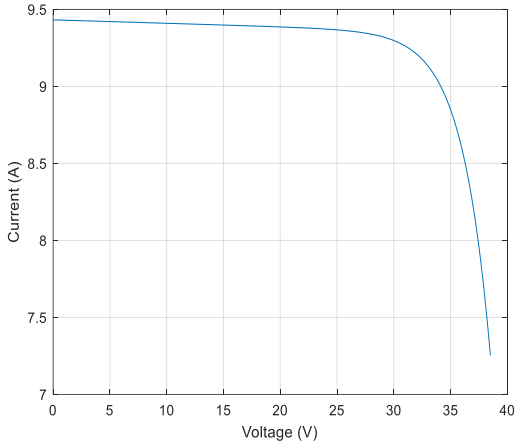

CCSO3

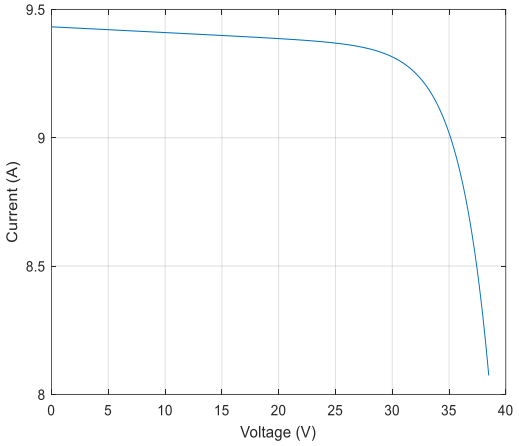

CCSO4

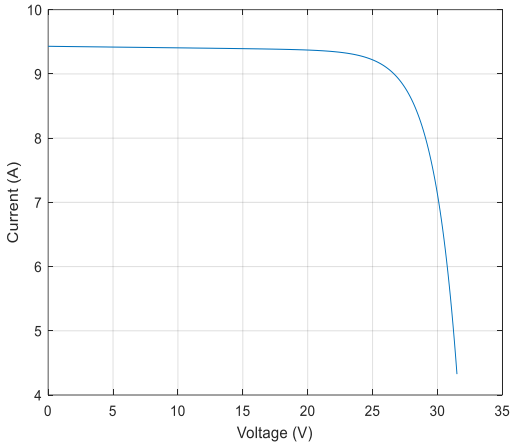

CCSO5

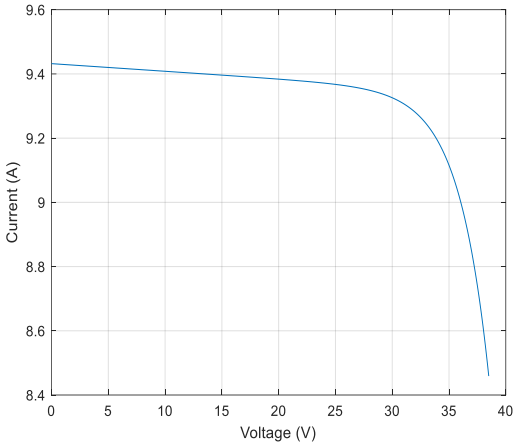

CCSO6

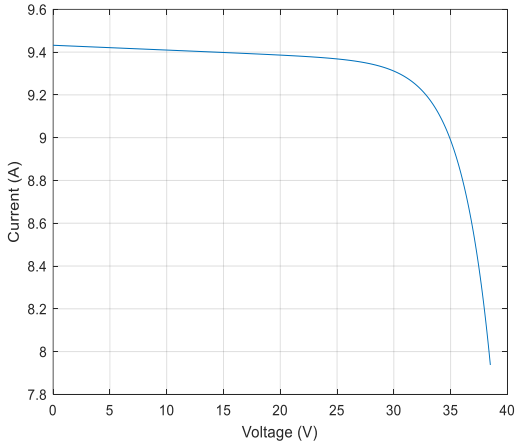

CCSO7

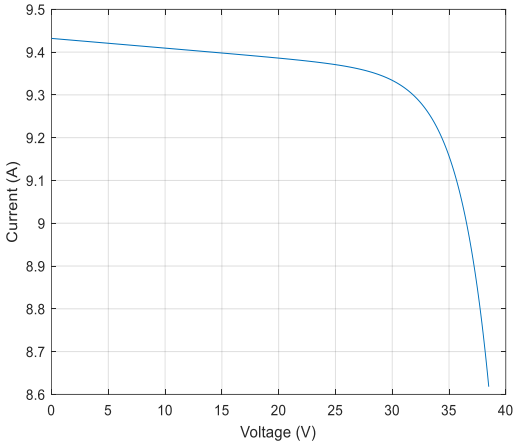

CCSO8

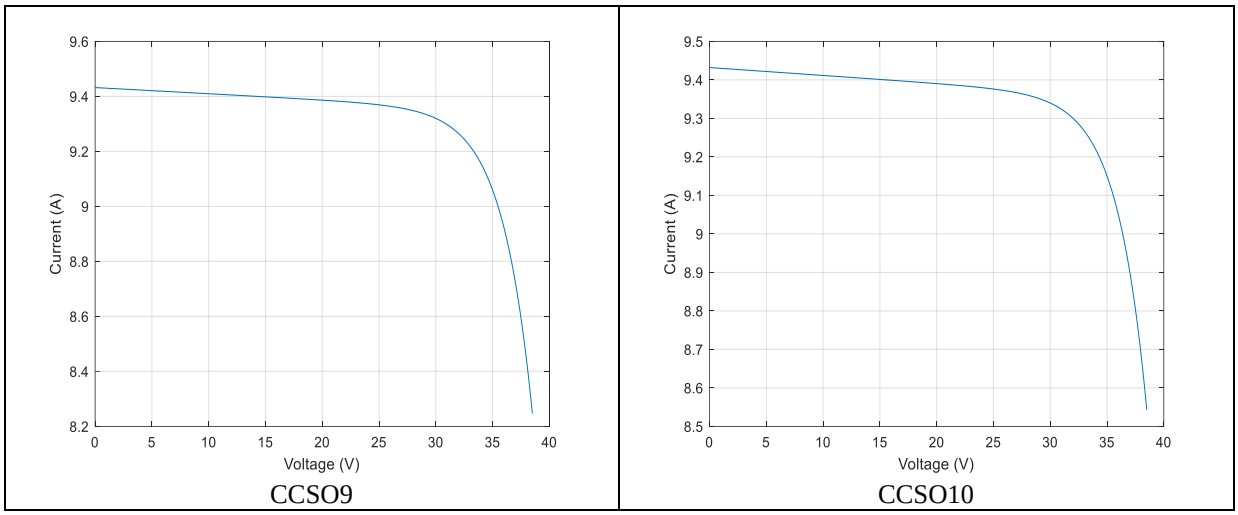

Fig. 2.27 I-V Curves of all the Variants CCSO for Canadian Solar model

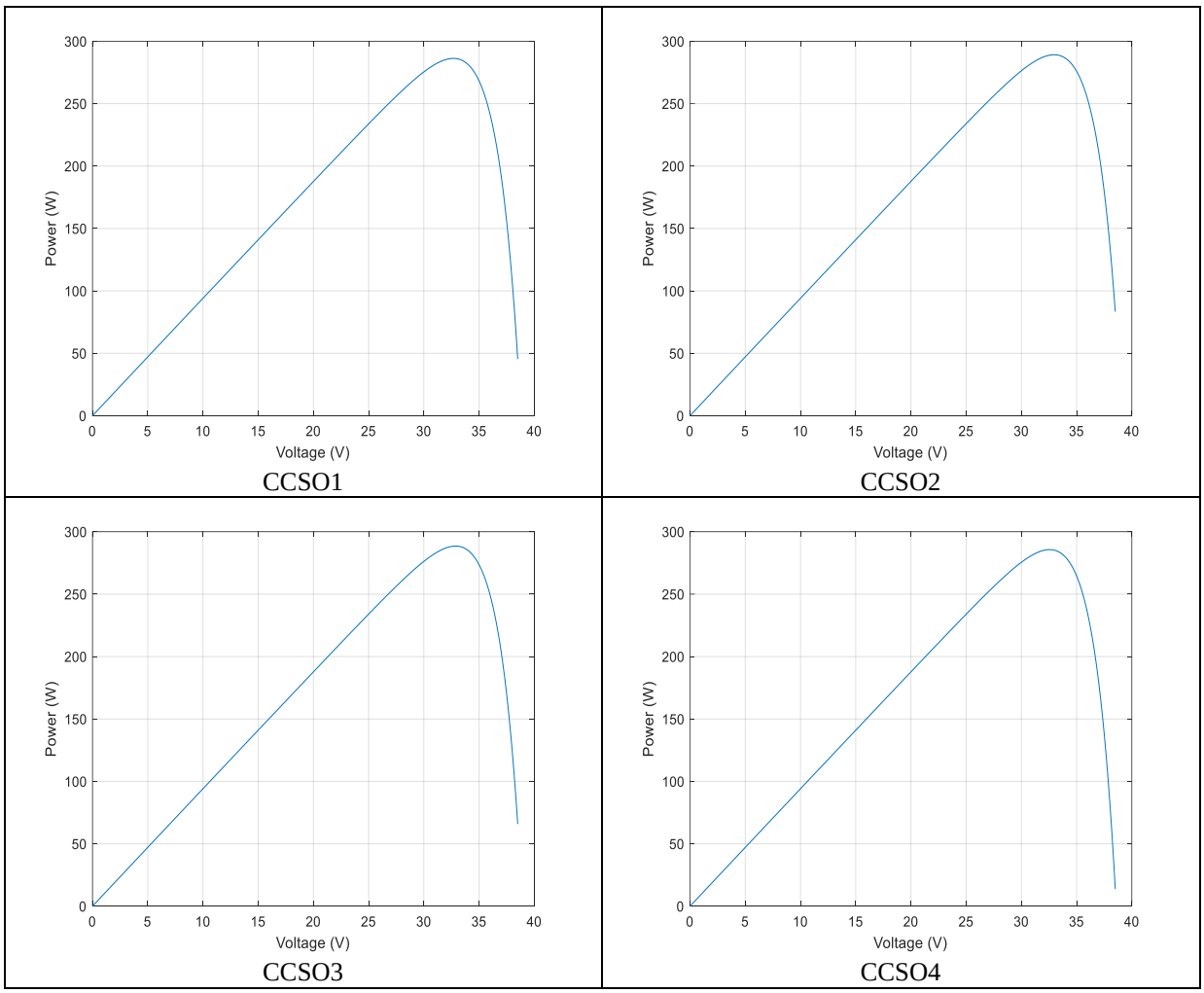

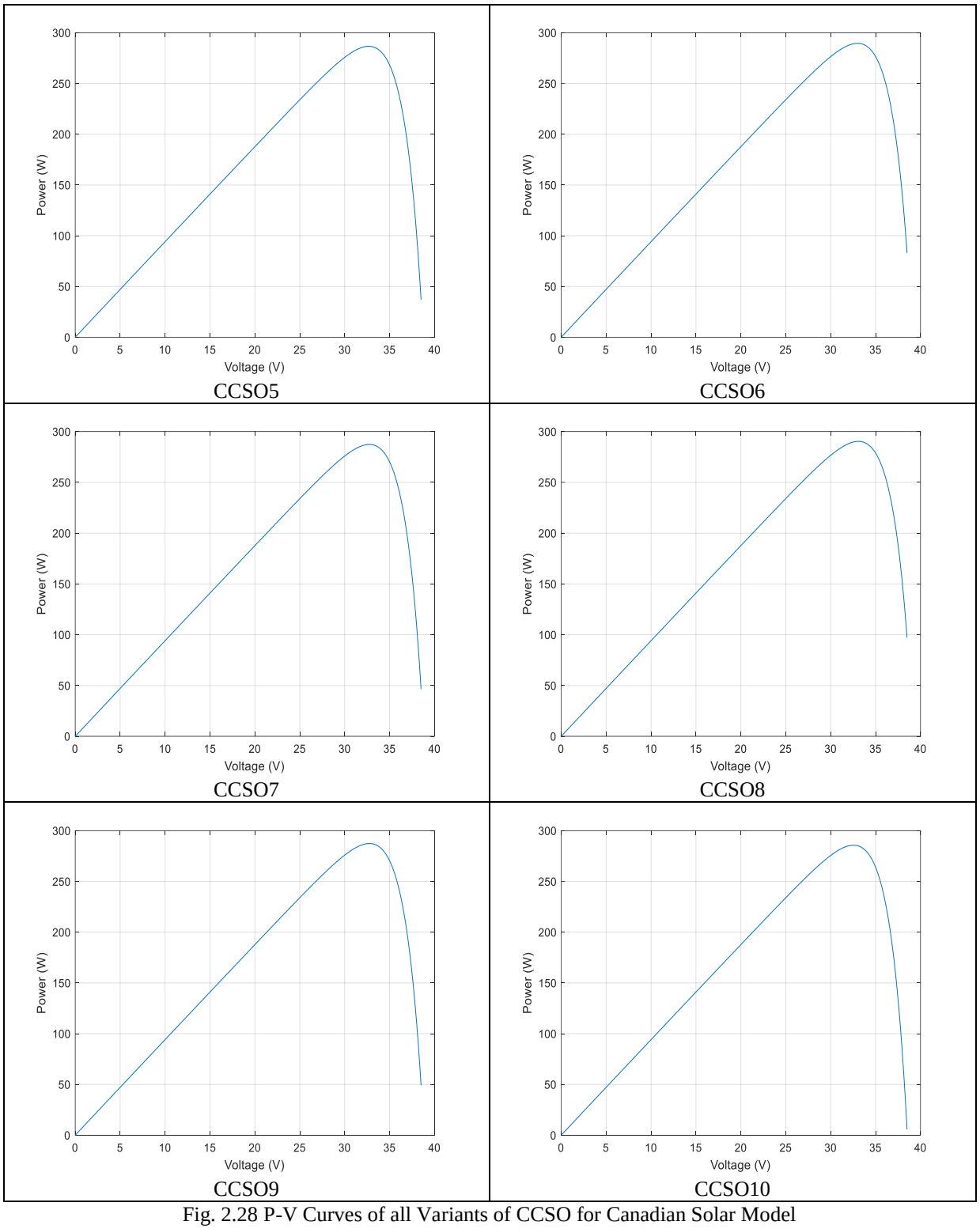

Fig. 2.28 P-V Curves of all Variants of CCSO for Canadian Solar Model

- **Non-Parametric test**

For better validation of the results, non-parametric tests are conducted. Initially, the rank-sum test of Wilcoxon's [113] is carried out. Table 2.28 (a) and 2.28 (b) lists the calculated p-values and justifies that the performances of all variants of CCSO are significant, with the significance level of 95%.

Table 2.28 (a) p-values for the Wilcoxon's rank-sum test of Canadian Solar Model

Algorithms	CSO	DA	ALO	MVO	WOA
CCSO1	3.0253E-11	3.0161E-11	2.9947E-11	3.0142E-11	3.0180E-11
CCSO2	3.0467E-11	2.9770E-11	3.0259E-11	3.0021E-11	2.9966E-11
CCSO3	3.0148E-11	3.0516E-11	3.0422E-11	3.0570E-11	3.0719E-11
CCSO4	3.0856E-11	3.0187E-11	3.0905E-11	3.0164E-11	3.0804E-11
CCSO5	3.0910E-11	3.0850E-11	3.0611E-11	3.0349E-11	3.0133E-11
CCSO6	3.0619E-11	3.0912E-11	3.0388E-11	3.0949E-11	3.0481E-11
CCSO7	3.0321E-11	2.9428E-11	3.0815E-11	3.0073E-11	3.0349E-11
CCSO8	3.0437E-11	3.0666E-11	3.0803E-11	3.0121E-11	3.0091E-11
CCSO9	3.0705E-11	3.0009E-11	3.0052E-11	3.1017E-11	2.9914E-11
CCSO10	3.0193E-11	3.0061E-11	2.9969E-11	3.0501E-11	3.0801E-11

Table 2.28 (b) p-values for the Wilcoxon's rank-sum test of Canadian Solar Model

Algorithms	GOA	SCA	SSA	HHO	ASO
CCSO1	2.9921E-11	3.0999E-11	3.0104E-11	3.0617E-11	2.9957E-11
CCSO2	2.9175E-11	3.0123E-11	3.0597E-11	3.0102E-11	2.9891E-11
CCSO3	2.9564E-11	3.0357E-11	3.0091E-11	3.0199E-11	2.9530E-11
CCSO4	2.9991E-11	3.0638E-11	2.9964E-11	2.9983E-11	2.9204E-11
CCSO5	3.0042E-11	3.0529E-11	3.0137E-11	3.0544E-11	2.9384E-11
CCSO6	2.9709E-11	3.0246E-11	3.0339E-11	3.0489E-11	2.9901E-11
CCSO7	2.9613E-11	3.0814E-11	3.0815E-11	3.0261E-11	2.9407E-11
CCSO8	2.9381E-11	3.0551E-11	3.0740E-11	3.0115E-11	2.9755E-11
CCSO9	2.9850E-11	3.0349E-11	3.0442E-11	3.0591E-11	2.9102E-11
CCSO10	3.0127E-11	3.0100E-11	3.1145E-11	3.0102E-11	2.9991E-11

Then the Kruskal Wallis test [114] is also applied to test the statistical differences amongst the various algorithms. Fig. 2.29 presents the graphs obtained from the test and shows that the mean ranks of the CCSO techniques are significantly different from the other algorithms.

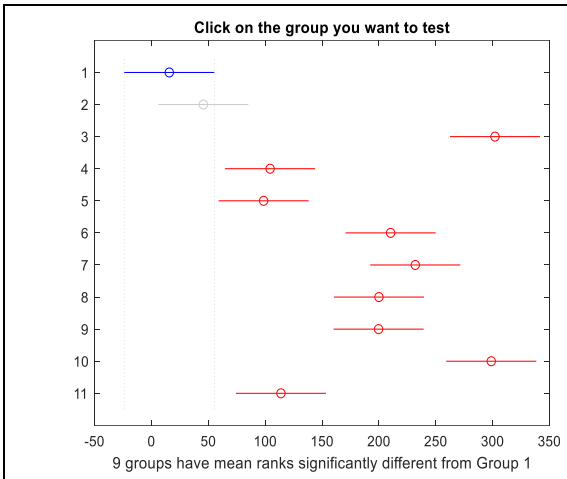

CCSO1

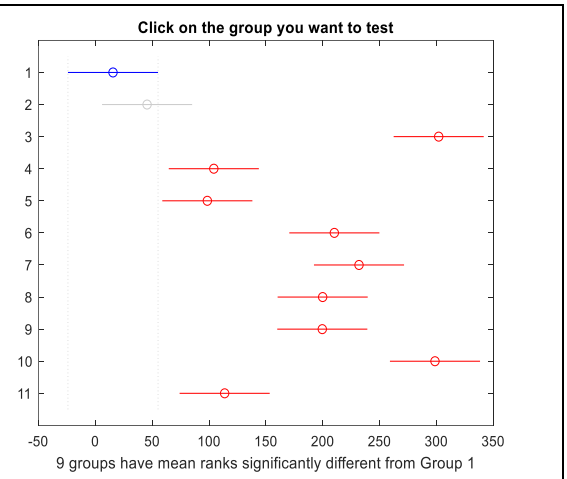

CCSO2

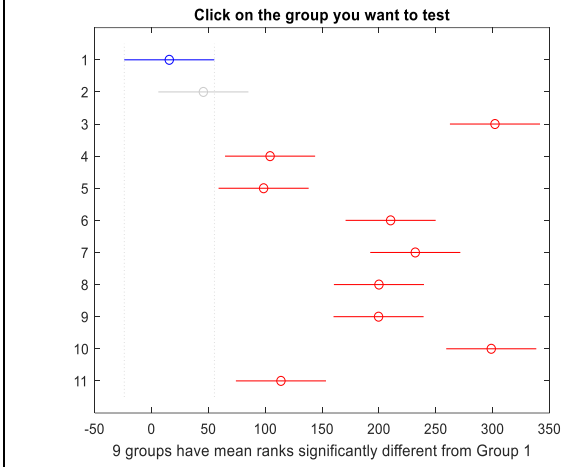

CCSO3

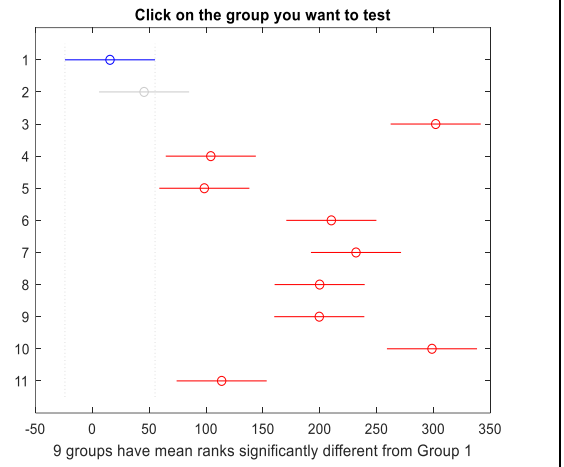

CCSO4

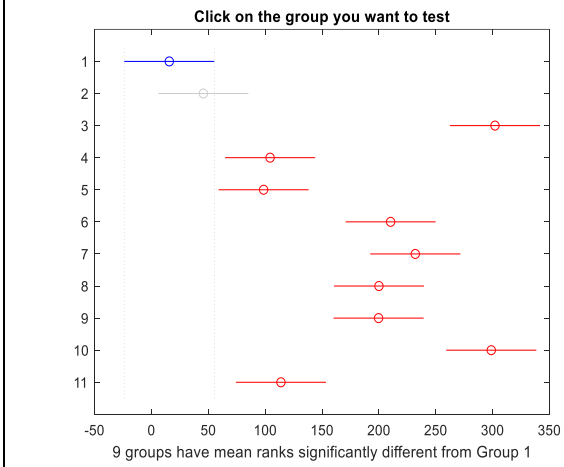

CCSO5

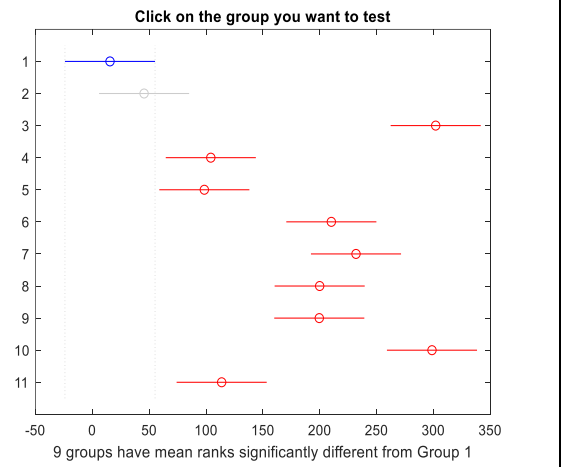

CCSO6

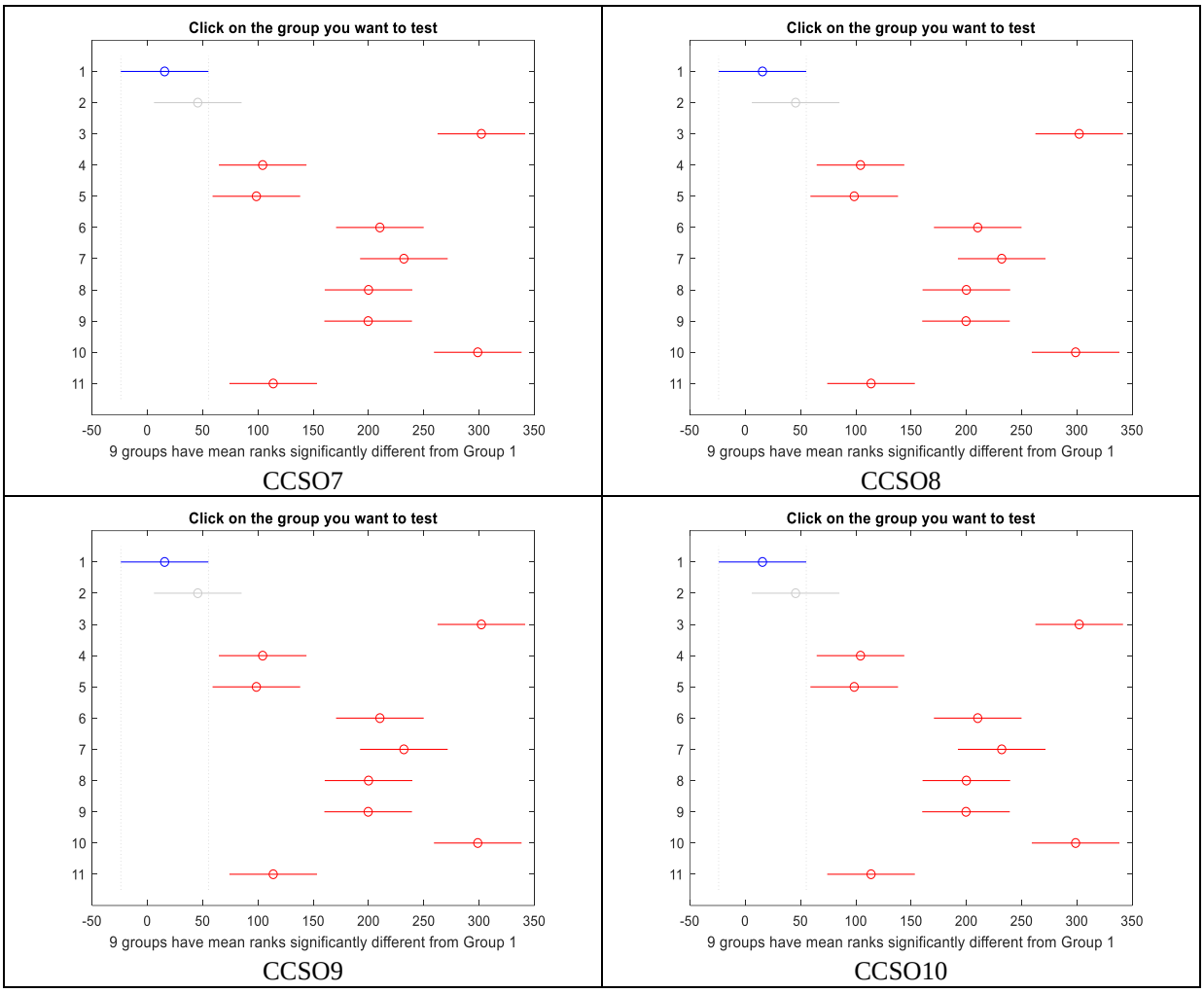

Fig. 2.29 Kruskal Wallis Test Diagram for the Canadian Solar Model

At last, p-values obtained by Wilcoxon's rank test is further evaluated using Holm-Bonferroni corrections method and the outcome values are presented in Table 2.29.

Table 2.29 Corrected p-Values by Holm-Bonferroni Corrections for Wilcoxon's Rank Test of Canadian Solar Model (Multiply the results with (1.0e-09) and test of significance (h) is 1)

Algorithms	CSO	DA	ALO	MVO	WOA	GOA	SCA	SSA	HHO	ASO
CCSO1	0.2930	0.0894	0.1785	0.1488	0.2077	0.2930	0.0597	0.2371	0.2666	0.1191
CCSO2	0.2651	0.0900	0.1797	0.1499	0.2091	0.2951	0.0601	0.2387	0.2684	0.1200
CCSO3	0.2936	0.0896	0.1788	0.2081	0.1491	0.2936	0.0598	0.2375	0.2671	0.1194
CCSO4	0.2949	0.0900	0.1796	0.1498	0.2090	0.2946	0.0601	0.2386	0.2682	0.1199
CCSO5	0.2962	0.0904	0.1804	0.1504	0.2099	0.2962	0.0604	0.2396	0.2694	0.1204
CCSO6	0.2956	0.0902	0.1801	0.1501	0.2095	0.2956	0.0602	0.2396	0.2689	0.1202
CCSO7	0.2643	0.0898	0.1793	0.1495	0.2086	0.2943	0.0600	0.2381	0.2677	0.1197
CCSO8	0.2643	0.0898	0.1793	0.1495	0.2086	0.2943	0.0600	0.2381	0.2677	0.1197
CCSO9	0.2941	0.0897	0.1792	0.1494	0.2085	0.2941	0.0599	0.2380	0.2676	0.1196
CCSO10	0.2906	0.0903	0.1803	0.1503	0.209	0.2960	0.0603	0.2395	0.2692	0.1203

Case 2: In this case, Kyocera (KC200GT multi-crystal) commercial module is investigated. Similar to case 1, all the earlier mentioned algorithms are executed to extract the nine parameters of the TDM. Table 2.30 narrates the extracted parameters of the model.

Table 2.30 Parameter Estimation of TDM for Kyocera Model

Parameters→ / **Algorithms ↓**	I_{pv}	α_1	α_2	α_3	R_S	R_{Sh}	I_{o1}	I_{o2}	I_{o3}
CCSO1	8.2130	1.6658	1.6556	1.7091	0.1193	333.9284	5.3308E-07	5.3267E-07	4.9854E-07
CCSO2	8.2129	1.6706	1.7231	1.7735	0.1141	312.5405	5.5423E-07	5.1728E-07	4.6744E-07
CCSO3	8.2131	1.7841	1.7700	1.6347	0.1111	292.0575	4.7194E-07	5.2759E-07	5.4345E-07
CCSO4	8.2131	1.6090	1.6955	1.7410	0.1165	327.0842	5.5305E-07	5.3586E-07	5.3085E-07
CCSO5	8.2131	1.6501	1.6966	1.7350	0.1146	312.4069	6.0508E-07	5.2196E-07	4.3595E-07
CCSO6	8.2132	1.6954	1.7424	1.6898	0.1211	326.4518	4.7269E-07	4.0068E-07	6.0666E-07
CCSO7	8.2132	1.6566	1.6252	1.7703	0.1163	316.2376	5.1367E-07	5.8212E-07	5.9493E-07
CCSO8	8.2130	1.6705	1.6734	1.7443	0.1128	313.8558	5.3980E-07	5.9118E-07	4.4266E-07
CCSO9	8.2130	1.6653	1.7153	1.6945	0.1119	318.3009	5.3401E-07	5.6077E-07	4.5432E-07
CCSO10	8.2128	1.6742	1.6924	1.7763	0.1017	280.9835	5.7969E-07	5.7292E-07	5.0378E-07
CSO	8.2313	1.6820	1.6859	1.6439	0.1085	306.7303	5.8186E-07	5.0013E-07	7.8819E-07
DA	8.2834	1.6078	1.6021	1.6533	0.1645	268.5313	4.3267E-07	5.4950E-07	4.7144E-07
ALO	8.2211	1.6809	1.5518	1.6750	0.1306	300.8825	5.9102E-07	4.5750E-07	5.1987E-07
MVO	8.2259	1.5584	1.4697	1.5597	0.0673	212.0287	4.4118E-07	5.0000E-07	4.7611E-07
WOA	8.3314	1.6144	1.6184	1.6021	0.2084	305.1682	4.8250E-07	5.1301E-07	5.0974E-07
GOA	8.4111	1.6294	1.6620	1.6589	0.2978	484.0321	4.2411E-07	3.5080E-07	4.5325E-07
SCA	8.1399	1.2748	1.1221	1.2842	0.0300	247.9600	2.0469E-07	1.2317E-07	1.5188E-07
SSA	8.2564	1.5924	1.6130	1.6547	0.1596	282.5653	4.5039E-07	4.2179E-07	4.5471E-07
HHO	8.4194	1.6210	1.5955	1.5878	0.2598	293.7824	5.5016E-07	5.2750E-07	5.3370E-07

ASO	8.0589	1.6176	1.6035	1.5932	0.0948	294.1035	4.7272E-07	4.1356E-07	5.6861E-07

Table 2.31 shows the statistical results of parameters (minimum, maximum, mean, and standard deviation) of SSE. The outcome of results the least SSE error is obtained by chaotic variants of proposed CSO algorithm in comparison to all compared algorithms. Hence proving the accuracy of proposed algorithm.

Table 2.31 Statistical Results of the SSE for Triple Diode Model for Kyocera Model

Statistical Results→ **Algorithms↓**	**Minimum**	**Average**	**Maximum**	**Standard Deviation**
CCSO1	1.0641E-10	1.7008E-09	4.5974E-10	3.2897E-10
CCSO2	1.0057E-10	9.9750E-10	3.6014E-10	2.3801E-10
CCSO3	1.1575E-10	9.9417E-10	5.1199E-10	2.7649E-10
CCSO4	1.1832E-10	9.3904E-10	4.0153E-10	2.4240E-10
CCSO5	1.0553E-10	9.7648E-10	4.1276E-10	2.4556E-10
CCSO6	1.1280E-10	9.5777E-10	3.9740E-10	2.2346E-10
CCSO7	1.1076E-10	9.8130E-10	4.4716E-10	2.8681E-10
CCSO8	1.1687E-10	8.1806E-10	3.8757E-10	1.9893E-10
CCSO9	1.0375E-10	9.3661E-10	4.0983E-10	2.3650E-10
CCSO10	1.0171E-10	9.2846E-10	3.6224E-10	2.3784E-10
CSO	1.1105E-06	9.2882E-06	3.4453E-06	2.8199E-06
DA	0.0126	0.0665	0.0384	0.0204
ALO	0.0011	0.0091	0.0035	0.0022
MVO	0.0001	0.0092	0.0039	0.0025
WOA	0.0101	0.0964	0.0418	0.0251
GOA	0.0106	0.0936	0.0390	0.0268
SCA	0.0102	0.0962	0.0442	0.0223
SSA	0.0014	0.0097	0.0050	0.0025
HHO	0.0111	0.0841	0.0440	0.0244
ASO	0.0011	0.0089	0.0040	0.0022

The chaotic map influenced CSO techniques perform significantly better as compared to as many ten latest heuristic methods as seen from the results of Table 2.32. The best outcomes are also marked in bold. The non-parametric tests are not shown to avoid repetition. Moreover, the convergences characteristics of the TDM are plotted to prove the significance of the extracted error value. The convergence curves are provided in Fig. 2.30. The proposed methods perform better in terms of convergence speed and accuracy as compared to the other algorithms. Fig. 2.31 shows the I-V curves of all variants of CCSO. The curves are pretty similar to the ideal characteristic curves of the solar model proving the accuracy of the proposed methodology. Similarly, P-V

curves under standard test conditions (STC) could also have been plotted to prove the consistency of the estimated parameter process by the suggested techniques as shown in Fig 2.32.

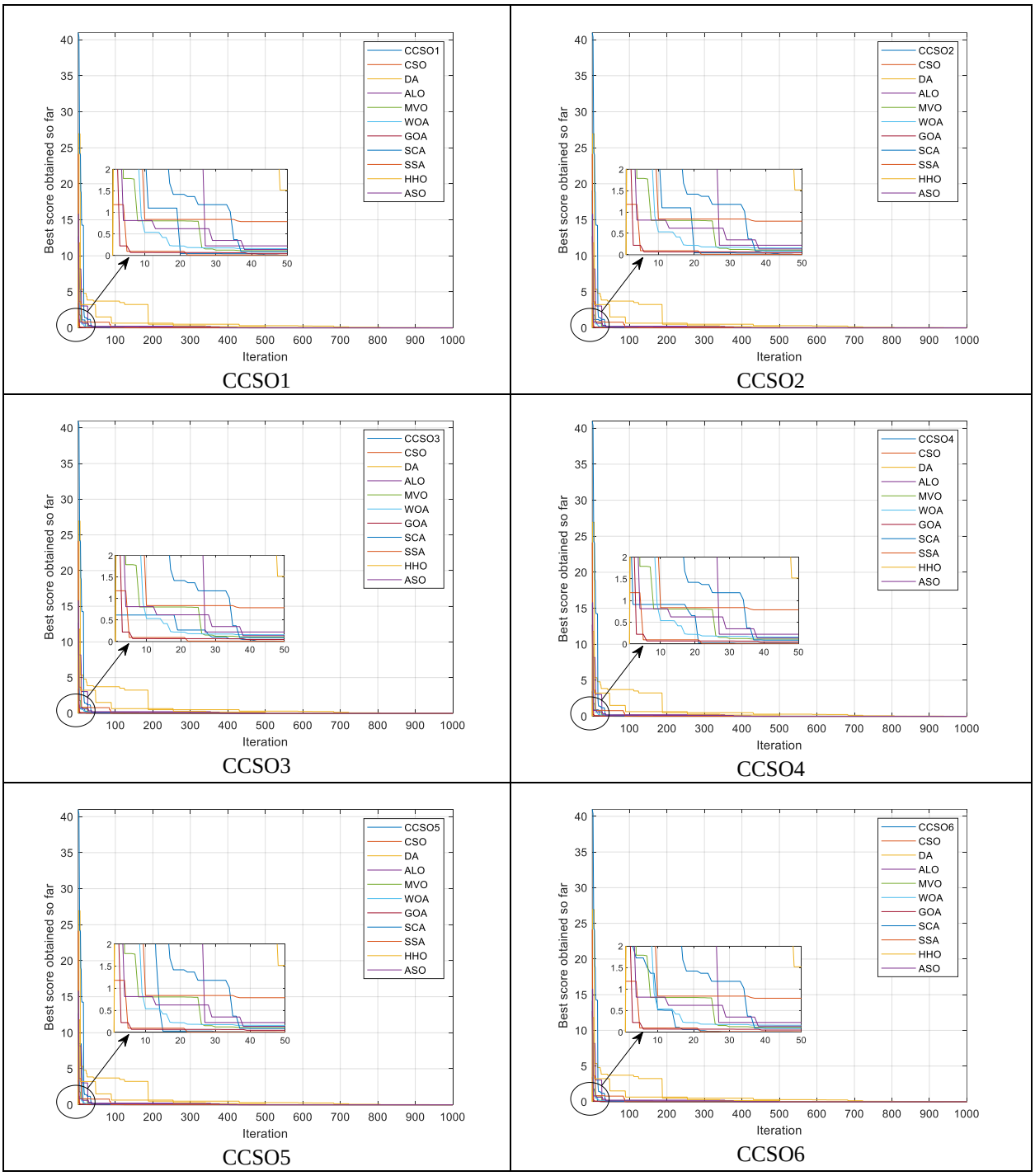

CCSO1 CCSO2

CCSO3 CCSO4

CCSO5 CCSO6

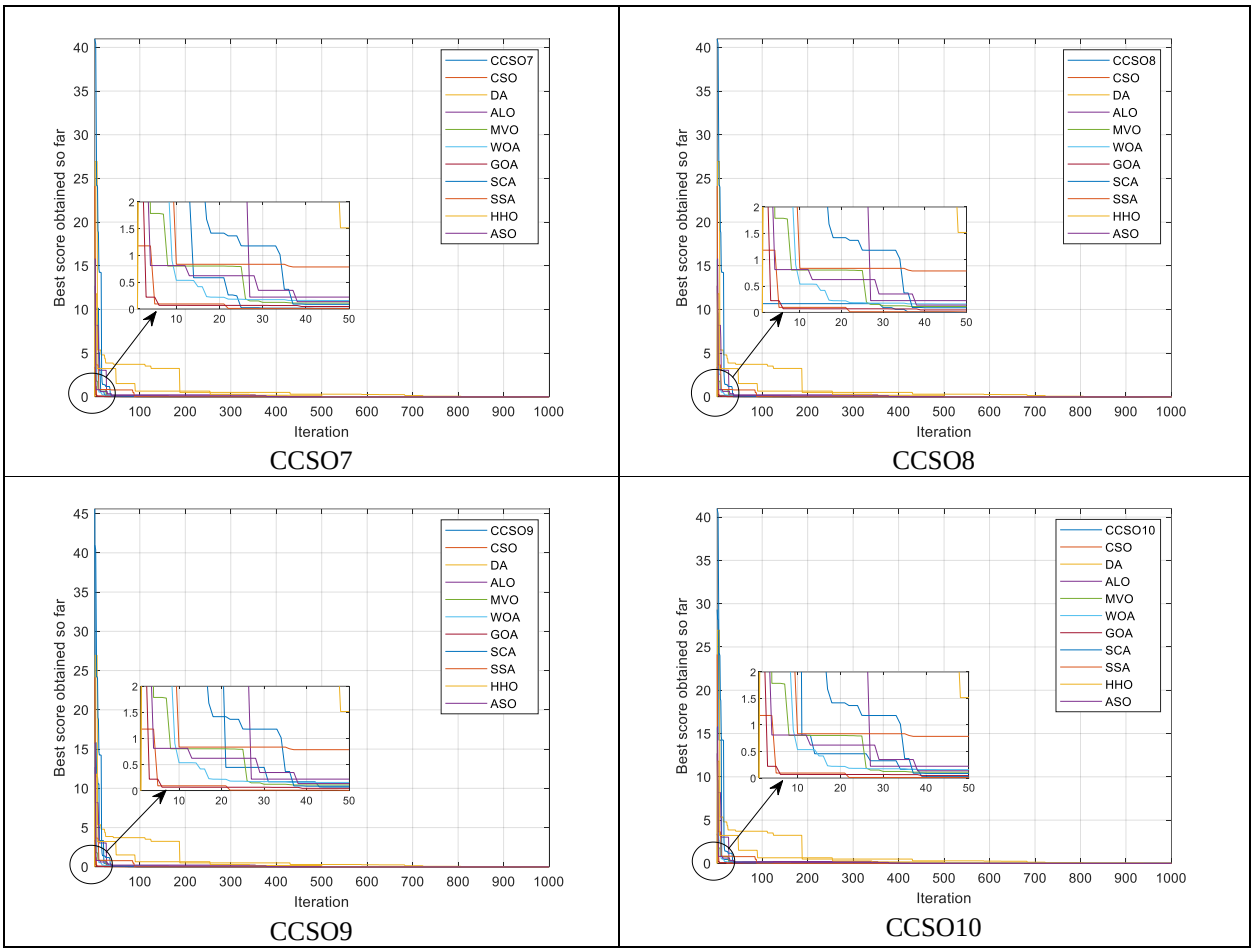

Fig. 2.30 Convergence Plots of Each Variant of CCSO with Other Compared Algorithms for Kyocera Model

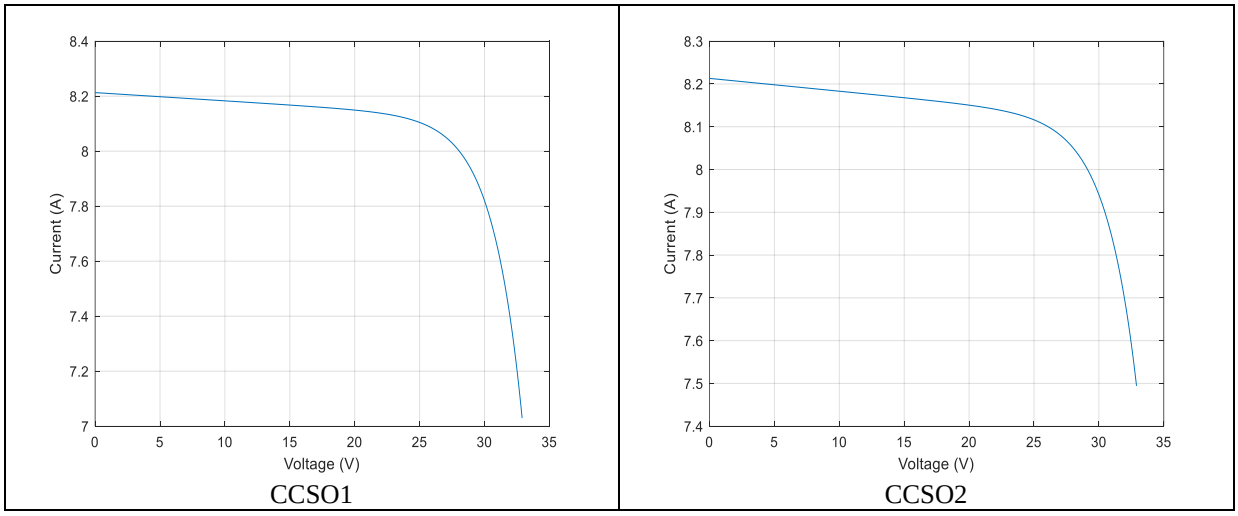

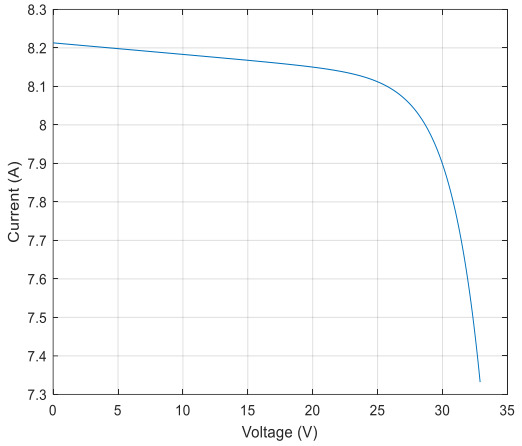

CCSO3

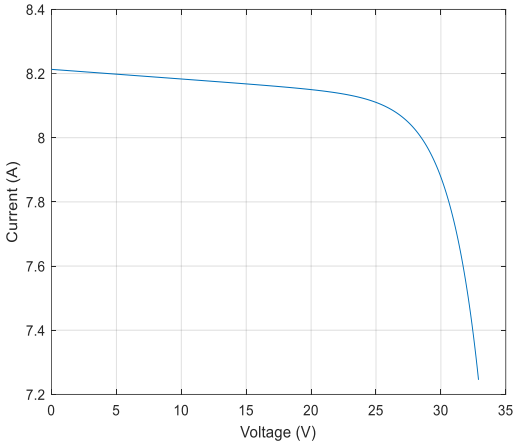

CCSO4

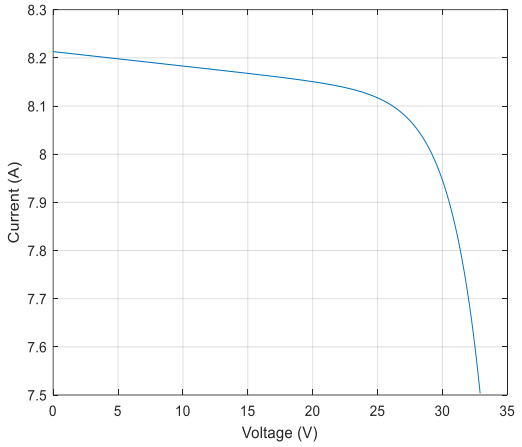

CCSO5

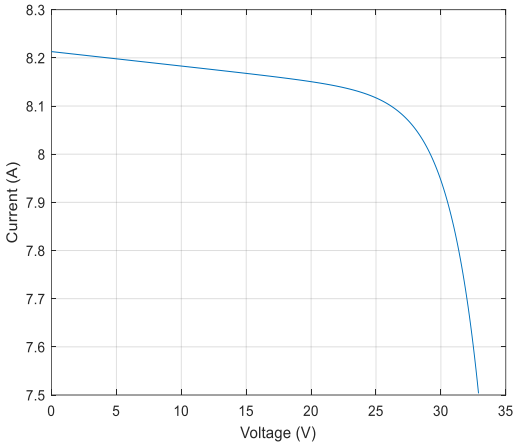

CCSO6

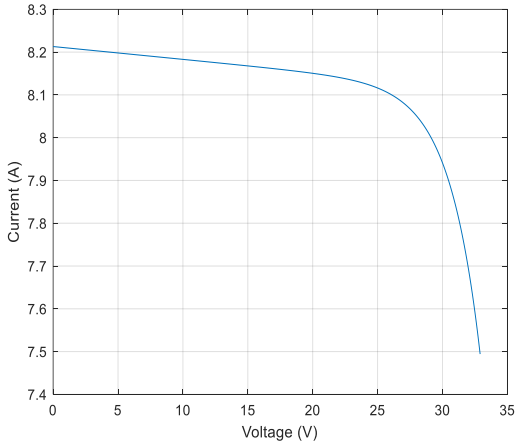

CCSO7

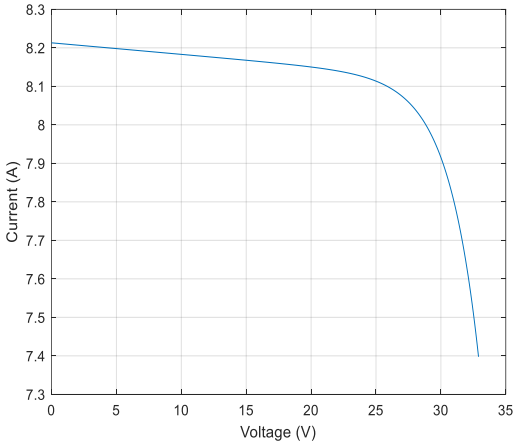

CCSO8

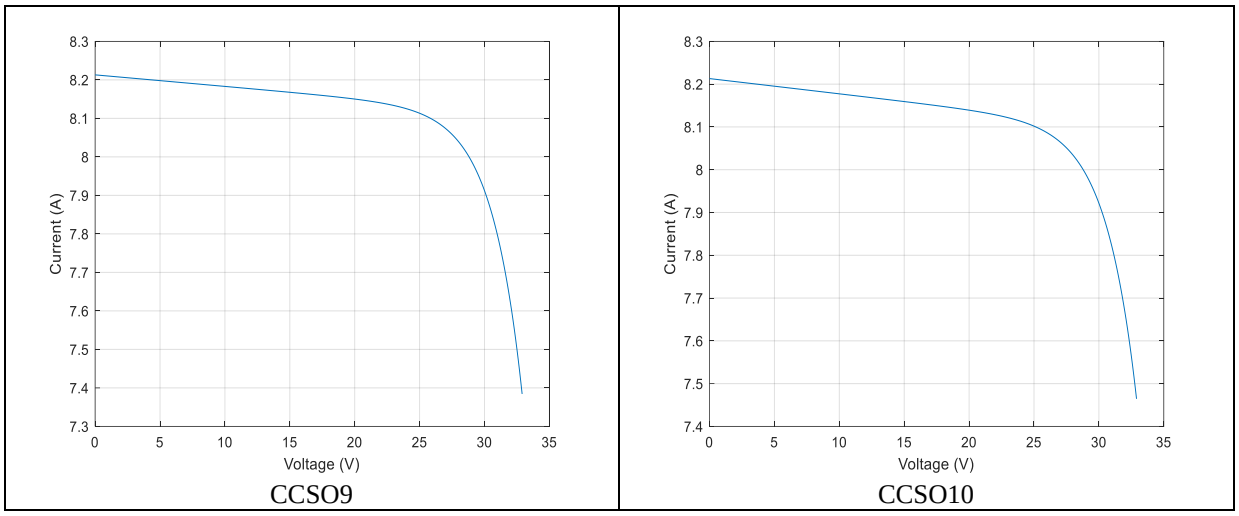

Fig. 2.31 I-V Curves for all Variants CCSO for Kyocera Model

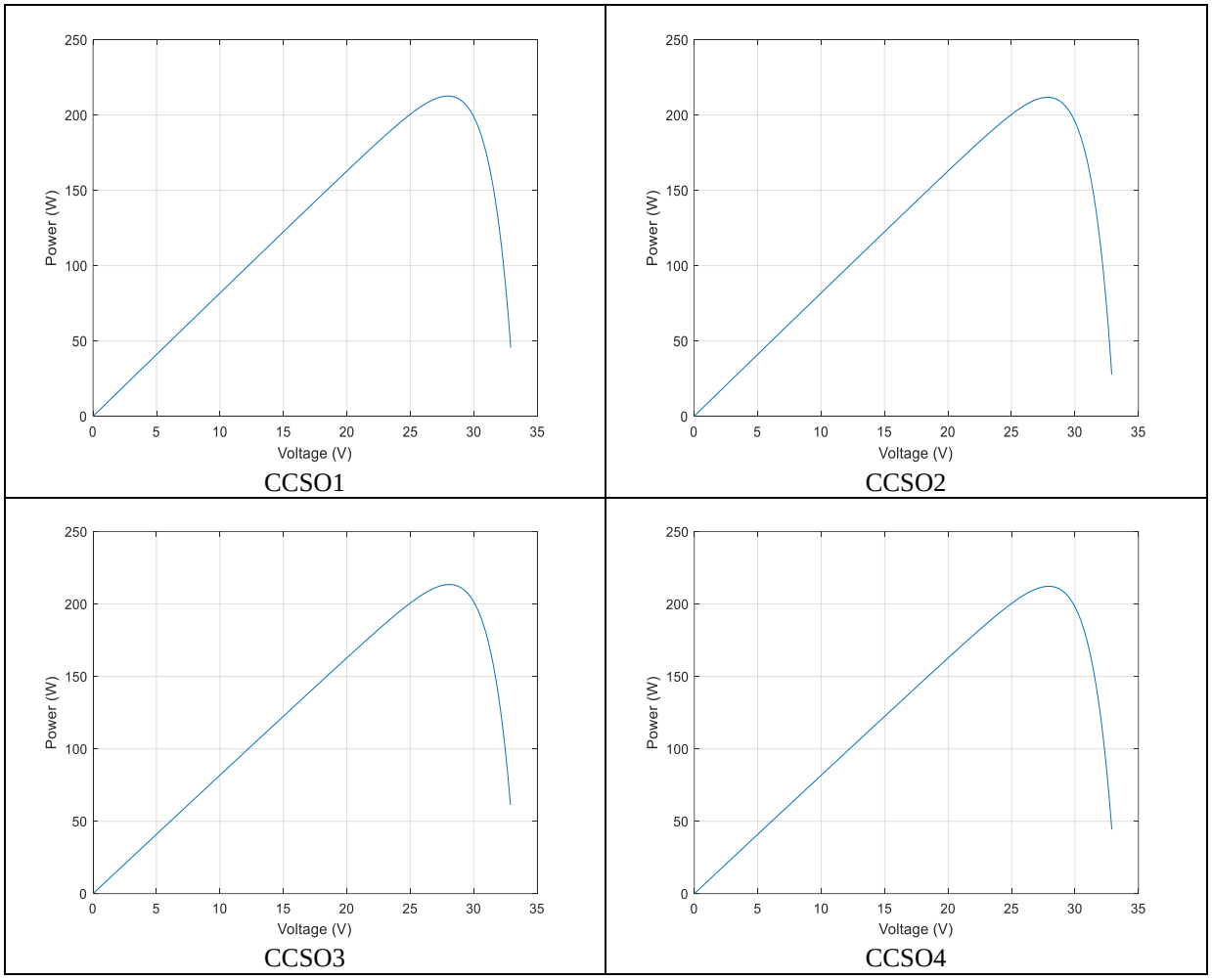

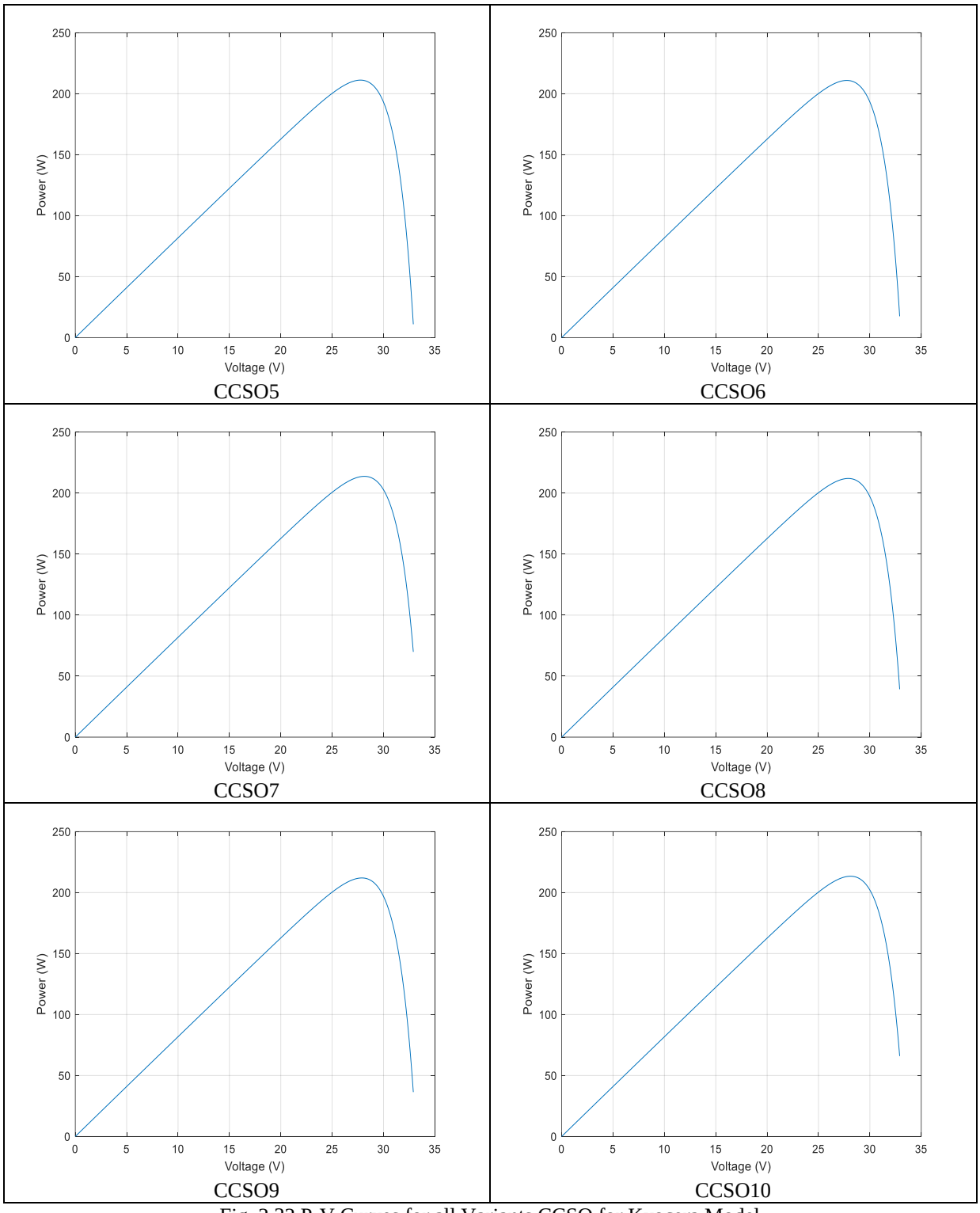

Fig. 2.32 P-V Curves for all Variants CCSO for Kyocera Model

- **Non – Parametric Tests**

Similar to case 1, for better validation of the results, non-parametric tests are conducted. Initially, the rank-sum test of Wilcoxon's is carried out [113]. Table 2.32 (a) and 2.32 (b) lists the calculated

p-values and justifies that the performances of all variants of CCSO are significant, with the significance level of 95%.

Table 2.32 (a) p-values for the Wilcoxon's Rank-Sum Test of Kyocera Model

Algorithms	CSO	DA	ALO	MVO	WOA
CCSO1	3.0510E-11	2.9785E-11	3.0647E-11	3.0466E-11	3.0161E-11
CCSO2	3.0947E-11	2.9112E-11	3.0141E-11	2.9992E-11	3.0598E-11
CCSO3	3.0128E-11	2.9394E-11	3.0858E-11	3.0104E-11	3.0796E-11
CCSO4	3.0392E-11	2.9830E-11	3.0571E-11	3.0815E-11	3.0975E-11
CCSO5	3.0812E-11	2.9502E-11	3.0785E-11	3.0396E-11	3.0249E-11
CCSO6	3.0651E-11	2.9457E-11	3.0438E-11	3.0731E-11	3.0886E-11
CCSO7	3.0166E-11	2.9981E-11	3.0291E-11	3.0901E-11	3.0771E-11
CCSO8	3.0449E-11	2.9196E-11	3.0112E-11	3.0584E-11	3.0494E-11
CCSO9	3.0906E-11	2.9997E-11	3.0537E-11	3.0477E-11	3.0161E-11
CCSO10	3.0510E-11	2.9785E-11	3.0647E-11	3.0466E-11	3.0161E-11

Table 2.32 (b) p-values for the Wilcoxon's Rank-Sum Test of Kyocera Model

Algorithms	GOA	SCA	SSA	HHO	ASO
CCSO1	3.0183E-11	3.0561E-11	3.0047E-11	3.0142E-11	3.0010E-11
CCSO2	3.0951E-11	3.0446E-11	2.9985E-11	3.0880E-11	2.9437E-11
CCSO3	2.9993E-11	3.0162E-11	2.9753E-11	3.0564E-11	2.9074E-11
CCSO4	3.0597E-11	3.0984E-11	2.9831E-11	3.0248E-11	2.9549E-11
CCSO5	3.0675E-11	3.0471E-11	2.9329E-11	3.0792E-11	2.9756E-11
CCSO6	3.0342E-11	3.0259E-11	2.9195E-11	3.0439E-11	3.0105E-11
CCSO7	3.0766E-11	3.0962E-11	3.0108E-11	3.0195E-11	2.9177E-11
CCSO8	3.0899E-11	3.0589E-11	2.9582E-11	3.0953E-11	2.9913E-11
CCSO9	3.0261E-11	2.9855E-11	3.0137E-11	3.0322E-11	2.9321E-11
CCSO10	3.0183E-11	3.0561E-11	3.0047E-11	3.0142E-11	3.0010E-11

Similar to first case, the next test preformed is Kruskal Wallis test [114]. The outcome graphs presented in Fig. 2.33 shows that the mean ranks of the CCSO techniques are significantly different from the other algorithms.

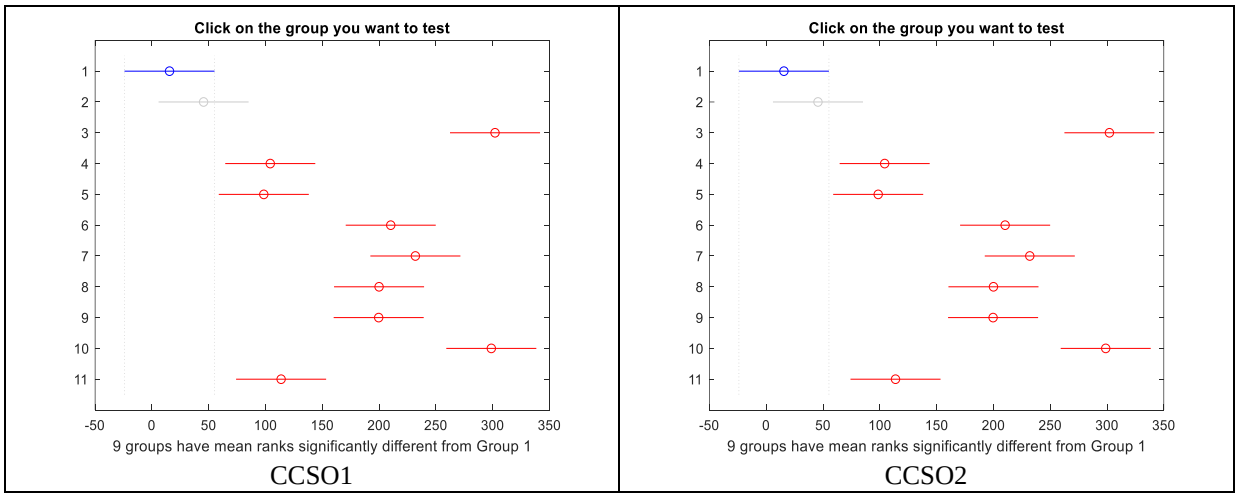

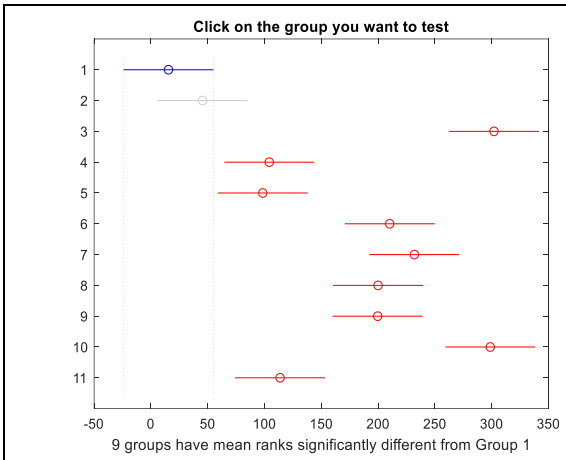

CCSO3

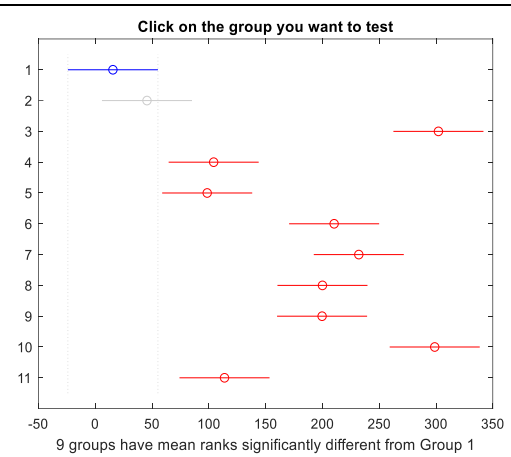

CCSO4

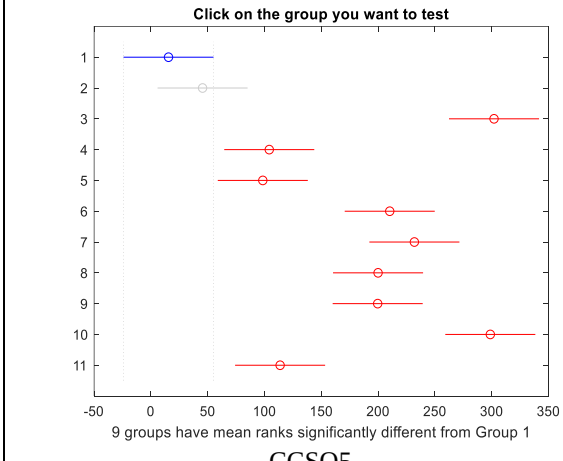

CCSO5

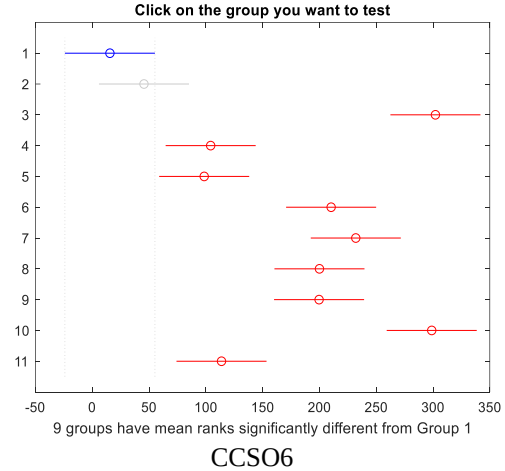

CCSO6

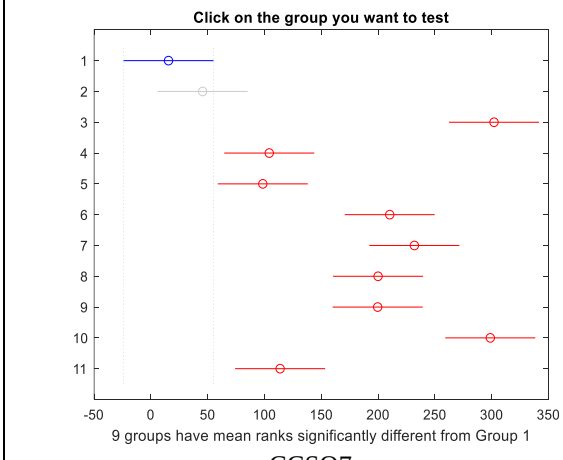

CCSO7

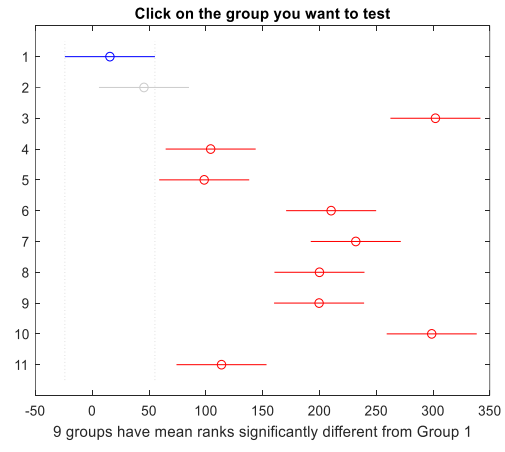

CCSO8

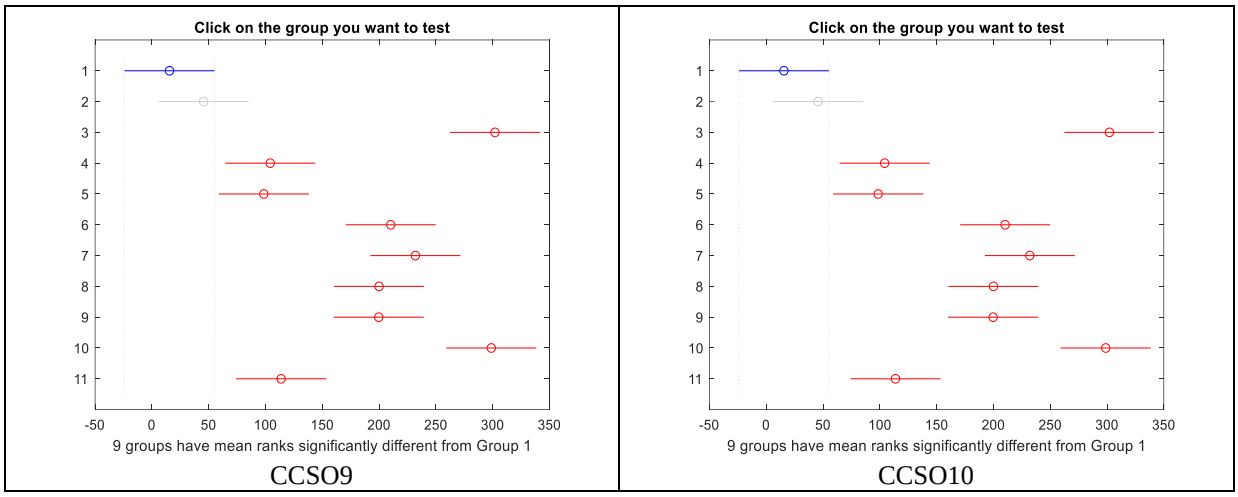

Fig. 2.33 Kruskal Wallis Test Diagram for the Kyocera Model

Similar to first case, p-values obtained by Wilcoxon's rank test is further evaluated using Holm-Bonferroni corrections method. The outcomes result is presented in Table 2.34 validate the proposed CCSO algorithm.

Table 2.33 Corrected p-Values by Holm-Bonferroni Corrections for Wilcoxon's Rank Test of Kyocera Model (Multiply the results with (1.0e-09) and test of significance (h) is 1)

Algorithms	CSO	DA	ALO	MVO	WOA	GOA	SCA	SSA	HHO	ASO
CCSO1	0.1219	0.2978	0.0611	0.1509	0.2110	0.1810	0.0915	0.2701	0.2404	0.2978
CCSO2	0.0926	0.2911	0.2099	0.2399	0.1522	0.0619	0.1808	0.2649	0.1224	0.2911
CCSO3	0.1806	0.2907	0.0616	0.2100	0.0917	0.2380	0.1506	0.2645	0.1206	0.2907
CCSO4	0.2117	0.2955	0.1824	0.1224	0.0924	0.1529	0.0619	0.2685	0.2386	0.2955
CCSO5	0.2982	0.2982	0.2404	0.1805	0.1207	0.0906	0.0604	0.2106	0.1505	0.2704
CCSO6	0.1218	0.2919	0.1821	0.0920	0.0615	0.2118	0.2408	0.2919	0.1522	0.2651
CCSO7	0.2409	0.2918	0.1812	0.0923	0.1231	0.1515	0.0618	0.2698	0.2112	0.2918
CCSO8	0.2108	0.2920	0.2393	0.1525	0.1827	0.0918	0.1223	0.2920	0.0618	0.2662
CCSO9	0.0611	0.2687	0.0914	0.1213	0.2110	0.1810	0.2932	0.2400	0.1513	0.2932
CCSO10	0.2982	0.2982	0.2404	0.1805	0.1207	0.0906	0.0604	0.2106	0.1505	0.2704

Case 3: The Solarex (MSX-60 poly-crystalline) commercial module is considered as a test system. Similar to cases 1 and 2, the unknown parameters of the TDM are identified using the different CCSO methods. The results of the extracted parameters are thus provided in Table 2.34. As many algorithms are used for comparison.

Table 2.34 Parameter Estimation of Triple Diode Model for Solarex Model

Parameters→ **Algorithms↓**	I_{pv}	α_1	α_2	α_3	R_S	R_{Sh}	I_{o1}	I_{o2}	I_{o3}
CCSO1	3.8007	1.6604	1.7414	1.6594	0.0670	350.2424	5.0405E-07	4.6675E-07	5.3207E-07

CCSO2	3.8006	1.7181	1.7262	1.6622	0.0630	364.9196	5.6228E-07	5.7694E-07	5.8448E-07
CCSO3	3.8006	1.7042	1.7418	1.7418	0.0651	365.5107	4.3119E-07	5.2946E-07	6.2651E-07
CCSO4	3.8007	1.7001	1.7067	1.7137	0.0737	357.3770	5.2362E-07	4.9889E-07	4.7401E-07
CCSO5	3.8007	1.6789	1.7363	1.7350	0.0757	352.1045	5.0795E-07	4.8644E-07	5.0921E-07
CCSO6	3.8007	1.7032	1.6968	1.7404	0.0656	369.1128	5.2000E-07	4.9932E-07	5.5763E-07
CCSO7	3.8007	1.7096	1.7483	1.6990	0.0681	351.9238	5.4566E-07	4.6693E-07	5.8948E-07
CCSO8	3.8007	1.6900	1.7097	1.6988	0.0662	348.0949	4.6966E-07	4.8532E-07	5.3252E-07
CCSO9	3.8007	1.7169	1.7298	1.6774	0.0727	355.8210	6.1338E-07	5.0430E-07	4.2880E-07
CCSO10	3.8007	1.6979	1.7408	1.6983	0.0672	357.1666	5.7214E-07	5.5199E-07	5.9184E-07
CSO	3.8006	1.6632	1.7108	1.6821	0.0603	365.4920	4.8014E-07	5.9008E-07	6.4198E-07
DA	3.8717	1.6284	1.5971	1.6059	0.2154	279.7127	4.1435E-07	4.0480E-07	4.6731E-07
ALO	3.8281	1.7267	1.7508	1.5790	0.1536	294.9870	5.3044E-07	4.5884E-07	5.0700E-07
MVO	3.8474	1.4381	1.3948	1.4849	0.0250	209.2078	5.2000E-07	2.4568E-07	4.4000E-07
WOA	3.9114	1.6193	1.6186	1.6221	0.2614	277.0438	5.4277E-07	5.0518E-07	6.1349E-07
GOA	3.8783	1.6348	1.7285	1.5964	0.2935	496.4711	4.7526E-07	4.1047E-07	3.8245E-07
SCA	3.8121	1.2484	1.3479	1.2132	0.0175	247.1086	1.2736E-07	1.4829E-07	1.6517E-07
SSA	3.8484	1.6147	1.5814	1.6207	0.2069	299.8353	4.1442E-07	3.9549E-07	4.3418E-07
HHO	3.8998	1.5594	1.6070	1.5949	0.2314	281.2135	4.2884E-07	5.8137E-07	5.2916E-07
ASO	3.8320	1.6011	1.6191	1.6253	0.0818	263.7884	3.6828E-07	4.5886E-07	3.5679E-07

Table 2.35 shows the statistical results of parameters (minimum, maximum, mean, and standard deviation) of SSE. The outcome of results the least SSE error is obtained by chaotic variants of proposed CSO algorithm in comparison to all compared algorithms. Hence proving the accuracy of proposed algorithm.

Table 2.35 Statistical Results of the SSE for Triple Diode Model for Solarex Model

Statistical Results → Algorithms ↓	Minimum	Average	Maximum	Standard Deviation
CCSO1	1.0609E-10	9.8154E-10	5.1597E-10	3.0629E-10
CCSO2	1.1995E-10	8.7431E-10	3.8689E-10	2.4429E-10
CCSO3	1.0322E-10	9.1183E-10	3.9265E-10	2.3867E-10
CCSO4	1.0209E-10	9.5743E-10	4.3495E-10	2.7955E-10
CCSO5	1.0899E-10	9.2031E-10	3.6249E-10	2.2947E-10
CCSO6	1.1381E-10	8.8668E-10	4.1727E-10	2.4458E-10
CCSO7	1.1099E-10	7.5532E-10	3.7148E-10	2.2981E-10
CCSO8	1.1058E-10	9.7361E-10	4.2491E-10	2.6195E-10
CCSO9	1.1042E-10	8.1993E-10	4.2701E-10	2.4031E-10
CCSO10	1.0436E-10	9.5133E-10	4.1828E-10	2.5275E-10
CSO	1.1024E-06	9.4487E-06	3.6709E-06	2.5051E-06
DA	0.0104	0.0828	0.0393	0.0244
ALO	0.0001	0.0062	0.0031	0.0017
MVO	0.0107	0.0905	0.0365	0.0251
WOA	0.0101	0.0915	0.0364	0.0264
GOA	0.0001	0.0094	0.0037	0.0025
SCA	0.0101	0.0929	0.0362	0.0238
SSA	0.0001	0.0094	0.0037	0.0025
HHO	0.0118	0.0967	0.0469	0.0277
ASO	0.0011	0.0089	0.0033	0.0020

The convergence curves of the error functions are plotted in Fig. 2.34. The comparison shows that the proposed chaotic chicken swarm techniques are far from the well-known methods reported in the literature. Similarly, the I-V, P-V curves under standard test conditions (STC) also have been plotted in Fig. 2.35 and Fig. 2.36 respectively to prove the consistency of the estimated parameter process by the suggested techniques.

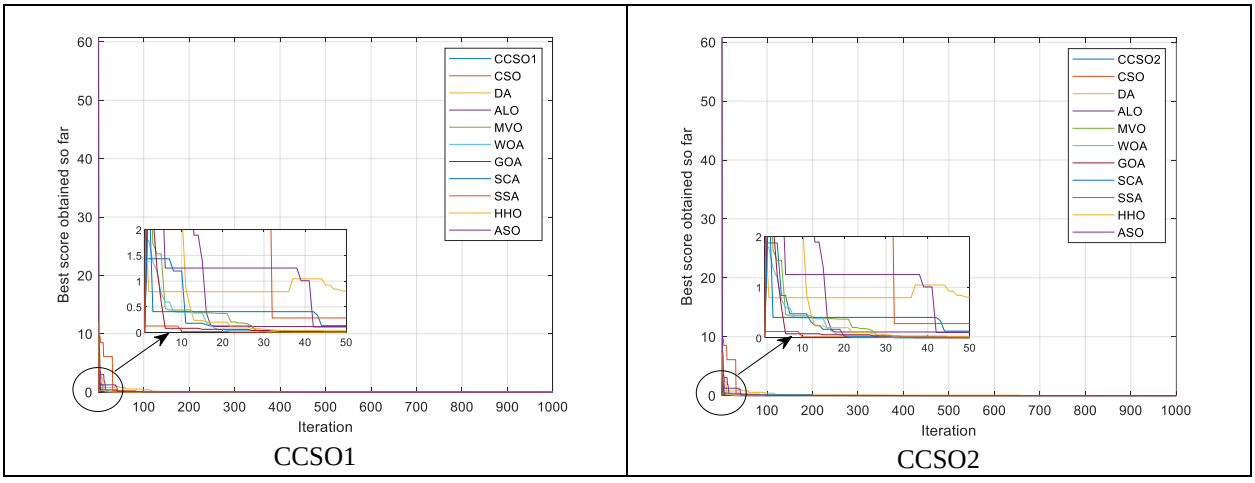

CCSO1 CCSO2

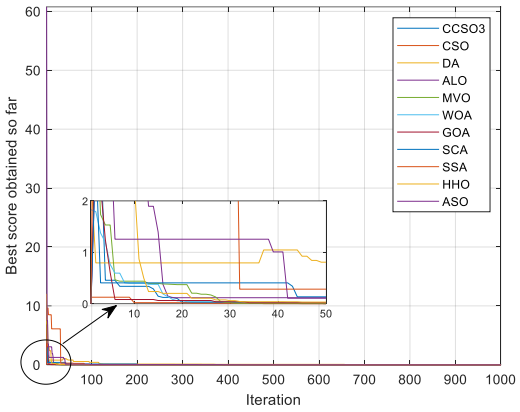

CCSO3

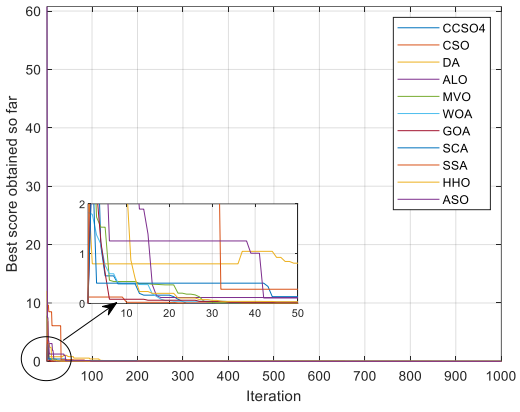

CCSO4

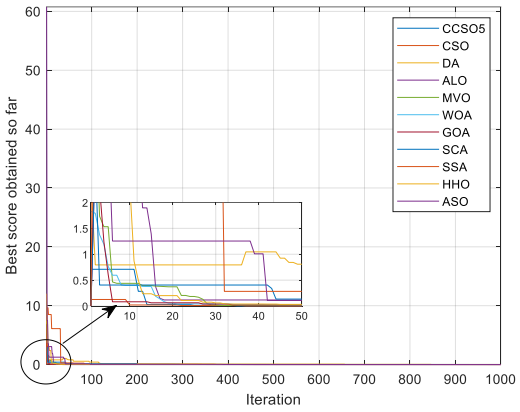

CCSO5

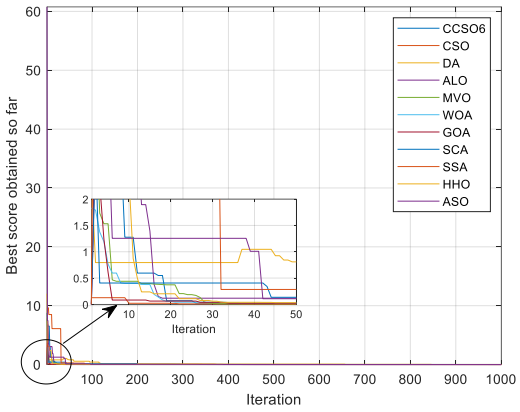

CCSO6

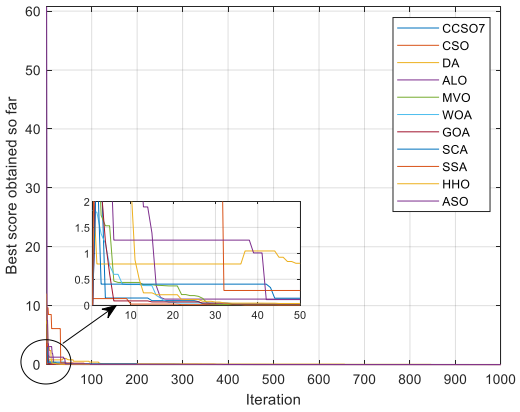

CCSO7

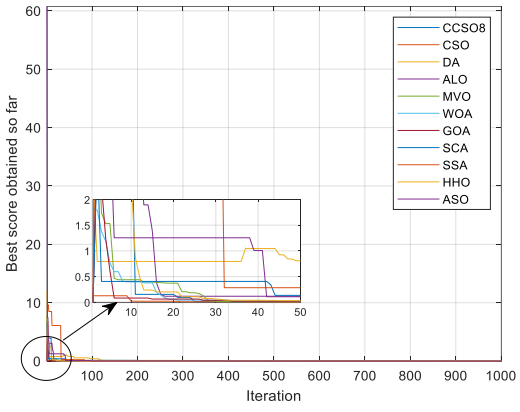

CCSO8

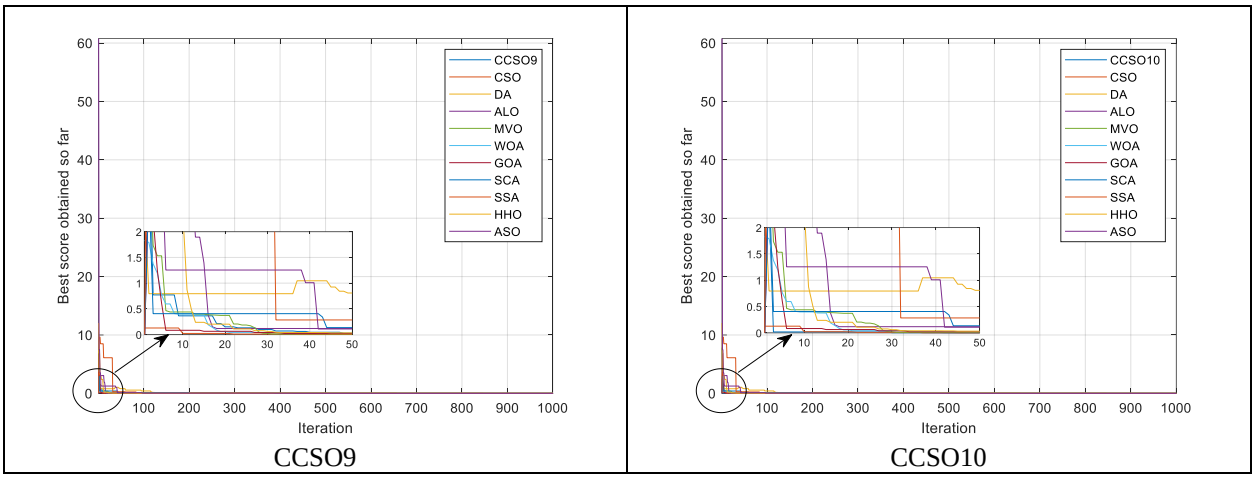

Fig. 2.34 Convergences Curves of Each Variant of CCSO with Other Compared Algorithms for Solarex Model

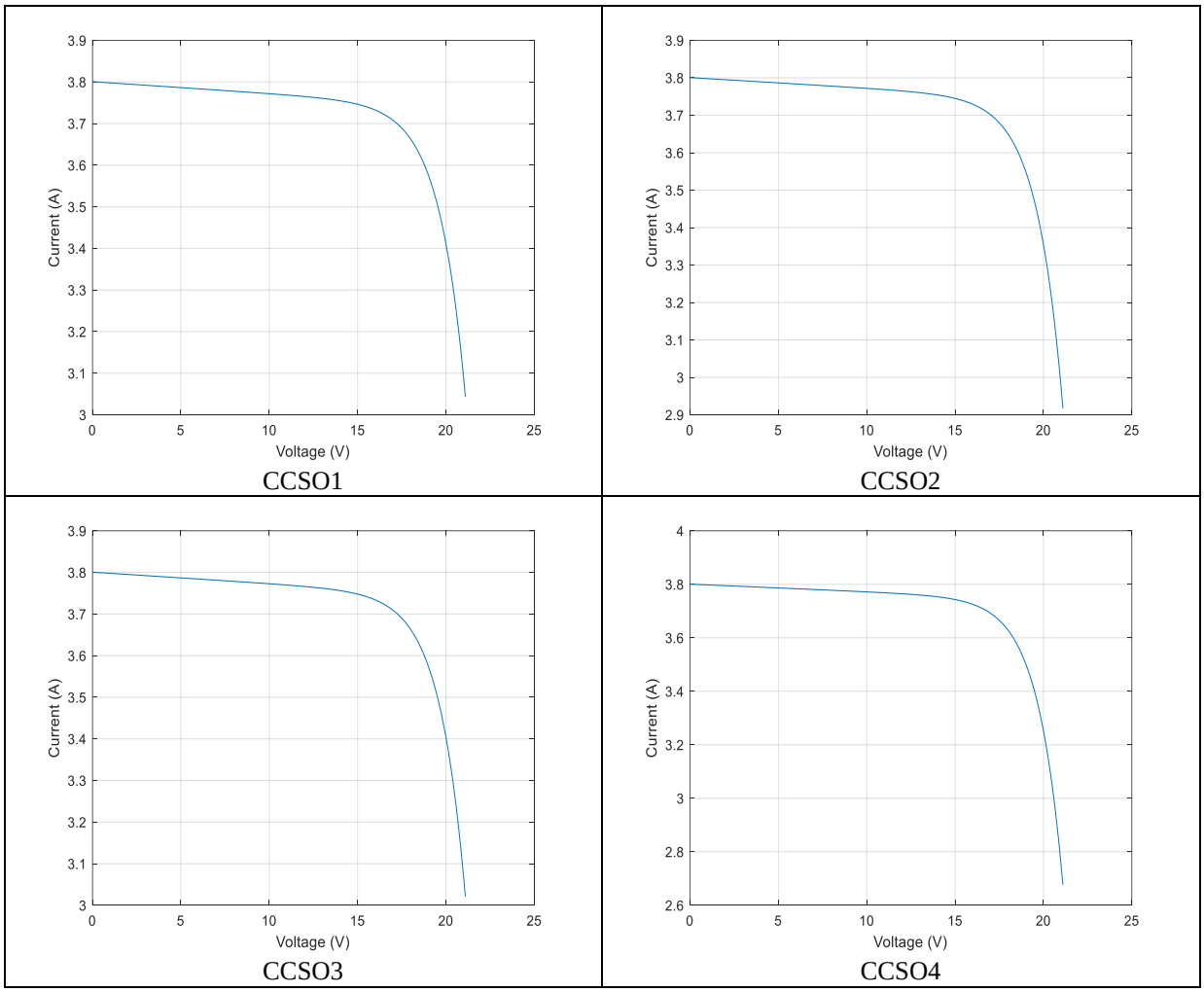

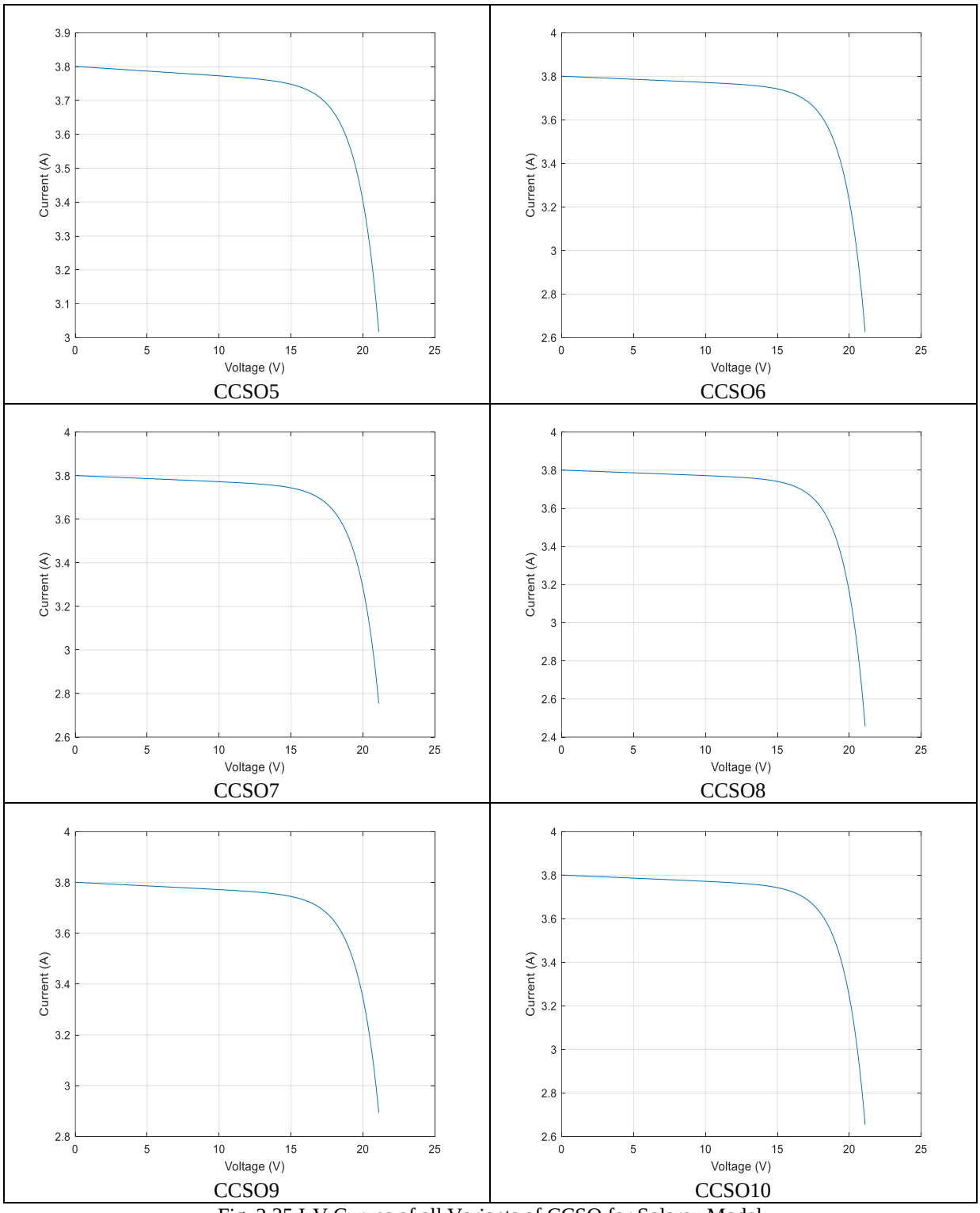

Fig. 2.35 I-V Curves of all Variants of CCSO for Solarex Model

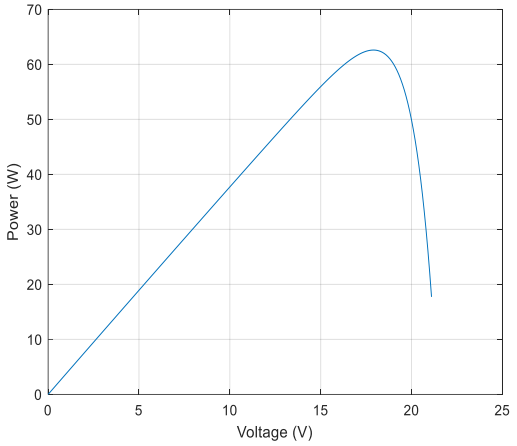

CCSO1

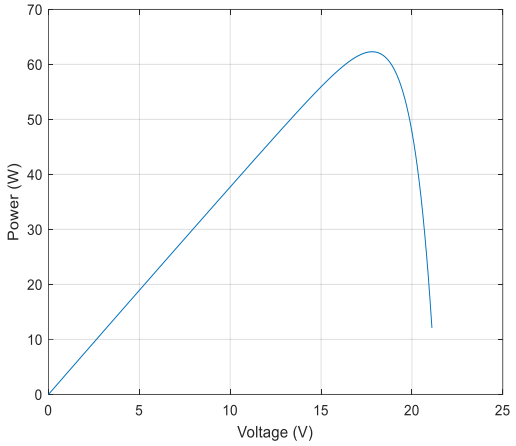

CCSO2

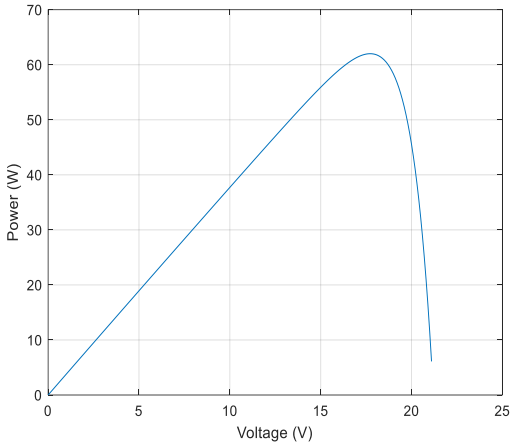

CCSO3

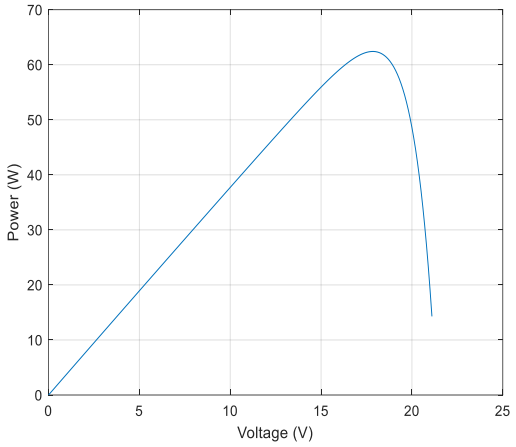

CCSO4

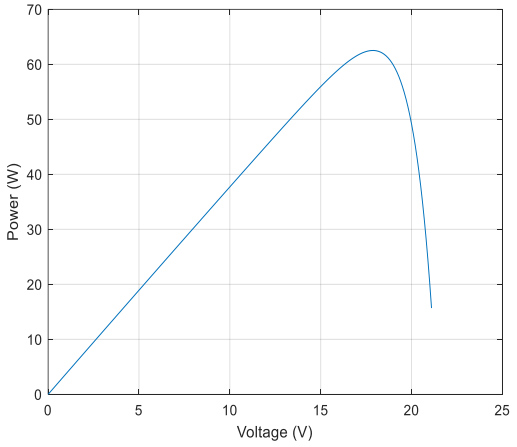

CCSO5

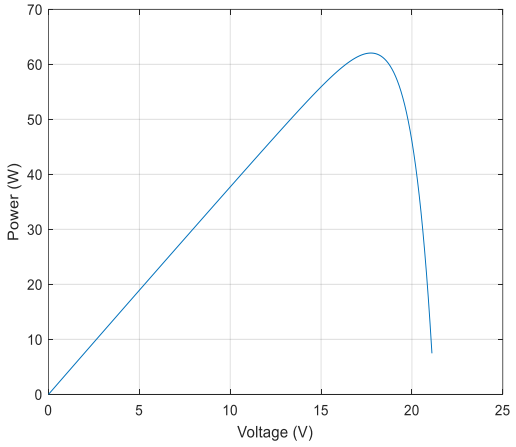

CCSO6

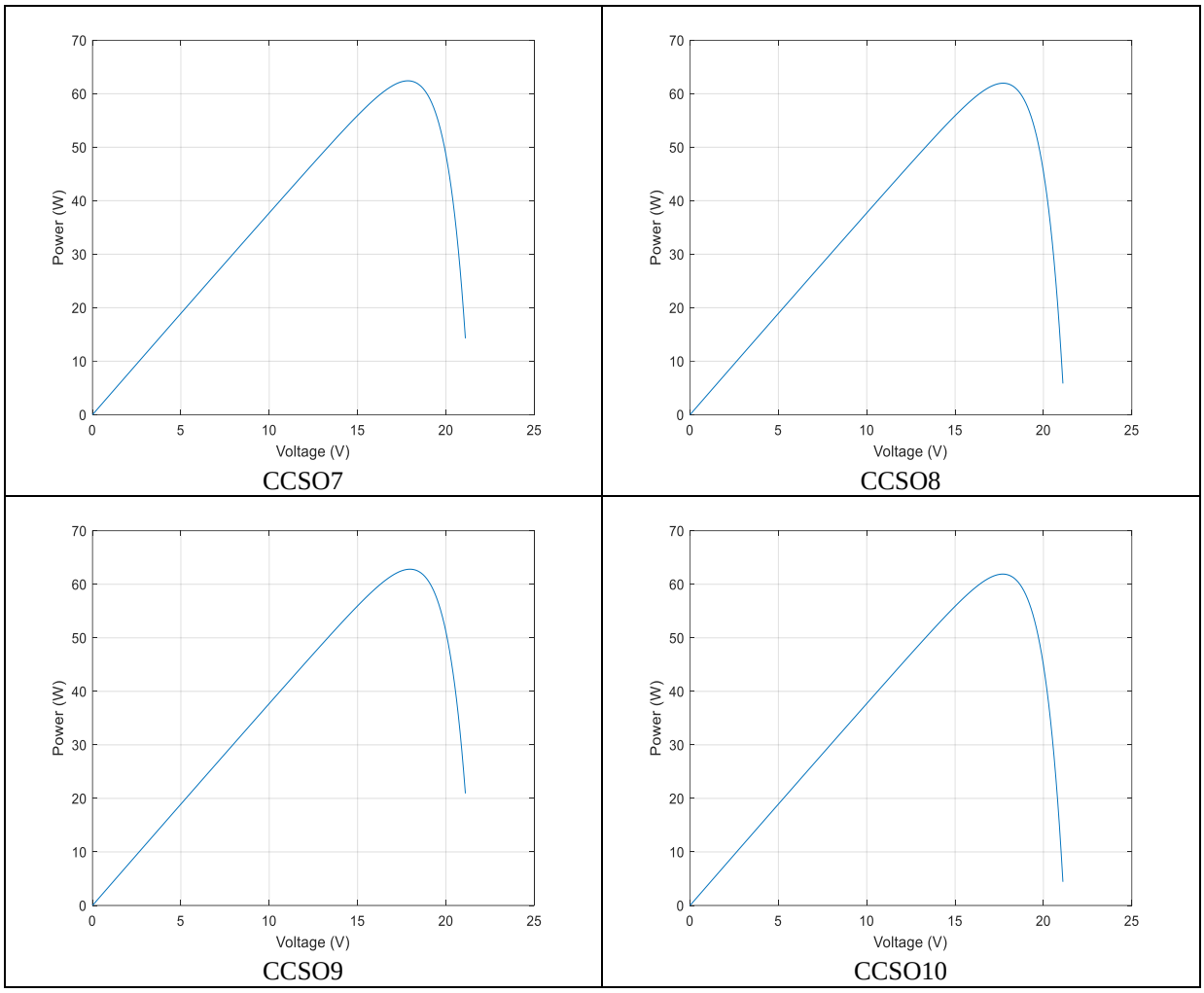

Fig. 2.36 P-V Curves of all Variants of CCSO from the Estimated Parameters

- **Non - Parametric Tests**

Similar to case 1, 2 for better validation of the results, non-parametric tests are conducted. Initially, the rank-sum test of Wilcoxon's is carried out [113]. Table 2.36 (a) and 2.36 (b) list the calculated p-values and justifies that the performances of all variants of CCSO are significant, with the significance level of 95%.

Table 2.36 (a) p-Values for the Wilcoxon's Rank-Sum Test of Solarex Model

Algorithms	CSO	DA	ALO	MVO	WOA
CCSO1	3.0253E-11	3.0161E-11	2.9947E-11	3.0142E-11	3.0180E-11
CCSO2	3.0467E-11	2.9770E-11	3.0259E-11	3.0021E-11	2.9966E-11
CCSO3	3.0148E-11	3.0516E-11	3.0422E-11	3.0570E-11	3.0719E-11
CCSO4	3.0856E-11	3.0187E-11	3.0905E-11	3.0164E-11	3.0804E-11
CCSO5	3.0910E-11	3.0850E-11	3.0611E-11	3.0349E-11	3.0133E-11
CCSO6	3.0619E-11	3.0912E-11	3.0388E-11	3.0949E-11	3.0481E-11
CCSO7	3.0321E-11	2.9428E-11	3.0815E-11	3.0073E-11	3.0349E-11

CCSO8	3.0437E-11	3.0666E-11	3.0803E-11	3.0121E-11	3.0091E-11
CCSO9	3.0705E-11	3.0009E-11	3.0052E-11	3.1017E-11	2.9914E-11
CCSO10	3.0193E-11	3.0061E-11	2.9969E-11	3.0501E-11	3.0801E-11

Table 2.36 (b) p-Values for the Wilcoxon's Rank-Sum Test of Solarex Model

Algorithms	**GOA**	**SCA**	**SSA**	**HHO**	**ASO**
CCSO1	2.9921E-11	3.0999E-11	3.0104E-11	3.0617E-11	2.9957E-11
CCSO2	2.9175E-11	3.0123E-11	3.0597E-11	3.0102E-11	2.9891E-11
CCSO3	2.9564E-11	3.0357E-11	3.0091E-11	3.0199E-11	2.9530E-11
CCSO4	2.9991E-11	3.0638E-11	2.9964E-11	2.9983E-11	2.9204E-11
CCSO5	3.0042E-11	3.0529E-11	3.0137E-11	3.0544E-11	2.9384E-11
CCSO6	2.9709E-11	3.0246E-11	3.0339E-11	3.0489E-11	2.9901E-11
CCSO7	2.9613E-11	3.0814E-11	3.0815E-11	3.0261E-11	2.9407E-11
CCSO8	2.9381E-11	3.0551E-11	3.0740E-11	3.0115E-11	2.9755E-11
CCSO9	2.9850E-11	3.0349E-11	3.0442E-11	3.0591E-11	2.9102E-11
CCSO10	3.0127E-11	3.0100E-11	3.1145E-11	3.0102E-11	2.9991E-11

Similar to first and second case, the next test preformed is Kruskal Wallis test [114]. The outcome graphs presented in Fig. 2.37 shows that the mean ranks of the CCSO techniques are significantly different from the other algorithms.

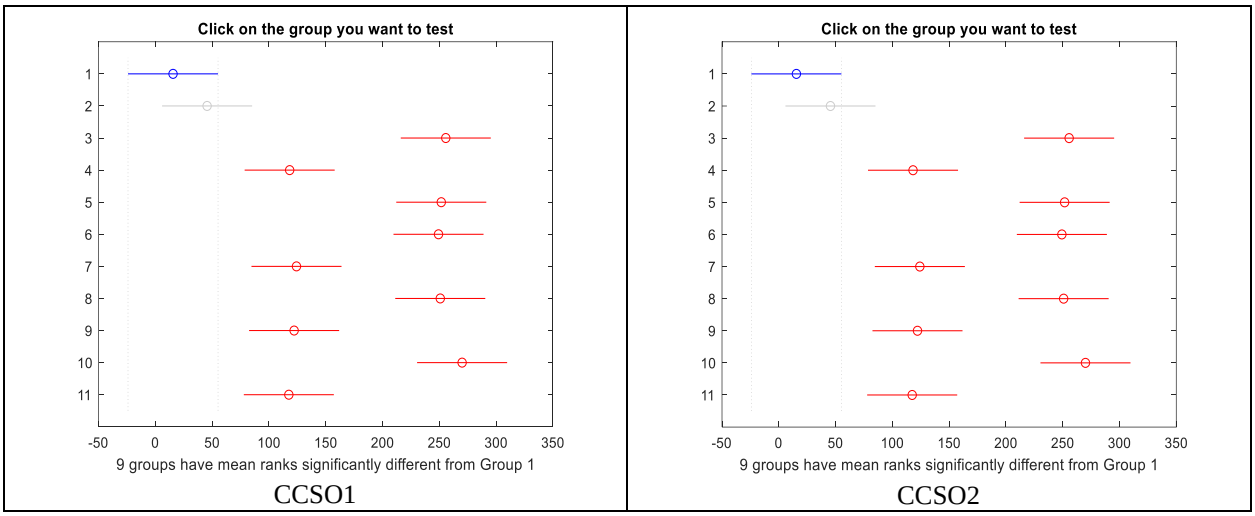

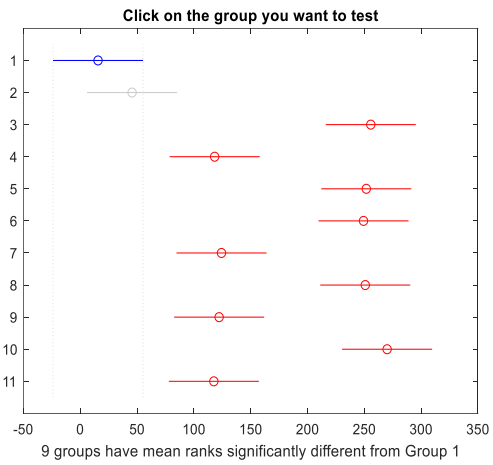

CCSO3

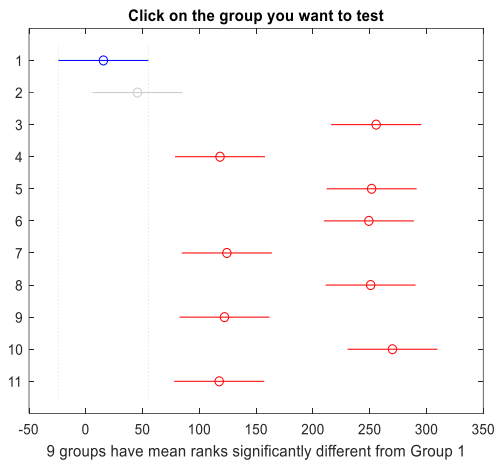

CCSO4

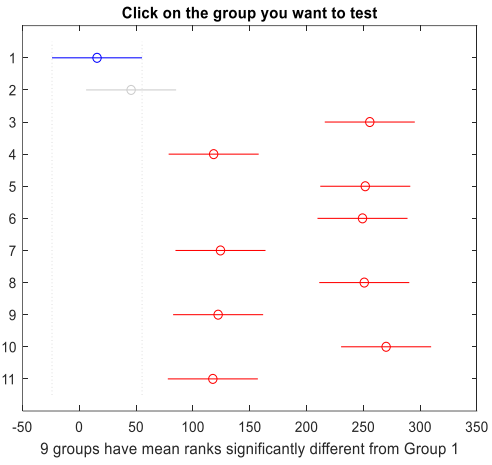

CCSO5

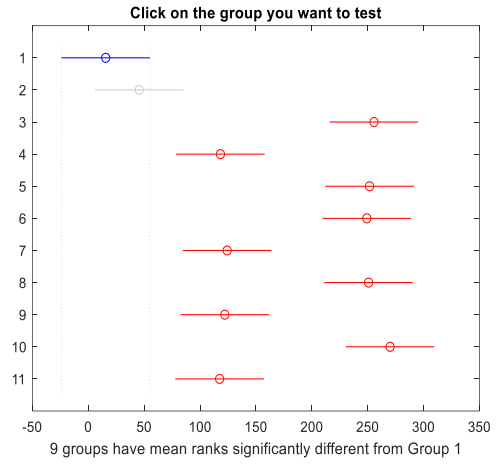

CCSO6

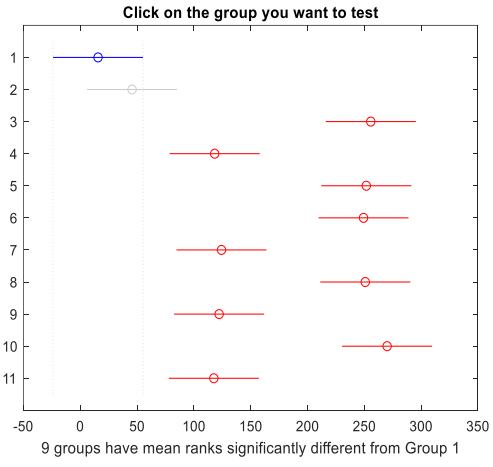

CCSO7

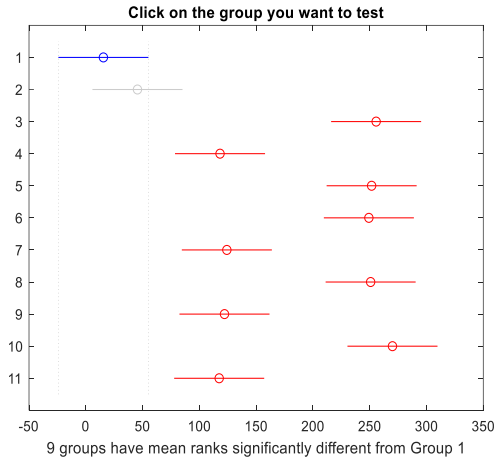

CCSO8

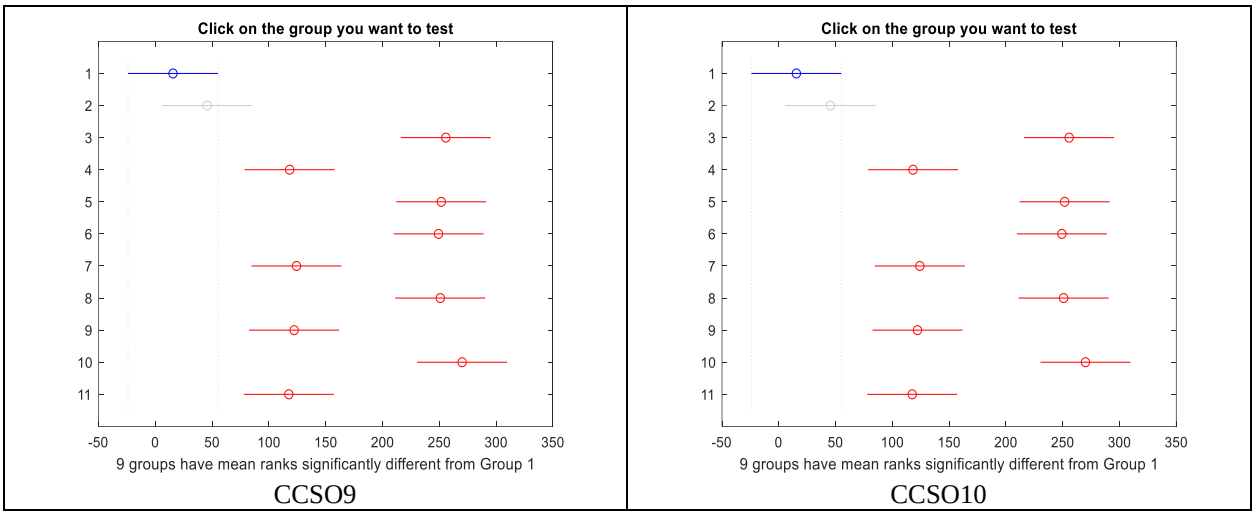

Fig. 2.37 Kruskal Wallis Test Diagram for the Solarex Model Results

Similar to first and second case, p-values obtained by Wilcoxon's rank test is further evaluated using Holm-Bonferroni corrections method. The outcome results are presented in Table 2.37 validate the proposed CCSO algorithm. Thus, it is found that the new swarm technique proves beneficial to extract successfully the parameters of TDM.

Table 2.37 Corrected p-Values by Holm-Bonferroni Corrections for Wilcoxon's Rank Test of Solarex Model (Multiply the results with (1.0e-09) and test of significance (h) is 1)

Algorithms	CSO	DA	ALO	MVO	WOA	GOA	SCA	SSA	HHO	ASO
CCSO1	0.1207	0.1809	0.2992	0.2107	0.1508	0.2992	0.0612	0.2397	0.0908	0.2695
CCSO2	0.0908	0.2918	0.1205	0.2098	0.2391	0.2918	0.1505	0.0609	0.1801	0.2679
CCSO3	0.2407	0.1217	0.1518	0.0915	0.0611	0.2953	0.1812	0.2661	0.2110	0.2953
CCSO4	0.0924	0.1810	0.0617	0.2099	0.1226	0.2399	0.1509	0.2920	0.2697	0.2920
CCSO5	0.0911	0.0610	0.2087	0.1794	0.2073	0.2383	0.1510	0.2073	0.1213	0.2383
CCSO6	0.1220	0.0919	0.2124	0.0618	0.1823	0.2971	0.2691	0.2420	0.1524	0.2971
CCSO7	0.1816	0.2941	0.0924	0.2369	0.1516	0.2649	0.1214	0.0616	0.2105	0.2941
CCSO8	0.1807	0.1222	0.0615	0.2108	0.2678	0.2938	0.1522	0.0920	0.2407	0.2938
CCSO9	0.0918	0.2393	0.2101	0.0614	0.2686	0.2910	0.1803	0.1517	0.1218	0.2910
CCSO10	0.1205	0.0905	0.2398	0.1799	0.2068	0.2398	0.1503	0.2068	0.0604	0.2099

2.4 Outcomes

A new chaotic algorithm, namely CTSA and CCSO, is suggested to resolve worldwide optimization concerns and to extract parameters from different solar cells. The findings are outlined as follows, based on the results so obtained.

- The accurate solution and speed of convergence of global optimization problems reveal that the chaotic variant family performs better than the rest of the compared algorithms

- The metaheuristic algorithms CTSA use RMSE as whereas CCSO uses SSE as an objective function to obtain the solar cell parameters.
- The performance of the suggested methods is analyzed by comparing them with some of the latest and standard heuristic techniques. The accuracy of proposed approach is verified through convergence characteristics.
- The I-V and P-V curves are presented which shows similarity to the curves under STC conditions.
- Further to validate the error result, the non-parametric statistical tests are also executed.

CHAPTER 3 PARAMETER ESTIMATION OF PROTON EXCHANGE MEMBRANE FUEL CELL

3.1 Introduction

Fuel cells can be used in many applications and have grown very quickly as well as the most common renewable sources of energy (wind and solar) and these renewable energies are a strong competitor. Fuel cells have drawn the interest of many scholars and producers in the previous years. Fuel cell directly transforms the chemical energy produced by the chemical reactions among hydrogen and oxygen into electrical energy in the presence of a catalyst [116-121]. There are several kinds of fuel cells depending on the form of electrolyte. Among these cells, the most frequent form is the Proton Exchange Membrane Fuel Cell (PEMFC) [120]. Owing to its large power density while operating under low temperatures and its rapid response against electrodynamics processes, PEMFC gained significant attention from researchers [122-123].

Because of the PEMFC significance and its developments in industrialized usage and cost reduction, it is important to construct a precise model in order to obtain the clear understanding about the dynamic processes and phenomena that would have occurred in the fuel cell without performing the complex experiments in order to save time and effort [122]. Multiple papers have attempted to identify the function of PEMFC in recent years and many models have been given in the literature [123]. Indeed, one of the important features of the fuel cell is the polarization curve, which describes relationship among both output cell voltage and the cell current.

There are large number of unidentified design parameters that are need to be precisely calculated, and the key challenge facing researchers while inspecting a mathematical PEMFC model to analyze the certain functions and its polarization curves. Usually, the statistics contained in the any PEMFC datasheet is typically not sufficient to locate the optimal set of parameters. However, if the exact parameters are not defined, there are considerable differences between the data obtained on the basis of the model and mentioned in the manufacturer's datasheet [122]. The identification of unknown parameters of PEMFC can then be treated as a problem of optimization and various algorithms can be used to find the optimal solution to this issue.

The conventional optimization strategies would result in the lack of matching of calculated information implemented by the vendor due to high nonlinearity of PEMFC polarization curves. Meta-heuristics are suggested for such issues as derivative-free approaches to solve the lack of conventional optimization strategies and their action allows stochastic motions to find the optimal

global solution. Numerous meta-heuristic optimization algorithms have been implemented over the past ten years to resolve the topic of PEMFC parameter estimation [124-126].

3.2 Mathematical Model of PEMFC Stacks

PEMFC is typically composed of cathode and anode electrodes which are separated by a polymer electrolyte membrane whose purpose is to inhibit the flow of electrons [127]. As depicted in Fig. 3.1, hydrogen is injected from the anode side and the cathode side oxygen is injected.

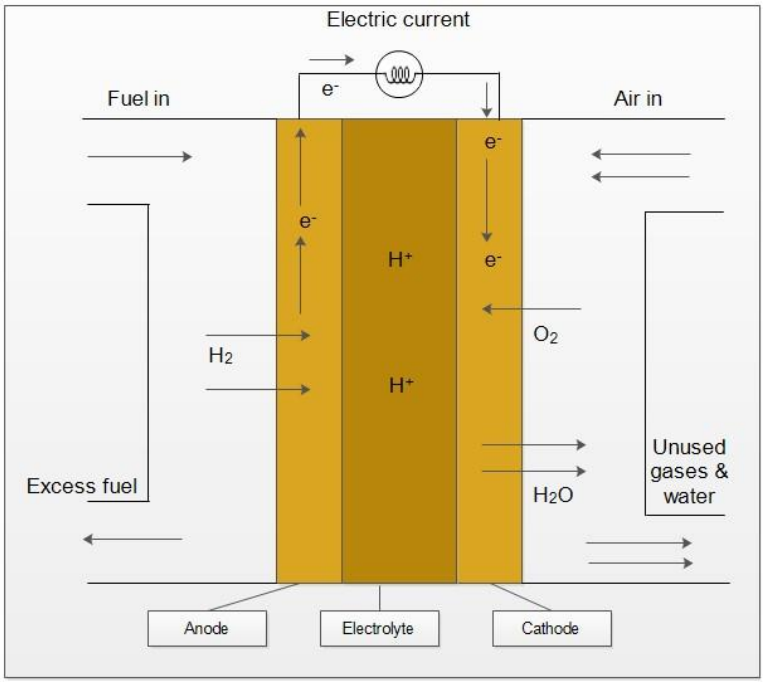

Fig. 3.1 Schematic Diagram of PEMFC

The electrochemical processes occurring at electrodes of a PEMFC can be described in equation 3.1 to 3.3:

$$\text{Anode side: } H_2 \rightarrow 2H^+ + 2e^- \tag{3.1}$$

$$\text{Cathode side: } 2H^+ + \frac{1}{2}O_2 \rightarrow H_2O \tag{3.2}$$

$$\text{Overall chemical reaction: } 2H^+ + \frac{1}{2}O_2 \rightarrow H_2O + \text{energy} \tag{3.3}$$

In equation 3.3, energy referred to describes the production of electrical energy. It is produced by the supply of electrons to the cathode electrode by an electrical load circuit at the anode electrode, as depicted in Fig. 3.1. A single PEMFC stack's output current and voltage are quite small. Therefore, multiple stacks are necessary to be combined and connected, either in series or parallel, based on specifications, to produce a sufficient amount of energy. When connected in series, the stack output voltage is defined in equation 3.4.

$$V_{stack} = N_{cells} * V_{cell} \tag{3.4}$$

Where the number of cells connected in series is denoted by N_{cells}, and the voltage of each cell is denoted by V_{cell}.

Each fuel cell's terminal output voltage consists mainly of three types of voltage, namely activation voltage drop is denoted by $V_{activation}$, an ohmic voltage drop is denoted by V_{ohmic}, and the concentration voltage drop is denoted by $V_{concentration}$. The single fuel cell's output voltage is mentioned in equation 3.5.

$$V_{cell} = E_{Nernst} - V_{activation} - V_{ohmic} - V_{concentration} \tag{3.5}$$

Where open circuit voltage is denoted by E_{Nernst} and, the below equation 2.6 represents the mathematical form of E_{Nernst}.

$$E_{Nernst} = 1.229 - 0.85 \times 10^{-3}\left(T_{fc} - 298.15\right) + 4.3085 \times 10^{-3} T_{fc} \times \left[\ln(P_{H2}) + \ln(\sqrt{P_{O2}})\right] \tag{3.6}$$

Where the operating cell temperature is denoted by T_{fc}, in the fuel cell stack the partial pressure of oxygen and hydrogen at the inlet channels is represented by P_{O2} and P_{H2} respectively.

P_{H2} and P_{O2} can be expressed by equation 3.7 and 3.8:

$$P_{H2} = 0.5(PH_a \times P_{H2O})\left[(\exp(\frac{1.635\left(\frac{I_{fc}}{A}\right)}{T_{fc}^{1.334}}) \times \frac{(PH_a \times P_{H2O})}{P_a})^{-1} - 1\right] \tag{3.7}$$

$$P_{O2} = (RH_C \times P_{H2O})\left[(\exp(\frac{4.192\left(\frac{I_{fc}}{A}\right)}{T_{fc}^{1.334}}) \times \frac{(PH_a \times P_{H2O})}{P_c})^{-1} - 1\right] \tag{3.8}$$

Where the pressure at the anode and cathode of the input channel is denoted by P_a and P_c; around anode and cathode the relative vapour humidity is represented by $PH_a$and RH_C; current generated by the cell is denoted by I_{fc}, a membrane of the surface area is denoted by A, P_{H2O} denotes water saturation pressure that can be represented by the equation 3.9:

$$P_{H2O} = 2.95 \times 10^{-2}\left(T_{fc} - 273.15\right) - 9.18 \times 10^{-5}\left(T_{fc} - 273.15\right)^2 + 1.44 \times 10^{-7}\left(T_{fc} - 273.15\right)^3 - 2.18 \tag{3.9}$$

The voltage loss due to the activation process $V_{activation}$ can be calculated as shown in equation 3.10:

$$V_{activation} = -\left[\xi_1 + \xi_2 T_{fc} + \xi_3 T_{fc} \ln(C_{O2}) + \xi_3 T_{fc} ln \ln\left(I_{fc}\right)\right] \tag{3.10}$$

Where the semi-empirical coefficients are denoted by ξ_1, ξ_2, ξ_3, ξ_4; in the cathode side the concentration of the oxygen is denoted by C_{O2} and is calculated as shown in equation 3.11:

$$C_{O2} = \frac{P_{O2}}{5.08\times10^6\times exp^{-(\frac{498}{T_{fc}})}} \tag{3.11}$$

Equation 3.12 represents the resistive ohmic voltage drop, in this equation, the membrane surface resistance is denoted by $R_{M,}$ and the connection of the resistance is denoted by R_C and the resistance of membrane is expressed in equation 3.13.

$$V_{ohmic} = I_{fc}(R_M + R_C) \tag{3.12}$$

$$R_M = \frac{\rho M\times l}{A} \tag{3.13}$$

Where the membrane material of specific resistance is denoted by ρM, the membrane thickness is denoted by *l*, and in the equation 3.14, ρM is expressed as:

$$\rho M = \frac{181.6[1+0.03\left(\frac{I_{fc}}{A}\right)+0.062(\frac{T_{fc}}{303})^2(\frac{I_{fc}}{A})^{2.5}}{\left[\lambda-0.634-3(\frac{I_{fc}}{A})\right]\times exp\left[4.18(\frac{T_{fc}-303}{T_{fc}})\right]} \tag{3.14}$$

Where the adjustable empirical variable is denoted by λ. In equation 3.15 $V_{concentration}$ is expressed as:

$$V_{concentration} = -b\ ln(1-\frac{J}{Jmax}) \tag{3.15}$$

Where the parametric variable is denoted as *b*, and the maximum current density is denoted by $Jmax$.

From the previous equations, it has been observed that the seven parameters have to be determined correctly. Generally, certain parameters are not defined in the vendor's datasheet. Accurate analysis of these parameters is therefore very necessary to guarantee adequate modeling of PEMFC under control and operation. Specifically, the PEMFC model has seven unknown parameters, such as ξ_1, ξ_2, ξ_3, ξ_4, λ, R_C, and *b*. Using the proposed algorithm, the unknown parameters are designed to have the best values between their lower and upper limits.

3.3 Proposed Algorithms and Outcomes

3.3.1 Slime Mould Algorithm (SMA)

The slime mould usually refers to physarum poly-cephalum [128]. Since it was first known as a fungus, it was then called a “slime mould” whose life cycle was initially described in a paper published in 1931 by Howard [129]. A eukaryote that inhabits cold and humid areas is the slime mould.

- **Mathematical Modeling of the SMA**

(a) Approach Food: Using a mathematical expression, SM behaviour is modeled. The phrase below emulates the SM's contraction mode as shown in equation 3.16.

$$\overrightarrow{E(l+1)} = \left\{\overrightarrow{E_b(l)} + \overrightarrow{A_b} * \left(\vec{W} * \overrightarrow{E_A(l)} - \overrightarrow{E_B(l)}\right), r < p\overrightarrow{A_c} * \overrightarrow{E(l)}, r \geq p\right\} \quad (3.16)$$

Where the parameter $\overrightarrow{A_b}$ is a variable with a range of [-a, a] and $\overrightarrow{A_c}$ reduces from 1 to 0 linearly. 'l' in the equations is referred to as the current iteration. $\vec{E}$ represents SM location, the individual current location is represented by $\overrightarrow{E_b}$ with the peak odour concentration, $\vec{W}$ represents SM weights, $\overrightarrow{E_A(l)}$ and $\overrightarrow{E_B(l)}$ represent individuals selected from the swarm randomly. The variable 'p' can be expressed as shown in equation 3.17:

$$\text{p} = |H(j) - C_f| \quad (3.17)$$

Where, C_f represents the best solution found by all iterations and $H(j)$ represents $\vec{E}$ fitness, $j \in$1,2,….n.

The $\overrightarrow{A_b}$ and $\vec{W}$ can be expressed as following equation 3.18-3.21:

$$\overrightarrow{A_b} = [-a, a] \quad (3.18)$$

$$a = \text{arctanh}\left(1 - \left(\frac{l}{\max\_l}\right)\right) \quad (3.19)$$

$$\overrightarrow{W(Smellindex(j))} = \begin{cases} 1 + r * log\left(\frac{C_f - H(j)}{C_f - w_f} + 1\right), condition \\ 1 - r * log\left(\frac{C_f - H(j)}{C_f - w_f} + 1\right), others \end{cases} \quad (3.20)$$

$$Smellindex = sort(H) \quad (3.21)$$

Where ‘r’ is any random value between [0, 1], the word 'condition' represents that $H(j)$ ranks half of the population of SM initially. The sorted fitness value set arranged in ascending order represents the ‘smell index’. The best and worst solution is depicted as ‘C_f’ and ‘w_f’ respectively.

(b) Wrap Food: It deals mathematically with the contraction method of the intravenous search arrangement of the SM. A vein with high food content creates a higher bio-oscillator propagation wave, which produces the maximum cytoplasm flow rate which allows the vein to get thicker. Mathematically, equation 3.20 simulated the positive and negative feedback between the thicknesses of the SM vein. Intravenous contraction mode volatility is represented as ‘r’ and log in equation 3.20 is used to maximize the significance of rate change. In equation 3.20, the ‘condition’ simulates the SM to change the search patterns depending on the consistency of food.

While the food concentration is high, the region's weight is more prevalent, and when the food concentration is smaller, the region's weight decreases, thereby shifting to looking in other areas. The position of the SM is modified according to the following equation 3.22 based on the discussion.

$$\overrightarrow{E^*} = \begin{cases} rand.(ub - lb) + lb, rand < z \\ \overrightarrow{E_b(l)} + \overrightarrow{A_b} * \left(\overrightarrow{W} * \overrightarrow{E_A(l)} - \overrightarrow{E_B(l)}\right), r < p \\ \overrightarrow{A_c} * \overrightarrow{E(l)}, r \geq p \end{cases} \quad (3.22)$$

The 'ub' depicts the upper bound and 'lb' depicts the lower bound, 'rand' is any random value between [0, 1]. The parameter 'z' value is set by experimental work.

(c) Grabble Food: To regulate the cytoplasmic flow in the veins, the SM is subject to the wave produced by the bio-oscillator so that it can transfer to the best food location. The SM intravenous width variance simulation is conducted with the aid of W, Ab, and Ac. The weight, W, mathematically simulates the oscillation frequency of the SM similar to one at different food concentrations. The SM will then reach the food easily if the SM discovers healthy food. When the food is approached steadily at lower food concentrations at a given site, the SM quality of food source collection is then increased optimally. The value of Ab differs, as defined in the discussion, between [-a, a] and slowly increases to zero. In the end, the value of Ac varies between [-1, 1] and zero is slowly reached. Fig. 3.2 presents pseudo code of SMA in a summarized manner and Fig. 3.3 flow chart of SMA.

Experimental values of V_{pv} and I_{pv}
Initialize the parameters pop size, Max iteration.
Initialize the positions of SM, E_j (j= 1,2,.....,p).
While (l < Max it)
Calculate the fitness of all SM,
Update best fitness, E_b
Calculate the weight, W
For each search phase
Update p, A_b, A_c.
Update search agent positions
End for
l = l+1;
Return best fitness, E_b.

Fig. 3.2 Pseudo code of SMA

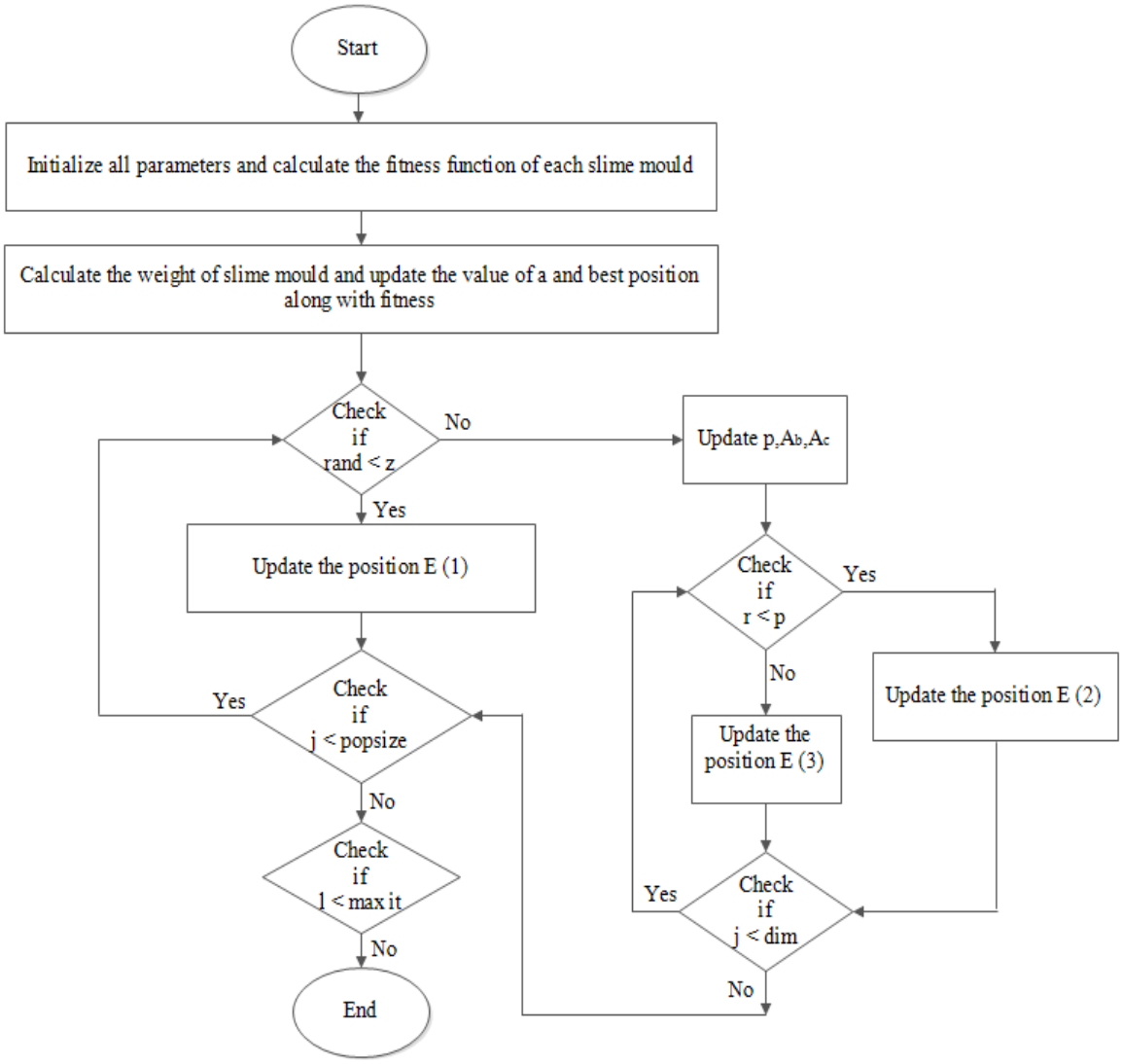

Fig. 3.3 Flow Chart of SMA

3.3.1.1 Discussion and Outcomes of SMA

A benchmark test research approach was adopted in this section, for the evaluation of the proposed algorithm in the case of parameter identification for PEMFC. Table 3.1 shows the ten-benchmark test function from which one to seven functions is uni-modal, eight to ten is multi-modal functions and the remaining function is CEC functions. To check the accuracy and performance of the proposed algorithm, some well-known meta-heuristic algorithms are compared i.e., PSO, ASO, ALO, HHO and GOA. Table 3.2 represents the statistical results of benchmark test functions. From Table 3.2 it is concluded that the proposed algorithm has the lowest mean and standard deviation (SD) values than the other compared algorithms. From the benchmark test function, it is concluded that the proposed algorithm has better performance, and accuracy than the rest of the compared

algorithms. Two test cases with the given experimental I-V data curves are conducted to determine the value of the proposed SMA in computing the unknown parameters of the PEMFC model for efficient simulation and modeling, on commercial typical ones such as Avista SR-12, and Ballard Mark V. These two commercial PEMFC stacks and the typical boundaries of seven unknown parameters is shown in Table 3.3 (a), Table 3.3 (b) and Table 3.3 (c). It is well known that the essence of the estimation of parameters is an off-line task; it is not a matter of computational time. Under steady-state conditions, the predicted test cases are illustrated as follows:

Table 3.1 Benchmark Test Function

Name of Function	**Function**	**Range**	**Dimension**
f_1= Sphere	$f_1(y) = \sum_{j=1}^{m} y_j^2$	[-100,100]	m=30
f_2= Schwefel 2.22	$f_2(y) = \sum_{j=1}^{m} \lvert y_j \rvert + \prod_{j=1}^{m} \lvert y_j \rvert$	[-10,10]	m=30
f_3= Schwefel 1.2	$f_3(y) = \sum_{j=1}^{m} \left(\sum_{i=1}^{j} y_i\right)^2$	[-100,100]	m=30
f_4= Schwefel 2.21	$f_4(y) = \max_j \{\lvert y_j \rvert, 1 \le j \le m\}$	[-100,100]	m=30
f_5= Rosen-brock	$f_5(y) = \sum_{j=1}^{m} 100\left(y_j + 1 - y_j^2\right)^2 + \left(y_j - 1\right)^2$	[-30,30]	m=30
f_6= Step	$f_6(y) = \sum_{j=1}^{m} \left(\left[y_j + 0.5\right]\right)^2$	[-100,100]	m=30
f_7= Quartic	$f_7(y) = \sum_{j=1}^{m} j y_j^4 + \text{randm } [0,1]$	[-128,128]	m=30
F_8= Schwefel	$f_{11}(y) = \sum_{j=1}^{m} -y_j \text{Sin}\left(\sqrt{\lvert y_j \rvert}\right)$	[-500,500]	m=30
F_9= Rastrigin	$f_{12}(y) = \sum_{j=1}^{m} \left[y_j^2 - 10\text{Cos}\left(2\pi y_j\right) + 10\right]$	[-5.12,5.12]	m=30
f_{10}= Ackley	$f_{13}(y) = -20\exp\left(-0.2\left(\frac{1}{m}\sum_{j=1}^{m} y_j^2\right)^{\Lambda} 0.5\right) - \exp\left(\frac{1}{m}\sum_{j=1}^{m} \text{Cos}\left(2\pi y_j\right)\right) + 20 + e$	[-32,32]	m=30
f_{11}= CEC1	$f1, f2, f3 \ldots f10 = Sphere\ function$ $\delta 1, \delta 2, \delta 3 \ldots \delta 10 = [1,1,1, \ldots 1]$ $\lambda 1, \lambda 2, \lambda 3 \ldots \lambda 10 = \left[\frac{5}{100}, \frac{5}{100}, \frac{5}{100}, \ldots \frac{5}{100}\right]$	[-5, 5]	m=30
f_{12}= CEC2	$f1, f2, f3 \ldots f10 = Griewanks'sfunction$ $\delta 1, \delta 2, \delta 3 \ldots \delta 10 = [1,1,1, \ldots 1]$ $\lambda 1, \lambda 2, \lambda 3 \ldots \lambda 10 = \left[\frac{5}{100}, \frac{5}{100}, \frac{5}{100}, \ldots \frac{5}{100}\right]$	[-5,5]	m=30
f_{13}= CEC3	$f1, f2, f3 \ldots f10 = Griewanks'sfunction$ $\delta 1, \delta 2, \delta 3 \ldots \delta 10 = [1,1,1, \ldots 1]$ $\lambda 1, \lambda 2, \lambda 3 \ldots \lambda 10 = [1,1,1, \ldots 1]$	[-5,5]	m=30
f_{14}= CEC4	$f1, f2 = Ackely'sfunction$ $f3, f4 = Rastrigin'sfunction$ $f5, f6 = Weierstrass\ function$ $f7, f8 = Griewanks'sfunction$ $f9, f10 = Sphere\ function$ $\delta 1, \delta 2, \delta 3 \ldots \delta 10 = [1,1,1, \ldots 1]$ $\lambda 1, \lambda 2, \lambda 3 \ldots \lambda 10 = \left[\frac{5}{32}, \frac{5}{32}, 1,1, \frac{5}{0.5}, \frac{5}{0.5}, \frac{5}{100}, \frac{5}{100}, \frac{5}{100}, \frac{5}{100}\right]$	[-5,5]	m=30

f_{15}= CEC5	$f1, f2 = Rastrigin'sfunction$ $f3, f4 = Weierstrass\ function$ $f5, f6 = Griewanks'sfunction$ $f7, f8 = Ackely'sfunction$ $f9, f10 = Sphere\ function$ $\delta1, \delta2, \delta3 \dots \delta10 = [1,1,1, \dots 1]$ $\lambda1, \lambda2, \lambda3 \dots \lambda10 = \left[\frac{1}{5}, \frac{1}{5}, \frac{5}{0.5}, \frac{5}{0.5}, \frac{5}{100}, \frac{5}{100}, \frac{5}{32}, \frac{5}{32}, , \frac{5}{100}, \frac{5}{100}\right]$	[-5,5]	m=30

Table 3.2 (a) Statistical Results of Benchmark Test Functions

Benchmark Test Functions →		**f_1**	**f_2**	**f_3**	**f_4**	**f_5**
Algorithms↓	**Statistical Results↓**					
SMA	**MEAN**	0	1.8715E-206	0	1.0978E-209	2.2735E-03
	SD	0	0	0	0	2.7975E-03
PSO	**MEAN**	6.9509	3.5447E+01	1.8690E+04	3.2352E+01	9.6377E+03
	SD	4.74391	4.9241E+01	8.6077E+03	2.9032E+01	1.3508E+04
ALO	**MEAN**	1.7862E-06	1.7344E+01	5.1201E+02	9.0774	7.5436E+01
	SD	1.3719E-06	2.8581E+01	2.0390E+02	3.0980	9.5474E+01
ASO	**MEAN**	4.1058E-25	1.2040E-12	2.3213E-23	6.8409	2.7190
	SD	2.79865E-25	2.7327E-13	3.7495E-23	5.6384	2.6205E-01
GOA	**MEAN**	2.2542E-01	2.5835E-29	2.7624E+03	1.4698E+01	3.1552E+01
	SD	8.4246E-02	1.2889E-28	1.2436E+03	4.4614	2.8770E+01
HHO	**MEAN**	3.4357E-187	4.6690E-96	2.3936E-146	3.7371E-116	2.6831E+01
	SD	0	1.7643E-95	1.3110E-145	5.7317E-132	4.8202E-01

Table 3.2 (b) Statistical Results of Benchmark Test Functions

Benchmark Test Functions →		**f_6**	**f_7**	**f_8**	**f_9**	**f_{10}**
Algorithms↓	**Statistical Results↓**					
SMA	**MEAN**	3.4229E-25	1.1722E-04	-1.2569E+04	0	8.8818E-16
	SD	2.1286E-25	9.1391E-05	6.6739E-02	0	4.0117E-31
PSO	**MEAN**	4.8303	6.7539E-02	-6.1144E+02	1.1019E+02	1.1345E+01
	SD	2.0015E-01	2.7655E-02	7.4059E+01	3.2363E+01	9.6867
ALO	**MEAN**	2.3298E-06	2.5383E-02	-6.2172E+03	7.9365E+01	2.6276
	SD	2.2787E-06	1.6572E-02	1.4997E+03	2.3460E+01	1.3884
ASO	**MEAN**	9.8011E-04	4.4398E-03	-2.5765E+03	4.9416	7.4720E-13
	SD	4.2763E-04	2.3053E-03	2.1950E+02	1.5782	3.1797E-13
GOA	**MEAN**	3.5270E+01	4.9206E-02	-7.4741E+03	4.5934E+01	5.1976
	SD	1.9676E+01	2.1885E-02	5.7741E+02	1.7104E+01	8.7172E-01
HHO	**MEAN**	5.3282E-05	8.0793E-04	-1.0713E+04	0	8.8818E-15
	SD	6.8647E-05	1.0936E-03	6.9181E+02	0	8.0235E-30

Table 3.2 (c) Statistical Results of Benchmark Test Functions

Benchmark Test Functions →		**f_{11}**	**f_{12}**	**f_{13}**	**f_{14}**	**f_{15}**
Algorithms↓	**Statistical Results↓**					
SMA	**MEAN**	4.8836E+04	1.7343E+01	1.2703E+01	1.4248E+01	1.2004

	SD	9.3437E+03	1.3984E-04	0	3.8810	9.6738E-02
PSO	**MEAN**	1.1594E+11	1.7343E+01	1.2702E+01	2.5414E+01	1.0755
	SD	9.0609E+10	1.0246E-10	6.6454E-13	1.1115E+01	3.1065E-02
ALO	**MEAN**	5.4744E+09	1.7346E+01	1.2702E+01	2.7660E+01	1.1344
	SD	6.5831E+09	9.4061E-03	1.8724E-15	1.2996E+01	5.2462E-02
ASO	**MEAN**	7.5829E+09	1.7539E+01	1.2702E+01	1.6191E+03	2.0122
	SD	1.2489E+10	3.8023E-01	1.8724E-15	4.6375E+02	1.8985E-01
GOA	**MEAN**	3.6120E+09	1.7359E+01	1.2702E+01	2.2463E+01	1.5038
	SD	1.8050E+09	4.4083E-04	1.8724E-15	1.024E+01	2.1728E-01
HHO	**MEAN**	6.0706E+04	1.7344E+01	1.2702E+01	2.3895E+03	2.8243
	SD	1.4288E+04	3.0865E-03	1.8724E-15	1.7513E+03	8.8467E-01

Table 3.3 PEMFC Parameter Search Range

Parameters	**Lower bound**	**Upper bound**
ξ_1	-1.1997	-0.08532
ξ_2*10^{-3}	0.8	6.00
ξ_3*10^{-5}	3.60	9.80
ξ_4*10^{-4}	-2.60	-0.954
λ	10.00	24.00
R_C*10^{-4}	1.00	8.00
b	0.0136	0.5

Table 3.4 represents the parameter estimation of the PEMFC datasheet [130]. In Table 3.4 J_{max} is the maximum current density, P_{H2} is the partial pressure of hydrogen, P_{O2} is the partial pressure of oxygen, T is the temperature, l is the thickness of the membrane, cells connected in series is denoted by n, and A is the area of the cell. In order to increase the high hydrogen reduction reaction (HRR) rate higher order of catalyst loading density has been used which is close to 5 milligram/cm^2, but usually catalyst loading density used is 1.5 milligram/cm^2. In the Avista SR-12 model the number of cells connected in series is 48, and the thickness of the membrane is 25um.

Table 3.4 Parameter Estimation of PEMFC Data Sheet

Model	**Avista SR-12**	**Ballard Mark V**
n	48	35
A [cm2]	62.5	50.6
l [um]	25	178
Jmax [A/cm2]	0.672	1.5
PH2 [bar]	1.47628	1
PO2 [bar]	0.2095	1
Power [W]	500	1000
T [K]	323.15	343.15

Case 1: Avista SR-12 Performance Assessment:

Table 3.5 represents the value of seven unknown parameters and the best results of SSE. In Table 3.5, the ξ_1, ξ_2, ξ_3, and ξ_4 is denoted as semi-empirical coefficients, λ is denoted as an adjustable empirical variable, b is the parametric variable, and R_C is the resistance connection From Table 3.5, it is seen that the average value of SSE is 2.9595E-01which is of the proposed algorithm. Table 3.6 represents the statistical results of case 1 which suggests that the proposed algorithm gives the lowest value of average and standard deviation. From Table 3.6 it is seen that the average value is 2.9595E-01, the minimum value is 2.6982E-01, the maximum value is 3.1941E-01, and the standard deviation (SD) value is 1.0858E-02 for the SSE which is of the proposed algorithm. Fig.3.4 represents the convergence curve of SMA with other compared algorithm of Avista SR-12 model. From this graph, it is concluded that the proposed algorithm is best than the rest of the compared algorithms.

Table 3.5 Parameter Estimation for Avista SR-12 Model

Parameters→ **Algorithms↓**	**ξ_1**	**ξ_2**	**ξ_3**	**ξ_4**	**λ**	**R_C**	**b**
SMA	-0.9736	0.0020	9.4777E-05	-2.4722E-04	17.3399	0.0003	0.3215
PSO	-0.8833	0.0010	9.3866E-05	-2.4746E-04	10	0.0002	0.1856
ALO	-0.9028	0.0011	9.5669E-05	-2.0218E-04	17.1769	0.0004	0.2715
ASO	-0.9615	0.0013	9.1022E-05	-1.8852E-04	15.0508	0.0004	0.2929
GOA	-1.0622	0.0013	8.8092E-05	-1.8502E-04	17.8139	0.0004	0.3259
HHO	-1.0558	0.0011	7.3030E-05	-1.6362E-04	13.8901	0.0004	0.2393

Table 3.6 Statistical Results of SSE for Avista SR-12 Model

Statistical Results→ **Algorithms↓**	**Minimum**	**Average**	**Maximum**	**S.D**
SMA	2.6982E-01	2.9595E-01	3.1941E-01	1.0858E-02
PSO	3.3213	6.0969	7.5373	1.5332
ALO	8.0060E-01	8.2048E-01	8.7775E-01	1.6352E-02
ASO	8.8065E-01	1.2605	5.7860	1.2307
GOA	8.1342E-01	1.1346	1.4206	1.6546E-01
HHO	8.2096E-01	1.1299	1.4335	2.6079E-01

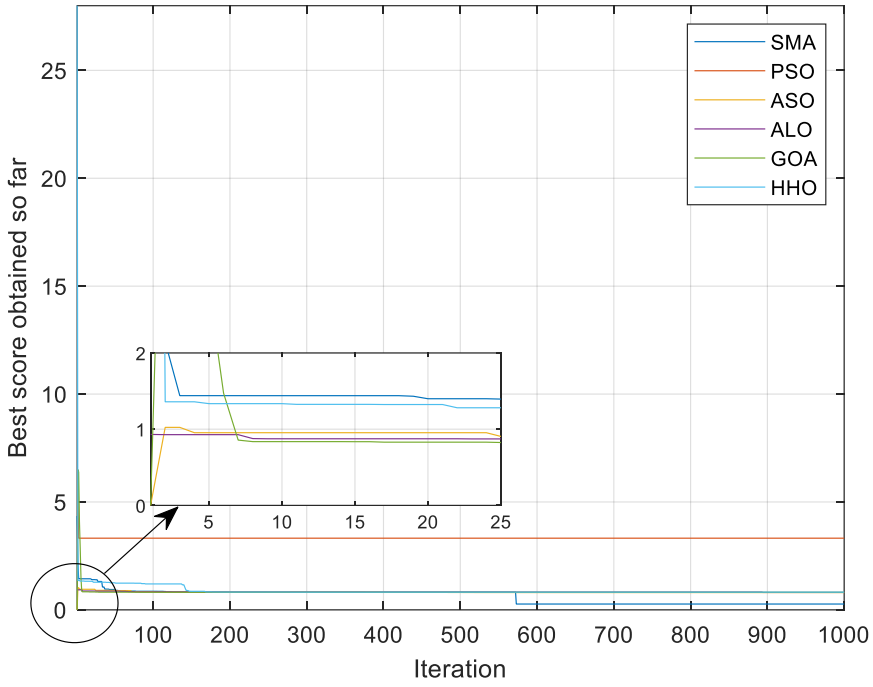

Fig. 3.4 Convergences Curves of SMA with Other Compared Algorithm for Avista SR-12 Model

After estimating the parameters of PEMFC the I-V and P-I curves are conducted as shown in Table 3.7 (a) and (b) and Table 3.8 (a) and (b) From Table 2.7 and Table 3.8, it is seen that the Absolute error (AE) of the proposed algorithm is minimum than the rest of the compared algorithms. The AE from both the tables of SMA is 3.04E-02, PSO is 4.83E-02, ALO is 3.07E-02, ASO is 4.62E-02, GOA is 4.74E-02 and HHO is 4.67E-02. Fig.3.5 and Fig. 3.68 depict the characteristics of the polarization curve of V-I and P-I. Moreover, from Fig. 3.5 and Fig. 3.6, it is concluded that the accuracy and reliability of the proposed algorithm are better than the rest of the compared algorithms.

Table 3.7 (a) Calculated Values of Voltage and Absolute Error for Avista SR-12 Model

Algorithms		**SMA**		**PSO**		**ALO**	
I_m Measured Current (A)	**V_m Measured Voltage (V)**	**V_c Calculated Voltage (V)**	**AE**	**V_c Calculated Voltage (V)**	**AE**	**V_c Calculated Voltage (V)**	**AE**
1.004	**43.17**	43.0225	3.8940E-03	43.0100	4.1845E-03	42.8935	6.9123E-03

3.166	**41.14**	41.0516	2.1533E-03	41.0011	3.3868E-03	41.1516	2.8202E-04
5.019	**40.09**	40.0335	1.4124E-03	39.9107	4.4919E-03	40.1235	8.3382E-04
7.027	**39.04**	39.0068	8.5115E-04	38.8914	3.8198E-03	39.1068	1.7078E-03
8.958	**37.99**	37.9737	4.3015E-04	37.8492	3.7194E-03	37.9937	9.6481E-05
10.97	**37.08**	37.0778	5.9490E-05	36.9958	2.2771E-03	37.1978	3.1667E-03
13.05	**36.03**	36.0399	2.7574E-04	35.9941	1.0727E-03	36.0401	2.8128E-04
15.06	**35.19**	35.2100	5.6765E-04	35.1461	1.2499E-03	35.2130	6.5279E-04
17.07	**34.07**	34.0988	8.4464E-04	33.9202	4.4166E-03	34.1008	9.0324E-04
19.07	**33.02**	33.0566	1.1078E-03	32.9939	7.9254E-04	33.1066	2.6164E-03
21.08	**32.04**	32.0837	1.3624E-03	31.9172	3.8480E-03	32.0937	1.6736E-03
23.01	**31.20**	31.2499	1.5977E-03	31.1201	2.5670E-03	31.2599	1.9171E-03
24.94	**29.80**	29.8557	1.8643E-03	29.7928	2.4081E-04	29.8057	1.8989E-04
26.87	**28.96**	29.0210	2.1012E-03	28.9053	1.8907E-03	29.0110	1.7572E-03
28.96	**28.12**	28.1863	2.3536E-03	28.0979	7.8659E-04	28.1063	4.8600E-04
30.81	**26.3**	26.3708	2.6842E-03	26.2800	7.6031E-04	26.3658	2.4951E-03
32.97	**24.06**	24.1357	3.1349E-03	24.0014	2.4435E-03	24.0957	1.4800E-03
34.90	**21.40**	21.4798	3.7137E-03	21.2643	6.3805E-03	21.4698	3.2496E-03
Sum of AE			**3.0409E-02**		**4.8329E-02**		**3.0701E-02**

Table 3.7(b) Calculated Values of Voltage and Absolute Error for Avista SR-12 Model

Algorithms		**ASO**		**GOA**		**HHO**	
I_m Measured Current (A)	**V_m Measured Voltage (V)**	**V_c Calculated Voltage (V)**	**AE**	**V_c Calculated Voltage (V)**	**AE**	**V_c Calculated Voltage (V)**	**AE**
1.004	**43.17**	43.0200	3.9511E-03	43.1825	1.7441E-04	43.1200	1.6228E-03

3.166	**41.14**	41.0061	3.2645E-03	41.0116	3.1307E-03	41.1061	8.2380E-04
5.019	**40.09**	39.9707	2.9841E-03	40.0135	1.9130E-03	39.9507	3.4862E-03
7.027	**39.04**	38.9314	2.7884E-03	39.0018	9.7982E-04	38.9114	3.3038E-03
8.958	**37.99**	37.8892	2.6598E-03	37.7937	5.1949E-03	37.9892	2.0424E-05
10.97	**37.08**	36.9858	2.5481E-03	37.0178	1.6804E-03	36.9958	2.2876E-03
13.05	**36.03**	35.9414	2.4653E-03	36.0199	2.7936E-04	35.8914	3.8618E-03
15.06	**35.19**	35.1061	2.3907E-03	35.1200	1.9935E-03	35.3061	3.2876E-03
17.07	**34.07**	33.9902	2.3481E-03	34.0588	3.2881E-04	33.7902	8.2809E-03
19.07	**33.02**	32.9439	2.3115E-03	33.0966	2.3150E-03	32.8439	5.3632E-03
21.08	**32.04**	31.9672	2.2778E-03	32.1237	2.6059E-03	31.9572	2.5915E-03
23.01	**31.20**	31.1301	2.2449E-03	31.3499	4.7824E-03	31.1001	3.2117E-03
24.94	**29.80**	29.7328	2.2593E-03	29.9557	5.1963E-03	29.8528	1.7695E-03
26.87	**28.96**	28.8953	2.2374E-03	29.0110	1.7572E-03	28.9453	5.0618E-04
28.96	**28.12**	28.0579	2.2133E-03	28.1543	1.2197E-03	28.0979	7.8659E-04
30.81	**26.3**	26.2400	2.2859E-03	26.3408	1.5484E-03	26.2200	3.0504E-03
32.97	**24.06**	24.0024	2.4017E-03	24.1557	3.9602E-03	24.0504	4.0112E-04
34.90	**21.40**	21.3443	2.6085E-03	21.5798	8.3304E-03	21.4443	2.0669E-03
Sum of AE			**4.6240E-02**		**4.7391E-02**		**4.6712E-02**

Table 3.8 (a) Calculated Values of Power and Absolute Error for Avista SR-12 Model

Algorithms		**SMA**		**PSO**		**ALO**	
I_m Measured Current (A)	**P_m Measured Power (W)**	**P_c Calculated Power (W)**	**AE**	**P_c Calculated Power (W)**	**AE**	**P_c Calculated Power (W)**	**AE**
1.004	**43.36**	43.1921	3.8940E-03	43.1821	4.1845E-03	43.0651	6.9123E-03
3.166	**130.25**	129.9694	2.1533E-03	129.8096	3.3868E-03	130.2860	2.8202E-04
5.019	**201.21**	200.9279	1.4124E-03	200.3119	4.4919E-03	201.3796	8.3382E-04
7.027	**274.33**	274.1007	8.5151E-04	273.2902	3.8198E-03	274.8034	1.7078E-03
8.958	**340.31**	340.1681	4.30155E-04	339.0533	3.7194E-03	340.3473	9.6481E-05
10.97	**406.77**	406.7434	5.9490E-05	405.8435	2.2771E-03	408.0598	3.1667E-03
13.05	**470.19**	470.3212	2.7574E-04	469.6877	1.0727E-03	470.3238	2.8128E-04
15.06	**529.96**	530.2624	5.6765E-04	529.2998	1.2499E-03	530.3076	6.5279E-04
17.07	**581.57**	582.0566	8.4464E-04	579.0176	4.4166E-03	582.1007	9.0324E-04
19.07	**629.69**	630.3897	1.1078E-03	629.1927	7.9254E-04	631.3432	2.6164E-03
21.08	**675.40**	676.3246	1.3624E-03	672.8142	3.8480E-03	676.5354	1.6736E-03
23.01	**717.91**	719.0608	1.5977E-03	716.0739	2.5670E-03	719.2909	1.9171E-03
24.94	**743.21**	744.6002	1.8643E-03	743.0331	2.4081E-04	743.3532	1.8989E-04
26.87	**778.16**	779.7937	2.1012E-03	776.6867	1.8907E-03	779.5250	1.7572E-03
28.96	**814.36**	816.2764	2.3536E-03	813.7151	7.8659E-04	813.9556	4.8600E-04
30.81	**810.30**	812.4839	2.6842E-03	809.6867	7.6031E-04	812.3298	2.4951E-03
32.97	**793.26**	795.7528	3.1349E-03	791.3246	2.4435E-03	794.4340	1.4800E-03
34.90	**746.86**	749.6439	3.7137E-03	742.1249	6.3805E-03	749.2949	3.2496E-03
Sum of AE			**3.0409E-02**		**4.8329E-02**		**3.0701E-02**

Table 3.8 (b) Calculated Values of Power and Absolute Error for Avista SR-12

Algorithms		**ASO**		**GOA**		**HHO**	
I_m Measured Current (A)	**P_m Measured Power (W)**	**P_c Calculated Power (W)**	**AE**	**P_c Calculated Power (W)**	**AE**	**P_c Calculated Power (W)**	**AE**
1.004	**43.36**	43.1921	3.9511E-03	43.3552	1.7441E-04	43.2925	1.6228E-03
3.166	**130.25**	129.8254	3.2645E-03	129.8427	3.1307E-03	130.1420	8.2380E-04
5.019	**201.21**	200.6131	2.9841E-03	200.8275	1.9130E-03	200.5127	3.4862E-03
7.027	**274.33**	273.5712	2.7884E-03	274.0655	9.7982E-04	273.4307	3.3038E-03
8.958	**340.31**	339.4117	2.6598E-03	338.5557	5.1949E-03	340.3075	2.0424E-05
10.97	**406.77**	405.7338	2.5481E-03	406.0852	1.6804E-03	405.8435	2.2876E-03
13.05	**470.19**	469.0352	2.4653E-03	470.0602	2.7936E-04	468.3827	3.8618E-03
15.06	**529.96**	528.6972	2.3907E-03	528.9070	1.9935E-03	531.7094	3.2876E-03
17.07	**581.57**	580.2125	2.3481E-03	581.3837	3.2881E-04	576.7985	8.2809E-03
19.07	**629.69**	628.2392	2.3115E-03	631.1525	2.3150E-03	626.3322	5.3632E-03
21.08	**675.40**	673.8682	2.2778E-03	677.1678	2.6059E-03	673.6574	2.5915E-03
23.01	**717.91**	716.3040	2.2449E-03	721.3618	4.7824E-03	715.6137	3.2117E-03
24.94	**743.21**	741.5367	2.2593E-03	747.0942	5.1963E-03	744.5295	1.7695E-03
26.87	**778.16**	776.4180	2.2374E-03	779.5250	1.7572E-03	777.7615	5.0618E-04
28.96	**814.36**	812.5567	2.2133E-03	815.3497	1.2197E-03	813.7151	7.8659E-04
30.81	**810.30**	808.4550	2.2859E-03	811.5596	1.5484E-03	807.8388	3.0504E-03
32.97	**793.26**	791.3576	2.4017E-03	796.4122	3.9602E-03	792.9401	4.0112E-04
34.90	**746.86**	744.9169	2.6085E-03	753.1339	8.3304E-03	748.4069	2.0669E-03
Sum of AE			**4.6240E-02**		**4.7391E-02**		**4.6712E-02**

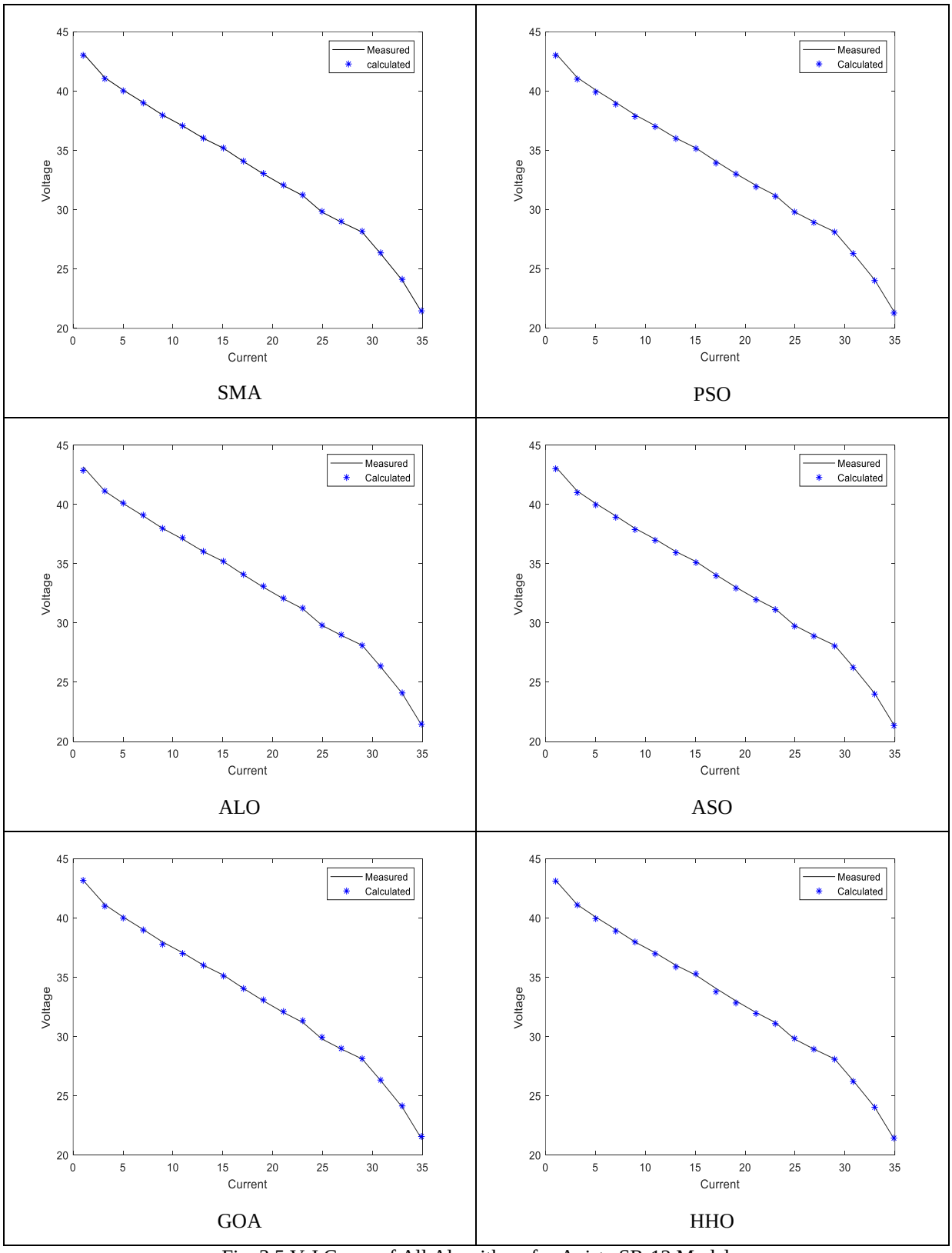

Fig. 3.5 V-I Curve of All Algorithms for Avista SR-12 Model

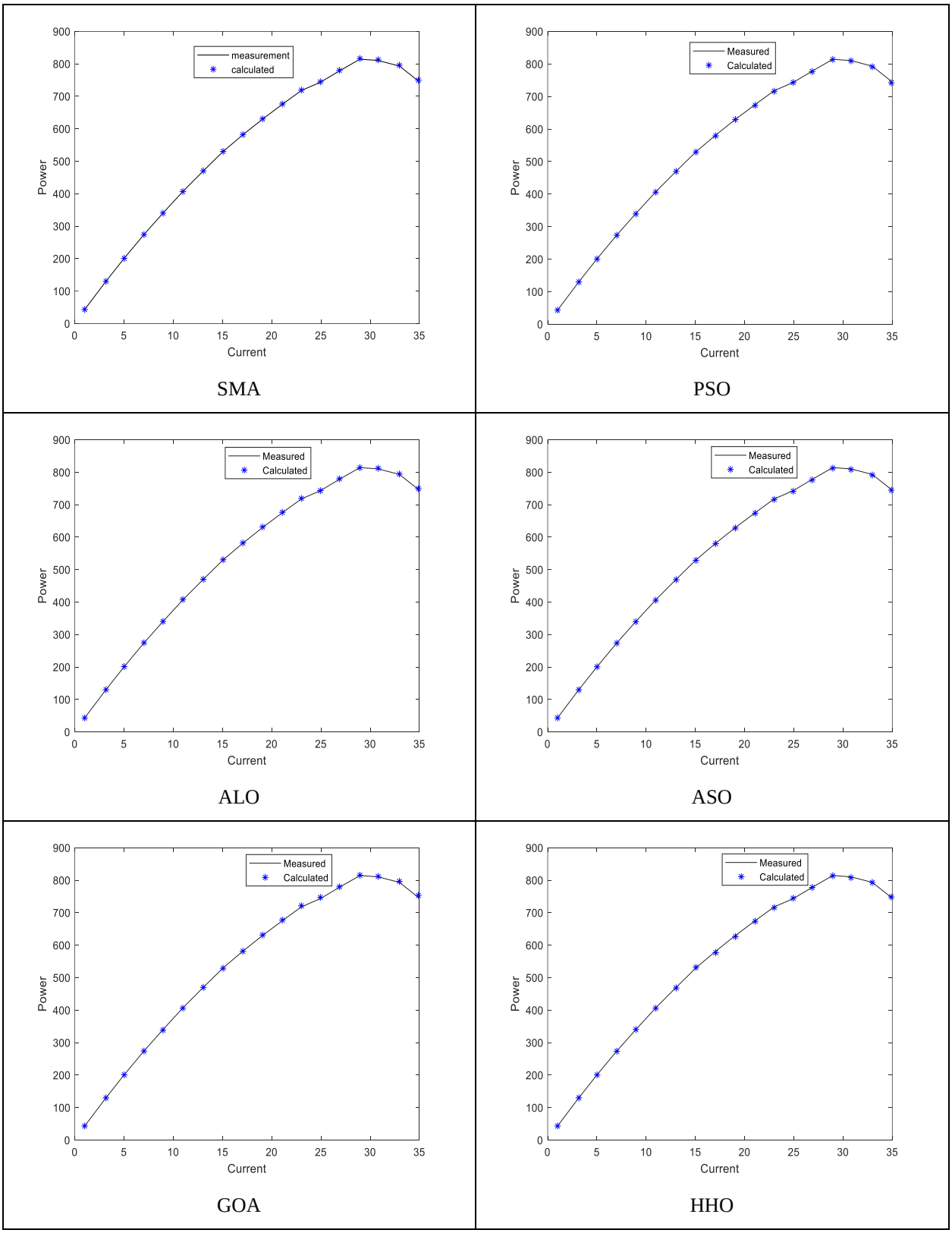

Fig. 3.6 P-V Curve of All Algorithms for Avista SR-12 Model

Case 2: Ballard Mark V Performance Assessment:

Table 3.4 represents the parameter estimation of the PEMFC datasheet. In the Ballard Mark V model, the number of cells connected in series is 35, and the thickness of the membrane is 178um. Table 3.9 represents the value of seven unknown parameters and the best results of SSE. From Table 3.9, it is seen that the average value of SSE is 1.7729E-05 which is of the proposed algorithm Table 3.10 represents the statistical results of case 2, from this table it is seen that the lowest value of average and standard deviation is of the proposed algorithm. From Table 3.10 it is seen that the average value is 1.7729E-05, the minimum value is 1.1473E-05, the maximum value is 2.6989E-05, and the standard deviation (SD) value is 4.7202E-06 for the SSE which is of the proposed algorithm. It can be concluded from the Table 3.10 that the proposed algorithm has better accuracy than compared algorithm.

Table 3.9 Parameter Estimation for Ballard Mark V Model

Parameters→ **Algorithms↓**	ξ_1	ξ_2	ξ_3	ξ_4	λ	R_C	**b**
SMA	-1.1942	0.0010	4.1234E-05	-1.6807E-04	15.3311	0.0002	0.2083
PSO	-0.9728	0.0024	6.4933E-05	-1.9965E-04	16.0716	0.0003	0.2094
ALO	-1.0376	0.0032	6.8699E-05	-1.7408E-04	17.7055	0.0004	0.3101
ASO	-1.0384	0.0031	6.877E-05	-1.8011E-04	17.1662	0.0004	0.3059
GOA	-1.0535	0.0025	6.8145E-05	-1.7356E-04	18.2932	0.0004	0.2010
HHO	-1.0315	0.0021	5.8528E-05	-1.6022E-04	13.8862	0.0003	0.1782

Table 3.10 Statistical results of SSE for Ballard Mark V Model

Statistical Results→ **Algorithms↓**	**Minimum**	**Average**	**Maximum**	**S.D**
SMA	1.1473E-05	1.7729E-05	2.6989E-05	4.7202E-06
PSO	5.2056E-03	6.4550E-03	7.1502E-03	5.3141E-04
ALO	1.0207E-04	1.6519E-04	2.9530E-04	6.7638E-05
ASO	1.0146E-04	1.5357E-04	2.1896E-04	3.5300E-05
GOA	1.0746E-04	1.5373E-04	2.2789E-04	3.9873E-05
HHO	1.0090E-04	1.7190E-04	2.8425E-04	5.1806E-05

Fig. 3.7 represents the convergence graph for the Ballard Mark V model. From this graph, it is observed that the blue line i.e. SMA has the lowest convergence curve among all the curves plotted. Hence it is concluded that the proposed algorithm (SMA) is best than the rest of the compared algorithms.

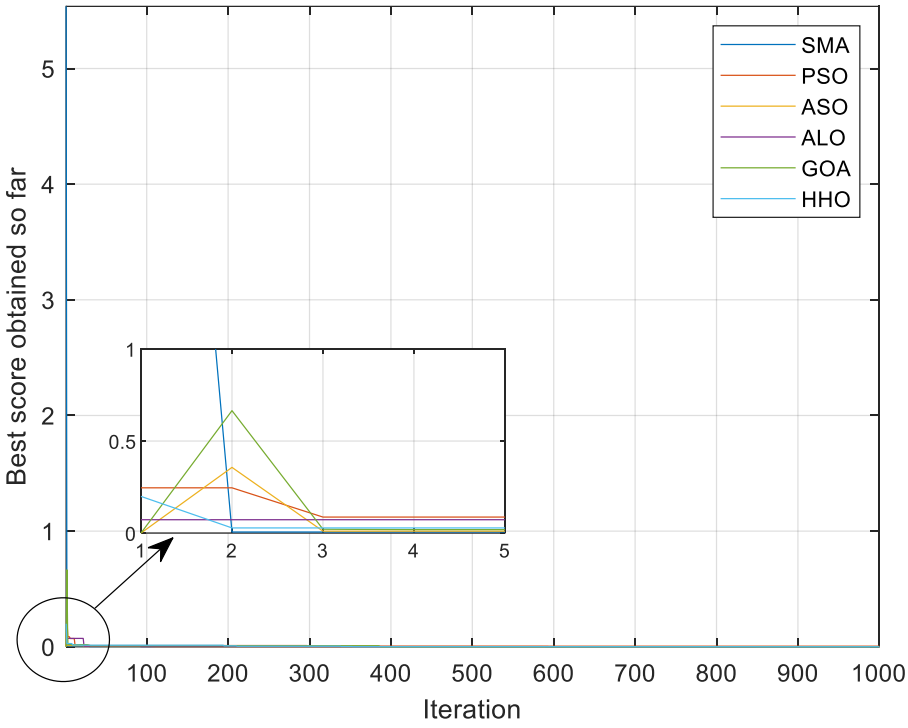

Fig. 3.7 Convergences Curves of SMA with Other Compared Algorithm for Ballard Mark V Model

After estimating the parameters of PEMFC the I-V and P-I curves are conducted as shown in Table 3.11 (a) and (b) and Table 3.12 (a) and (b). From both Table 3.11 and Table 3.12, it is seen that the Absolute error (AE) of the proposed algorithm is minimum than the rest of the compared algorithms. The AE from both the tables of SMA is 3.77E-02, PSO is 4.26E-02, ALO is 3.85E-02, ASO is 4.09E-02, GOA is 3.92E-02 and HHO is 4.13E-02.

Table 3.11 (a) Calculated Values of Voltage and Absolute Error for Ballard Mark V Model

Algorithms		**SMA**		**PSO**		**ALO**	
I_m Measured Current (A)	**V_m Measured Voltage (V)**	**V_c Calculated Voltage (V)**	**AE**	**V_c Calculated Voltage (V)**	**AE**	**V_c Calculated Voltage (V)**	**AE**
5.4	**0.92**	0.9198	2.1744E-04	0.9211	1.1942E-03	0.9179	2.2878E-03
10.8	**0.88**	0.8810	1.1351E-03	0.8791	1.0238E-03	0.8807	7.9458E-04
16.2	**0.85**	0.8504	4.7037E-04	0.8512	1.4098E-03	0.8476	2.8315E-03

21.6	**0.82**	0.8182	2.2000E-03	0.8221	3.2819E-03	0.8191	1.0988E-03
27.0	**0.79**	0.7921	2.6512E-03	0.7885	1.9023E-03	0.7919	2.3993E-03
32.4	**0.77**	0.7701	1.2985E-04	0.7679	2.7347E-03	0.7673	3.5188E-03
37.8	**0.74**	0.7388	1.6243E-03	0.7439	5.2426E-03	0.7381	2.5742E-03
43.2	**0.72**	0.7221	2.9082E-03	0.7184	2.2272E-03	0.7249	6.7596E-03
48.6	**0.69**	0.6941	5.9069E-03	0.6879	3.0528E-03	0.6932	4.6163E-03
54.0	**0.66**	0.6638	5.7246E-03	0.6574	3.9550E-03	0.6590	1.5175E-03
59.4	**0.62**	0.6171	4.6994E-03	0.6231	7.2058E-03	0.6184	2.5873E-03
64.8	**0.60**	0.6030	4.9751E-03	0.5974	4.3522E-03	0.6028	4.6450E-03
70.2	**0.55**	0.5472	5.1170E-03	0.5528	5.0651E-03	0.5484	2.9176E-03
Sum of AE			**3.7759E-02**		**4.2647E-02**		**3.8548E-02**

Table 3.11 (b) Calculated Values of Voltage and Absolute Error for Ballard Mark V Model

Algorithms		**ASO**		**GOA**		**HHO**	
I_m Measured Current (A)	**V_m Measured Voltage (V)**	**V_c Measured Voltage (V)**	**AE**	**V_c Measured Voltage (V)**	**AE**	**V_c Measured Voltage (V)**	**AE**
5.4	**0.92**	0.9224	2.6019E-03	0.9218	1.9527E-03	0.9185	1.6331E-03
10.8	**0.88**	0.8814	1.5884E-03	0.8786	1.5934E-03	0.8826	2.9458E-03
16.2	**0.85**	0.8482	2.1221E-03	0.8511	1.2924E-03	0.8536	4.2174E-03
21.6	**0.82**	0.8276	9.1832E-03	0.8221	2.5544E-03	0.8228	3.4030E-03
27.0	**0.79**	0.7885	1.9023E-03	0.7919	2.3993E-03	0.7949	6.1643E-03
32.4	**0.77**	0.7730	3.8810E-03	0.7725	3.2362E-03	0.7724	3.1072E-03
37.8	**0.74**	0.7409	1.2147E-03	0.7416	2.1575E-03	0.7393	9.4684E-03
43.2	**0.72**	0.7182	2.5063E-03	0.7171	4.0441E-03	0.7211	1.5254E-03
48.6	**0.69**	0.6889	1.5967E-03	0.6888	1.7422E-03	0.6891	1.3061E-03

54.0	**0.66**	0.6634	5.1251E-03	0.6578	3.3445E-03	0.6627	4.0742E-03
59.4	**0.62**	0.6185	2.4252E-03	0.6231	4.9751E-03	0.6237	5.9323E-03
64.8	**0.60**	0.6024	3.9841E-03	0.5982	3.0090E-03	0.5982	3.0090E-03
70.2	**0.55**	0.5515	2.7199E-03	0.5538	6.8617E-03	0.5483	3.1005E-03
Sum of AE			**4.0851E-02**		**3.9163E-02**		**4.1365E-02**

Table 3.12 (a) Calculated Values of Power and Absolute Error for Ballard Mark V Model

Algorithms		**SMA**		**PSO**		**ALO**	
I_m Measured Current (A)	**P_m Measured Power (W)**	**P_c Calculated Power (W)**	**AE**	**P_c Calculated Power (W)**	**AE**	**P_c Calculated Power (W)**	**AE**
5.4	**4.9680**	4.9669	2.1744E-04	4.9739	1.1942E-03	4.9567	2.2878E-03
10.8	**9.5040**	9.5148	1.1351E-03	9.4943	1.0238E-03	9.5116	7.9458E-04
16.2	**13.7700**	13.7765	4.7037E-04	13.7894	1.4098E-03	13.7311	2.8315E-03
21.6	**17.7120**	17.6731	2.2000E-03	17.7703	3.2819E-03	17.6926	1.0988E-03
27.0	**21.9620**	22.0204	2.6512E-03	21.9203	1.9023E-03	22.0148	2.3993E-03
32.4	**24.9480**	24.9512	1.2985E-04	24.8800	2.7347E-03	24.8605	3.5188E-03
37.8	**27.9720**	27.9266	1.6243E-03	28.1194	5.2426E-03	27.9002	2.5742E-03
43.2	**31.1040**	31.1947	2.9082E-03	31.0349	2.2272E-03	31.3157	6.7596E-03
48.6	**33.5340**	33.7333	5.9069E-03	33.4319	3.0528E-03	33.6895	4.6163E-03
54.0	**35.6400**	35.8452	5.7246E-03	35.4996	3.9550E-03	35.5860	1.5175E-03
59.4	**36.8280**	36.6557	4.6994E-03	37.0953	7.2058E-03	36.7330	2.5873E-03
64.8	**38.8800**	39.0744	4.9751E-03	38.7115	4.3522E-03	39.0614	4.6450E-03
70.2	**38.6100**	38.4134	5.1170E-03	38.8066	5.0651E-03	38.4977	2.9176E-03
Sum of AE			**3.7759E-02**		**4.2647E-02**		**3.8548E-02**

Table 3.12 (b) Calculated Values of Power and Absolute Error for Ballard Mark V Model

Algorithms		**ASO**		**GOA**		**HHO**	
I_m Measured Current (A)	**P_m Measured Power (W)**	**P_c Calculated Power (W)**	**AE**	**P_c Calculated Power (W)**	**AE**	**P_c Calculated Power (W)**	**AE**
5.4	**4.9680**	4.9810	2.6019E-03	4.9777	1.9527E-03	4.9567	1.6331E-03
10.8	**9.5040**	9.5191	1.5884E-03	9.4889	1.5934E-03	9.5321	2.9458E-03
16.2	**13.7700**	13.7408	2.1221E-03	13.7878	1.2924E-03	13.8283	4.2174E-03
21.6	**17.7120**	17.8762	9.1832E-03	17.7574	2.5544E-03	17.7725	3.4030E-03
27.0	**21.9620**	21.9203	1.9023E-03	22.0148	2.3993E-03	22.0982	6.1643E-03
32.4	**24.9480**	25.0452	3.8810E-03	25.0290	3.2362E-03	25.0258	3.1072E-03
37.8	**27.9720**	28.0060	1.2147E-03	28.0325	2.1575E-03	27.9455	9.4684E-03
43.2	**31.1040**	31.0262	2.5063E-03	30.9787	4.0441E-03	31.1515	1.5254E-03
48.6	**33.5340**	33.4805	1.5967E-03	33.4757	1.7422E-03	33.4903	1.3061E-03
54.0	**35.6400**	35.8236	5.1251E-03	35.5212	3.3445E-03	35.7858	4.0742E-03
59.4	**36.8280**	36.7389	2.4252E-03	37.0121	4.9751E-03	37.0478	5.9323E-03
64.8	**38.8800**	39.0355	3.9841E-03	38.7634	3.0090E-03	38.7634	3.0090E-03
70.2	**38.6100**	38.7153	2.7199E-03	38.8768	6.8617E-03	38.4907	3.1005E-03
Sum of AE			**4.0851E-02**		**3.9163E-02**		**4.1365E-02**

Fig. 3.8 depict the characteristics of the polarization curve of V-I. Similarly, P-I characteristic curves of each algorithm is also plotted as shown in Fig. 3.9. Moreover, from Fig. 3.8 and Fig. 3.9 it is concluded that the accuracy and reliability of the proposed algorithm are better than the rest of the compared algorithms. In this case, it is well intended to affirm that the measured outcomes using the proposed algorithm model match with the results from the experiments, whereas the measured value of compared algorithm deviate from the path of calculated value.

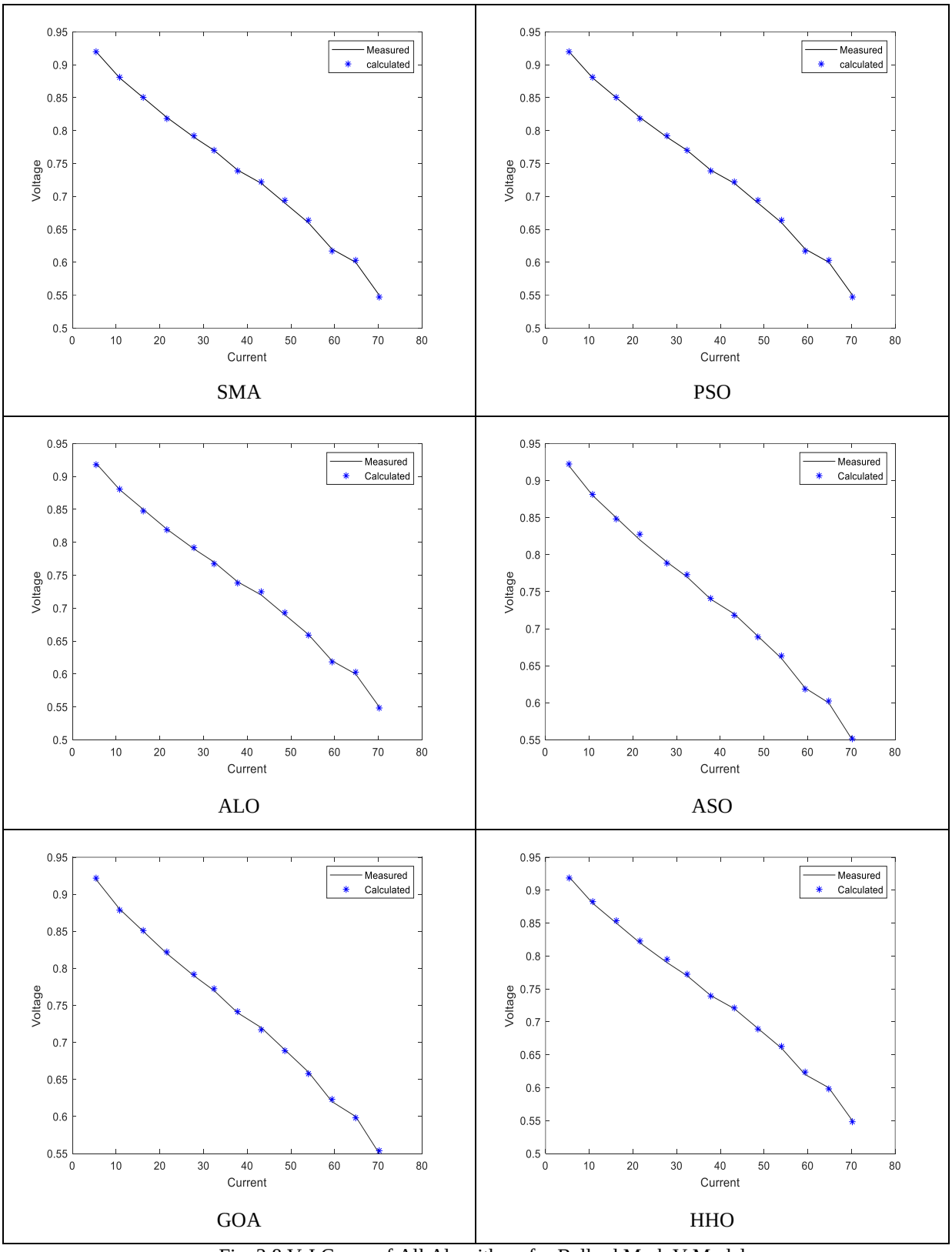

Fig. 3.8 V-I Curve of All Algorithms for Ballard Mark V Model

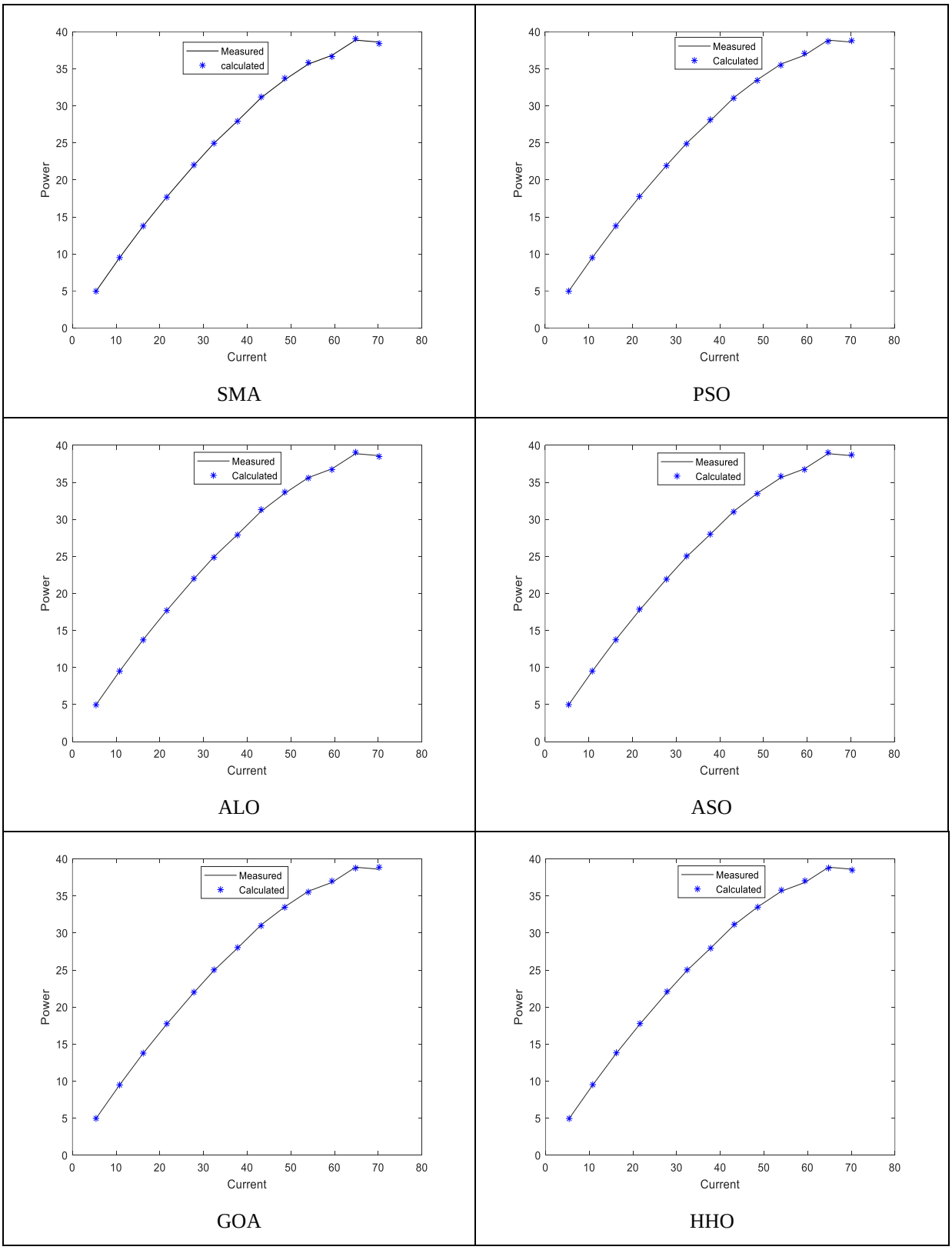

Fig. 3.9 P-I Curve of All Algorithms of Ballard Mark V Model

- **Non-Parametric Test**

The first non-parametric test performed is the Friedman ranking test [112]. From this test, it is clear that the proposed algorithm is far more accurate and precise than the rest of the compared algorithms for both the datasheets of PEMFC. From Table 3.13 and Table 3.14 it is seen that the proposed algorithm SMA secured the first rank in both cases. This non-parametric test clearly proves that SMA is a better algorithm for parameter estimation of the PEMFC model as compared to the rest of the algorithms being compared in both the datasheets.

Table 3.13 Friedman ranking test for Avista SR-12 Model

Algorithms	Friedman Ranking
SMA	1
PSO	6
ALO	2
ASO	3
GOA	5
HHO	4

Table 3.14 Friedman ranking test for Ballard Mark V Model

Algorithms	Friedman Ranking
SMA	1
PSO	6
ALO	2
ASO	4
GOA	3
HHO	5

.

Second Wilcoxon's rank-sum non-parametric test is also applied [113]. This test seems to be an easy but secure and reliable non-parametric method for combined statistical analysis when samples are independent and in dynamic programming it is prominent. Wilcoxon's rank-sum test is applied in comparison of SMA with other algorithms as shown in Table 3.15 and Table 3.16 for both the datasheets of PEMFC models. The p-value is the probability of getting results at least as extreme as the observed results of a statistical hypothesis test, assuming the null hypothesis is accurate. The p-value is used as an alternative to rejection points to provide the smallest level of significance at which the null hypothesis would be rejected. A smaller p-value means that there is stronger evidence in favor of the alternative hypothesis. From this test, it justifies that the performance of SMA is better than the other algorithms, with the significance level of probability range of 95%.

Table 3.15 Wilcoxon's Rank Sum Test for Avista SR-12 Model

Algorithms	PSO	ALO	HHO	GOA	ASO
SMA	2.9841E-11	2.9247 E-11	2.9754 E-11	2.9484 E-11	2.9841 E-11

Table 3.16 Wilcoxon's Rank Sum Test for Ballard Mark V Model

Algorithms	PSO	ALO	HHO	GOA	ASO
SMA	2.9506 E-11	2.9660 E-11	2.9450 E-11	2.9271 E-11	2.9376 E-11

Third, the Kruskal-Wallis test is applied to test the statistical differences amongst the various algorithms [114]. In Fig. 3.10 and Fig. 3.11, the list of graphs obtained from the test along with the mean rank of SMA has been shown. The mean rank of SMA is significantly different from other groups. In Fig. 3.12and Fig. 3.13 the lists of graphs obtained from the test along with the median rank of SMA has been shown. The median rank of SMA is also significantly different and better from other groups. Table 3.17 and Table 3.18 represent the results of the ANOVA Kruskal-Wallis test. To test the value of probability, chi-square is found.

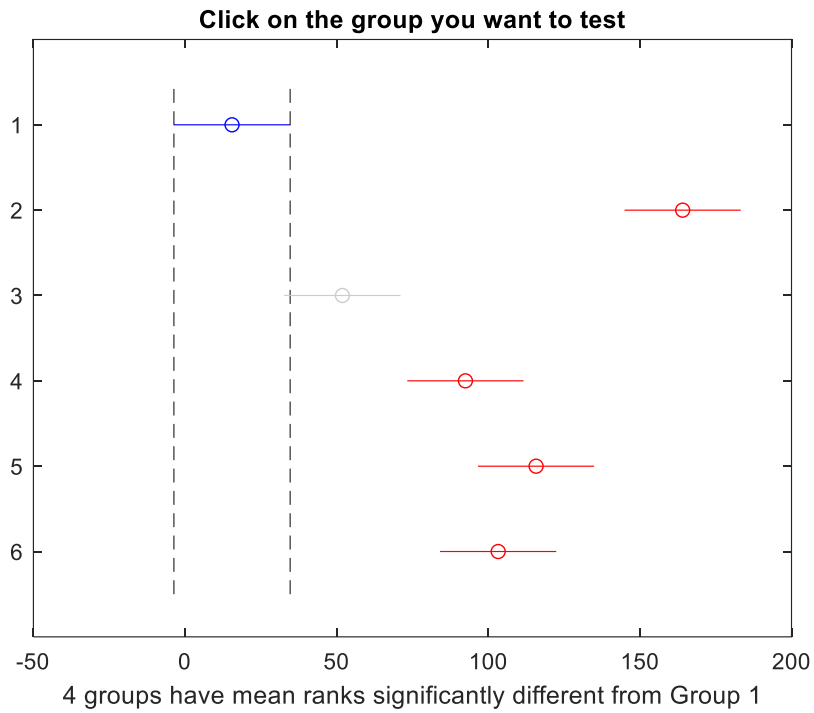

Fig. 3.10 Mean Ranking using Kruskal-Wallis Test for Avista SR-12 Model

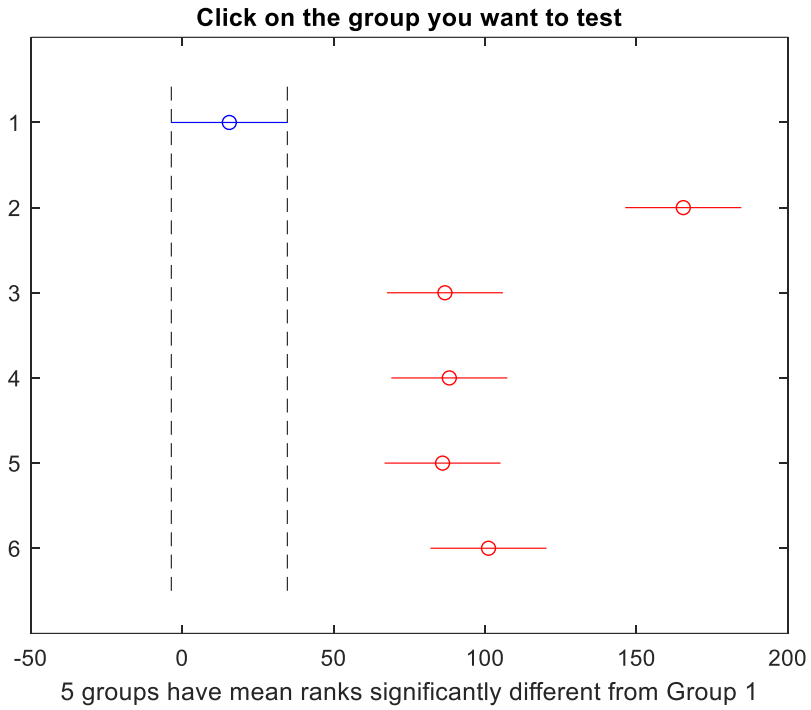

Fig. 3.11 Mean Ranking using Kruskal-Wallis Test for Ballard Mark V Model

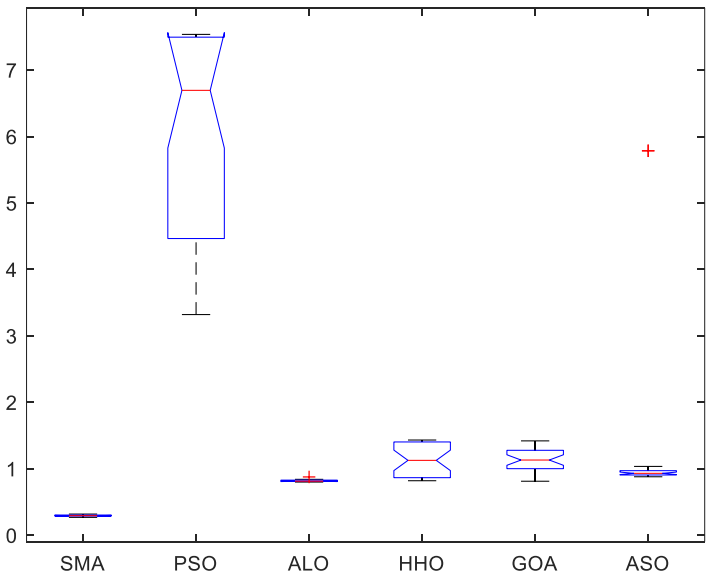

Fig. 3.12 Median Ranking using Kruskal-Wallis Test for Avista SR-12 Model

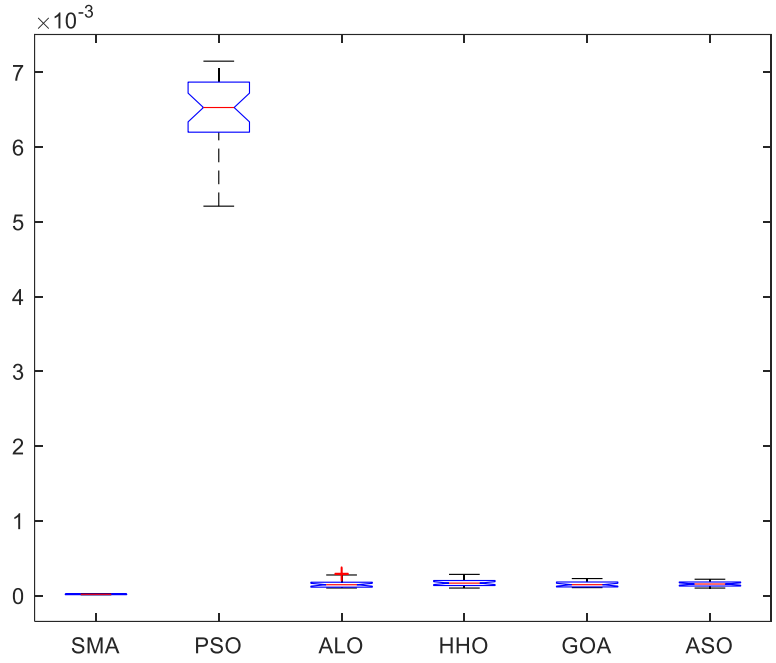

Fig. 3.13 Median Ranking using Kruskal-Wallis Test for Ballard Mark V Model

Table 3.17 Anova Kruskal-Wallis Test for Avista SR-12 Model

Source	Sum of Square	degree of freedom	Mean Square	Chi-square	Prob>Chi-square
Columns	414158.9	5	82831.8	152.56	3.80824e-31
Error	71780.6	174	412.5	-	-
Total	485939.5	179	-	-	-

Table 3.18 Anova Kruskal-Wallis Test for Ballard Mark V Model

Source	Sum of Square	degree of freedom	Mean Square	Chi-square	Prob>Chi-square
Source	340153.5	5	68030.7	152.56	2.35603e-25
Source	145755	174	837.7	-	-
Source	485908.5	179	-	-	-

3.3.2 Mayflies Algorithm (MA)

Mayflies are insects of the Ephemeroptera order that belongs to an ancient insect group called Palaeoptera. About 3000 varieties of mayflies are estimated to exist globally. Their name stems from the fact that they occur mostly in the UK during May. Immature mayflies are visible to the naked eye after hatching from the egg, and they spend many years emerging as aquatic nymphs

until they can rise as adults to the surface. An adult mayfly only lives for a few days before it reaches its ultimate aim of reproduction [128-129].

To lure females, most male adults assemble in swarms a few meters above the water, performing a nuptial dance, by distinctive up-and-down rhythms of behaviour. Females migrate into these swarms, to compete with a male in the sky. The mating will last just a few seconds, and once it is done, the females release their eggs on the water surface, and their life cycle begins [131-132].

(a) Mayflies Inspiration:

A PSO modification can be seen in the proposed optimization approach which combines major PSO [133-134] benefits. In general, it provides an effective hybrid algorithmic framework for investigators seeking to advance the efficiency of the PSO algorithm using crossover and local search techniques, as it has been shown that PSO involves certain modifications to ensure optimum performance in high-dimensional space [135]. The literature reports previously modified optimization algorithms that combine the benefits of existing algorithms. It is influenced by the social actions of the Mayflies and, in particular, by their mating phase. Humans agree that mayflies are grown and fittest mayflies survive even after the hatching of the egg, irrespective of how long they survive [136]. The location of each fly in the search space is a possible solution to the problem. The algorithm is operating as follows. Initially, the male and female population is produced random ally by two sets of mayflies. In other words, every fly is positioned arbitrarily as a solution depicted by a d-dimensional (dim) vector $x = (x_1, x_2, \ldots\ldots x_d)$ as shown in equation 3.23 in the space of issue, and its output is assessed on a preset objective function f (x). The velocity $v = (v_1, v_2, \ldots\ldots v_d)$ as shown in equation 3.24 of a mayfly is characterized as a change of position, and the flight path of each mayfly is a complex interaction of both individual and social flying experiences. In general, each mayfly changes its path to its personal best position (pbest) so far, as well as to the best position obtained by any swarm mayfly so far (gbest).

$$J = (J_1, J_2, \ldots\ldots J_{dim}) \tag{3.23}$$

$$V = (V_1, V_2, \ldots\ldots V_{dim}) \tag{3.24}$$

(b) Male Mayflies Movement

The aggregation of males in swarms means that each mayfly's position is balanced according to both its own experience and that of its neighbours as well as shown in equation 3.25 and 3.26.

$$J_a^{t+1} = J_a^t + V_a^{t+1} \tag{3.25}$$

$$J_a^o \sim (J_{min}, J_{max}) \tag{3.26}$$

Where the current position of mayflies is represented as J_a^t and the search space is represented as a at time step t+1.

Provided that the male mayflies are still performing the nuptial dance a few meters above the water, we presume that they cannot establish high velocities and that they run continuously. As a consequence, the velocity of male mayflies is determined in equation 3.27.

$$J_{ab}^{t+1} = J_{ab}^{t+1} + \Omega_1 M^{-\alpha R_I^2}\left(P_{bestab} - J_{ab}^t\right) + \Omega_2 M^{-\alpha R_I^2}\left(G_{bestab} - J_{ab}^t\right) \tag{3.27}$$

Where J_{ab}^{t+1} the ab position of mayflies in dimension at a time is step, $\Omega_1 M^{-\alpha R_I^2}$ and $\Omega_2 M^{-\alpha R_I^2}$ are the constants used to scale the contribution of cognitive and social component respectively. Considering the minimization of the problem, the P_{best} is calculated as in equation 3.28.

$$P_{bestab} = \begin{cases} J_{ab}^{t+1}, & \text{if } f\left(J_{ab}^{t+1}\right) < f P_{bestab}, \\ \text{is kept the same, 0 otherwise.} \end{cases} \tag{3.28}$$

To evaluate the quality of a solution, the f is the objective function. At the time step, the global best position and distance is calculated as in equation 3.29.

$$\|J_a - Y_a\| = \sqrt{\left(\sum_{b=1}^{N} J_{ab} - Y_{ab}\right)^2} \tag{3.29}$$

(c) Female Mayflies Movement

Female mayflies, unlike males, do not congregate in swarms. Instead, they fly toward males to reproduce as mentioned below in equation 3.30 and 3.31.

$$V_a^{t+1} = V_a^t + V_a^{t+1} \tag{3.30}$$

$$V_a^o \sim (V_{min}, V_{max}) \tag{3.31}$$

They preferred to design it as a probabilistic method, while attraction could be randomized as shown in equation 3.32.

$$V_{ab}^{t+1} = \begin{cases} J_{ab}^{t+1} + \Omega_2 M^{-\alpha R_I^2}\left(J_{ab}^t - Y_{ab}^t\right), \text{if } (Y_a \geq f(J_a) \\ V_{ab}^t + f * \text{Rand}, \text{if } (Y_a \leq f(J_a) \end{cases} \tag{3.32}$$

Where the velocity of female mayflies is represented as V_{ab}^{t+1}, the random walk coefficient is denoted as $f * \text{Rand}$, is used when a female is not attracted by the male mayflies, so it flies randomly and the range of random value is [-1,1].

(d) Mating

The mating mechanism between two mayflies is defined by the crossover operator as follows: One parent is chosen from the male population and one from the female population. The way parents are preferred is the same as the way that males attract females. In specific, the selection can be either random or dependent on their fitness function. For better females, the better males will pair with them. Then, the next best females will pair with the next best males, and so on. Two offspring that are produced as shown in equations 3.33 and 3.34 are the outcomes of the crossover.

$$\text{Offspring 1} = M * \text{Male parent} + (1-M) * \text{female} \tag{3.33}$$

$$\text{Offspring 2} = M * \text{Female parent} + (1-M) * \text{male} \tag{3.34}$$

Where the specific range of random value is denoted by M, the female parent is denoted by the word 'female', and the male parent is denoted by the word 'male'. The initial velocities of the offspring are set to be zero. The pseudo-code is represented in Fig. 3.14. Flow chart of Mayfly algorithm is shown in Fig. 3.15.

```
Objective function f(x).
Initialize the male mayfly population, and velocities.
Initialize the female mayfly population, and velocities.
Evaluate solutions,
Find global best,
Do While stopping criteria are not met,
    Update velocities and solutions of males and females,
    Evaluate solutions,
    Rank the mayflies,
    Mate the mayflies,
    Evaluate offspring,
    Separate offspring to male and female randomly,
    Replace worst solutions with the best new ones,
    Update pbest and gbest.
End while
Post process results and visualization.
```

Fig. 3.14 Pseudo code of MA

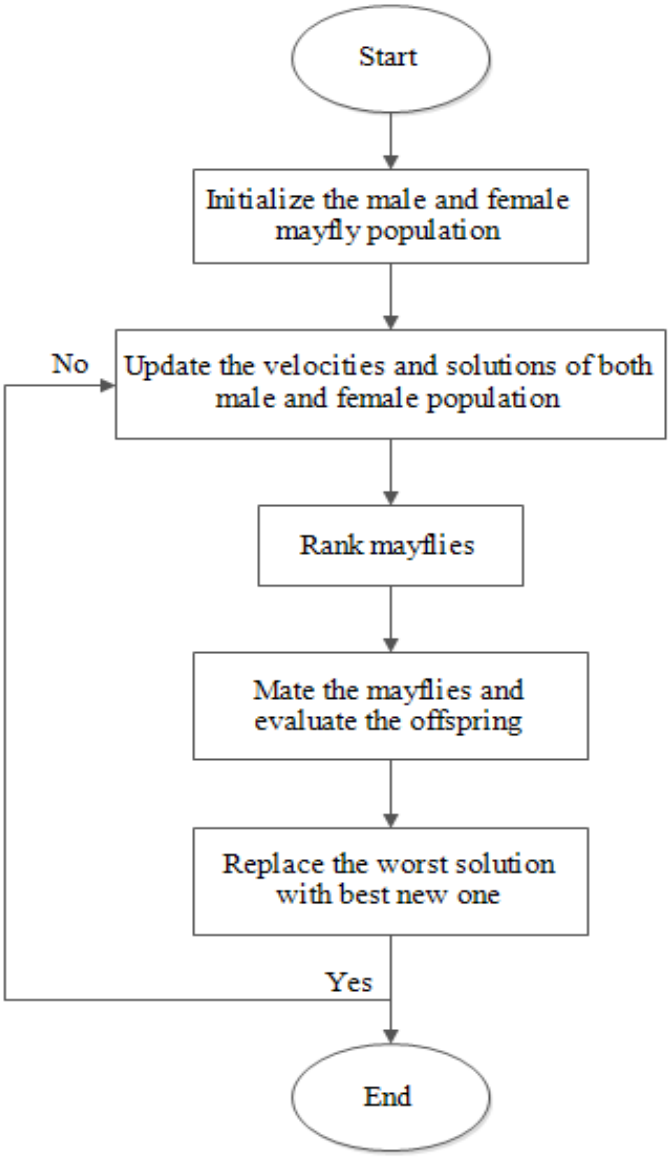

Fig. 3.15 Flow Chart of MA

- **New Chaotic Mayfly Algorithm (CMA)**

The literature has shown that chaotic maps have multiple advantages in metaheuristic algorithms [121]. The advantages of chaotic maps are investigated in our suggested algorithm. The problem of the MA becoming trapped at the local minimum can be solved by using chaotic maps to aid the algorithm in better exploring the search space. The mutation rate of the standard MA, is altered chaotically using the maps, in this study to get better results than the original methodology. Pseudo-code of Chaotic Mayfly Algorithm is shown in Fig. 3.16. Flow chart of Mayfly algorithm is represented in Fig. 3.17.

Objective function f(x).
Initialize the male mayfly population, and velocities.
Initialize the female mayfly population, and velocities.
Mutation rate is regulated using chaotic maps.
Evaluate solutions,
Find global best,
Do While stopping criteria are not met,
    Update velocities and solutions of males and females,
    Evaluate solutions,
    Rank the mayflies,
    Mate the mayflies,
    Evaluate offspring,
    Separate offspring to male and female randomly,
    Replace worst solutions with the best new ones,
    Update pbest and gbest.
End while
Post process results and visualization.

Fig. 3.16 Pseudo code of CMA

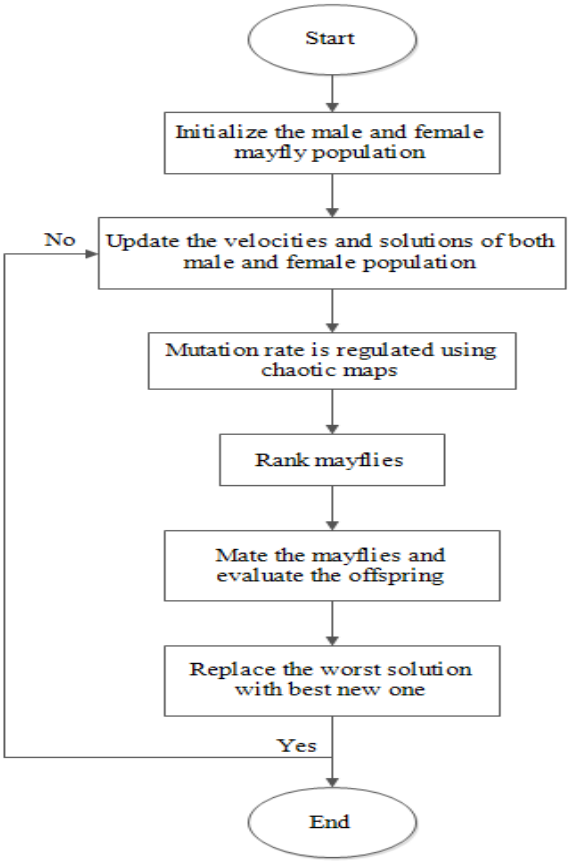

Fig. 3.17 Flow Chart of CMA

3.3.2.1 Outcome and Discussion of CMA

In this section, the PEMFC model parameter extraction issues are solved by the chaotic variant family. To check the performance of the chaotic variant family, some well-known meta-heuristics algorithms are compared that are PSO, ASO, ALO, HHO, SMA, TSA, CSO and MA. One model of PEMFC is considered which Ballard Mark V [130] as discussed below in Table 3.4. Table 2.1 explains the five chaotic maps used by CMA whereas five chaotic maps are represented by Table 3.19.

Table 3.19 List of Chaotic Maps

Name	Maps Number
Chebyshev	CMA1
Circle	CMA2
Gauss/Mouse	CMA3
Iterative	CMA4
Logistic	CMA5

Table 3.20 shows the seven unknown parameters as well as the sum of square error and computation time per second. From the computation time, it is clear that the variants of the chaotic family have run in less time as compared to other algorithms. The minimum value for SSE is 3.2244E-09 from this table, which belongs to the variant of the chaotic family. The statistical result of this model is seen in Table 3.21 and the convergence graph is shown in Fig. 3.18. The chaotic variant family outperforms the rest of the compared algorithms, according to this graph. The polarization curve of I-V and P-I is shown in Fig. 3.19 and Fig. 3.20

Table 3.20 Parameter Estimation of PEMFC

Parameters→ Algorithms↓	ξ_1	ξ_2	ξ_3	ξ_4	λ	R_C	**b**	**Computation time/ second**
CMA1	-0.9575	0.0019	5.1827E-05	-0.00016	12.6055	0.00032	0.1879	5.5215
CMA2	-1.1603	0.0011	5.3728E-05	-0.00020	15.5433	0.00030	0.1103	2.8451
CMA3	-1.0177	0.0028	6.6621E-05	-0.00017	15.9889	0.00052	0.2710	4.2569
CMA4	-1.0107	0.0027	6.8447E-05	-0.00019	16.8330	0.00042	0.2274	4.9787
CMA5	-1.0364	0.0027	6.9692E-05	-0.00018	15.9574	0.00039	0.2392	2.1523

MA	-0.8692	0.0023	4.4663E-05	-0.00013	10.3924	0.00020	0.1266	9.2134
SMA	-1.1942	0.0010	4.1234E-05	-0.00016	15.3311	0.00020	0.2083	11.4205
TSA	-1.0390	0.0024	6.9428E-05	-0.00019	16.8429	0.00038	0.2925	9.8950
CSO	-1.0701	0.0026	5.5273E-05	-0.00018	15.6439	0.00043	0.2249	10.5877
PSO	-0.9031	0.0015	5.4600E-05	-0.00011	12.8730	0.00017	0.0665	24.5582
ALO	-1.1799	0.0011	5.0620E-05	-0.00019	13.5090	0.00019	0.0666	20.2591
ASO	-1.0554	0.0028	6.8984E-05	-0.00017	15.1905	0.00047	0.2526	16.1455
HHO	-1.0937	0.0018	4.7761E-05	-0.00015	12.7963	0.00021	0.1383	14.5897

Table 3.21 Statistical Results of SSE

Statistical Results→ Algorithms↓	**Minimum**	**Average**	**Maximum**	**S.D**
CMA1	1.0313E-08	4.8894E-08	8.7186E-08	2.7939E-08
CMA2	1.3133E-09	4.1836E-09	8.4204E-09	2.2094E-09
CMA3	1.1802E-08	3.6360E-08	9.1337E-08	1.9694E-08
CMA4	1.0255E-08	3.7132E-08	8.6146E-08	2.4223E-08
CMA5	1.2321E-09	3.2244E-09	6.9744E-09	1.5466E-09
MA	1.0087E-06	3.3852E-06	7.0971E-06	1.7477E-06
SMA	1.1473E-05	1.7729E-05	2.6989E-05	4.7202E-06
TSA	1.0351E-06	3.6082E-06	8.8437E-06	1.8686E-06
CSO	1.0049E-06	4.8296E-06	9.8121E-06	2.4544E-06
PSO	1.1596E-02	3.1792E-02	9.5653E-02	2.0490E-02
ALO	1.1545E-03	4.4915E-03	8.8848E-03	2.6598E-03
ASO	1.3107E-04	5.1699E-04	9.8557E-04	2.5892E-04
HHO	1.2729E-04	3.7255E-04	8.7043E-04	2.4143E-04

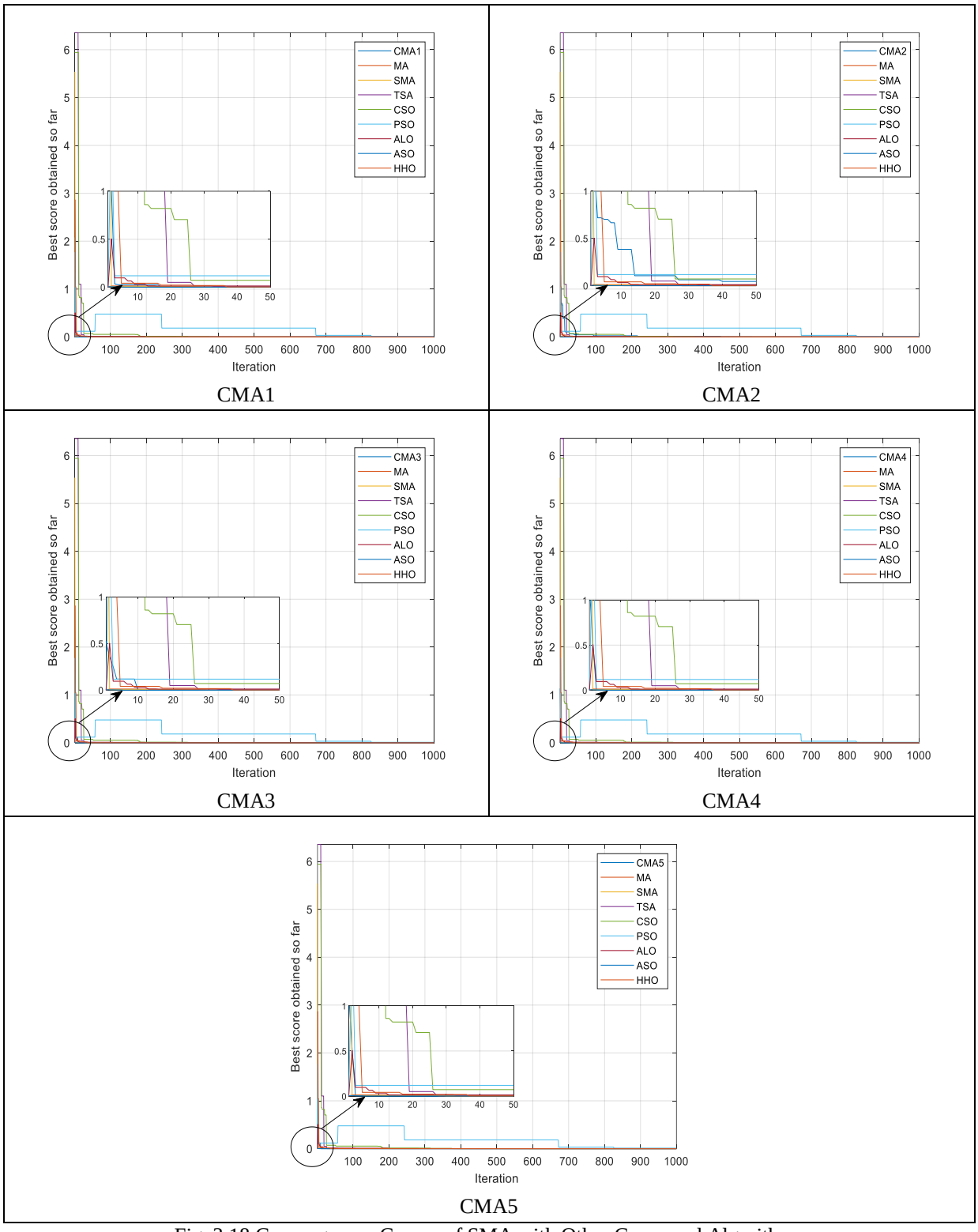

Fig. 3.18 Convergences Curves of SMA with Other Compared Algorithms

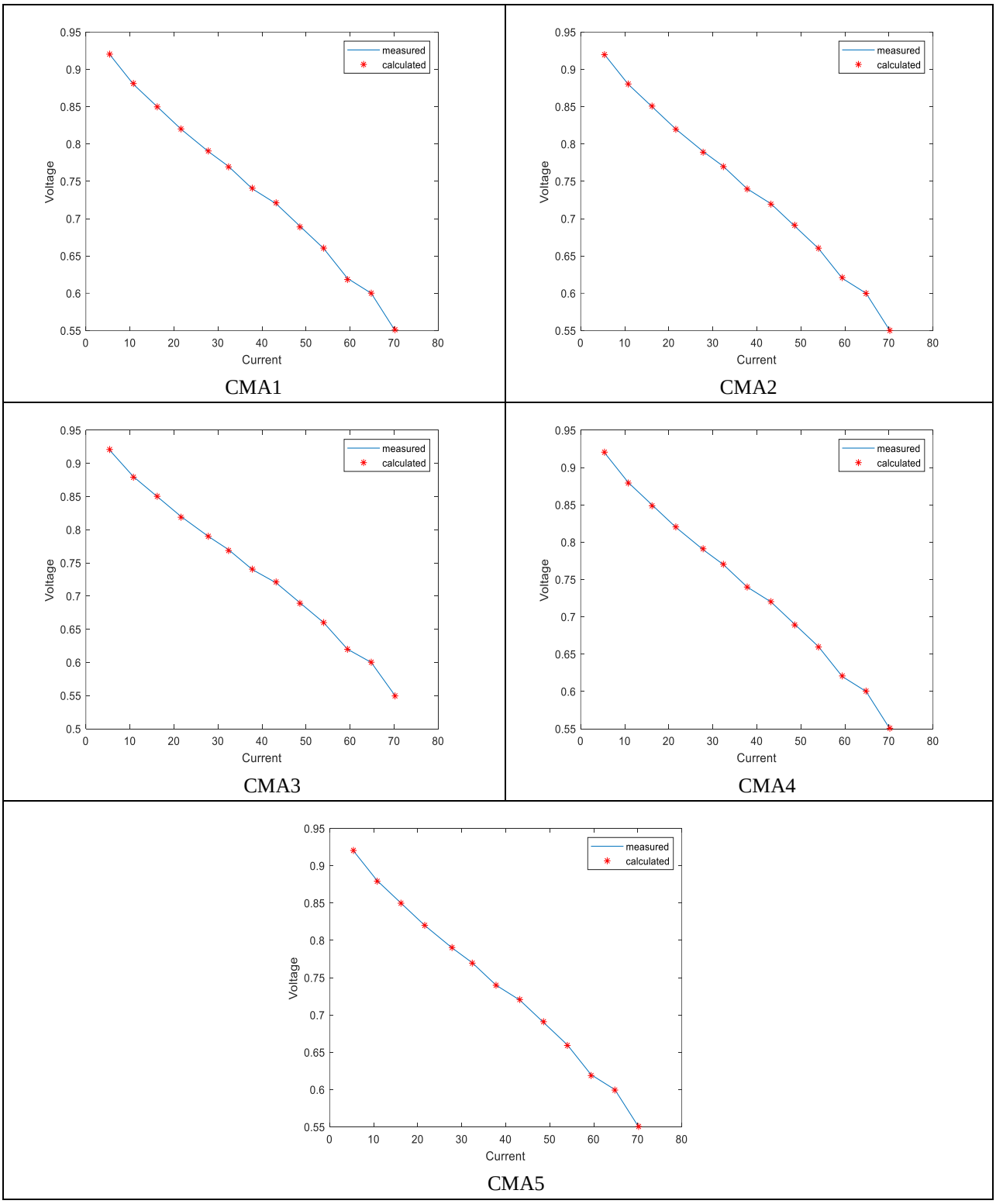

Fig. 3.19 V-I Curve of All Algorithms

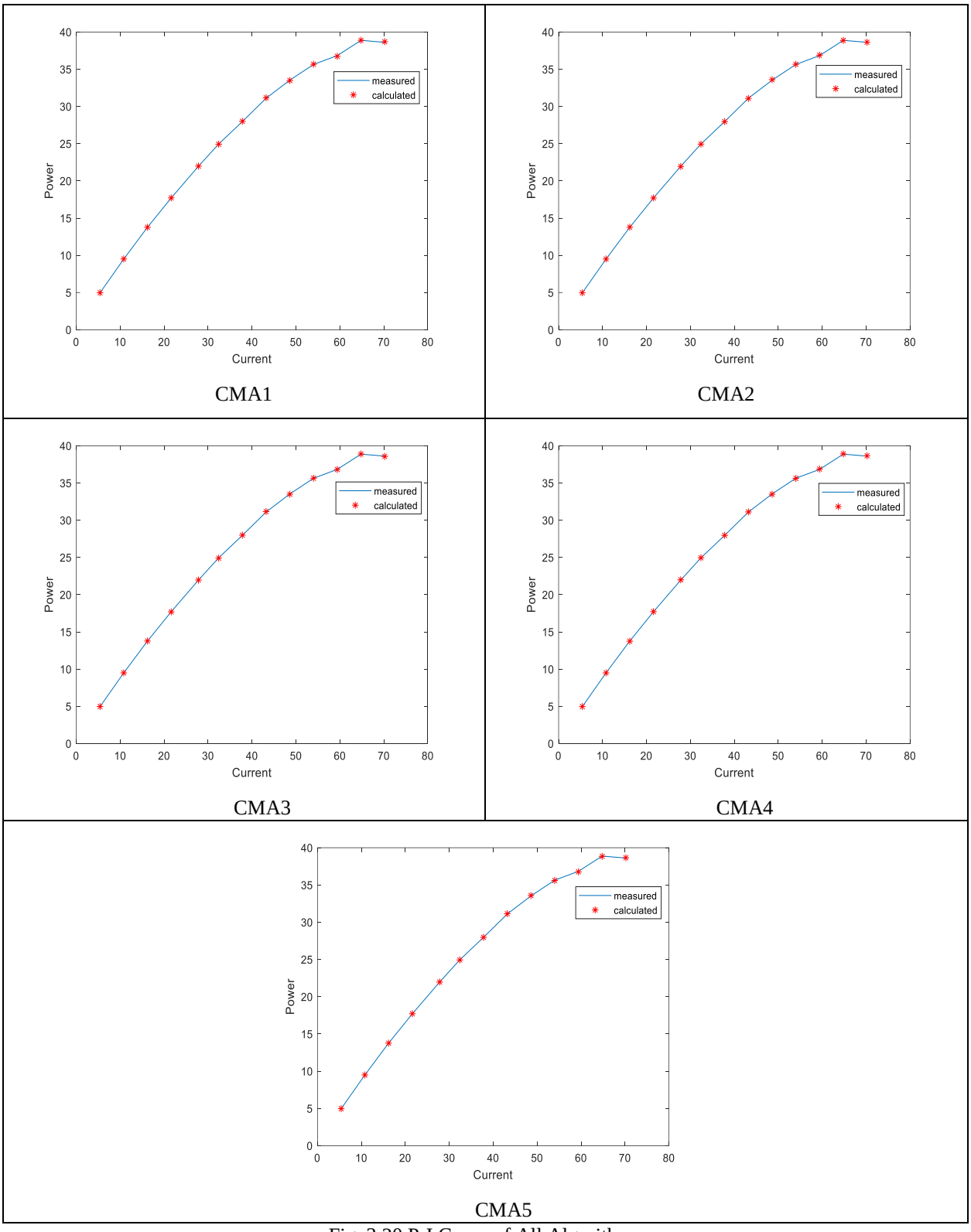

Fig. 3.20 P-I Curve of All Algorithms

- **Non-Parametric Tests**

Nonparametric statistics is a statistical approach in which the data is not expected to originate from pre-determined models with a small number of parameters. Milton Friedman created the Friedman test, which is a non-parametric statistical test [112]. It is used for the detection of changes in treatments during several test trials, similar to the repeated parametric ANOVA measurements. Each row (or block) is ranked collectively, and the values of the ranks are then considered by columns. Table 3.22 depicts the results of Friedman ranking non-parametric test. The chaotic variant family outperforms the compared meta-heuristic algorithms in this test. The chaotic variant family has secured one to five ranks; MA has secured the sixth rank with PSO, ASO, ALO, SMA, TSA, CSO and HHO to follow in this test.

Table 3.22 Friedman Ranking Test

Algorithms	Friedman Ranking
CMA1	5
CMA2	2
CMA3	4
CMA4	3
CMA5	1
MA	6
SMA	9
TSA	7
CSO	8
PSO	13
ALO	12
ASO	11
HHO	10

The second non-parametric test performed in this article is the Kruskal-Wallis test [114]. The multiple comparisons of mean ranking are shown in Fig. 3.21. The chaotic variant family means rank is considerably different and better from the other groups. The multiple comparisons of median ranking are shown in Fig. 3.22. The chaotic variant family median rank is considerably different and better from the other groups. Table 3.23 represents the results of Mood's Median test. Chi-square is used to measure the significance of probability. Based on the results of the above non-parametric tests, it can be inferred that the suggested technique, the chaotic variant family, outperformed the other algorithms in terms of reliability and speed.

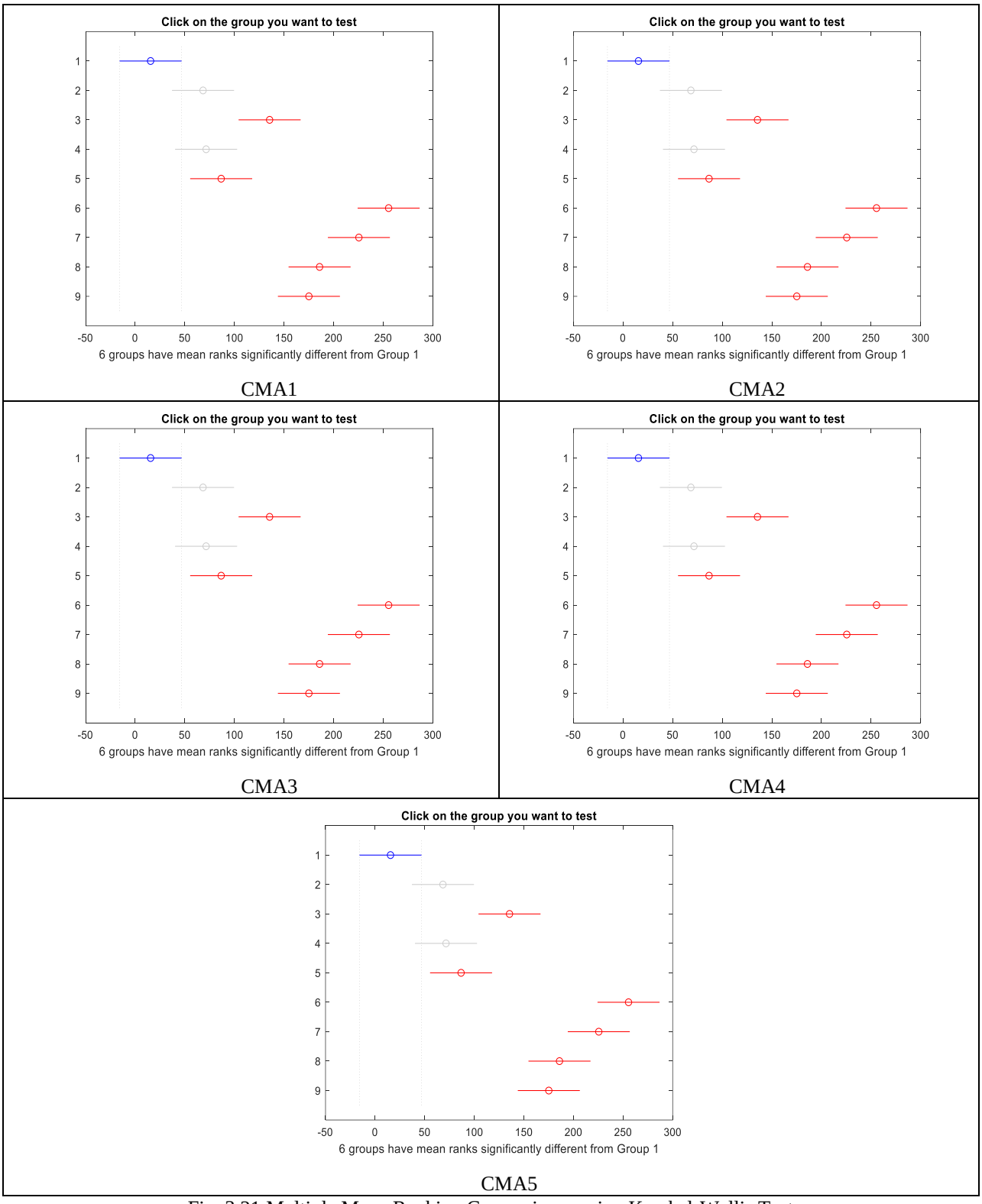

Fig. 3.21 Multiple Mean Ranking Comparisons using Kruskal-Wallis Test

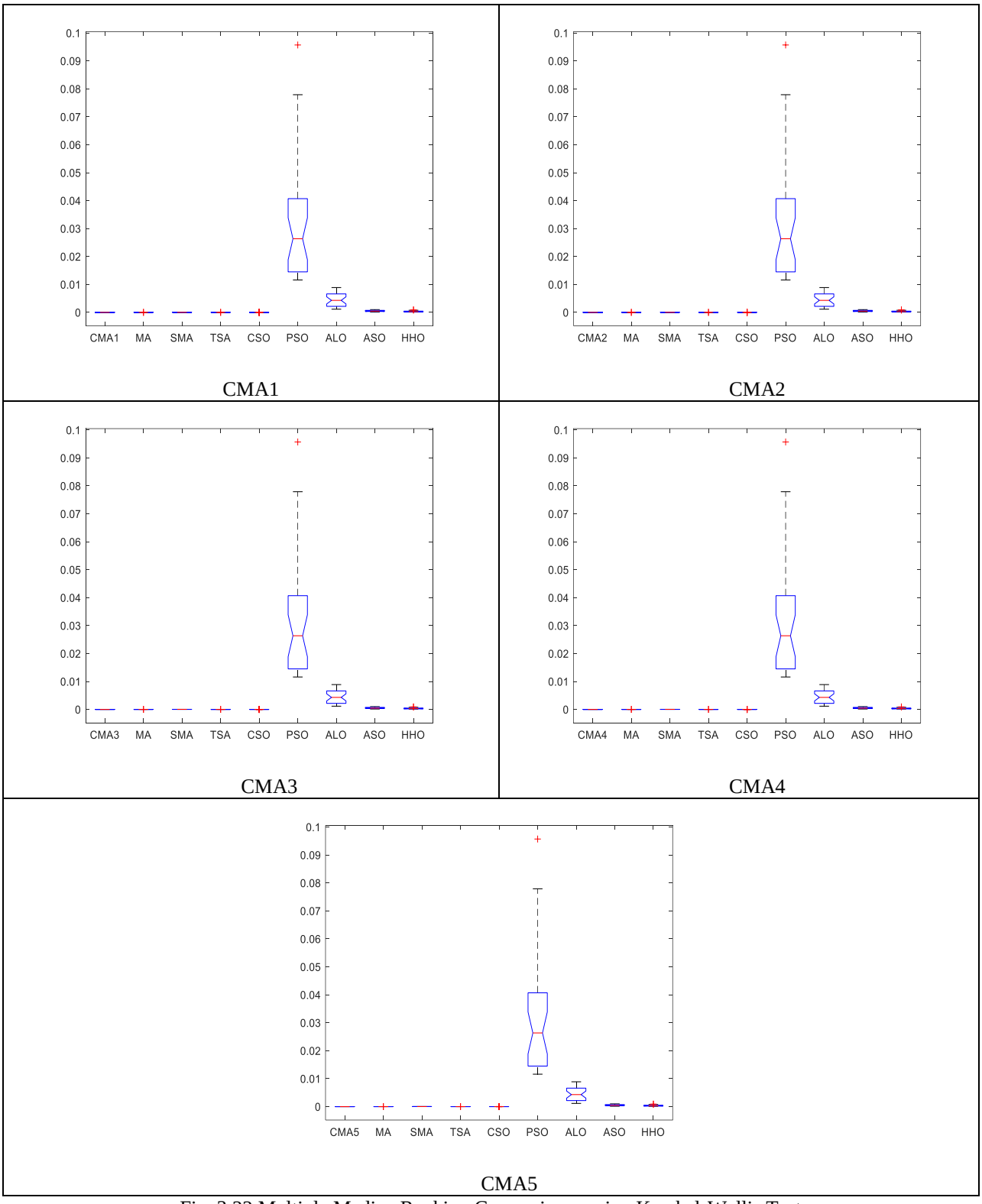

Fig. 3.22 Multiple Median Ranking Comparisons using Kruskal-Wallis Test

Table 3.23 Mood's Median Test

Algorithms	CMA1	CMA2	CMA3	CMA4	CMA5
P-Value	3.91E-25	3.91E-25	3.91E-25	3.91E-25	3.91E-25
Chi-Square	11.0705	11.0705	11.0705	11.0705	11.0705
Chi-Square Observed	124.2667	124.2667	124.2667	124.2667	124.2667

3.4 Outcomes

To solve the global optimization problems and extracting the parameters of various PEMFCs, a two algorithm are proposed i.e. SMA and CMA. Based on the obtained result, the following conclusions have been drawn.

- A meta-heuristic efficient algorithm Slime Mould Algorithm (SMA) along with Chaotic Mayfly Algorithm (CMA) meta-heuristic efficient algorithm is introduced.
- The SSE is the objective function for the evaluation of the PEMFCs.
- The parameter extraction and error is calculated. Furthermore, the convergence graph, as well as the I-V and P-V Characteristics curves, validates the proposed algorithm's speed and accuracy.
- From the non-parametric tests, it is justified that the proposed algorithms are much better than the rest of the compared algorithms.

CHAPTER 4 OPTIMAL SIZING OF PHOTOVOLTAIC, FUEL CELL, AND BIOMASS BASED HYBRID ENERGY SYSTEMS

4.1 Introduction

From the second half of the twentieth century onwards, there has been an enormous growth in environmental pollution [138]. Currently, fossil fuels account for nearly 80% of the world's primary energy supply, and estimates suggest that global energy consumption will grow at a rate of about 2.3 percent per year from 2015 to 2040, implying a visible increase in CO_2 levels in the atmosphere, given that the global average CO_2 level in the atmosphere in 2019 was 409.8 ppm, [139-140]. Despite the fact that today's society is more aware of the problem, effective solutions such as increased investment in the development of renewable technologies, as well as a search for renewable energy sources, are urgently needed. These solutions need to be cost-effective, efficient, and, most importantly, reduce or do not increase polluting emissions, globally.

Renewable energy sources such as solar PV, wind, fuel cells, biogas, and biomass are ecologically beneficial and sustainable those are fast increasing sources of energy in the process of developing a strong economy of a nation. However, when employed as a stand-alone source of energy, renewable energy has a number of limitations. The electricity generated by wind turbines and solar PV is highly reliant on environmental variables, whereas fuel cells require hydrogen-enriched fuel to function properly. Biomass/biogas energy producing systems have significant features that have recently been created and are widely employed in stand-alone mode to meet the energy demands of rural areas. Fuel cells have a lot of potential as emerging green energy sources because of its many features, such as high efficiency, zero emissions, and a flexible structure. Solar and wind energy are coupled with other sources to ensure 24x7 electricity availability. The combination of two or more renewable sources from the hybrid renewable energy system (HRES). To increase the overall working efficiency of HRES the understanding and optimization of the working variables that improve their characteristics taking into account their constraints [141-142]. Rural electrification is hampered by technical obstacles such as limited transmission capacity, difficult terrain, and a geographically distributed population that is characterized by lower levels of education, lower load density, and lower incomes.

4.2 Description of System

In this section, hybrid renewable energy system is evaluated i.e. (Solar PV/Biomass/ FC) using HOMER to analyze and quantify the cost of the system. In order to assess the optimization

outcomes for the proposed model, HOMER simulation program requires additional input data, which is discussed in the following section.

- Load Profile Data: The community load is considered for the area Patiala which is located in Punjab and the latitude and Longitude of this location is 30.3398^{o} N, 76.3867^{o} E respectively. The Patiala is located at 846ft above the sea level. Figure 1 shows the load profile data of proposed location. From Fig. 4.1, the average (kWh/day) baseline load is 171.04 and scaled load is 165.59, the average (kW) baseline load is 7.13 and scaled load is 6.9, the peak (kW) baseline load is 23.32 and scaled load is 22.57, and the load factor for the baseline and scaled load is 0.31 which is to be assumed. The Table 4.1 and Table 4.2 show the yearly load data of weekdays and weekend.

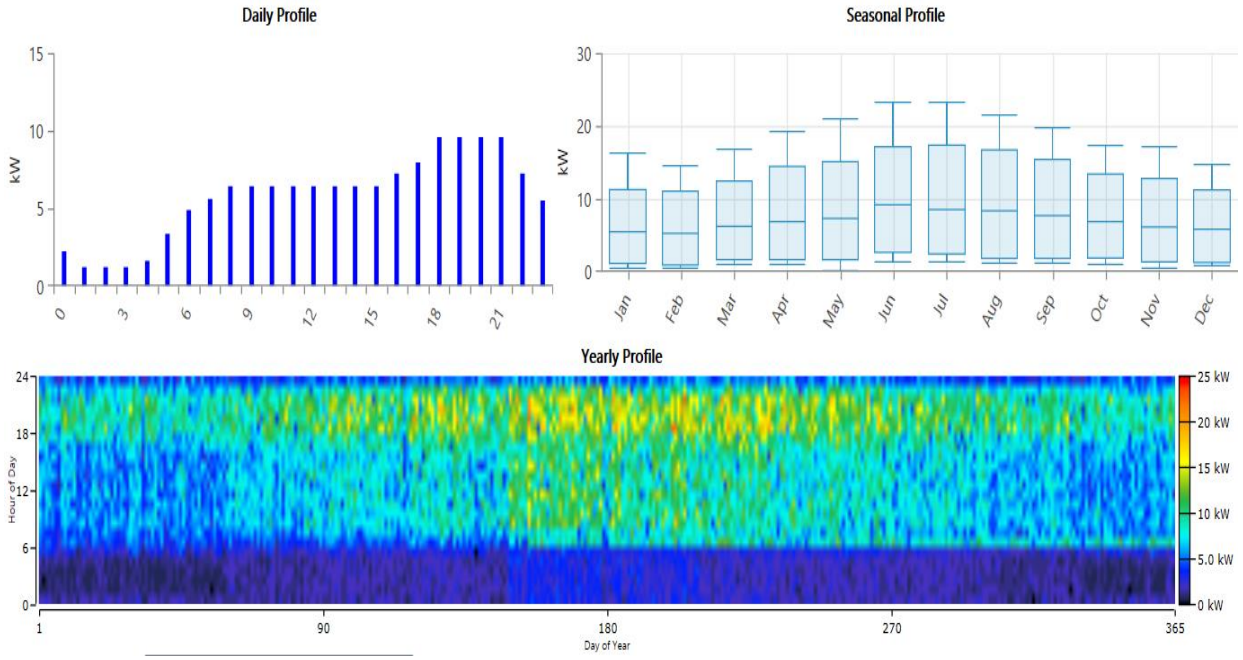

Fig. 4.1 Load Profile Data

Table 4.1 Weekdays Load Data Profile

Hour	Jan	Feb	Mar	Apr	May	Jun	Jul	Aug	Sep	Oct	Nov	Dec
0	2.200	2.200	1.800	2.000	2.200	3.400	3.400	2.340	2.200	2.000	1.800	2.200
1	1.200	1.200	1.800	2.000	2.200	3.400	3.400	2.340	2.200	2.000	1.800	1.200
2	1.200	1.200	1.800	2.000	2.200	3.400	3.400	2.340	2.200	2.000	1.800	1.200
3	1.200	1.200	1.800	2.000	2.200	3.400	3.400	2.340	2.200	2.000	1.800	1.200
4	1.600	1.600	1.800	2.000	2.200	3.600	3.600	2.340	2.200	2.000	1.800	1.600

5	3.400	3.400	2.700	3.000	3.300	3.600	3.600	3.510	3.300	3.000	2.700	3.400
6	4.900	4.900	4.500	5.000	5.500	8.850	8.850	5.850	5.500	5.000	4.500	8.850
7	5.600	5.600	6.300	7.000	7.700	8.400	8.400	8.190	7.700	7.000	6.300	5.600
8	6.400	6.400	7.200	8.000	8.800	11.050	11.050	9.360	8.800	8.000	7.200	6.400
9	6.400	6.400	7.200	8.000	8.800	11.050	11.050	9.360	8.800	8.000	7.200	6.400
10	6.400	6.400	7.200	8.000	8.800	11.050	11.050	9.360	8.800	8.000	7.200	6.400
11	6.400	6.400	7.200	8.000	8.800	11.050	11.050	9.360	8.800	8.000	7.200	6.400
12	6.400	6.400	7.200	8.000	8.800	11.050	11.050	9.360	8.800	8.000	7.200	6.400
13	6.400	6.400	7.200	8.000	8.800	11.050	11.050	9.360	8.800	8.000	7.200	6.400
14	6.400	6.400	7.200	8.000	8.800	11.050	11.050	9.360	8.800	8.000	7.200	6.400
15	6.400	6.400	7.200	8.000	8.800	11.050	11.050	9.360	8.800	8.000	7.200	6.400
16	7.200	7.200	8.100	9.000	9.900	10.800	10.800	10.530	9.900	9.000	8.100	7.200
17	8.000	8.000	9.000	10.000	11.000	12.000	12.000	11.700	11.000	10.000	9.000	8.000
18	9.600	9.600	10.800	12.000	13.200	14.400	14.400	14.040	13.200	12.000	10.800	9.600
19	9.600	9.600	10.800	12.000	13.200	14.400	14.400	14.040	13.200	12.000	10.800	9.600
20	9.600	9.600	10.800	12.000	13.200	14.400	14.400	14.040	13.200	12.000	10.800	9.600
21	9.600	9.600	10.800	12.000	13.200	14.400	14.400	14.040	13.200	12.000	10.800	9.600
22	7.200	7.200	8.100	9.000	9.900	10.800	10.800	10.530	9.900	9.000	8.100	7.200
23	5.500	5.500	4.500	5.000	5.500	6.000	6.000	5.850	5.500	5.000	4.500	5.500

Table 4.2 Weekend Load Data Profile

Hour	Jan	Feb	Mar	Apr	May	Jun	Jul	Aug	Sep	Oct	Nov	Dec
0	1.600	1.600	1.800	2.000	2.200	3.400	2.400	2.340	2.200	2.000	1.800	1.600
1	1.600	1.600	1.800	2.000	2.200	3.400	2.400	2.340	2.200	2.000	1.800	1.600
2	1.600	1.600	1.800	2.000	2.200	3.400	2.400	2.340	2.200	2.000	1.800	1.600
3	1.600	1.600	1.800	2.000	2.200	3.400	2.400	2.340	2.200	2.000	1.800	1.600
4	1.600	1.600	1.800	2.000	2.200	3.600	2.400	2.340	2.200	2.000	1.800	1.600
5	2.160	2.160	2.430	2.700	2.970	3.600	3.240	3.159	2.970	2.700	2.430	2.160

6	3.600	3.600	4.050	4.500	4.950	8.850	5.400	5.265	4.950	4.500	4.050	8.850
7	5.040	5.040	5.670	6.300	6.930	8.400	7.560	7.371	6.930	6.300	5.670	5.040
8	5.760	5.760	6.480	7.200	7.920	11.050	8.640	8.424	7.920	7.200	6.480	5.760
9	5.760	5.760	6.480	7.200	7.920	11.050	8.640	8.424	7.920	7.200	6.480	5.760
10	5.760	5.760	6.480	7.200	7.920	11.050	8.640	8.424	7.920	7.200	6.480	5.760
11	5.760	5.760	6.480	7.200	7.920	11.050	8.640	8.424	7.920	7.200	6.480	5.760
12	5.760	5.760	6.480	7.200	7.920	11.050	8.640	8.424	7.920	7.200	6.480	5.760
13	5.760	5.760	6.480	7.200	7.920	11.050	8.640	8.424	7.920	7.200	6.480	5.760
14	5.760	5.760	6.480	7.200	7.920	11.050	8.640	8.424	7.920	7.200	6.480	5.760
15	5.760	5.760	6.480	7.200	7.920	11.050	8.640	8.424	7.920	7.200	6.480	5.760
16	6.480	6.480	7.290	8.100	8.910	10.800	9.720	9.477	8.910	8.100	7.290	6.480
17	9.200	9.200	8.100	9.000	9.900	12.000	10.800	10.530	9.900	9.000	8.100	9.200
18	9.200	9.200	9.720	10.800	11.880	14.400	12.960	12.636	11.880	10.800	9.720	9.200
19	9.200	9.200	9.720	10.800	11.880	14.400	12.960	12.636	11.880	10.800	9.720	9.200
20	9.200	9.200	9.720	10.800	11.880	14.400	12.960	12.636	11.880	10.800	9.720	9.200
21	9.200	9.200	9.720	10.800	11.880	14.400	12.960	12.636	11.880	10.800	9.720	9.200
22	7.240	7.240	7.290	8.100	8.910	10.800	9.720	9.477	8.910	8.100	7.290	7.240
23	3.600	3.600	4.050	4.500	4.950	6.000	5.400	5.265	4.950	4.500	4.050	3.600

- Solar Radiation and Biomass Gasifier: Fig. 4.2 represents the average solar radiation and clearness data per annum. From Table 4.3, it is concluded that the average solar radiation is 5.17 (kWh/m^2/day). Fig. 4.3 shows the average temperature data per annum. From Table 4.4, it is clearly indicated that the maximum temperature is in the month of June which 36.030 ^{o}C, and the average temperature is 25.46^{o}C. Table 4.5 represents the electrical data information of the solar PV model taken (Fronius Symo 20.0-3-M with Generic PV).

Fig. 4.2 Solar Radiation and Clearness Index per Annum for Solar

Table 4.3 Clearness Index and Solar Radiation per Annum for Solar

Month	Clearness Index	Daily Radiation (kWh/m^2/day)
Jan	0.598	3.507

Feb	0.608	4.319
Mar	0.616	5.379
Apr	0.622	6.343
May	0.619	6.877
Jun	0.601	6.870
Jul	0.506	5.690
Aug	0.516	5.418
Sep	0.607	5.589
Oct	0.656	4.963
Nov	0.641	3.924
Dec	0.582	3.181

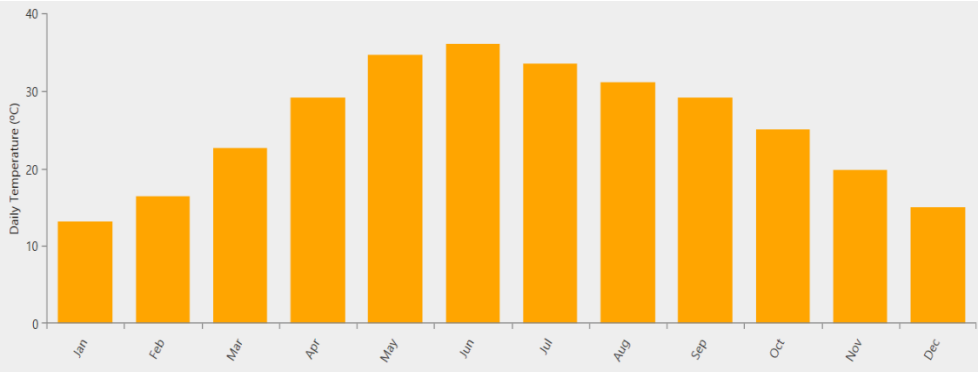

Fig. 4.3 Average Temperature Data per Annum for Solar

Table 4.4 Average Temperature Data per Annum for Solar

Month	**Daily Temperature (°C)**
Jan	13.190
Feb	16.360
Mar	22.600
Apr	29.160
May	34.670
Jun	36.030
Jul	33.500
Aug	31.090
Sep	29.060
Oct	25.010
Nov	19.820
Dec	15.050

The functioning of the PV is highly influenced by climatic factors such as solar radiation and temperature. The method may be used to calculate the output of solar photovoltaic as shown in equation 4.1.

$$S_{o/p} = \eta . Ae . N_q \quad (4.1)$$

Where, the efficiency of solar photovoltaic is denoted by η, Ae is denoted as the area of the solar photovoltaic generator, and solar radiation is denoted by N_q. The solar photovoltaic efficiency is given as in equation 4.2.

$$\eta = f_r . f_{cp} . \left(1 - \beta\left(Q_c - Q_{ref}\right)\right) \tag{4.2}$$

Where, the module efficiency, energy conditioning efficiency is denoted as f_r , f_{cp} and temperature coefficient is denoted as β. The reference cell temperature is denoted as Q_{ref}, and cell temperature is denoted as Q_c. The cell temperature is calculated as given by equation 4.3.

$$Q_c = Q_a + \left((N_{oct} - 20)/800\right) . N_q \tag{4.3}$$

Where, the ambient temperature is denoted as Q_a, and Nominal operating temperature is denoted as N_{oct}.

Table 4.5 Electrical Data of Solar PV

Solar Model Name	FroniusSymo 20.0-3-M with Generic PV
Max. Permitted PV Power	30.00 kW
Max. Voltage Range	450-800 V
Operating Voltage Range	200-1,000 V
Max. Input Voltage	1,000 V
Nominal Input Voltage	710 V
Max. Output Power	19.995 VA
Max. Output fault Current /Duration	30.9 A RMS / 150.4 ms
Max. Continuous Output Current	24.0 A
Max. Efficiency	98.0 %
CEC Efficiency	97.5 %
Total Harmonic Distortion	< 1.75%
Power Factor	0-1 inductor/capacitor

Solid bio-residue is converted into a gaseous fuel that is then utilized to generate power in biomass gasification technology. The producer gas, which is a flammable gas composed of H_2 (20%), CO (20%), CH_4 (1–2%), and inert gases, is formed during partial combustion. The producer gas is utilized as an input fuel in the case of a biomass gasifier. A biomass gasifier's yearly output electricity (F_{bg}) may be calculated as shown in equation 4.4. Fig. 4.4 shows the average monthly data of biomass availability. From Table 4.6, it is clearly indicated that the average biomass availability is 0.63 (tonnes/day).

$$F_{bg} = Q_{bg}(8760 * CUF) \quad (4.4)$$

Where, biomass gasifier system rating is denoted as Q_{bg}, and capacity utilization factory is denoted as CUF. Few characteristics such as biomass calorific value, biomass availability (Ton/yr), and biomass gasifier utilization hours are playing a major role in a biomass system. A biomass gasifier with the highest possible rating can be characterized as in equation 4.5 when placed in a certain area:

$$Q_{bg} = \frac{Total\ available\ biomass\ (\frac{Ton}{yr}) * 1000 * DW_{bg} * \eta_{bg}}{365 * 860 * Operating\ hours/day} \quad (4.5)$$

Where the overall efficiency of the biomass gasifier is denoted as η_{bg}, and the calorific value of biomass gasifier is denoted as DW_{bg}.

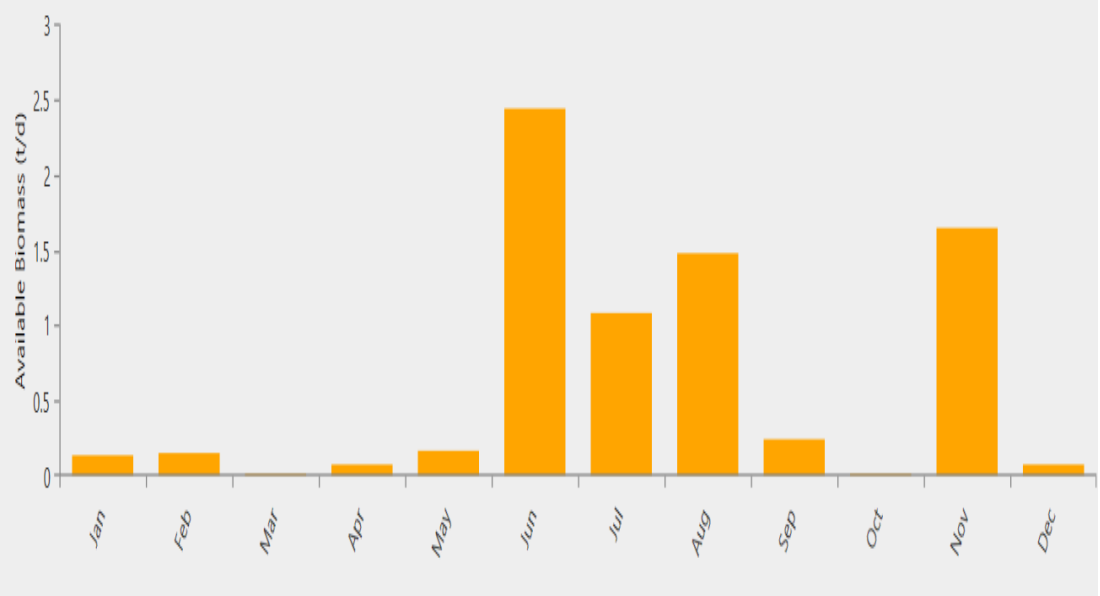

Fig. 4.4 Average Biomass Availability Monthly

Table 4.6 Monthly Average Available Biomass Data

Month	Average (tonnes/day)
Jan	0.130
Feb	0.150
Mar	0.017
Apr	0.077
May	0.170
Jun	2.433
Jul	1.079

Aug	1.480
Sep	0.240
Oct	0.016
Nov	1.650
Dec	0.076

Fig. 4.5 represents the biomass gasifier fuel consumption on the yearly basis. The total fuel consumed in a year is 20,287 m^3, the average fuel consumed per day is 55.6 m^3, and the average fuel consumed per hour is 2.32 m^3.

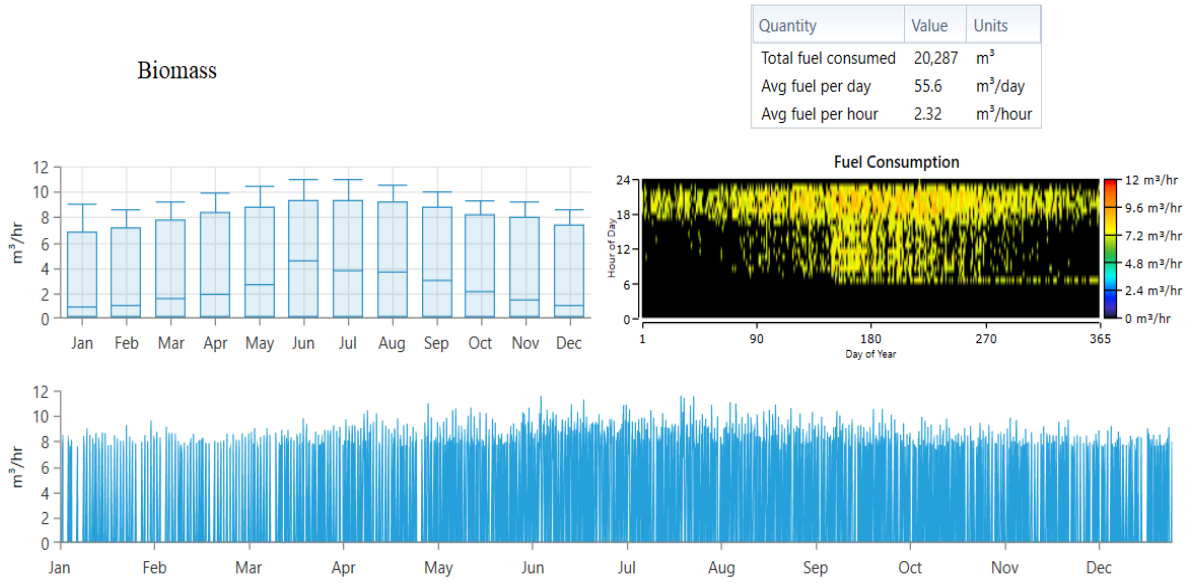

Fig. 4.5 Biomass Gasifier Fuel Consumed on Yearly Basis

- Fuel Cell (FC): Similar to battery, FC is an electro-chemical device that converts chemical energy to electrical energy. FC is available in various designs depending upon electrode types, operating characteristics and power ranges. But in this work, the Polymer Electrolyte Membrane fuel cell (PEMFC) is used because of its excellent start up time and shut down time [108, 143]. In the PEMFC, there are two electrodes (anode and cathode), which is separated by a semi-permeable membrane. The explanation of PEMFC is provided [144]. The overall electro-chemical equation of fuel cell is represented in equation 4.6.

$$2H_2 + O_2 = 2H_2O \tag{4.6}$$

The overall efficiency of fuel cell is given in equation 4.7:

$$M_{FC} = M_E . M_T . M_R \tag{4.7}$$

Where, the electrical efficiency is denoted by M_E, the thermal efficiency is denoted by M_T, and the efficiency of fuel cell reaction is denoted by M_R.

Fig. 4.6 represents the yearly fuel consumption of a fuel cell. The total fuel consumed in a year is 6,343 liters, the average fuel consumer per day is 17.4 liters, and the average fuel consumption per hour is 0.724 liters.

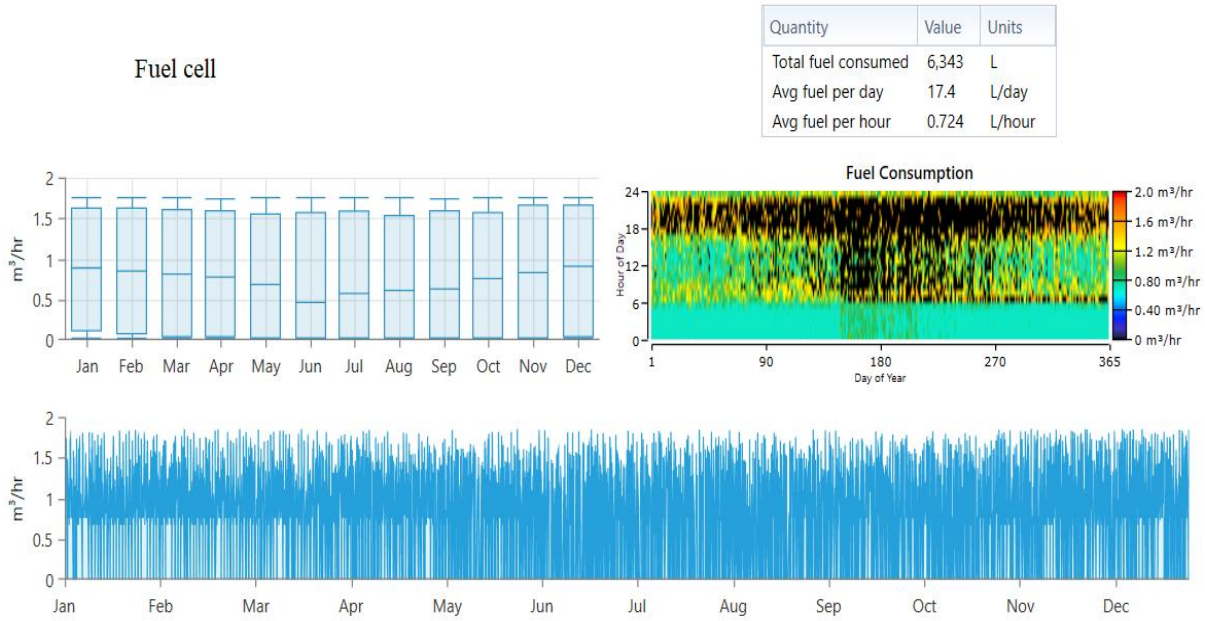

Fig. 4.6 Fuel Cell Fuel Consumption on Yearly Basis

- Electrolyzer: By conducting electric current through water, hydrogen may be generated by decomposing it into its constituent elements. A water electrolyzer is made up of multiple cells that are linked together in a series. The electrolyte separates the two electrodes of the electrolyzer from one another. Water is decomposed into hydrogen and oxygen by passing electrical current via the electrolyzer [145].
- Hydrogen Storage: An electrolyzer will be used to produce the hydrogen which we need. This device acts in the opposite manner of a fuel cell, in that it employs the electrolysis process, which is based on the separation of the components that combine to produce a compound by the application of electrical current. In order for electrolysis to occur, the direct current voltage must surpass a voltage threshold that varies depending on the kind of material and is referred to as the breakdown voltage. It is necessary to fill the electrolyzer with water that has been combined with the residue in order for it to function. Afterwards, a voltage is supplied to it by the use of electrodes

that are connected in series at the bottom of the container, resulting in the occurrence of the appropriate chemical reactions, which will result in the production of the hydrogen.

4.3 Proposed Algorithm

4.3.1 Slime Mould Algorithm (SMA)

The slime mould usually refers to physarum poly-cephalum [128]. Since it was first known as a fungus, it was then called a “slime mould” whose life cycle was initially described in a paper published in 1931 by Howard [129]. A eukaryote that inhabits cold and humid areas is the slime mould. There are three main behaviour of SMA forms the basis of mathematical modelling i.e. approach food, wrap food, grabble food The detailed mathematical modelling of SMA is explained in chapter 3 in sub section 3.3.1. Pseudo code as well as flow chart is shown in Fig. 3.2 and Fig. 3.3 respectively.

4.3.2 Particle Swarm Optimization (PSO)

Particle swarm optimization is a swarm-intelligence-based optimization method inspired by the social behaviour of birds and shoals of fish. It uses a population-based search technique to find the optimum solution to a problem by moving particles about in the search space. Particles in PSO go through a multidimensional search space [146-147]. During flight, each particle modifies its location based on its own and neighbouring particles' experiences, utilizing the optimal position discovered by itself and its neighbour’s. A particle's swarm direction is determined by the collection of particles that surround it as well as its past experience [148-149]. PSO is a nondeterministic, stochastic optimization technique that provides a population-based search procedure for global optimization. Its main advantage is that it is simple to implement and has a small number of parameters to adjust. Pseudo code of PSO is shown in Fig. 4.7 and Fig. 4.8 represents the flow chart of PSO.

4.3.3 Hybrid Chaotic Particle Swarm Optimization Slime Mould Algorithm (HCPSOSMA)

Hybridization and chaotic maps have numerous remunerations in meta-heuristic algorithm and it can be observed from previous work [150, 13]. The benefits of chaotic maps are explored in our proposed hybrid proposed algorithm. As PSO algorithm being the parental algorithm of the swarm group of optimization algorithm helps SMA algorithm to increase the precision of outcomes. In this, the proposed hybrid chaotic algorithm eliminates the problem of local min using chaotic maps along with it increases the accuracy of the system. Pseudo code of HCPSOSMA is shown in Fig. 4.9 and Fig. 4.10 represents the flow chart of HCPSOSMA.

Initialize all parameters

For every particle, calculate fitness value

If the fitness value is better than the best fitness value from previous one, then set this value as new best particle (pbest)

End

Choose the particle with the best fitness value of all the particles as gbest

For each particle, calculate particle velocity and update position

End

If the maximum iteration is reached

End

Fig. 4.7 Pseudo code of PSO

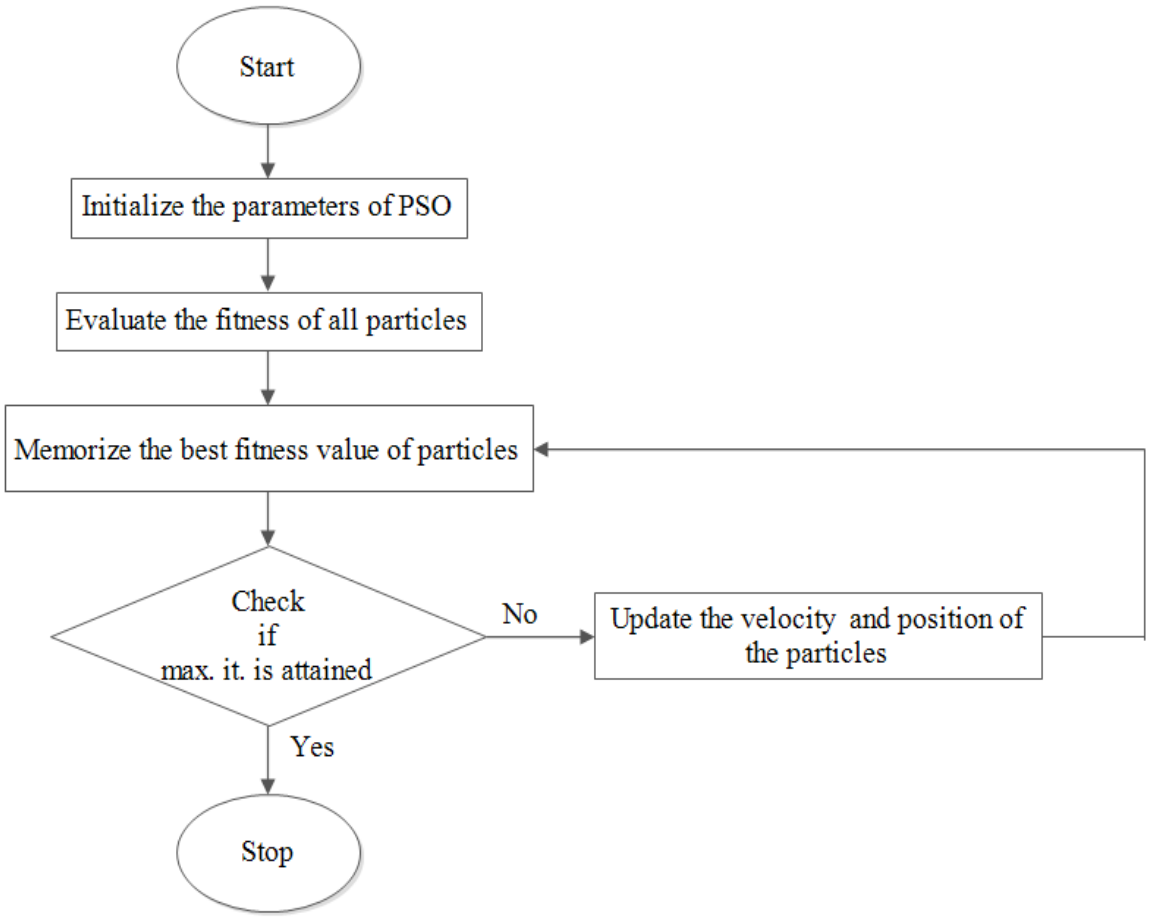

Fig. 4.8 Flow Chart of PSO

4.3.4 Problem Formulation

In this method of cost optimization, HOMER replicates each system configuration, and shows in the graphical form, sorted by net present cost, and levelised cost of energy. After the simulation process done in the HOMER, then the cost is found by the proposed algorithm. Authors proposed a hybrid renewable energy system. The primary goal of this research is to reduce overall NPC of the HRES while maintaining optimal flow of energy in the proposed hybrid system. Three major choice variables, namely the biomass gasifier, solar PV panels, and fuel cell have been determined in order to get the best possible design. To conduct the economic analysis, the principle of annualized system cost (ASC) is employed. Once all constraints and criteria are satisfied, it is seen that the outcome with the lowest ASC is the most optimum one to achieve. The objective function taken into consideration is the overall system cost, which is comprised of the total capital cost, the replacement cost, and the operating and maintenance costs of the various components.

Initialize all parameters

For i =1 to max_iter

Run PSO

Update the velocity of particles

If rand (0,1) < prob, then (to avoid local minima)

Initialize the parameters of SMA where 'z' parameter is evaluated using chaotic maps

Run SMA

Calculate the best position and fitness

Update the position of current particle according to best position

end

Fig. 4.9 Pseudo code of HCPSOSMA

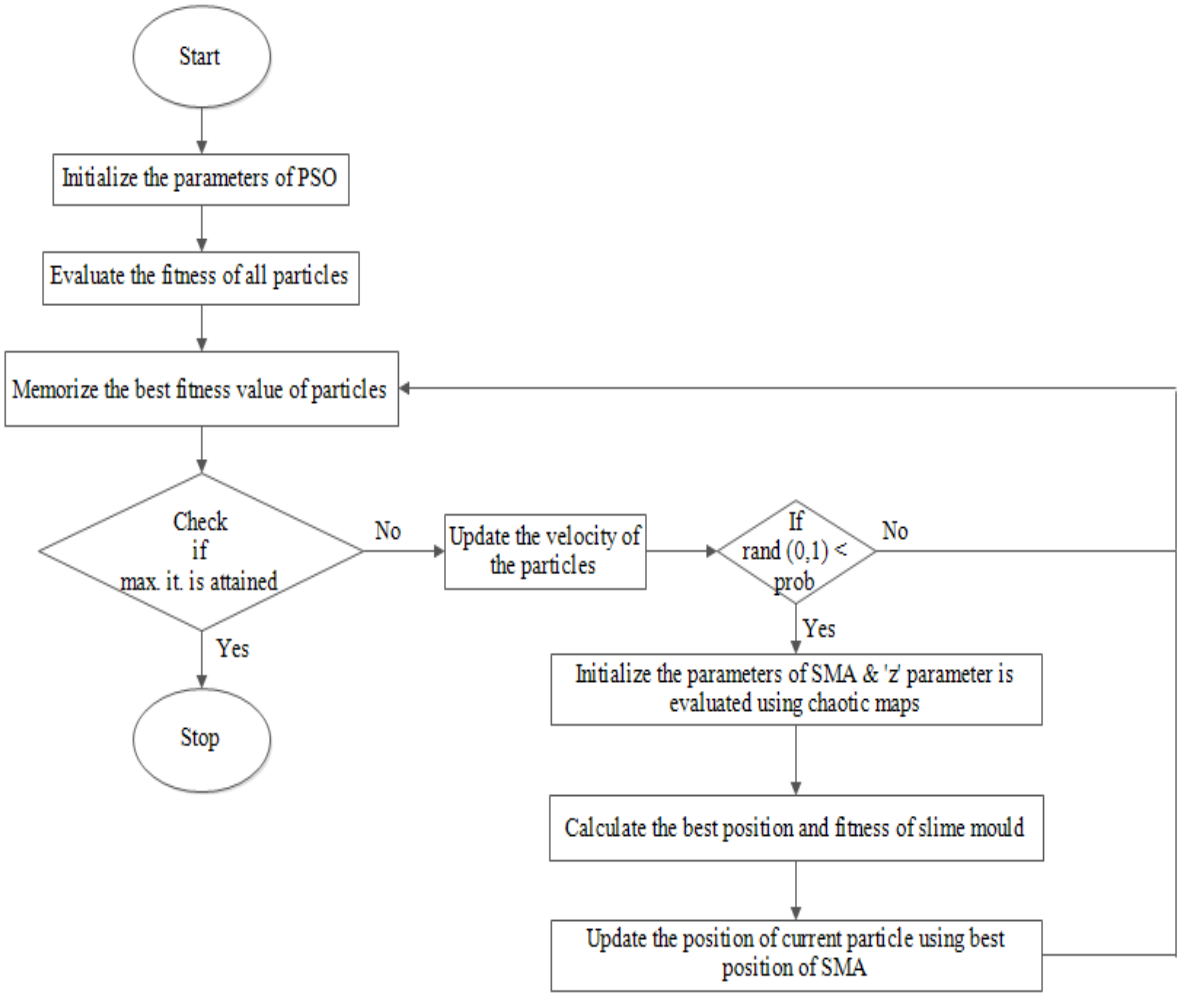

Fig. 4.10 Flow Chart of HCPSOSMA

All the components used in the proposed system have their own capital and installation cost, replacement cost, operating cost, salvage cost and annual maintenance cost. Annualized system cost is defined as in equation 4.9:

$$ASC = CRF * NPC \tag{4.9}$$

Here, NPC stands for net present cost, and CRF stands for capital recovery factor. Equation 4.10 gives the formula to calculate CRF.

$$CRF\ (j,m) = \frac{j(1+j)^m}{(1+j)^m - 1} \tag{4.10}$$

The constraint for the proposed system is shown in equation 4.11:

$$J_{IHRES} = J_{spv} + J_{bio} + J_{fc} + J_{converter} + J_e + J_{ht} \tag{4.11}$$

Where the sum of cost integrated hybrid renewable energy system is denoted as J_{IHRES}, cost of the solar PV panel is denoted as J_{spv}, cost of biomass gasifier is denoted as J_{bio}, cost of converter is denoted as $J_{converter}$, cost of electrolyzer is denoted as J_e, cost of hydrogen tank is denoted as J_{ht}, and cost of fuel cell is denoted as J_{fc}.

The most cost-effective and reliable configuration is chosen based on the LCOE and dependability. The levelised cost of energy (LCOE) is defined as the average price per kWh of usable energy provided by the system and may be expressed in equation 4.12:

$$\text{LCOE} = \text{ASC}/\text{Total useful energy provided} \quad (4.12)$$

4.4 Simulation and Optimization Results:

The two most important aspects for developing and implementing HRES are reliability and LCOE. This section evaluates the suggested optimally-designed HRES to fulfill AC (Alternating Current) and DC (Direct Current) primary load requirement of a community. For the bi-directional converter, the efficiency is assumed to be 90%. After simulating the system in HOMER software, the simulation studies are also carried out in MATLAB 2020a for the comparison purpose. A whole year of data was used to test all of the algorithms, which included the PSO, SMA, and chaotic variant family. Each algorithm was tested for a maximum of 1000 iterations during a 1-hour time period on the data set.

Solar PV/Biomass/FC:

This hybrid system consists of solar photovoltaic, biomass and fuel cell as shown in Fig. 4.11. In this case the main source of supply is Solar PV, biomass and for the storage purpose fuel cell is used instead of battery the life time of this system is also same. The energy generated by the solar PV panels, biomass and fuel cell sources is used to power the fundamental AC load.

The average generated electricity produced by the solar PV panels, biomass and fuel cell is represented in Fig. 4.12. From the figure it is clearly concluded that the production of electricity is maximum by biomass system is 29,787 kWh/yr, (44.70 % of the total electricity production), solar PV panel is producing electricity is 8,347 kWh/yr (12.60% of the total production of electricity), and the fuel cell is producing electricity is 28,417 kWh/yr (42.70% of the total production of electricity), the total production of electricity of the system is 66,551 kWh/yr. The total electricity consumption of the AC load is 60,442 kWh/yr, which is 100% of the total consumption load. For the proposed system, the excess electricity is 4,078 kWh/yr.

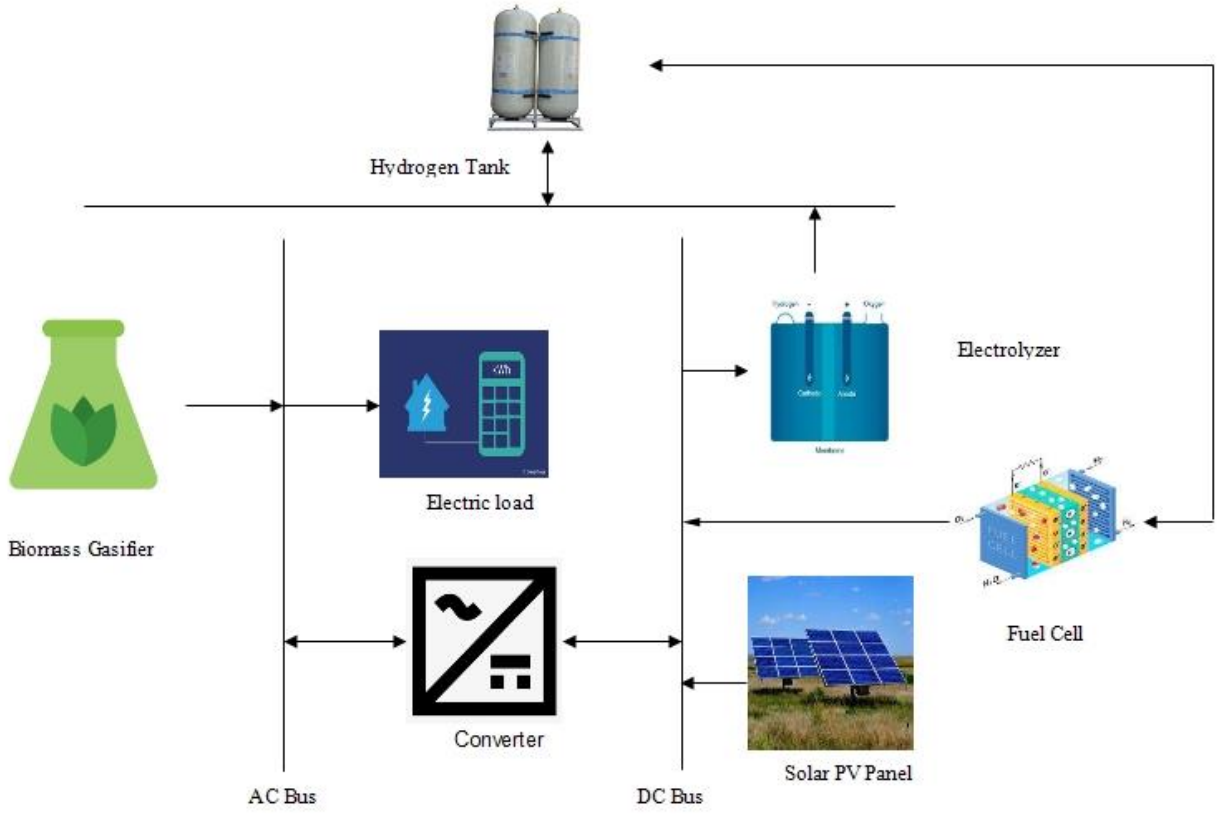

Fig. 4.11 Proposed Hybrid Diagram

Production	kWh/yr	%
Fronius Symo 20.0-3-M with Generic PV	8,347	12
Cummins 30kW RX30 C30 N6H	29,787	44
CAT-HFO-4919kW-50Hz-CP	28,417	42
Total	66,551	10

Consumption	kWh/yr	%
AC Primary Load	60,442	99.3
DC Primary Load	0	0
Deferrable Load	0	0
Total	60,859	100

Quantity	kWh/yr	%
Excess Electricity	4,078	6.13
Unmet Electric Load	0	0
Capacity Shortage	0	0

Quantity	Value	Units
Renewable Fraction	3.70	%
Max. Renew. Penetration	151	%

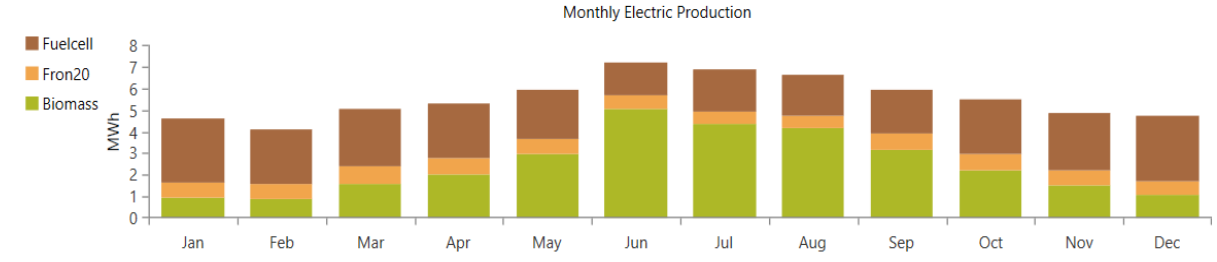

.

Fig. 4.12 Average Generated Electricity Produced in a Year

Fig. 4.13 shows the solar PV electricity production in a year. The total production of electricity in a year by solar PV system is 8,347 kWh. The rated capacity of the solar PV panel is 4.67 kW, mean output is 0.953 kW, mean output per day is 22.9 kWh, the dedicated converter is 20.0 kW, and the capacity factor the solar system is 20.4%. The maximum output which solar PV system gives 4.96 kW, PV penetration is 13.8%, per year solar PV hours of operation is 4,371 hours, and the LCOE of solar PV system is 0.135 $/kWh.

Quantity	Value	Units
Rated Capacity	4.67	kW
Mean Output	0.953	kW
Mean Output	22.9	kWh/d
Capacity Factor	20.4	%
Total Production	8,347	kWh/yr
Dedicated converter	20.0	kW

Quantity	Value	Units
Minimum Output	0	kW
Maximum Output	4.96	kW
PV Penetration	13.8	%
Hours of Operation	4,371	hrs/yr
Levelized Cost	0.135	$/kWh

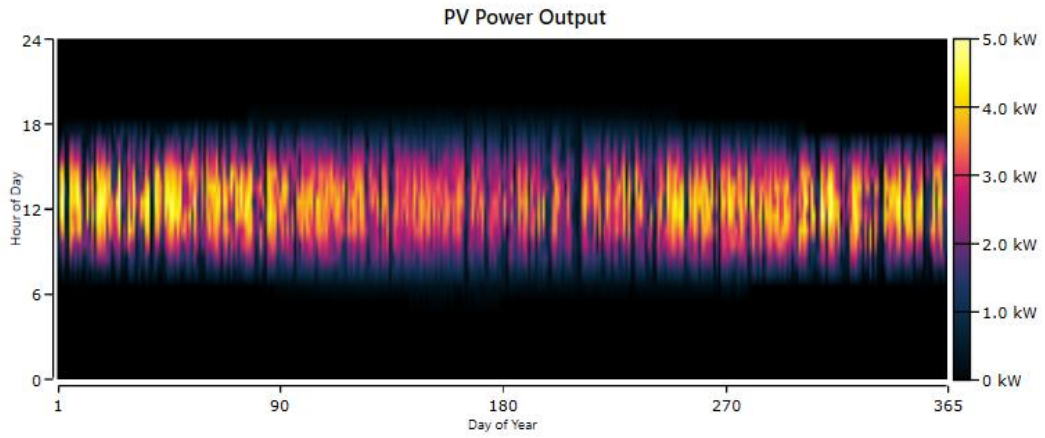

Fig. 4.13 Solar PV Electricity Production Yearly

Fig. 4.14 shows the biomass gasifier electricity production in a year. The total production of electricity in a year by biomass gasifier system is 29,787 kWh. The total rated capacity factor of the biomass gasifier is 11.3 %, mean output is 11.5 kW, the minimum electrical output is 8.64 kW, and the maximum electrical output is 22.6 kW. The maximum fuel consumption system gives 20.287 m^3, specific fuel consumption is 0.681 m^3/kWh, per year biomass gasifier hours of operation is 2,593 hours, and the mean electrical efficiency of system is 14.9%.

Quantity	Value	Units
Hours of Operation	2,593	hrs/yr
Number of Starts	896	starts/yr
Operational Life	0.386	yr
Capacity Factor	11.3	%
Fixed Generation Cost	3.60	$/hr
Marginal Generation Cost	0.145	$/kWh

Quantity	Value	Units
Electrical Production	29,787	kWh/yr
Mean Electrical Output	11.5	kW
Minimum Electrical Output	8.64	kW
Maximum Electrical Output	22.6	kW

Quantity	Value	Units
Fuel Consumption	20,287	m^3
Specific Fuel Consumption	0.681	m^3/kWh
Fuel Energy Input	200,334	kWh/yr
Mean Electrical Efficiency	14.9	%

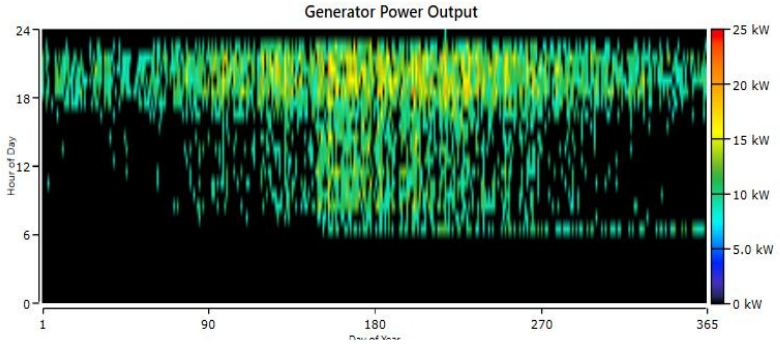

Fig. 4.14 Biomass Gasifier Production Yearly

Fig. 4.15 shows the converter yearly consumption. The rated capacity of the inverter is 10.3 kW, mean output of inverter is 3.50 kW, the maximum output of the inverter system is 9.27 kW, and the overall capacity factor of the inverter is 34.1 %. The per year inverter hours of operation is 6,167 hours, the energy out of inverter per year is 30,654 kWh, the energy in per year of inverter is 32,268 kWh, and the total losses in the inverter per year is 1,613 kWh.

Quantity	Inverter	Rectifier	Units
Capacity	10.3	0	kW
Mean Output	3.50	0	kW
Minimum Output	0	0	kW
Maximum Output	9.27	0	kW
Capacity Factor	34.1	0	%

Quantity	Inverter	Rectifier	Units
Hours of Operation	6,167	0	hrs/yr
Energy Out	30,654	0	kWh/yr
Energy In	32,268	0	kWh/yr
Losses	1,613	0	kWh/yr

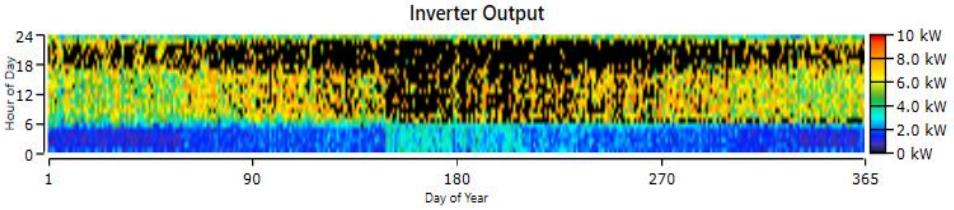

Fig. 4.15 Converters Yearly Consumption

Fig. 4.16 shows the production and consumption of fuel cell in a year. The electrical production of the fuel cell in a year is 28,417 kWh, the mean electrical output is 4.6 kW, Minimum electrical

output is 3.00 kW, and the maximum electrical output is 9.08 kW. The fuel consumption is 6,343 liters, the specific fuel consumption is 0.223 L/kWh, the fuel energy input per year is 70,573 kWh, and the mean electrical efficiency is 40.3%. The hours of operation of fuel cell per year is 6,167 hours, the number of starts per year is 897 starts, the operating life of fuel cell is 32.4 year, the capacity factor is 32.4 %, the fixed generation cost per hour is 0.673 $, and the marginal generation cost per kilowatt hour is 0.164$.

Quantity	Value	Units
Hours of Operation	6,167	hrs/yr
Number of Starts	897	starts/yr
Operational Life	32.4	yr
Capacity Factor	32.4	%
Fixed Generation Cost	0.673	$/hr
Marginal Generation Cost	0.164	$/kWh

Quantity	Value	Units
Electrical Production	28,417	kWh/yr
Mean Electrical Output	4.61	kW
Minimum Electrical Output	3.00	kW
Maximum Electrical Output	9.08	kW

Quantity	Value	Units
Fuel Consumption	6,343	L
Specific Fuel Consumption	0.223	L/kWh
Fuel Energy Input	70,573	kWh/yr
Mean Electrical Efficiency	40.3	%

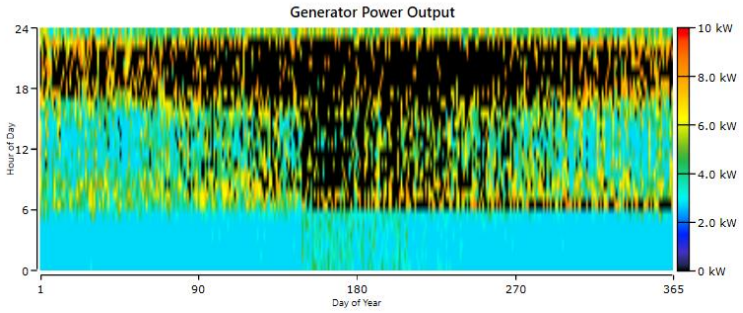

Fig. 4.16 Production and Consumption of Fuel Cell

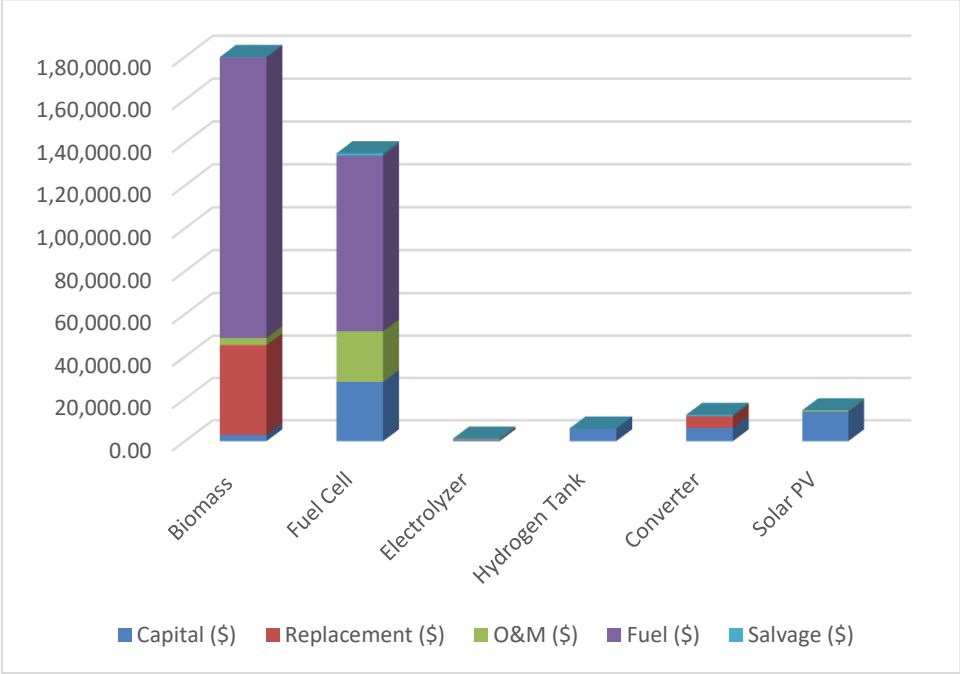

Fig. 4.17 Components Total Capital Cost

Fig. 4.17 describes the component cost of the proposed system, which include capital, replacement, fuel, salvage, operational and maintenance cost. The overall total system cost comes out to be $ 345, 443.60. The overall system component cost is shown in Table 4.7 and Fig. 4.18 represents the cost analysis of overall proposed system. The time series plot of the proposed system is shown in Fig. 4.19. Fig. 4.20 represents the graph between the year and cumulative nominal cash flow, and Table 4.8 represents the economic metrics of the proposed hybrid system.

Table 4.7 Overall System Component Cost

Component	Capital ($)	Replacement ($)	O&M ($)	Fuel ($)	Salvage ($)	Total ($)
Biomass	3,000.00	42,401.87	3,352.11	131,130.00	52.40	179,831.64
Fuel Cell	28,000.00	0	23,917.20	82,002.21	1,097.77	132,821.64
Electrolyzer	610.00	258.81	323.19	0	48.71	1,143.28
Hydrogen Tank	6,000.00	0	3.88	0	0	6,003.88
Converter	6,225.96	5,526.75	0	0	749.33	11,033.39
Solar PV	14,006.25	0	603.55	0	0	14,609.80
System	57,872.21	48,187.43	28,199.92	213,132.22	1,948.22	345,443.56

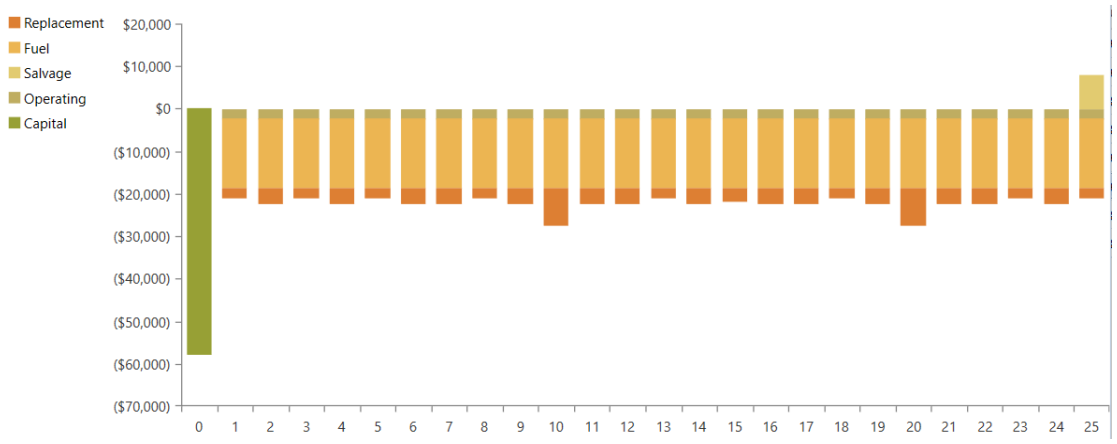

Fig. 4.18 Cost Analysis

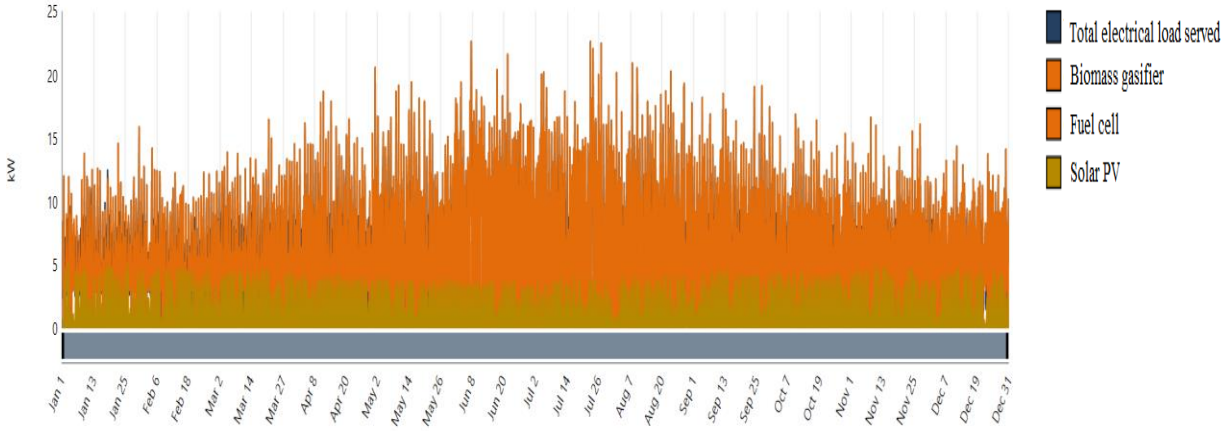

Fig. 4.19 Time Series Plot

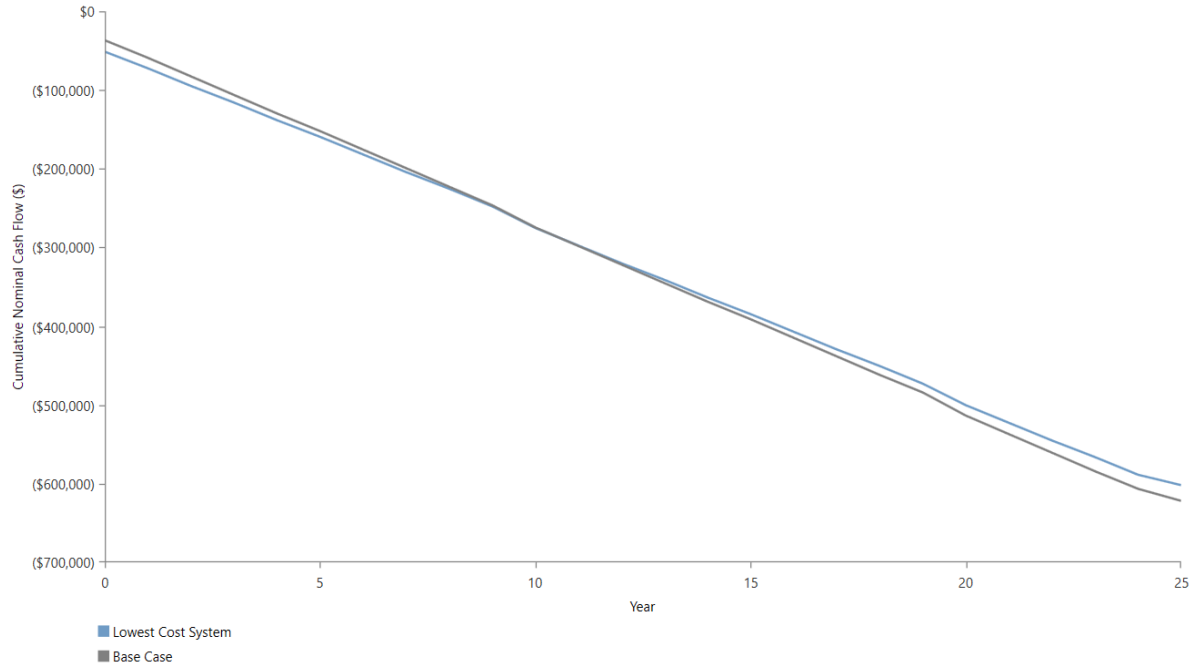

Fig. 4.20 Graph between Year and Cumulative Nominal Cash Flow ($)

Table 4.8 Economic Metric of the Proposed Hybrid System

Present Worth ($)	3,591
Annual Worth ($/yr)	278
Return on Investment (%)	2.3
Internal Rate of Return (%)	3.9
Simple Payback (yr)	15.96

After calculating all the component costs with HOMER software, the three parameters i.e. NPC, LCOE, and total operating cost of the proposed system are also calculated. These three parameters are also compared with the proposed algorithm and their parent algorithm (PSO and SMA) as mentioned above. Table 4.9 shows the results in the form of ASC, NPC, and LCOE using HOMER, SMA, PSO, HCPSOSMA1, HCPSOSMA2, HCPSOSMA3, HCPSOSMA4, and HCPSOSMA5 case studies.

Table 4.9 Optimal Sizing Results

Algorithm	ASC ($/yr)	NPC ($)	LCOE ($/kWh)
HOMER	26716.44	345,443.60	0.4420
PSO	26330.46	340,452.90	0.4356
SMA	25892.47	334,789.75	0.4283
HCPSOSMA1	24954.22	322,658.12	0.4128
HCPSOSMA2	24178.05	312,622.23	0.4000
HCPSOSMA3	25556.14	330,440.90	0.4228
HCPSOSMA4	23834.68	308,182.50	0.3943
HCPSOSMA5	25134.02	324,982.90	0.4158

A comparative analysis of the convergence rates of proposed algorithm and their comparison with parental algorithm is shown in Fig 4.21. The proposed hybrid system took hours to simulate with HOMER, but with the help of algorithms the time to simulate is reduced. From the results so obtained, it is concluded that the proposed algorithm (HCPSOSMA) is better than the parent algorithms (PSO and SMA) and the HOMER simulation.

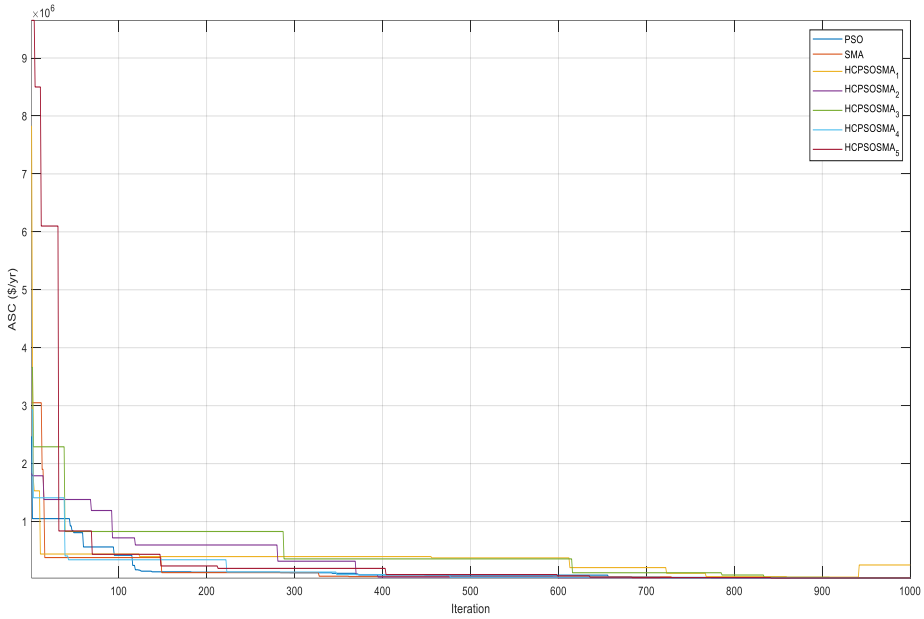

Fig. 4.21 Convergence Graph for All Algorithms

4.5 Outcomes

The number of researchers designed hybrid renewable energy system (HRES) models in different configurations. Based on the identified gap in the literature, a fuel cell based HRES model is

purposed. For the considered system, modeling and optimization of an off-grid HRES is undertaken. To resolve the optimal sizing and optimization difficulties, a novel proposed hybrid chaotic algorithm (HCPSOSMA) is applied. The results so obtained have been compared with those obtained using HOMER software. The best configuration of HRES is identified along with the lowest NPC and LCOE using the proposed algorithm, parent algorithm and HOMER software. The key finding of this chapter are outlined below:

- A new hybrid renewable energy system (HRES) was designed for the size and cost optimization.
- The proposed algorithm gives better results as compared to other algorithms and HOMER software in terms of reasonable environmental benefits.
- The system's performance was assessed with solar PV/biomass/fuel cell of stand-alone HRES with the lowest NPC and LCOE values.

CHAPTER 5 CONCLUSIONS AND FUTURE SCOPE

5.1 Conclusions

The thesis contribution of all chapters is discussed as follows:

Chapter 2: The key findings of this chapter are outlined below:

The key findings of chaotic tunicate swarm algorithm are:

- The accurate solution and speed of convergence of global optimization problems reveal that the chaotic variant family performs better than the rest of the compared algorithms in the chapter.
- For the DDM the computation time of the chaotic variants is better than the rest of the compared algorithms.
- For the TDM the computation time of the chaotic variants is better than the rest of the compared algorithms.
- Convergence curves indicate that the family of chaotic variants has a higher convergence rate than other algorithms compared to each other.
- Focusing on the effects of the solution stability, operating at various temperatures, the characteristic curves of I-V and P-V, the Friedman ranking test, the results of the Wilcoxon rank sum test, and the Kruskal-Wallis test, the family of chaotic variants displays greater or equal performance than the other compared methods on the solar PV cell model.
- The statistical finding shows that the family of chaotic variants has increased the efficiency of the Solar PV model parameter extraction problem. As error outcome of the proposed algorithm is least among all algorithms. This ensures that the unknown parameters obtained are of optimal value which in return decrease losses and increase efficiency of the solar PV cell.

The key findings of chaotic chicken swarm optimization are:

- In this chapter, a swarm-based approach is introduced to estimate the undetermined parameters of the three-diode PV models.
- Ten widely popular chaotic maps are used to enhance the performance of chicken swarm optimization (CSO).
- The metaheuristic algorithms use SSE as an objective function to obtain the solar cell parameters.
- The performance of the suggested methods is analyzed by comparing them with some of the latest and standard heuristic techniques. The accuracy of proposed approach is verified through convergence characteristics.

- The I-V and P-V curves are presented which shows similarity to the curves under STC conditions.
- Further to validate the error result, the non-parametric statistical tests are also executed.

Chapter 3: The key findings of this chapter are outlined below:

The key findings of slime mould algorithm are:

- The Sum of Square error (SSE) defines the objective function for the evaluation of PEMFC.
- In this chapter, firstly the proposed algorithm is checked by ten benchmark test functions. Moreover, the convergence graph and I-V and P-V Characteristics curves justify the accuracy of the proposed algorithm.
- The average value of SSE for both the cases of the proposed algorithm is better than the rest of the compared algorithms.
- Non-parametric statistical tests are also performed to signify the outcome parameter results.

The key findings of chaotic mayfly algorithm are:

- For the extraction of PEMFC, a proposed algorithm is introduced i.e. CMA.
- Firstly, the proposed algorithm is performed on ten benchmark test functions.
- The precise solution and convergence speed of global optimization problems demonstrate that CMA performs better than the rest of the compared algorithms.
- Focused on the solution consistency results, working on I-V and P-I characteristics curve, the non-parametric tests, CMA demonstrates better based on equivalent efficiency, then the other algorithms being compared.
- The statistical findings indicate that CMA has increased effectiveness on the issue of parameter extraction of the PEMFC model.

Chapter 4: The key findings of this chapter are outlined below:

The key objective of this chapter is to develop a cost-effective and dependable hybrid PV- biomass energy system with fuel cell storage to fulfill the electrical load requirement of a community with abundant natural resources. The mathematical modeling of numerous components, as well as the operational approach for the proposed system, has been thoroughly explored. A proposed algorithm and software tool are used to do a detailed cost analysis of the proposed hybrid system, which is presented in detail. The results produced by employing these diverse approaches have been evaluated in order to determine the most optimum size and scheduling. It has been determined that the proposed hybrid chaotic algorithm outperforms both parental algorithm (PSO and SMA)

and HOMER in order to evaluate the effectiveness of the approach used. A comparative analysis is performed on the basis of LCOE, from this it is concluded that the most cost-effective configuration is the one with the least LCOE. The major goals of this effort are described below:

- For size and cost optimization concerns in community, a new hybrid renewable energy system (HRES) was designed.
- To overcome size and expense concerns, novel proposed hybrid chaotic algorithm (HCPSOSMA) is applied. The results so obtained have been compared with those obtained between parent algorithms and HOMER Pro software.
- The system's performance was assessed with solar PV/biomass/fuel cell of stand-alone HRES with the lowest NPC and LCOE values.

5.2 Future Scope

In this thesis, numerous algorithms are explored for parameter estimation of PEMFC and PV. Further, optimal sizing of hybrid renewable energy system is also studied. However, the designing of different types of fuel cell is yet to be explored. Similarly, more variant of PV diode models can form the basis of strong future study. There is great scope for further improvement in metaheuristic algorithms. The chaotic and hybrid algorithms are very sensitive to parameters for tuning so it appropriate selection of parameters are very important. Similarly, the termination criteria of optimization of algorithm need specific attention.

Optimal sizing of various hybrid renewable energy systems:

The present system involves only biomass, solar and fuel cell hybrid energy system. The optimal sizing of different types of hybrid energy system can be explored using different hybrid and chaotic based algorithm.

Multi-objective algorithm:

The current work in this thesis was limited to single-objective optimization problems. The multi-objective optimization approach is necessary for very intricate optimization issues involving many competing objectives to be addressed. So, all proposed optimization algorithms have great potential for different application also.

Development of hybrid algorithms:

The present work focuses only on one hybrid algorithm. Various hybridization of algorithm can be explored and be tested on various engineering applications.

Study on irradiance effect on solar PV cell:

This thesis only explores the effect of temperature variation on solar PV cell. The effect of variation in the solar irradiance can be studied.

REFERENCES

[1] Cao, Y., Li, Y., Zhang, G., Jermsittiparsert, K., & Razmjooy, N. (2019). Experimental modeling of PEM fuel cells using a new improved seagull optimization algorithm. Energy Reports, 5, 1616-1625.

[2] Eslami, M., Moghadam, H. A., Zayandehroodi, H., & Ghadimi, N. (2019). A new formulation to reduce the number of variables and constraints to expedite SCUC in bulky power systems. Proceedings of the national academy of sciences, India section a: physical sciences, 89(2), 311-321.

[3] Liu, Y. (2017). Continuous dependence for a thermal convection model with temperature-dependent solubility. Applied Mathematics and Computation, 308, 18-30.

[4] Mirzapour, F., Lakzaei, M., Varamini, G., Teimourian, M., & Ghadimi, N. (2019). A new prediction model of battery and wind-solar output in hybrid power system. Journal of Ambient Intelligence and Humanized Computing, 10(1), 77-87.

[5] Hosseini Firouz, M., & Ghadimi, N. (2016). Optimal preventive maintenance policy for electric power distribution systems based on the fuzzy AHP methods. Complexity, 21(6), 70-88.

[6] Hekler, A., Utikal, J. S., Enk, A. H., Hauschild, A., Weichenthal, M., Maron, R. C., & Thiem, A. (2019). Superior skin cancer classification by the combination of human and artificial intelligence. European Journal of Cancer, 120, 114-121.

[7] Gong, H., Hu, Q., Walther, A., Koo, C. W., Takahashi, E. A., Levin, D. L., ... & Yu, L. (2020). Deep-learning-based model observer for a lung nodule detection task in computed tomography. Journal of Medical Imaging, 7(4), 042807.

[8] Bhushan, B., & Singh, M. (2011). Adaptive control of nonlinear systems using bacterial foraging algorithm. International journal of computer and electrical engineering, 3(3), 335-342.

[9] Gollapudi, S. V., Pattnaik, S. S., Bajpai, O. P., Devi, S., VidyaSagar, C., Pradyumna, P. K., &Bakwad, K. M. (2008). Bacterial foraging optimization technique to calculate resonant frequency of rectangular microstrip antenna. International Journal of RF and Microwave Computer-Aided Engineering: Co-sponsored by the Center for Advanced Manufacturing and Packaging of Microwave, Optical, and Digital Electronics (CAMPmode) at the University of Colorado at Boulder, 18(4), 383-388.

[10] Del Ser, J., Osaba, E., Molina, D., Yang, X. S., Salcedo-Sanz, S., Camacho, D., ... & Herrera, F. (2019). Bio-inspired computation: Where we stand and what's next. Swarm and Evolutionary Computation, 48, 220-250.

[11] Sörensen, K. (2015). Metaheuristics—the metaphor exposed. International Transactions in Operational Research, 22(1), 3-18.

[12] Dos Santos Coelho, L., & Mariani, V. C. (2008). Use of chaotic sequences in a biologically inspired algorithm for engineering design optimization. Expert Systems with Applications, 34(3), 1905-1913.

[13] Gandomi, A. H., Yang, X. S., Talatahari, S., & Alavi, A. H. (2013). Firefly algorithm with chaos. Communications in Nonlinear Science and Numerical Simulation, 18(1), 89-98.

[14] Chen, X., Xu, B., Mei, C., Ding, Y., & Li, K. (2018). Teaching–learning–based artificial bee colony for solar photovoltaic parameter estimation. Applied energy, 212, 1578-1588.

[15] Mohanty, S., Subudhi, B., & Ray, P. K. (2015). A new MPPT design using grey wolf optimization technique for photovoltaic system under partial shading conditions. IEEE Transactions on Sustainable Energy, 7(1), 181-188.

[16] Gao, X., Cui, Y., Hu, J., Xu, G., Wang, Z., Qu, J., & Wang, H. (2018). Parameter extraction of solar cell models using improved shuffled complex evolution algorithm. Energy conversion and management, 157, 460-479.

[17] Campana, P. E., Wästhage, L., Nookuea, W., Tan, Y., & Yan, J. (2019). Optimization and assessment of floating and floating-tracking PV systems integrated in on-and off-grid hybrid energy systems. solar energy, 177, 782-795.

[18] Allam, D., Yousri, D. A., & Eteiba, M. B. (2016). Parameters extraction of the three diode model for the multi-crystalline solar cell/module using Moth-Flame Optimization Algorithm. Energy Conversion and Management, 123, 535-548.

[19] Jiang, L. L., Maskell, D. L., & Patra, J. C. (2013). Parameter estimation of solar cells and modules using an improved adaptive differential evolution algorithm. Applied Energy, 112, 185-193.

[20] Ortiz-Conde, A., Sánchez, F. J. G., & Muci, J. (2006). New method to extract the model parameters of solar cells from the explicit analytic solutions of their illuminated I–V characteristics. Solar Energy Materials and Solar Cells, 90(3), 352-361.

[21] Niu, Q., Zhang, H., & Li, K. (2014). An improved TLBO with elite strategy for parameters identification of PEM fuel cell and solar cell models. International journal of hydrogen energy, 39(8), 3837-3854.

[22] Yu, K., Chen, X., Wang, X., & Wang, Z. (2017). Parameters identification of photovoltaic models using self-adaptive teaching-learning-based optimization. Energy Conversion and Management, 145, 233-246.

[23] Niu, Q., Zhang, L., & Li, K. (2014). A biogeography-based optimization algorithm with mutation strategies for model parameter estimation of solar and fuel cells. Energy conversion and management, 86, 1173-1185.

[24] Ma, J., Bi, Z., Ting, T. O., Hao, S., & Hao, W. (2016). Comparative performance on photovoltaic model parameter identification via bio-inspired algorithms. Solar Energy, 132, 606-616.

[25] Humada, A. M., Hojabri, M., Mekhilef, S., & Hamada, H. M. (2016). Solar cell parameters extraction based on single and double-diode models: A review. Renewable and Sustainable Energy Reviews, 56, 494-509.

[26] Jordehi, A. R. (2018). Enhanced leader particle swarm optimisation (ELPSO): An efficient algorithm for parameter estimation of photovoltaic (PV) cells and modules. Solar Energy, 159, 78-87.

[27] Nunes, H. G. G., Pombo, J. A. N., Mariano, S. J. P. S., Calado, M. R. A., & De Souza, J. F. (2018). A new high performance method for determining the parameters of PV cells and modules based on guaranteed convergence particle swarm optimization. Applied energy, 211, 774-791.

[28] Jamadi, M., Merrikh-Bayat, F., & Bigdeli, M. (2016). Very accurate parameter estimation of single-and double-diode solar cell models using a modified artificial bee colony algorithm. International Journal of Energy and Environmental Engineering, 7(1), 13-25.

[29] Nishioka, K., Sakitani, N., Uraoka, Y., & Fuyuki, T. (2007). Analysis of multicrystalline silicon solar cells by modified 3-diode equivalent circuit model taking leakage current through periphery into consideration. Solar energy materials and solar cells, 91(13), 1222-1227

[30] Akbary, P., Ghiasi, M., Pourkheranjani, M. R. R., Alipour, H., & Ghadimi, N. (2019). Extracting appropriate nodal marginal prices for all types of committed reserve. Computational Economics, 53(1), 1-26.

[31] Fei, X., Xuejun, R., & Razmjooy, N. (2019). Optimal configuration and energy management for combined solar chimney, solid oxide electrolysis, and fuel cell: a case study in Iran. Energy sources, part A: Recovery, utilization, and environmental effects, 1-21.

[32] Fawzi, M., El-Fergany, A. A., & Hasanien, H. M. (2019). Effective methodology based on neural network optimizer for extracting model parameters of PEM fuel cells. International Journal of Energy Research, 43(14), 8136-8147.

[33] Yin, Z., &Razmjooy, N. (2020). PEMFC identification using deep learning developed by improved deer hunting optimization algorithm. Int J Power Energy Syst, 40(2).

[34] El-Hay, E. A., El-Hameed, M. A., & El-Fergany, A. A. (2019). Improved performance of PEM fuel cells stack feeding switched reluctance motor using multi-objective dragonfly optimizer. Neural Computing and Applications, 31(11), 6909-6924.

[35] El-Fergany, A. A. (2017). Electrical characterisation of proton exchange membrane fuel cells stack using grasshopper optimiser. IET Renewable Power Generation, 12(1), 9-17.

[36] Chugh, S., Chaudhari, C., Sonkar, K., Sharma, A., Kapur, G. S., & Ramakumar, S. S. V. (2020). Experimental and modelling studies of low temperature PEMFC performance. international journal of hydrogen energy, 45(15), 8866-8874.

[37] Mir, M., Dayyani, M., Sutikno, T., MohammadiZanjireh, M., & Razmjooy, N. (2020). Employing a Gaussian Particle Swarm Optimization method for tuning Multi Input Multi Output-fuzzy system as an integrated controller of a micro-grid with stability analysis. Computational Intelligence, 36(1), 225-258.

[38] Wang, Y., Diaz, D. F. R., Chen, K. S., Wang, Z., & Adroher, X. C. (2020). Materials, technological status, and fundamentals of PEM fuel cells–a review. Materials today, 32, 178-203.

[39] Corrêa, J. M., Farret, F. A., Canha, L. N., & Simoes, M. G. (2004). An electrochemical-based fuel-cell model suitable for electrical engineering automation approach. IEEE Transactions on industrial electronics, 51(5), 1103-1112.

[40] Correa, J. M., Farret, F. A., Popov, V. A., & Simoes, M. G. (2005). Sensitivity analysis of the modeling parameters used in simulation of proton exchange membrane fuel cells. IEEE Transactions on energy conversion, 20(1), 211-218.

[41] Kanase-Patil, A. B., Saini, R. P., & Sharma, M. P. (2010). Integrated renewable energy systems for off grid rural electrification of remote area. Renewable Energy, 35(6), 1342-1349.

[42] Singh, J., Panesar, B. S., & Sharma, S. K. (2008). Energy potential through agricultural biomass using geographical information system—A case study of Punjab. Biomass and Bioenergy, 32(4), 301-307.

[43] Kanase-Patil, A. B., Saini, R. P., & Sharma, M. P. (2011). Sizing of integrated renewable energy system based on load profiles and reliability index for the state of Uttarakhand in India. Renewable Energy, 36(11), 2809-2821.

[44] Nehrir, M. H., Wang, C., Strunz, K., Aki, H., Ramakumar, R., Bing, J., ... & Salameh, Z. (2011). A review of hybrid renewable/alternative energy systems for electric power generation: Configurations, control, and applications. IEEE transactions on sustainable energy, 2(4), 392-403.

[45] Mirjalili, S. (2015). The ant lion optimizer. Advances in engineering software, 83, 80-98.

[46] Mirjalili, S. (2016). SCA: a sine cosine algorithm for solving optimization problems. Knowledge-based systems, 96, 120-133.

[47] Mirjalili, S. (2016). Dragonfly algorithm: a new meta-heuristic optimization technique for solving single-objective, discrete, and multi-objective problems. Neural computing and applications, 27(4), 1053-1073.

[48] Mirjalili, S., Mirjalili, S. M., & Hatamlou, A. (2016). Multi-verse optimizer: a nature-inspired algorithm for global optimization. Neural Computing and Applications, 27(2), 495-513.

[49] Wang, G. G. (2018). Moth search algorithm: a bio-inspired metaheuristic algorithm for global optimization problems. Memetic Computing, 10(2), 151-164.

[50] Mirjalili, S., & Lewis, A. (2016). The whale optimization algorithm. Advances in engineering software, 95, 51-67.

[51] Saremi, S., Mirjalili, S., & Lewis, A. (2017). Grasshopper optimisation algorithm: theory and application. Advances in Engineering Software, 105, 30-47.

[52] Zhao, W., Wang, L., & Zhang, Z. (2019). A novel atom search optimization for dispersion coefficient estimation in groundwater. Future generation computer systems, 91, 601-610.

[53] Pierezan, J., & Coelho, L. D. S. (2018, July). Coyote optimization algorithm: a new metaheuristic for global optimization problems. In 2018 IEEE congress on evolutionary computation (CEC) (pp. 1-8). IEEE.

[54] Heidari, A. A., Mirjalili, S., Faris, H., Aljarah, I., Mafarja, M., & Chen, H. (2019). Harris hawks optimization: Algorithm and applications. Future generation computer systems, 97, 849-872.

[55] Khishe, M., & Mosavi, M. R. (2020). Chimp optimization algorithm. Expert systems with applications, 149, 113338.

[56] Abualigah, L., Yousri, D., AbdElaziz, M., Ewees, A. A., Al-Qaness, M. A., & Gandomi, A. H. (2021). Aquila optimizer: a novel meta-heuristic optimization algorithm. Computers & Industrial Engineering, 157, 107250.

[57] Allam, D., Yousri, D. A., & Eteiba, M. B. (2016). Parameters extraction of the three diode model for the multi-crystalline solar cell/module using Moth-Flame Optimization Algorithm. Energy Conversion and Management, 123, 535-548.

[58] Jadli, U., Thakur, P., & Shukla, R. D. (2017). A new parameter estimation method of solar photovoltaic. IEEE Journal of Photovoltaics, 8(1), 239-247.

[59] Ouada, M., Meridjet, M. S., & Dib, D. (2018). Comprehensive three-diode model of photovoltaic array with partial shading capability. International Journal of Power and Energy Conversion, 9(2), 159-173.

[60] Chenche, L. E. P., Mendoza, O. S. H., & Bandarra Filho, E. P. (2018). Comparison of four methods for parameter estimation of mono-and multi-junction photovoltaic devices using experimental data. Renewable and Sustainable Energy Reviews, 81, 2823-2838.

[61] Qais, M. H., Hasanien, H. M., Alghuwainem, S., & Nouh, A. S. (2019). Coyote optimization algorithm for parameters extraction of three-diode photovoltaic models of photovoltaic modules. Energy, 187, 116001.

[62] Wei, T., Yu, F., Huang, G., & Xu, C. (2019). A Particle-Swarm-Optimization-Based Parameter Extraction Routine for Three-Diode Lumped Parameter Model of Organic Solar Cells. IEEE Electron Device Letters, 40(9), 1511-1514.

[63] Qais, M. H., Hasanien, H. M., & Alghuwainem, S. (2019). Identification of electrical parameters for three-diode photovoltaic model using analytical and sunflower optimization algorithm. Applied Energy, 250, 109-117.

[64] Yousri, D., Thanikanti, S. B., Allam, D., Ramachandaramurthy, V. K., & Eteiba, M. B. (2020). Fractional chaotic ensemble particle swarm optimizer for identifying the single, double, and three diode photovoltaic models' parameters. Energy, 195, 116979.

[65] Chenouard, R., & El-Sehiemy, R. A. (2020). An interval branch and bound global optimization algorithm for parameter estimation of three photovoltaic models. Energy Conversion and Management, 205, 112400.

[66] Elazab, O. S., Hasanien, H. M., Alsaidan, I., Abdelaziz, A. Y., & Muyeen, S. M. (2020). Parameter estimation of three diode photovoltaic model using grasshopper optimization algorithm. Energies, 13(2), 497.

[67] Qais, M. H., Hasanien, H. M., & Alghuwainem, S. (2020). Parameters Extraction of Three-diode Photovoltaic Model using Computation and Harris Hawks Optimization. Energy, 117040.

[68] Bisht, R., & Sikander, A. (2021). A New Soft Computing-Based Parameter Estimation of Solar Photovoltaic System. Arabian Journal for Science and Engineering, 1-13.

[69] Singla, M. K., & Nijhawan, P. (2021). Triple diode parameter estimation of solar PV cell using hybrid algorithm. International Journal of Environmental Science and Technology, 1-24.

[70] Ali, M., El-Hameed, M. A., & Farahat, M. A. (2017). Effective parameters' identification for polymer electrolyte membrane fuel cell models using grey wolf optimizer. Renewable energy, 111, 455-462.

[71] El-Fergany, A. A. (2017). Electrical characterization of proton exchange membrane fuel cells stack using grasshopper optimizer. IET Renewable Power Generation, 12(1), 9-17.

[72] El-Fergany, A. A. (2018). Extracting optimal parameters of PEM fuel cells using Salp Swarm Optimizer. Renewable Energy, 119, 641-648.

[73] Fathy, A., & Rezk, H. (2018). Multi-verse optimizer for identifying the optimal parameters of PEMFC model. Energy, 143, 634-644.

[74] Gong, W., Yan, X., Hu, C., Wang, L., & Gao, L. (2018). Fast and accurate parameter extraction for different types of fuel cells with decomposition and nature-inspired optimization method. Energy conversion and management, 174, 913-921.

[75] Fathy, A., Elaziz, M. A., & Alharbi, A. G. (2020). A novel approach based on hybrid vortex search algorithm and differential evolution for identifying the optimal parameters of PEM fuel cell. Renewable Energy, 146, 1833-1845.

[76] Priya, K., & Rajasekar, N. (2019). Application of flower pollination algorithm for enhanced proton exchange membrane fuel cell modelling. International Journal of Hydrogen Energy, 44(33), 18438-18449.

[77] Duan, B., Cao, Q., & Afshar, N. (2019). Optimal parameter identification for the proton exchange membrane fuel cell using Satin Bowerbird optimizer. International Journal of Energy Research, 43(14), 8623-8632.

[78] Han, W., Li, D., Yu, D., & Ebrahimian, H. (2019). Optimal parameters of PEM fuel cells using chaotic binary shark smell optimizer. Energy Sources, Part A: Recovery, Utilization, and Environmental Effects, 1-15.

[79] Xu, S., Wang, Y., & Wang, Z. (2019). Parameter estimation of proton exchange membrane fuel cells using eagle strategy based on JAYA algorithm and Nelder-Mead simplex method. Energy, 173, 457-467.

[80] Kler, D., Rana, K. P., & Kumar, V. (2019). Parameter extraction of fuel cells using hybrid interior search algorithm. International Journal of Energy Research, 43(7), 2854-2880.

[81] El-Fergany, A. A., Hasanien, H. M., & Agwa, A. M. (2019). Semi-empirical PEM fuel cells model using whale optimization algorithm. Energy Conversion and Management, 201, 112197.

[82] Miao, D., Chen, W., Zhao, W., & Demsas, T. (2020). Parameter estimation of PEM fuel cells employing the hybrid grey wolf optimization method. Energy, 193, 116616.

[83] Fathy, A., Abdel Aleem, S. H., & Rezk, H. (2021). A novel approach for PEM fuel cell parameter estimation using LSHADE-EpSin optimization algorithm. International Journal of Energy Research, 45(5), 6922-6942.

[84] Singla, M. K., Nijhawan, P., & Oberoi, A. S. (2021). Parameter estimation of proton exchange membrane fuel cell using a novel meta-heuristic algorithm. Environmental Science and Pollution Research, 28(26), 34511-34526.

[85] Heydari, A., & Askarzadeh, A. (2016). Optimization of a biomass-based photovoltaic power plant for an off-grid application subject to loss of power supply probability concept. Applied Energy, 165, 601-611.

[86] Singh, S., & Kaushik, S. C. (2016). Optimal sizing of grid integrated hybrid PV-biomass energy system using artificial bee colony algorithm. IET Renewable Power Generation, 10(5), 642-650.

[87] Lai, C. S., & McCulloch, M. D. (2016). Sizing of standalone solar PV and storage system with anaerobic digestion biogas power plants. IEEE Transactions on Industrial Electronics, 64(3), 2112-2121.

[88] Singh, S., Singh, M., & Kaushik, S. C. (2016). Feasibility study of an islanded microgrid in rural area consisting of PV, wind, biomass and battery energy storage system. Energy Conversion and Management, 128, 178-190.

[89] Sawle, Y., Gupta, S. C., & Bohre, A. K. (2017). Optimal sizing of standalone PV/Wind/Biomass hybrid energy system using GA and PSO optimization technique. Energy Procedia, 117, 690-698.

[90] Sawle, Yashwant, S. C. Gupta, and Aashish Kumar Bohre. "Socio-techno-economic design of hybrid renewable energy system using optimization techniques." Renewable energy 119 (2018): 459-472.

[91] Eteiba, M. B., Barakat, S., Samy, M. M., & Wahba, W. I. (2018). Optimization of an off-grid PV/Biomass hybrid system with different battery technologies. Sustainable cities and society, 40, 713-727.

[92] Zheng, Y., Jenkins, B. M., Kornbluth, K., & Træholt, C. (2018). Optimization under uncertainty of a biomass-integrated renewable energy microgrid with energy storage. Renewable energy, 123, 204-217.

[93] Gonzalez, A., Riba, J. R., Esteban, B., & Rius, A. (2018). Environmental and cost optimal design of a biomass–Wind–PV electricity generation system. Renewable energy, 126, 420-430.

[94] Zheng, Y., Jenkins, B. M., Kornbluth, K., Kendall, A., & Træholt, C. (2018). Optimization of a biomass-integrated renewable energy microgrid with demand side management under uncertainty. Applied Energy, 230, 836-844.

[95] Samy, M. M., Elkhouly, H. I., & Barakat, S. (2021). Multi-objective optimization of hybrid renewable energy system based on biomass and fuel cells. International Journal of Energy Research, 45(6), 8214-8230.

[96] Kumar, A., &Verma, A. (2021). Optimal techno-economic sizing of a solar-biomass-battery hybrid system for off-setting dependency on diesel generators for microgrid facilities. Journal of Energy Storage, 36, 102251.

[97] Alam, D. F., Yousri, D. A., & Eteiba, M. B. (2015). Flower pollination algorithm based solar PV parameter estimation. Energy Conversion and Management, 101, 410-422.

[98] Derick, M., Rani, C., Rajesh, M., Farrag, M. E., Wang, Y., & Busawon, K. (2017). An improved optimization technique for estimation of solar photovoltaic parameters. Solar Energy, 157, 116-124.

[99] Fathy, A., Elaziz, M. A., Sayed, E. T., Olabi, A. G., &Rezk, H. (2019). Optimal parameter identification of triple-junction photovoltaic panel based on enhanced moth search algorithm. Energy, 188, 116025.

[100] Bastidas-Rodriguez, J. D., Petrone, G., Ramos-Paja, C. A., & Spagnuolo, G. (2017). A genetic algorithm for identifying the single diode model parameters of a photovoltaic panel. Mathematics and Computers in Simulation, 131, 38-54.

[101] Biswas, P. P., Suganthan, P. N., Wu, G., & Amaratunga, G. A. (2019). Parameter estimation of solar cells using datasheet information with the application of an adaptive differential evolution algorithm. Renewable Energy, 132, 425-438.

[102] Ebrahimi, S. M., Salahshour, E., Malekzadeh, M., & Gordillo, F. (2019). Parameters identification of PV solar cells and modules using flexible particle swarm optimization algorithm. Energy, 179, 358-372.

[103] Abdelghany, R. Y., Kamel, S., Sultan, H. M., Khorasy, A., Elsayed, S. K., & Ahmed, M. (2021). Development of an Improved Bonobo Optimizer and Its Application for Solar Cell Parameter Estimation. Sustainability, 13(7), 3863.

[104] Saleem, H., & Karmalkar, S. (2009). An analytical method to extract the physical parameters of a solar cell from four points on the illuminated $ J {-} V $ curve. IEEE Electron Device Letters, 30(4), 349-352.

[105] Mahmoud, Y., Xiao, W., & Zeineldin, H. H. (2011). A simple approach to modeling and simulation of photovoltaic modules. IEEE transactions on Sustainable Energy, 3(1), 185-186.

[106] Jordehi, A. R. (2016). Parameter estimation of solar photovoltaic (PV) cells: A review. Renewable and Sustainable Energy Reviews, 61, 354-371.

[107] Qais, M. H., Hasanien, H. M., & Alghuwainem, S. (2020). Parameters extraction of three-diode photovoltaic model using computation and Harris Hawks optimization. Energy, 195, 117040.

[108] Berrill, J. J. (1950). The Tuniccafa. The Royal Society: London.

[109] Kaur, S., Awasthi, L. K., Sangal, A. L., & Dhiman, G. (2020). Tunicate swarm algorithm: a new bio-inspired based metaheuristic paradigm for global optimization. Engineering Applications of Artificial Intelligence, 90, 103541.

[110] Lu, H. J., Zhang, H. M., & MaShi, J. (2019). A multi-compartment vehicle routing problem with time windows for urban distribution–A comparison study on particle swarm optimization algorithms. Computers A, 7(4), 539-542.

[111] Easwarakhanthan, T., Bottin, J., Bouhouch, I., & Boutrit, C. (1986). Nonlinear minimization algorithm for determining the solar cell parameters with microcomputers. International journal of solar energy, 4(1), 1-12.

[112] Friedman, M. (1939). A Correction. Journal of the American Statistical Association, 34(205), 109-109.

[113] Tamizharasan, T., Senthilkumar, N., Selvakumar, V., & Dinesh, S. (2019). Taguchi's methodology of optimizing turning parameters over chip thickness ratio in machining P/M AMMC. SN Applied Sciences, 1(2), 160.

[114] Kruskal, W. H., & Wallis, W. A. Use of Ranks in One-Criterion Variance Analysis [Internet]. J, 535, 583-621.

[115] Meng, X., Liu, Y., Gao, X., & Zhang, H. (2014, October). A new bio-inspired algorithm: chicken swarm optimization. In International conference in swarm intelligence (pp. 86-94). Springer, Cham.

[116] Fathy, A., & Rezk, H. (2018). Multi-verse optimizer for identifying the optimal parameters of PEMFC model. Energy, 143, 634-644.

[117] Zhang, L., & Wang, N. (2013). An adaptive RNA genetic algorithm for modeling of proton exchange membrane fuel cells. International Journal of Hydrogen Energy, 38(1), 219-228.

[118] Priya, K., Babu, T. S., Balasubramanian, K., Kumar, K. S., & Rajasekar, N. (2015). A novel approach for fuel cell parameter estimation using simple genetic algorithm. Sustainable Energy technologies and assessments, 12, 46-52.

[119] Turgut, O. E., & Coban, M. T. (2016). Optimal proton exchange membrane fuel cell modelling based on hybrid Teaching Learning Based Optimization–Differential Evolution algorithm. Ain Shams Engineering Journal, 7(1), 347-360.

[120] Rao, Y., Shao, Z., Ahangarnejad, A. H., Gholamalizadeh, E., & Sobhani, B. (2019). Shark Smell Optimizer applied to identify the optimal parameters of the proton exchange membrane fuel cell model. Energy conversion and management, 182, 1-8.

[121] Chen, Y., & Wang, N. (2019). Cuckoo search algorithm with explosion operator for modeling proton exchange membrane fuel cells. International Journal of Hydrogen Energy, 44(5), 3075-3087.

[122] Guarnieri, M., Negro, E., Di Noto, V., & Alotto, P. (2016). A selective hybrid stochastic strategy for fuel-cell multi-parameter identification. Journal of Power Sources, 332, 249-264.

[123] Askarzadeh, A., & Rezazadeh, A. (2013). A new heuristic optimization algorithm for modeling of proton exchange membrane fuel cell: bird mating optimizer. International journal of energy research, 37(10), 1196-1204.

[124] Yuan, Z., Wang, W., & Wang, H. (2020). Optimal parameter estimation for PEMFC using modified monarch butterfly optimization. International Journal of Energy Research, 44(11), 8427-8441.

[125] Houssein, E. H., Hashim, F. A., Ferahtia, S., & Rezk, H. (2021). An efficient modified artificial electric field algorithm for solving optimization problems and parameter estimation of fuel cell. International Journal of Energy Research, 45(14), 20199-20218.

[126] Balasubramanian, K., Thanikanti, S. B., & Natarajan, R. (2018, May). An innovative approach of PEMFC parameter extraction using artificial immune system. In 2018 IEEE Innovative Smart Grid Technologies-Asia (ISGT Asia) (pp. 167-171). IEEE.

[127] Singla, M. K., Oberoi, A. S., & Nijhawan, P. (2019). Trends so far in Hydrogen Fuel Cell Technology: State of the art. International Journal of Advanced in Computer Science and Engineering, 8(4), 1146-1155.

[128] Domínguez, E. (2006). Ephemeroptera of south America (Vol. 2). Pensoft Publishers.

[129] McCafferty, W. P. (1991). Comparison of old and new world Acanthametropus (Ephemeroptera: Acanthametropodidae) and other psammophilous mayflies. Entomological News, 102(5), 205-214.

[130] Geem, Z. W., & Noh, J. S. (2016). Parameter estimation for a proton exchange membrane fuel cell model using GRG technique. Fuel Cells, 16(5), 640-645.

[131] Allan, J. D., & Flecker, A. S. (1989). The mating biology of a mass-swarming mayfly. Animal Behaviour, 37, 361-371.

[132] Peckarsky, B. L., McIntosh, A. R., Caudill, C. C., & Dahl, J. (2002). Swarming and mating behavior of a mayfly Baetisbicaudatus suggest stabilizing selection for male body size. Behavioral Ecology and Sociobiology, 51(6), 530-537.

[133] Li, Q., Chen, W., Wang, Y., Liu, S., & Jia, J. (2010). Parameter identification for PEM fuel-cell mechanism model based on effective informed adaptive particle swarm optimization. IEEE Transactions on Industrial Electronics, 58(6), 2410-2419.

[134] Addis, B., Cassioli, A., Locatelli, M. et al. A global optimization method for the design of space trajectories. Comput Optim Appl 48, 635–652 (2011).

[135] Yang, X. S. (2010). Nature-inspired metaheuristic algorithms. Luniver press.

[136] Mansouri, N., Zade, B. M. H., & Javidi, M. M. (2019). Hybrid task scheduling strategy for cloud computing by modified particle swarm optimization and fuzzy theory. Computers & Industrial Engineering, 130, 597-633.

[137] Chen, J., & Shi, J. (2019). A multi-compartment vehicle routing problem with time windows for urban distribution–A comparison study on particle swarm optimization algorithms. Computers & Industrial Engineering, 133, 95-106.

[138] Abdin, Z., & Mérida, W. (2019). Hybrid energy systems for off-grid power supply and hydrogen production based on renewable energy: A techno-economic analysis. Energy Conversion and management, 196, 1068-1079.

[139] Mehrjerdi, H. (2020). Modeling and optimization of an island water-energy nexus powered by a hybrid solar-wind renewable system. Energy, 197, 117217.

[140] Ahmad, J., Imran, M., Khalid, A., Iqbal, W., Ashraf, S. R., Adnan, M., & Khokhar, K. S. (2018). Techno economic analysis of a wind-photovoltaic-biomass hybrid renewable energy system for rural electrification: A case study of KallarKahar. Energy, 148, 208-234

[141] Doshi, R., &Kute, V. (2020, February). A Review Paper on Security Concerns in Cloud Computing and Proposed Security Models. In 2020 International Conference on Emerging Trends in Information Technology and Engineering (ic-ETITE) (pp. 1-4). IEEE.

[142] Rajanna, S., & Saini, R. P. (2016). Modeling of integrated renewable energy system for electrification of a remote area in India. Renewable Energy, 90, 175-187.

[143] Singla, M. K., Oberoi, A. S., & Nijhawan, P. (2019). Solar-PV & fuel cell based hybrid power solution for remote locations. International Journal of Engineering and Advanced Technology, 9(1), 861-867.

[144] Singla, M. K., Nijhawan, P., & Oberoi, A. S. (2021). Hydrogen fuel and fuel cell technology for 61a cleaner future: 61a review. Environmental Science and Pollution Research, 1-20.

[145] Santarelli, M., Calì, M., & Macagno, S. (2004). Design and analysis of stand-alone hydrogen energy systems with different renewable sources. International Journal of Hydrogen Energy, 29(15), 1571-1586.

[146] Chauhan, P., Deep, K., & Pant, M. (2013). Novel inertia weight strategies for particle swarm optimization. Memetic computing, 5(3), 229-251.

[147] Panda, S., & Padhy, N. P. (2007). Comparison of particle swarm optimization and genetic algorithm for TCSC-based controller design. International Journal of computer science and engineering, 1(1), 41-49.

[148] Dhillon JS, Kothari DP (2010) Power system optimization, 2ndedn. PHI, New Delhi

[149] Das, S., Abraham, A., & Konar, A. (2008). Particle swarm optimization and differential evolution algorithms: technical analysis, applications and hybridization perspectives. In Advances of computational intelligence in industrial systems (pp. 1-38). Springer, Berlin, Heidelberg.

[150] Dey, B., Bhattacharyya, B., & Márquez, F. P. G. (2021). A hybrid optimization-based approach to solve environment constrained economic dispatch problem on microgrid system. Journal of Cleaner Production, 307, 127196.